

A General Theory of Elastic Stability

J. M. T. Thompson

and

G. W. Hunt

*Department of Civil Engineering
University College London*

A Wiley-Interscience Publication

JOHN WILEY & SONS

@Seismicisolation

London · New York · Sydney · Toronto

Copyright © 1973 John Wiley & Sons Ltd.
All Rights Reserved. No part of this publication
may be reproduced, stored in a retrieval system,
or transmitted, in any form or by any means,
electronic, mechanical, photocopying, recording
or otherwise, without the prior written permission
of the Copyright owner.

Library of Congress Catalog Card No. 73-8199
ISBN 0 471 85991 5

PREFACE

Working as a research student at Cambridge University in the early sixties under the guidance of Dr A. H. Chilver, the first author soon became aware of what appeared to be a complete lack of any general theoretical framework on which his studies of shell buckling could be based. Linear stability theories, to be sure, were fairly well developed, but following the exploratory work of Karman and Tsien in 1939 it was well known that many structural problems of engineering significance demanded a nonlinear large-deflection approach.

A research fellowship at Peterhouse gave him the opportunity to lay the seeds of a general discrete-coordinate theory, which has since borne fruit in the Stability Research Group at University College London with the encouragement and support first of Professor A. H. Chilver and now of Professor K. O. Kemp.

For several years the first author was blissfully unaware of the classic dissertation of Professor W. T. Koiter which had surprisingly lain largely unknown since 1945, and has in fact only recently been translated into English by the National Aeronautics and Space Administration of America. This was indeed most fortunate, since the weight of Professor Koiter's contribution could well have discouraged him from proceeding with his own development of the subject. As it transpired, the full significance of Professor Koiter's work has filtered slowly into our consciousness in a gentle stream, moderated by the Dutch language and by our temperaments which have invariably preferred to explore the field for ourselves. This having been said, we must nevertheless hasten to admit our deep indebtedness to Professor Koiter's work, which we hope is adequately acknowledged in the text.

This book, then, is the fruit of a decade of research activity and presents a general nonlinear mathematical theory of elastic stability for conservative systems. Generalized coordinates are employed, and the treatise represents a sizeable contribution to bifurcation theory of classical mechanics in the spirit of H. Poincaré. It has important applications in the nonlinear eigenvalue analyses of practical solids and structures, making it of immediate concern to structural engineers, as well as to wider audiences across the physical sciences in such areas as crystallography and cosmology.

A Lagrangian energy formulation is employed, and starting from a firm axiomatic base a number of fundamental theorems are established. A wide

Printed in Great Britain by William Clowes & Sons Limited
London, Colchester and Beccles



@Seismicisolation

variety of instability phenomena are delineated and classified, and recent experimental studies of frames and arches are presented. Intrinsic perturbation schemes are systematically employed within both diagonal and non-diagonal formulations, and a rigorous elimination of passive coordinates is introduced. Branching points corresponding to both distinct and compound eigenvalues are examined, and particular attention is given to the important topic of imperfection-sensitivity.

Worked examples from engineering structures include comparative continuum and numerical studies of the initial post-buckling of struts and plates, and the finite-element results are shown to converge rapidly to the exact continuum values. Structural models with one, two and n degrees of freedom are presented, and a computer analysis of a frame yields excellent agreement with experimental results. Rings and spherical shells are also studied, the latter serving as an illustration of simultaneous buckling.

Some original material on the compound failure of columns is included, and the treatise closes on a divergent note with an examination of the dangers of highly optimized structural designs, which inevitably exhibit severe and usually compound instabilities.

Although it is essentially an advanced treatise aimed at research workers and stability specialists we have been at pains to present a most readable introduction to the nonlinear phenomena of elastic stability which is in many ways unique. Indeed as far as we are aware the only other book that deals with these phenomena in a systematic way is the recent undergraduate text by our colleagues Dr J. G. A. Croll and Dr A. C. Walker which we can recommend as an introduction to the field.

The closing chapter on the very real dangers of structural optimization is a second original and readable feature which we feel could most profitably be studied by undergraduates, postgraduates and structural engineers in the civil and aeronautical fields.

We are deeply indebted to our colleagues, both within and outside the Stability Research Group, for the simulating environment in which our ideas have developed and to the Science Research Council for their generous financial support. Although framed in generalized coordinates rather than in continuum terms, our approach owes much to the afore-mentioned work of Professor W. T. Koiter and we are pleased once again to acknowledge our indebtedness to this source, and to the later contributions of Dr M. J. Sewell.

A general outline of the book can be found in Section 2.8, and we hope that the reader will find this excursion into bifurcation theory a rewarding experience. We are indeed fortunate to have contributed to a field of classical mechanics in which practical usefulness and natural beauty are so harmoniously united.

SOME NOTES ON TERMINOLOGY

All equilibrium states of a system are characterized as either *normal* or *critical*. A normal equilibrium state has no zero stability coefficients, while a critical equilibrium state has one or more zero stability coefficients. A critical equilibrium state with a single zero coefficient is termed *distinct*, while a critical equilibrium state with more than one zero coefficient is termed *compound*. A compound critical point can be viewed as two or more *coincident* critical points.

We see that we are here using the word *distinct* to replace the word *discrete* which has been used in the past to describe a critical equilibrium state with a single zero coefficient. *Discrete* can thus be reserved for systems described by a set of generalized coordinates to distinguish them from *continuous* systems.

The adjective *neutral*, which is much abused in the engineering literature and is often used synonymously with *critical*, will be reserved for the pathological situation in which a system can be displaced indefinitely along an equilibrium path at a given value of the loading parameter with no change in its total potential energy.

The monograph is applicable both to engineering structures and to the much wider class of conservative physical systems, and for some concepts two words will be introduced corresponding to these two fields of interest. A point of bifurcation will for example be viewed as the intersection of a *primary* or *fundamental* equilibrium path with one or more *secondary* or *post-buckling* paths. This will allow us to retain the established terms fundamental and post-buckling for structural examples, while employing the broader terms in sections of more general interest. The term *post-buckling* will hardly strike a chord in an astro-physicist interested in stellar evolution, or a crystallographer studying lattice stability.

Finally, we shall use the term *buckling* to describe loosely the loss of stability of an engineering structure, and at a compound critical point we shall speak of *simultaneous* buckling.

CONTENTS

Preface	v
Some Notes on Terminology	vii
1 INTRODUCTORY EXAMPLES	1
1.1 Introduction	1
1.2 Simple link models Simple arch... Hinged cantilever... Propped cantilever... Asymmetric model... Two-hinged strut	1
1.3 The elastica	26
Introduction... Energy formulation... Continuum analysis... General theory for discrete systems... Harmonic analysis... Finite-element analysis... Post-buckling solution	
2 GENERAL INTRODUCTION	46
2.1 Introduction	46
Historical notes... Practical relevance	
2.2 Structural system	49
2.3 Some basic phenomena	50
Limit and branching points... Meta-stability... Shallow arch... Structural examples... Cosmology and crystallography	
2.4 Two fundamental theorems	61
Topological proofs of theorems	
2.5 Initial imperfections	65
Limit point... Asymmetric point of bifurcation... Stable-symmetric point of bifurcation... Unstable-symmetric point of bifurcation	
2.6 A criterion for classification	69
Far-field stability	

2.7	Experimental study	70	6	DISTINCT BRANCHING POINTS	141
	Work of Roorda on frames		6.1	Introduction	141
2.8	Theoretical developments	76	6.2	Sliding coordinates	141
	General outline of the book		6.3	General analysis	141
				The <i>W</i> -transformation... General form of equations...	
				Rayleigh–Ritz theorem... Corresponding deflection	
3	STABILITY OF EQUILIBRIUM	86	6.4	Analysis with diagonalization	150
3.1	Structural system	86		The <i>A</i> -transformation... Sliding and rotating coordinates	
	Kinetic and potential energies... Liapunov stability...				
	Two axioms		6.4	The elastic ring	155
3.2	Stability of an equilibrium state	89		Donnell equations	
	Principal coordinates... Stability coefficients... Degree of instability				
3.3	Stability of an equilibrium path	98	7	THE CIRCULAR PLATE	160
	The <i>A</i> -transformation... The Euler strut		7.1	General outline	160
3.4	Multi-link model	99	7.2	Formulation	161
				Energy functional... Calculus of variations	
4	NORMAL BEHAVIOUR	103	7.3	Continuum analyses	165
4.1	The general system	103		Contraction procedure	
	Perturbation equations... Kirchhoff uniqueness theorem		7.4	Finite-element analyses	170
4.2	The specialized system	106		Energy coefficients... Banding of arrays	
	Some theorems for the load versus corresponding deflection plot				
✓ 4.3	The finite-element method	110	8	IMPERFECT SYSTEMS	179
	Introduction... Continuum formulation... Localized Ritz formulation... Finite-element solution		8.1	Introduction	179
4.4	The laterally-loaded beam	117		Imperfection-sensitivity	
	Introduction... Energy formulation... Continuum analysis... Harmonic analysis... Finite-element analysis... Perturbation solutions		8.2	The limit point	180
5	CRITICAL BEHAVIOUR	127	8.3	Branching analysis with diagonalization	181
5.1	Introduction	127		One-half power law... Two-thirds power law	
5.2	Perturbation equations	127	8.4	Two illustrative examples	187
	Stability determinant			Stable-symmetric bifurcation... Unstable-symmetric bifurcation	
5.3	The limit point	129	8.5	General branching analysis	191
	Spatial form of equilibrium paths			Spiralling eigenvector	
5.4	Simple arch	132	8.6	Perturbation patterns	196
5.5	Branching points	134		Contraction mechanism	
	Classification... Poincaré's exchange of stability		8.7	Asymptotic equations of imperfection-sensitivity	202
9	STRUTS AND FRAMES	205			
9.1	Strut on an elastic foundation	205			
	Energy formulation... Perfect system... Imperfect systems				

9.2	Finite-element method for frames	211
	Generalized coordinates... Perfect system... Imperfect systems... Correlation with experiments	
10	COINCIDENT BRANCHING POINTS	221
10.1	Introduction	221
10.2	Analysis with diagonalization	222
	Elimination of passive coordinates... Preservation of equilibrium and stability conditions... Perturbation equations and the theorem of Bezout... Some particular solutions... Critical state stability analysis	
10.3	General branching analysis	238
	Elimination of passive coordinates... Post-buckling solutions	
10.4	Erosion of an optimum design	242
	The Augusti model... Secondary branching... Imperfection-sensitivity at coalescence	
11	THE SPHERICAL SHELL	251
11.1	Introduction	251
11.2	Energy formulation	253
	Energy functional... Expansion in Legendre functions ... Quadratic coefficients	
11.3	Analysis in principal coordinates	260
	Diagonalization and eigenvalue problem... Cubic coefficients... Post-buckling solutions	
11.4	Analysis in original coordinates	268
	Elimination of passive coordinates	
12	COMPOUND FAILURE OF COLUMNS	272
12.1	Introduction	272
12.2	The thin-walled strut	272
	Analysis of Van der Neut... Analysis of Koiter	
12.3	The reticulated strut	277
	Theory... Experiments	
12.4	The mild-steel strut	282
13	STRUCTURAL OPTIMIZATION	287
13.1	Introduction	287
	Optimization as a generator of severe instability	
13.2	The elastic arch	289
13.3	The yielding strut	290
13.4	The cylindrical panel	291
13.5	The Michell truss	292
13.6	The complete spherical shell	293
	Root-mean-square imperfection magnitude	
13.7	The complete cylindrical shell	294
13.8	The thin-walled column	295
	Optimum design of a thin-walled column... Erosion of the optimum solution	
13.9	Concluding remarks	299
	APPENDIX I BASIC THEOREMS	300
	Analytical proofs of theorems	
	APPENDIX II INDUCTION TECHNIQUES	303
	REFERENCES	307
	BIBLIOGRAPHY	317
	INDEX	319

INTRODUCTORY EXAMPLES

1.1 Introduction

Insight into the instability of structural systems is most readily gained by a study first of simple finite-dimensional models and then of simple continuous systems, and for this reason we have prefixed this monograph by a chapter of illustrative examples. These are used to introduce the reader gently and naturally to the basic concepts and ideas that will be introduced formally and rigorously in the subsequent chapters. This having been said, specialists in the field of structural stability may well care to omit this chapter from their reading, and proceed straight to the general introduction of Chapter 2, and we can assure them that in doing so they will miss nothing of the general development of the subject. Further examples are introduced throughout the body of the book, and if more are required the specialist reader can easily flick back to this chapter, which we might observe contains a fairly detailed study of the buckling and post-buckling of an Euler strut by continuum, harmonic and finite-element methods.

1.2 Simple link models

Simple arch

Let us consider first the shallow arch of Figure 1 comprising two linear extensional springs of stiffness k pinned to each other and to rigid supports as shown. The springs are assumed to be capable of resisting both tension and

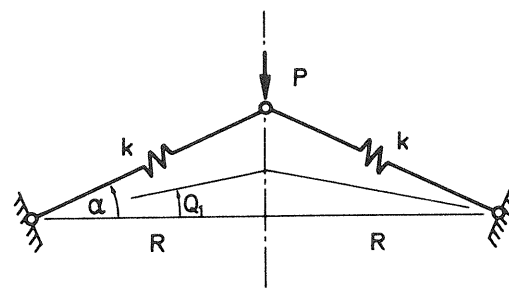


Figure 1 The simple arch

compression and the distance between the abutments is taken as $2R$. The initial angle of the springs is α and the central pin is loaded by a dead vertical force of magnitude P .

Only symmetric deformations of the arch are to be considered, so the system has one degree of freedom which we take to be the variable angle Q_1 .

The original length of either spring is $R/\cos\alpha$ and the subsequent length is $R/\cos Q_1$. Thus the strain energy of the two springs can be written as

$$U(Q_1) = 2 \cdot \frac{1}{2} \cdot k \left(\frac{R}{\cos \alpha} - \frac{R}{\cos Q_1} \right)^2$$

and assuming that the arch is and remains shallow we can take α and Q_1 to be small and write

$$\cos \alpha = 1 - \frac{\alpha^2}{2}, \quad \cos Q_1 = 1 - \frac{Q_1^2}{2}.$$

We thus obtain the strain energy as

$$U(Q_1) = \frac{1}{4}kR^2(\alpha^4 - 2\alpha^2 Q_1^2 + Q_1^4).$$

The corresponding deflection of the load P is simply

$$\mathcal{E}(Q_1) = R \tan \alpha - R \tan Q_1,$$

and approximating for small angles as before we have

$$\mathcal{E}(Q_1) = R(\alpha - Q_1).$$

The potential energy of the load is $-P\mathcal{E}(Q_1)$ so the total potential energy of the system (structure plus load) can be written as

$$\begin{aligned} V(Q_1, P) &= U(Q_1) - P\mathcal{E}(Q_1) \\ &= \frac{1}{4}kR^2(\alpha^4 - 2\alpha^2 Q_1^2 + Q_1^4) - PR(\alpha - Q_1). \end{aligned}$$

The condition for equilibrium is simply that

$$\frac{\partial V}{\partial Q_1} \equiv V_1 = 0$$

so we can quickly obtain the equilibrium solution by setting

$$V_1 = kR^2(-\alpha^2 Q_1 + Q_1^3) + PR = 0$$

to give

$$P(Q_1) = kRQ_1(\alpha^2 - Q_1^2),$$

which is shown in Figures 2 and 3. We see that P is stationary with respect to Q_1 when $Q_1 = \pm \alpha/\sqrt{3}$, and zero when $Q_1 = 0$ or $\pm\alpha$.

We see, as we would expect, that there are three equilibrium positions under zero P , given by $Q_1 = 0$ and $\pm\alpha$.

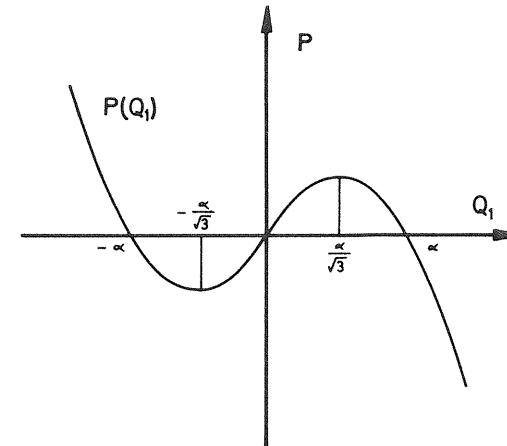


Figure 2 Nonlinear response

To study the stability of the equilibrium path we form the second derivative

$$\frac{\partial^2 V}{\partial Q_1^2} \equiv V_{11} = kR^2(3Q_1^2 - \alpha^2)$$

which varies with Q_1 as shown in Figure 3. In the equilibrium states $V_1 = 0$, so if V_{11} is positive we have a minimum of V and the equilibrium state is stable, while if V_{11} is negative we have a maximum of V and the equilibrium state is unstable. This is indicated in Figure 3 in which stable equilibrium states are represented by a solid line and unstable equilibrium states are represented by a broken line. As we would expect, we see that the two unloaded equilibrium states represented by $Q_1 = \pm\alpha$ are stable while the unloaded equilibrium state represented by $Q_1 = 0$ is unstable.

It remains to inquire whether the critical equilibrium states, C and E of Figure 3, are themselves stable or unstable. In these states we have $V_1 = V_{11} = 0$ and to examine the local form of V we must clearly examine the third derivative. This is readily obtained as

$$V_{111} = 6kR^2 Q_1$$

and we see that this is non-zero at the critical equilibrium states C and E . Thus considering a Taylor expansion of V about these states we see that V is locally cubic giving a horizontal point of inflection; so V is not a minimum and the two critical equilibrium states are themselves unstable.

A loading sequence can now be traced on Figure 3. Starting from the unloaded state B the arch will follow the stable rising path BC as the load is increased. On reaching the unstable critical equilibrium state C the arch will snap dynamically under the prescribed value of the dead load P and will

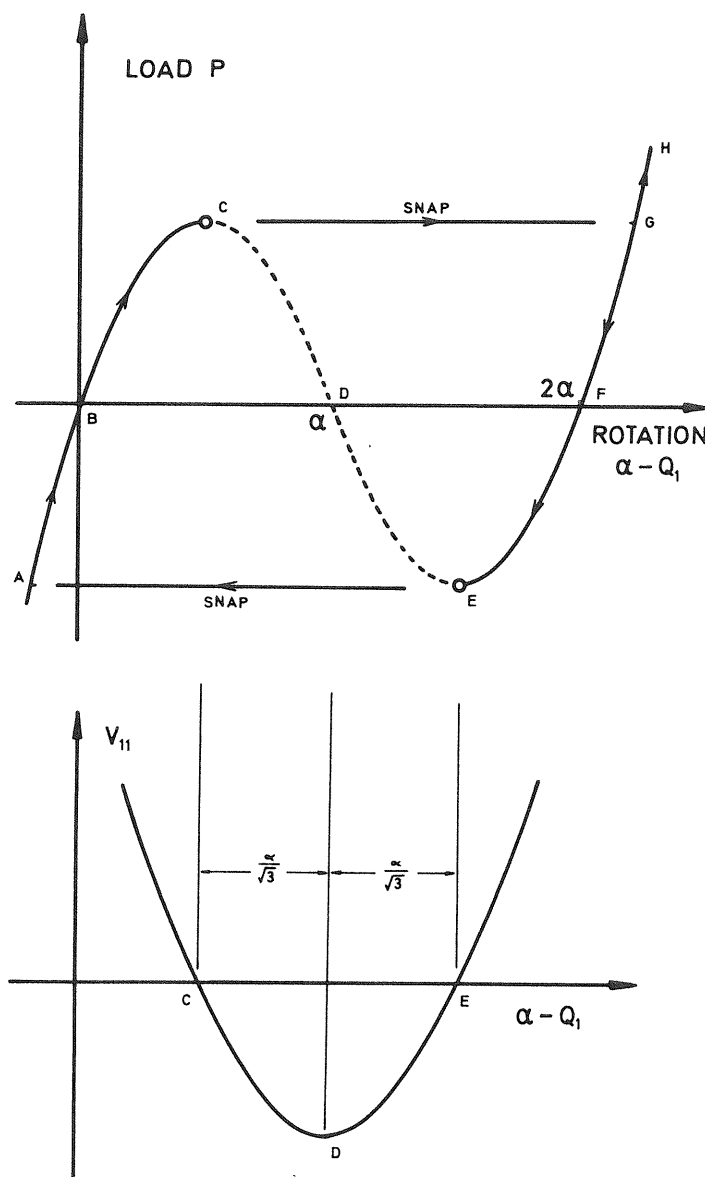


Figure 3 Variation of V_{11} determining regions of stability and instability

exhibit large-amplitude vibrations about the stable equilibrium state G . In the presence of some damping the energy released in the displacement from C to G (corresponding to the area $CDEFG$ on a plot of the load against its corresponding deflection) will eventually be dissipated and the system will come to rest in state G . On further loading the arch, now inverted, will follow the stable rising path GH as indicated.

On unloading a similar sequence is followed. Thus as P is decreased the arch will remain inverted along the stable path $HGFE$ and will then snap dynamically from E to A , an increase in P being then necessary to bring the arch back to the unloaded state B .

We see that the arch has followed a hysteresis loop $CGEA$, the corresponding energy having been dissipated in the two dynamic snaps. The region CE of the equilibrium path corresponding to unstable states of equilibrium is never encountered in a normal loading sequence, but the equilibrium states do of course exist and can be observed experimentally if some element of control is introduced.

The maxima and minima at which the stability of an equilibrium path changes, illustrated by points C and E of the present example, will be examined in some detail in later chapters, and will be termed *limit points*. They are well known to structural engineers in the response of shallow arches and domes which can snap through into an inverted configuration.

Hinged cantilever

Let us consider secondly the hinged cantilever of Figure 4(a) comprising a rigid link of length L , pinned to a rigid foundation and supported by a linear

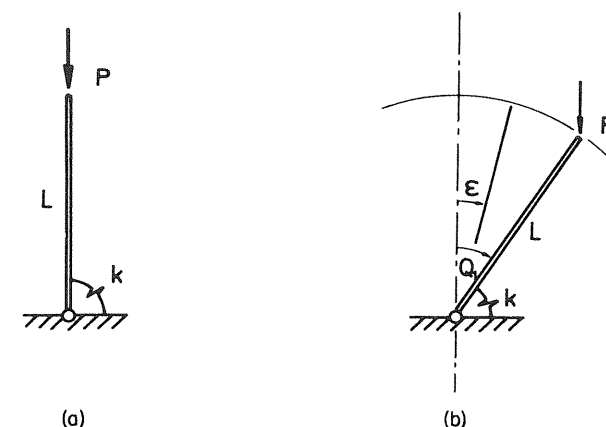


Figure 4 Hinged cantilever showing (a) undeflected perfect system and (b) deflected imperfect system

rotational spring of stiffness k . Assuming for the moment that the system is perfect in the sense that the spring is unstrained when the link is vertical, we shall denote the subsequent rotation of the link by Q_1 .

The strain energy of the system is now given by

$$U = \frac{1}{2}kQ_1^2$$

and the corresponding deflection of the dead vertical load P is given by

$$\delta = L(1 - \cos Q_1).$$

Thus the total potential energy of the perfect system can be written as

$$\begin{aligned} V(Q_1, P) &= U(Q_1) - P\delta(Q_1) \\ &= \frac{1}{2}kQ_1^2 - PL(1 - \cos Q_1). \end{aligned}$$

The equilibrium condition is that

$$V_1 \equiv \frac{\partial V}{\partial Q_1} = kQ_1 - PL \sin Q_1 = 0$$

and we see that the undeflected state $Q_1 = 0$ satisfies this equation for all values of P . Thus one equilibrium path, the trivial *fundamental* path, is coincident with the load axis while a second (post-buckling) equilibrium path is given by the expression

$$P(Q_1) = \frac{kQ_1}{L \sin Q_1}.$$

This path has the form shown in Figure 5 and intersects the fundamental path at the critical equilibrium state

$$Q_1 = 0, \quad P = P^c = \frac{k}{L}.$$

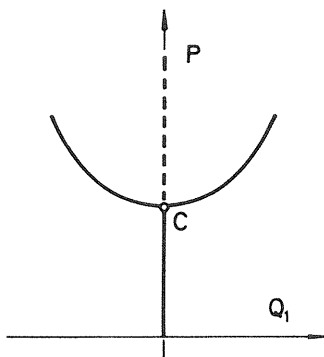


Figure 5 Equilibrium paths of the perfect system ($P^c = k/L$)

To study the stability of these equilibrium solutions we form

$$V_{11} \equiv \frac{\partial^2 V}{\partial Q_1^2} = k - PL \cos Q_1.$$

We see that on the fundamental path for which $Q_1 = 0$ the *stability coefficient* V_{11} is given by

$$V_{11}^F = k - PL.$$

It varies linearly with P changing from positive to negative at the critical equilibrium state C , indicating that the fundamental path is stable for $P < P^c$ and unstable for $P > P^c$. This is indicated in Figure 5 in which solid lines represent stable equilibrium paths while broken lines represent unstable equilibrium states.

It is readily verified that the rising post-buckling path is everywhere stable, so it remains to discuss the stability of the critical equilibrium state itself. At this state $V_1 = V_{11} = 0$ and we have further

$$V_{111} = PL \sin Q_1 \quad \text{giving} \quad V_{111}^C = 0,$$

$$V_{1111} = PL \cos Q_1 \quad \text{giving} \quad V_{1111}^C = PL.$$

Thus considering a Taylor expansion of $V(Q_1, P^c)$ we see that the first non-zero term will be

$$\frac{1}{24}V_{1111}^C Q_1^4 = \frac{1}{24}P^c L Q_1^4 = \frac{1}{24}k Q_1^4$$

so that V is a local minimum and the critical equilibrium state is thus stable.

On loading from the origin the perfect system would remain undeflected until the value of P equals $P^c = k/L$ and on further loading it would follow one limb of the stable rising post-buckling path, the limb chosen depending on the small dynamic disturbances assumed to be present.

Suppose now that the system is imperfect in the sense that the rotational spring is unstrained when the link has a small rotation denoted by ε . We see that variation of this *imperfection parameter* generates a family of imperfect systems degenerating to the perfect system when $\varepsilon = 0$.

Denoting once again the total rotation of the link by Q_1 , as shown in Figure 4(b), the strain energy of the system can now be written as

$$U(Q_1, \varepsilon) = \frac{1}{2}k(Q_1 - \varepsilon)^2$$

and the corresponding deflection of the load as

$$\delta(Q_1) = L(1 - \cos Q_1).$$

Thus the total potential energy of an imperfect system can be written as

$$V(Q_1, P, \varepsilon) = \frac{1}{2}k(Q_1 - \varepsilon)^2 - PL(1 - \cos Q_1),$$

giving

$$V_1 \equiv \frac{\partial V}{\partial Q_1} = k(Q_1 - \varepsilon) - PL \sin Q_1,$$

$$V_{11} \equiv \frac{\partial^2 V}{\partial Q_1^2} = k - PL \cos Q_1.$$

Equilibrium paths are thus given by

$$P(Q_1, \varepsilon) = \frac{k(Q_1 - \varepsilon)}{L \sin Q_1}$$

and we have stability if

$$k - PL \cos Q_1 > 0,$$

and instability if

$$k - PL \cos Q_1 < 0.$$

The response of the family of systems is summarized in Figure 6 which is taken from the analysis of Augusti.¹⁹⁷ Here heavy lines represent the response of the perfect system and light lines represent the response of imperfect systems, continuous lines denoting stable equilibrium paths and broken lines denoting unstable equilibrium paths. We see that systems with a positive ε give equilibrium paths in two opposite quadrants, while systems with a negative ε give equilibrium paths in the remaining two quadrants. The equilibrium paths of

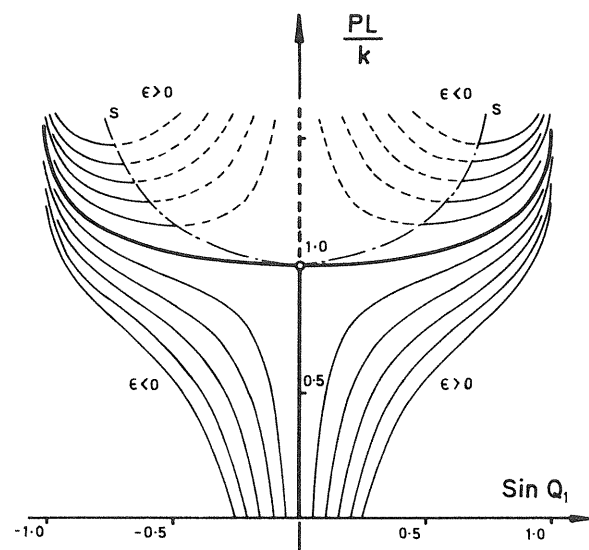


Figure 6 Equilibrium paths of the perfect and imperfect systems (after Augusti 1964)

the imperfect systems collapse onto the equilibrium paths of the perfect system as ε tends to zero. The locus of critical equilibrium states given by the equation

$$P = \frac{k}{L \cos Q_1}$$

separates the stable and unstable domains and is shown on the figure as curve ss .

We see that a given imperfect system loaded from its unloaded state will follow a constantly rising stable path so that no instability is encountered, the deflections merely growing more rapidly as the critical load of the perfect system is passed. In addition to this *natural* equilibrium path such an imperfect system will also have a *complementary* equilibrium path in the opposite quadrant, but this path (partly stable and partly unstable) would not be encountered in a natural loading sequence from $P = 0$.

The response shown in this figure (Figure 6) is well known to structural engineers and is exhibited by the familiar Euler strut which will be discussed later in this chapter. The particular critical point which initiates this response is termed a *stable-symmetric point of bifurcation* and will be studied in depth later in the book.

Propped cantilever

Consider now the propped cantilever of Figure 7 comprising a rigid link of length L , pinned to a rigid foundation and supported by a linear extensional

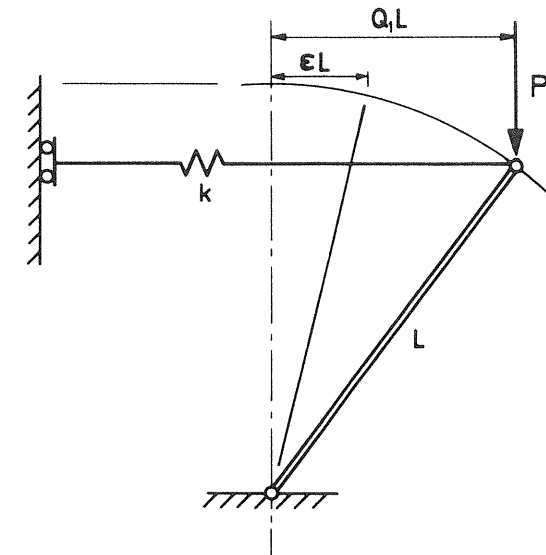


Figure 7 The propped cantilever

spring of stiffness k . The spring is assumed to be capable of resisting both tension and compression and retains its horizontal orientation as the system deflects. An *imperfection parameter* is introduced into the system by allowing the link to have a small horizontal displacement εL when the spring is unstrained. The family of imperfect systems which are generated by this imperfection parameter of course degenerate to the perfect system when $\varepsilon = 0$. The total displacement of the system from the vertical is denoted by $Q_1 L$.

The strain energy of the system is given by

$$\begin{aligned} U &= \frac{1}{2}k(Q_1 L - \varepsilon L)^2 \\ &= \frac{1}{2}kL^2(Q_1 - \varepsilon)^2 \end{aligned}$$

and the corresponding deflection of the dead vertical load P is given by

$$\varepsilon = L[1 - (1 - Q_1^2)^{\frac{1}{2}}].$$

Thus the total potential energy of the system becomes

$$V(Q_1, P, \varepsilon) = \frac{1}{2}kL^2(Q_1 - \varepsilon)^2 - PL[1 - (1 - Q_1^2)^{\frac{1}{2}}].$$

The equilibrium condition for the family of systems is

$$V_1 = kL^2(Q_1 - \varepsilon) - PLQ_1(1 - Q_1^2)^{-\frac{1}{2}} = 0$$

and the second variation of potential energy may be written

$$V_{11} = kL^2 - PL(1 - Q_1^2)^{-\frac{1}{2}} - PLQ_1^2(1 - Q_1^2)^{-\frac{3}{2}}.$$

Let us first consider the behaviour of the perfect system by setting $\varepsilon = 0$ in the potential energy expression. The equilibrium equation now provides a trivial fundamental path $Q_1 = 0$ and a further post-buckling path which may be written

$$P(Q_1) = kL(1 - Q_1^2)^{\frac{1}{2}}$$

and which intersects the fundamental path at the critical point $Q_1 = 0, P^C = kL$. The stability coefficient

$$V_{11}(0, P) = kL^2 - PL$$

clearly demonstrates that the fundamental path is stable below and unstable above the critical point; it may also readily be verified that the post-buckling path is everywhere unstable as shown in Figure 8. It therefore remains for us to investigate the stability of the critical point itself. At this state $V_1 = V_{11} = 0$ and we have further

$$V_{111} = -3PLQ_1(1 - Q_1^2)^{-\frac{3}{2}} - 3PLQ_1^3(1 - Q_1^2)^{-\frac{5}{2}} \quad \text{giving} \quad V_{111}^C = 0,$$

$$V_{1111} = -3PL(1 - Q_1^2)^{-\frac{5}{2}} - 18PLQ_1^2(1 - Q_1^2)^{-\frac{7}{2}} - 15PLQ_1^4(1 - Q_1^2)^{-\frac{9}{2}} \quad \text{giving} \quad V_{1111}^C = -3kL^2.$$

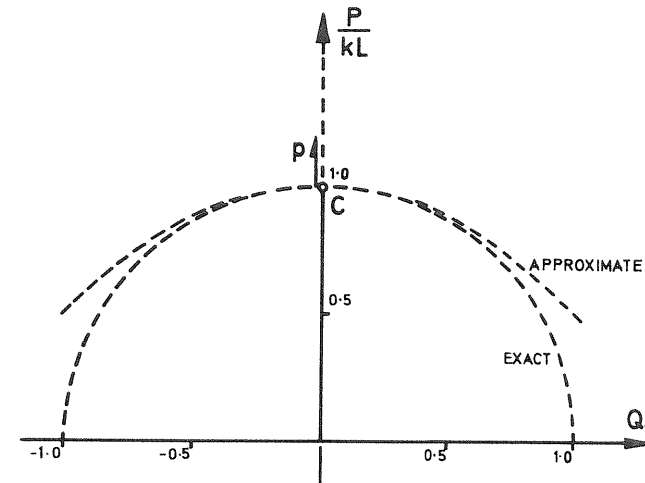


Figure 8 Approximate and exact paths of the perfect system

Thus considering a Taylor expansion of $V(Q_1, P^C)$ we see that the first non-zero term will be

$$\frac{1}{24}V_{1111}^C Q_1^4 = -\frac{1}{8}kL^2 Q_1^4$$

so that V is a local maximum and the critical equilibrium state is thus unstable.

We now move on to consider the family of imperfect systems generated by the imperfection parameter. The equilibrium condition now gives

$$P(Q_1, \varepsilon) = kL(1 - Q_1^2)^{\frac{1}{2}} \left(1 - \frac{\varepsilon}{Q_1} \right).$$

The response of the family of perfect and imperfect systems is summarized in Figure 9 which again is taken from the analysis of Augusti.¹⁹⁷ Here, once more, systems with a positive ε give equilibrium paths in two opposite quadrants, while systems with negative ε give equilibrium paths in two remaining quadrants. The equilibrium paths of the imperfect systems again collapse onto the equilibrium paths of the perfect system as ε tends to zero. However we can observe one important difference between these response curves and those of the previous example in that an imperfect equilibrium path which emerges from the unloaded state is not always rising and stable but exhibits a limit point after which the path falls and becomes unstable. Clearly it would be a rewarding step to obtain a relationship between the maximum load P^M and the imperfection parameter ε .

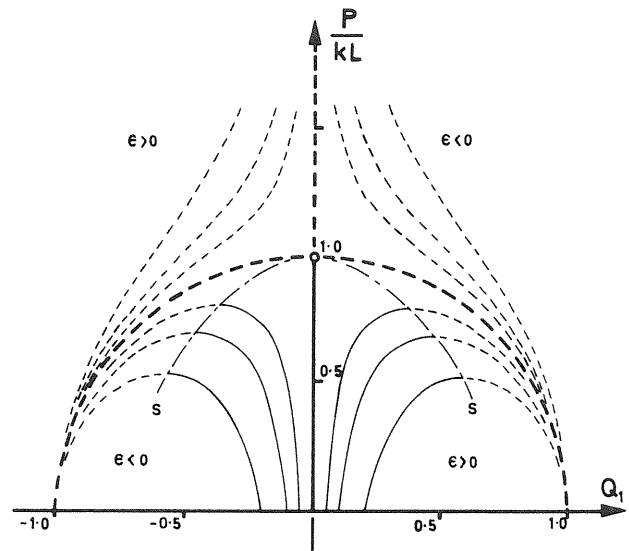


Figure 9 Equilibrium paths of the imperfect systems (after Augusti 1964)

The maximum load P^M for an imperfect system can be defined by setting the stability coefficient V_{11} to zero. This then yields

$$V_{11} = kL^2 - P^M L (1 - Q_1^2)^{\frac{1}{2}} - P^M L Q_1^2 (1 - Q_1^2)^{-\frac{1}{2}} = 0$$

which becomes

$$P^M = kL(1 - Q_1^2)^{\frac{1}{2}}.$$

This $P^M(Q_1)$ relationship is represented in Figure 9 by the curve ss : we note that this curve separates the total domain into stable and unstable regions. We can also obtain the $Q_1(\epsilon)$ relationship for this curve by combining the above result with that obtained from the equilibrium condition. This then leads to

$$kL(1 - Q_1^2)^{\frac{1}{2}} = kL(1 - Q_1^2)^{\frac{1}{2}} \left(1 - \frac{\epsilon}{Q_1}\right)$$

which may be reduced to give

$$Q_1 = \epsilon^{\frac{1}{2}},$$

and hence we obtain the important variation of maximum load P^M with imperfection parameter ϵ ,

$$P^M(\epsilon) = kL(1 - \epsilon^{\frac{1}{2}})^{\frac{1}{2}}.$$

This measure of the *imperfection-sensitivity* of the system is illustrated in Figure 10. We might note that it could have been obtained purely from equilibrium considerations by replacing the stability condition $V_{11} = 0$ by the path condition that $\partial P/\partial Q_1 = 0$.

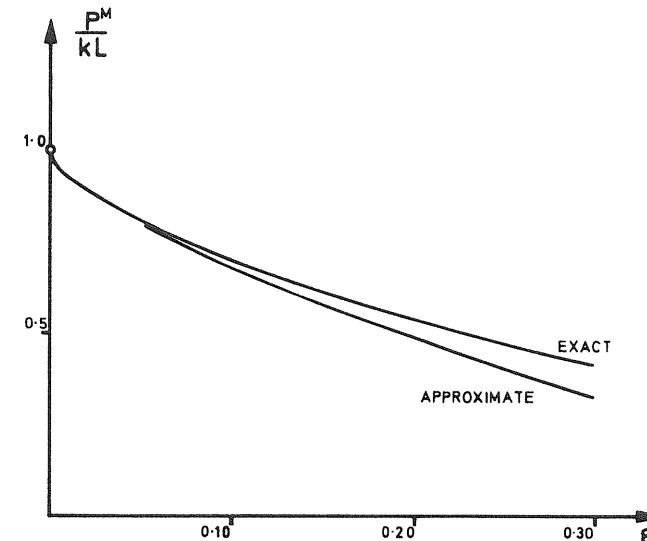


Figure 10 Imperfection-sensitivity relationship

In nonlinear problems of elastic stability it is rare that we can obtain a closed-form solution such as the above. We can however usually obtain local information by first truncating the total potential energy expression, and to demonstrate this we shall first expand the total potential energy as a power series in the variables Q_1 and ϵ ,

$$\begin{aligned} V - V^C = & -\frac{1}{8}kL^2 Q_1^4 - \frac{1}{16}kL^2 Q_1^6 + \dots \\ & -pL(\frac{1}{2}Q_1^2 + \frac{1}{8}Q_1^4 + \dots) \\ & -kL^2 Q_1 \epsilon (\frac{1}{2}kL^2 \epsilon^2) \end{aligned}$$

where $p = P - P^C$. It is now our intention to construct an approximate analysis by truncating these power series forms; the natural first-order truncations are of course introduced after the first non-zero term of each type, as shown by the solid lines above. Approximate expressions for the post-buckling path of the perfect system and the imperfection-sensitivity of imperfect systems may now be obtained by performing an exact analysis on this truncated form of the potential energy function. The equilibrium condition now becomes

$$V_{11} = -\frac{1}{2}kL^2 Q_1^3 - pLQ_1 - kL^2 \epsilon = 0$$

and the second variation of potential energy is written

$$V_{11} = -\frac{3}{2}kL^2 Q_1^2 - PL.$$

Let us first consider the perfect system by setting $\varepsilon = 0$ in the above expressions. The equilibrium equation now gives an approximate post-buckling path which may be written

$$p(Q_1) = -\frac{1}{2}kLQ_1^2.$$

The comparison between this approximate path and the known exact path is shown in Figure 8; it can be seen to represent a good approximation to the exact path for values of Q_1 up to 0.5. Expanding the preceding exact post-buckling solution as a Taylor series about the critical point we can readily confirm that our energy truncation has supplied the leading term and thus gives rise to a correct first-order solution for the path.

The approximate imperfection-sensitivity relationship can also readily be found by combining the equilibrium condition with a vanishing second variation of potential energy. This leads to

$$p^M = -\frac{1}{2}kLQ_1^2 - kL \frac{\varepsilon}{Q_1} = -\frac{3}{2}kLQ_1^2$$

which becomes

$$Q_1 = \varepsilon^{\frac{1}{3}}.$$

We can now obtain an approximate $p^M(\varepsilon)$ relationship,

$$p^M(\varepsilon) = -\frac{3}{2}kL\varepsilon^{\frac{2}{3}}.$$

The comparison between this relationship and the known exact curve is shown in Figure 10; again we have a good approximation to the exact curve for values of the imperfection parameter ε up to 0.1. Expanding the earlier exact equation of imperfection-sensitivity as an asymptotic power series about the critical point of the perfect system, it is readily verified that our energy truncation has again supplied the leading term and has thus again led us to a correct first-order solution. This first non-zero term illustrates an important property of the system, namely that the $P^M(\varepsilon)$ curve exhibits an infinite slope at $P^M = P^C$ and $\varepsilon = 0$. This suggests that the system is extremely sensitive to small imperfections since the introduction of a very small imperfection will considerably reduce the maximum load which the structure can sustain. We shall find that this 'infinite slope' phenomenon arises frequently in the nonlinear world of elastic stability.

The response shown in Figure 9 is well known to structural engineers and is exhibited by many structural systems including a wide variety of thin shells; the behaviour of non-shallow arches under point load, and the cylindrical panel as discussed by Koiter,⁶ are particularly worthy of mention. The particular critical point which initiates this response is termed an *unstable-symmetric point of bifurcation* and will be studied in depth later in the book.

Asymmetric model

Let us now consider the structural system shown in Figure 11 comprising a rigid link of length L , supported by a linear spring of stiffness k in both tension

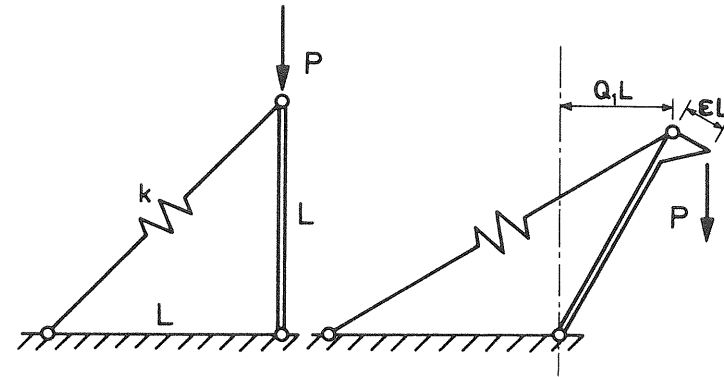


Figure 11 The asymmetric model showing undeflected perfect system and deflected imperfect system

and compression and inclined initially at 45°. The structure is loaded by a vertical dead load of magnitude P . To generate a family of imperfect systems we suppose that the load is offset by a distance εL , and to show the effect of introducing a second imperfection we shall assume additionally that the spring is initially too long by $\sqrt{2}\gamma\varepsilon L$ where γ is an arbitrary constant. The side-sway of the structure is denoted by $Q_1 L$, the single degree of freedom of the system therefore being represented by the non-dimensional generalized coordinate Q_1 .

The strain energy of the system is given by

$$U = kL^2\{(1 + Q_1)^{\frac{1}{2}} - 1 - \gamma\varepsilon\}^2$$

and the corresponding deflection of the load P becomes

$$\delta = L\{1 + Q_1\varepsilon - (1 - Q_1^2)^{\frac{1}{2}}\}$$

so the total potential energy of the system may be written as

$$V(Q_1, P, \varepsilon) = kL^2\{(1 + Q_1)^{\frac{1}{2}} - 1 - \gamma\varepsilon\}^2 - PL\{1 + Q_1\varepsilon - (1 - Q_1^2)^{\frac{1}{2}}\}$$

Let us first consider the behaviour of the perfect system by setting $\varepsilon = 0$ in the potential energy expression; this ensures that *both* of the two imperfections are absent. The equilibrium condition now gives

$$V_1(Q_1, P) = kL^2\{1 - (1 + Q_1)^{-\frac{1}{2}}\} - PLQ_1(1 - Q_1^2)^{-\frac{1}{2}} = 0$$

and we see we have a trivial fundamental solution $Q_1 = 0$. We shall investigate the stability of this fundamental solution by a second differentiation

$$V_{11}(Q_1, P) = \frac{kL^2}{2}(1 + Q_1)^{-\frac{1}{2}} - PL(1 - Q_1^2)^{-\frac{1}{2}} - PLQ_1^2(1 - Q_1^2)^{-\frac{1}{2}}$$

giving the stability coefficient

$$V_{11}^F = \frac{kL^2}{2} - PL.$$

This clearly demonstrates that we have a critical point at $Q_1 = 0$, $P^c = kL/2$, the fundamental path being stable below and unstable above this critical load. The critical equilibrium state itself can be seen to be unstable by a further differentiation of the total potential energy function,

$$V_{111} = -\frac{3}{4}kL^2(1 + Q_1)^{-\frac{3}{2}} - 3PLQ_1(1 - Q_1^2)^{-\frac{3}{2}} - 3PLQ_1^3(1 - Q_1^2)^{-\frac{3}{2}},$$

giving

$$V_{111}^F = -\frac{3}{4}kL^2.$$

It now remains for us to consider the post-buckling behaviour of this perfect system.

In each of the previous examples of this chapter we have obtained an exact expression for the post-buckling path, but such closed form solutions are possible in only the most simple problems. In the last example the straightforward truncation of the energy function supplied us with a consistent first-order solution, but the situation is less clear cut in problems involving more than one generalized coordinate, since they may have different orders of magnitude. But the greatest drawback to an initial energy truncation is that while it can yield a first-order solution, it is not clear how one should subsequently proceed if one wants to improve the solution. It is here that a *perturbation approach*, yielding as it does an ordered sequence of (usually linear) problems for the path derivatives, offers such obvious advantages, and we shall now illustrate this approach. We develop first a scheme for the post-buckling path of the problem in hand: this will be achieved both implicitly from a formal representation of the potential energy function, and explicitly from our particular known potential energy expression.

We are seeking a Taylor expansion of P as a function of Q_1 so anticipating this representation we first substitute $P(Q_1)$ into the equilibrium equation. Once this parametric substitution has been carried out, the equilibrium equation applies only to points on the post-buckling path and so becomes the identity

$$V_1[Q_1, P(Q_1)] \equiv kL^2\{1 - (1 + Q_1)^{-\frac{1}{2}}\} - P(Q_1)LQ_1(1 - Q_1^2)^{-\frac{1}{2}} \equiv 0.$$

The left-hand side is now merely a function of Q_1 and so we may differentiate the expression with respect to Q_1 as many times as we please: the right-hand

side remaining zero for all differentiations. The first such differentiation generates the equation

$$\begin{aligned} V_{11} + V'_1 P^{(1)} &= \frac{kL^2}{2}(1 + Q_1)^{-\frac{1}{2}} - P^{(1)}LQ_1(1 - Q_1^2)^{-\frac{1}{2}} \\ &\quad - PL(1 - Q_1^2)^{-\frac{1}{2}} - PLQ_1^2(1 - Q_1^2)^{-\frac{1}{2}} = 0, \end{aligned}$$

in which a bracketed superscript denotes partial differentiation with respect to Q_1 and a prime denotes partial differentiation with respect to P . If we now evaluate at the critical point C we find that this equation gives no information, so differentiating again with respect to Q_1 we obtain

$$\begin{aligned} V_{111} + 2V'_{11}P^{(1)} + V''_1 P^{(1)}P^{(1)} + V'_1 P^{(2)} &= -\frac{3}{4}kL^2(1 + Q_1)^{-\frac{5}{2}} \\ &\quad - P^{(2)}LQ_1(1 - Q_1^2)^{-\frac{3}{2}} \\ &\quad - 2P^{(1)}L(1 - Q_1^2)^{-\frac{1}{2}} \\ &\quad - 2P^{(1)}LQ_1^2(1 - Q_1^2)^{-\frac{3}{2}} \\ &\quad - 3PLQ_1(1 - Q_1^2)^{-\frac{3}{2}} \\ &\quad - 3PLQ_1^3(1 - Q_1^2)^{-\frac{1}{2}} = 0. \end{aligned}$$

Evaluating this equation at the critical point, several of the terms vanish and we are left with an expression for the slope of the post-buckling path

$$P^{(1)c} = -\left.\frac{V_{111}}{2V'_{11}}\right|_C = -\frac{3}{8}kL.$$

This will be the dominant term in the Taylor series expansion $P(Q_1)$ in the region of the critical point. It is of course possible to continue the perturbation scheme to the next equation thereby obtaining the curvature of the post-buckling path at the critical point but it is felt that this scheme, which constitutes an ordered series of linear equations, has been effectively illustrated when discontinued at this stage. We have arrived at the important result that at the critical point the post-buckling path has a *non-zero slope*, and after investigating the stability of this post-buckling path we find that the perfect system exhibits the bifurcating behaviour illustrated *schematically* in Figure 12.

This figure illustrates the load P plotted against the generalized coordinate Q_1 , but it may also be of interest to plot P against its corresponding deflection \mathcal{E} . By inverting $\mathcal{E}(Q_1)$ for the perfect system we see that

$$Q_1 = \pm \sqrt{\frac{\mathcal{E}}{L}} \left(2 - \frac{\mathcal{E}}{L} \right)^{\frac{1}{2}}$$

and hence by substituting $Q_1(\mathcal{E})$ into the Taylor expansion we obtain the first-order result,

$$P = P^c \pm \frac{3\sqrt{2}}{8}kL \left(\frac{\mathcal{E}}{L} \right)^{\frac{1}{2}}.$$

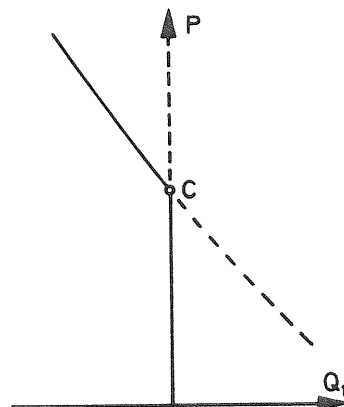


Figure 12 Schematic representation of the equilibrium paths of the perfect system ($P^c = kL/2$)

The complete $P-\varepsilon$ relationship is shown schematically in Figure 13 and we can see from the first-order approximation which is valid close to the critical point that the $P-\varepsilon$ plot has an infinite slope at $P = P^c$ and $\varepsilon = 0$; this contrasts sharply with the finite slope of the $P-Q_1$ diagram of Figure 12. We shall see in the later chapters that this contrast is common to all points of bifurcation, and that the $P-\varepsilon$ plot will normally be different in form from a typical load-generalized coordinate plot.

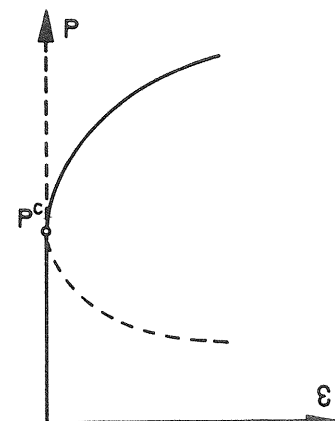


Figure 13 Schematic plot of the load versus the corresponding deflection

We now move on to consider the family of imperfect systems which is generated by variation of the imperfection parameter ε . As in the earlier examples we have a particular interest in the locus of the critical limit points which can arise in imperfect responses, and with this in mind we now write the characterizing equations of this locus. The equilibrium equation may be written

$$V_1(Q_1, P, \varepsilon) = kL^2\{1 - (1 + \gamma\varepsilon)(1 + Q_1)^{-\frac{1}{2}}\} - PL\{\varepsilon + Q_1(1 - Q_1^2)^{-\frac{1}{2}}\} = 0$$

and the limit points are further defined by the vanishing stability coefficient

$$V_{11}(Q_1, P, \varepsilon) = \frac{kL^2}{2}(1 + \gamma\varepsilon)(1 + Q_1)^{-\frac{3}{2}} - PL(1 - Q_1^2)^{-\frac{1}{2}} - PLQ_1^2(1 - Q_1^2)^{-\frac{3}{2}} = 0.$$

Again in the nonlinear world of elastic stability it is rare that we can obtain the path of interest in a closed form, so we are obliged to turn to a perturbation process which culminates in a Taylor series approximation to this path about the critical point of the perfect system. We thus define the locus of critical limit points by the parametric representations

$$P = P^M(Q_1^M), \varepsilon = \varepsilon^M(Q_1^M)$$

and substitute these into the characterizing equations to obtain the identities

$$\begin{aligned} V_1[Q_1^M, P^M(Q_1^M), \varepsilon^M(Q_1^M)] &\equiv kL^2\{1 - [1 + \gamma\varepsilon^M(Q_1^M)](1 + Q_1^M)^{-\frac{1}{2}}\} \\ &\quad - P^M(Q_1^M)L\{\varepsilon^M(Q_1^M) + Q_1^M(1 - Q_1^{M2})^{-\frac{1}{2}}\} \equiv 0, \end{aligned}$$

$$\begin{aligned} V_{11}[Q_1^M, P^M(Q_1^M), \varepsilon^M(Q_1^M)] &\equiv \frac{kL^2}{2}[1 + \gamma\varepsilon^M(Q_1^M)](1 + Q_1^M)^{-\frac{3}{2}} \\ &\quad - P^M(Q_1^M)L(1 - Q_1^{M2})^{-\frac{1}{2}} \\ &\quad - P^M(Q_1^M)LQ_1^{M2}(1 - Q_1^{M2})^{-\frac{3}{2}} \equiv 0. \end{aligned}$$

The perturbation scheme constitutes successive differentiations of each identity in turn with respect to Q_1^M , and subsequent evaluation of the resulting equations at the critical point of the perfect system to obtain the results of interest. The first such differentiation of the first identity generates the equation

$$V_{11} + V'_1 P^{M(1)} + \dot{V}_1 \varepsilon^{M(1)} = 0$$

where a dot denotes partial differentiation with respect to ε^M . On evaluation at C this leads to the result

$$\varepsilon^{M(1)c} = 0.$$

Differentiation of the second identity with respect to Q_1^M now gives the equation

$$V_{111} + V'_{11} P^{M(1)} + \dot{V}_{11} \varepsilon^{M(1)} = 0$$

which on evaluation at C leads to the result

$$P^{M(1)c} = -\left.\frac{V_{111}}{V'_{11}}\right|_C = -\frac{3}{4}kL.$$

This is an expression for the slope of the locus of critical limit points at the critical point of the perfect system, and we note that this slope is equal to twice the slope of the post-buckling path. The second differentiation of the equilibrium identity now generates the equation

$$\begin{aligned} V_{111} + 2V'_{11}P^{M(1)} + 2\dot{V}_{11}\varepsilon^{M(1)} + V''_1(P^{M(1)})^2 + 2\dot{V}'_1P^{M(1)}\varepsilon^{M(1)} \\ + V'_1P^{M(2)} + \dot{V}_1(\varepsilon^{M(1)})^2 + \dot{V}_1\varepsilon^{M(2)} = 0 \end{aligned}$$

which on evaluation at C gives the expression

$$\varepsilon^{M(2)c} = \frac{V_{111}}{V_1} \Big|_C = \frac{3}{2(1+2\gamma)}.$$

We have now obtained the first non-zero term in each of the Taylor series expansions $P^M(Q_1^M)$ and $\varepsilon^M(Q_1^M)$ about the critical point of the perfect system and so this is the stage at which we decide to leave the analysis. We have therefore obtained the first-order relationships

$$P^M = P^c + P^{M(1)c}Q_1^M = \frac{kL}{2}(1 - \frac{3}{2}Q_1^M),$$

$$\varepsilon^M = \frac{1}{2}\varepsilon^{M(2)c}Q_1^{M2} = \frac{3}{4(1+2\gamma)}Q_1^{M2}.$$

The complete imperfect behaviour is shown schematically in Figure 14. Here, as in the previous examples, the locus of limit points ss (approximated to

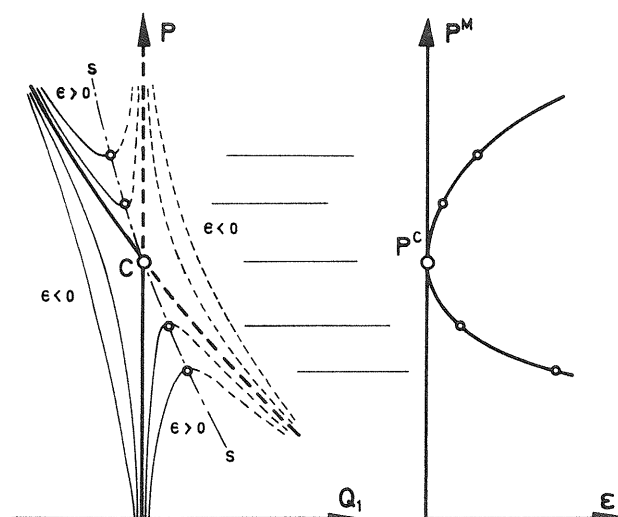


Figure 14 Schematic representation of the responses of the perfect and imperfect systems (for $1 + 2\gamma > 0$)

a first order by the first relationship above) separates the total domain into stable and unstable regions. The imperfection-sensitivity relationship $P^M(\varepsilon^M)$ may be obtained to a first order by writing $Q_1^M(\varepsilon^M)$ from the second relationship and substituting this into the first expression. This becomes

$$P^M = \frac{kL}{2} \left\{ 1 \pm \left(\frac{9}{2\varepsilon^{M(2)c}} \right)^{\frac{1}{2}} \varepsilon^{M\frac{1}{2}} \right\} = \frac{kL}{2} \{ 1 \pm [3(1 + 2\gamma)\varepsilon^M]^{\frac{1}{2}} \}.$$

The complete $P^M(\varepsilon)$ curve is also shown schematically in Figure 14, and we know that the above parabolic relationship represents a good approximation to this curve close to $P^M = P^c$ and $\varepsilon = 0$; this parabolic form is of course contaminated by higher-order terms in a complete power expansion as ε is increased. It is also interesting to note that, for imperfect systems loaded from $P = 0$, the critical limit points are only present when $\varepsilon > 0$ and so the system only experiences a high degree of sensitivity to positive imperfections.

The critical point of bifurcation which provokes the response of Figure 14 is well known to structural engineers and is termed an *asymmetric point of bifurcation*. This occurs in practice somewhat less frequently than symmetric points of bifurcation since bifurcations are often accompanied by some degree of physical symmetry and this often ensures a symmetric point of bifurcation. However the asymmetric point of bifurcation does arise in the buckling of rigid-jointed frames⁵³ and also occurs in the rotationally-symmetric buckling of a complete spherical shell.⁵⁷

Two-hinged strut

Finally, to conclude this discussion of some simple finite-dimensional models, we shall look at a problem with two degrees of freedom. Let us therefore consider the two-hinged strut of Figure 15 comprising three rigid links

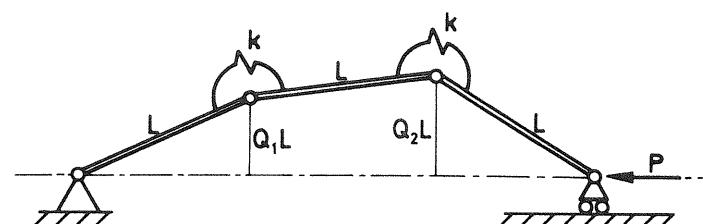


Figure 15 The two-hinged strut

of length L , pinned at their joints as shown, and restrained by the two rotational springs of stiffness k at the internal joints. The load P is assumed to retain its magnitude and direction as the system deflects. The vertical deflections of the internal joints are denoted by Q_1L and Q_2L as shown, so the total deflected

form of the system may be fully represented by specifying the non-dimensional generalized coordinates Q_1 and Q_2 . The strut is assumed to be perfect in the sense that the springs are unstrained when Q_1 and Q_2 are equal to zero.

The strain energy of the system is

$$U = \frac{1}{2}k[\sin^{-1} Q_1 - \sin^{-1}(Q_2 - Q_1)]^2 + [\sin^{-1} Q_2 + \sin^{-1}(Q_2 - Q_1)]^2$$

which, by expanding each of the terms as a power series, may be written

$$U = \frac{1}{2}k(5Q_1^2 - 8Q_1 Q_2 + 5Q_2^2 + \text{higher-order terms}).$$

The corresponding deflection of the dead load P is

$$\mathcal{E} = L\{3 - (1 - Q_1^2)^{\frac{1}{2}} - (1 - Q_2^2)^{\frac{1}{2}} - [1 - (Q_2 - Q_1)^2]^{\frac{1}{2}}\}$$

which likewise may be written

$$\mathcal{E} = L(Q_1^2 - Q_1 Q_2 + Q_2^2 + \text{higher-order terms}).$$

Thus the total potential energy of the system becomes

$$\begin{aligned} V(Q_1, Q_2, P) &= \frac{1}{2}k(5Q_1^2 - 8Q_1 Q_2 + 5Q_2^2 + \text{higher-order terms}) \\ &\quad - PL(Q_1^2 - Q_1 Q_2 + Q_2^2 + \text{higher-order terms}). \end{aligned}$$

Let us look closely at the quadratic terms in this potential energy function. In both the strain energy contribution and the corresponding deflection of the load the appropriate quadratic form is not diagonal (the cross-term $Q_1 Q_2$ is non-zero) so a useful first step in the analysis is to simultaneously diagonalize both quadratic forms of the potential energy. This can certainly be done since one of the quadratic forms, namely that of the strain energy, is positive definite and it is in fact achieved by the non-singular linear coordinate transformation

$$u_1 = \frac{Q_1 + Q_2}{2}, \quad u_2 = \frac{Q_1 - Q_2}{2},$$

which has the inverted relationships

$$Q_1 = u_1 + u_2, \quad Q_2 = u_1 - u_2.$$

We can now substitute these expressions into the V -function to obtain a new potential energy function in u_1 , u_2 and P with a fully diagonalized quadratic form,

$$\begin{aligned} A(u_1, u_2, P) &\equiv V[Q_1(u_1, u_2), Q_2(u_1, u_2), P] \\ &= \frac{1}{2}k(2u_1^2 + 18u_2^2 + \text{higher-order terms}) \\ &\quad - PL(u_1^2 + 3u_2^2 + \text{higher-order terms}). \end{aligned}$$

The generalized coordinates associated with a diagonalized potential energy function—in this case u_1 and u_2 —shall henceforth be referred to as *principal coordinates*.

We shall now investigate the equilibrium and stability of the system by studying the new potential energy function. Clearly for equilibrium the potential energy must be stationary with respect to both principal coordinates and so we obtain the two equilibrium conditions

$$A_1 = \frac{1}{2}k(4u_1 + \text{higher-order terms}) - PL(2u_1 + \text{higher-order terms}) = 0,$$

$$A_2 = \frac{1}{2}k(36u_2 + \text{higher-order terms}) - PL(6u_2 + \text{higher-order terms}) = 0.$$

Both conditions are certainly satisfied by $u_1 = u_2 = 0$ and so we have a trivial fundamental path in $P - u_1 - u_2$ space coincident with the P -axis. We shall now investigate the stability of points on the fundamental path by the second differentiations

$$A_{11} = \frac{1}{2}k(4 + \text{higher-order terms}) - PL(2 + \text{higher-order terms}),$$

$$A_{12} = A_{21} = \frac{1}{2}k(0 + \text{higher-order terms}) - PL(0 + \text{higher-order terms}),$$

$$A_{22} = \frac{1}{2}k(36 + \text{higher-order terms}) - PL(6 + \text{higher-order terms}).$$

With evaluation on the fundamental path the higher-order terms vanish and we obtain

$$A_{11}^F = 2k - 2PL,$$

$$A_{12}^F = A_{21}^F = 0,$$

$$A_{22}^F = 18k - 6PL.$$

The advantage of adopting a diagonalized potential energy function now becomes clear. The cross-derivatives A_{12}^F and A_{21}^F being zero, the stability of the fundamental path now depends entirely on the derivatives A_{11}^F and A_{22}^F . We may therefore state that if A_{11}^F and A_{22}^F are both greater than zero at a particular equilibrium state then this state is stable: alternatively if either A_{11}^F or A_{22}^F is less than zero at a particular equilibrium state then this state is unstable. Furthermore if either of these derivatives vanishes we shall say that the equilibrium state is critical. The derivatives A_{11}^F and A_{22}^F are thus of fundamental significance and shall henceforth be referred to as the *stability coefficients* of the system along the fundamental path.

Let us now consider the variation of these stability coefficients with the load as shown in Figure 16. First we note that we have two critical loads $P^1 = k/L$ and $P^2 = 3k/L$ defined by $A_{11}^F = 0$ and $A_{22}^F = 0$ respectively. For a fixed load less than the first critical load both A_{11}^F and A_{22}^F are greater than zero: this is sufficient information to ensure that the potential energy is a *complete relative minimum* with respect to the principal coordinates and we may conclude that the fundamental path is stable below the first critical load. However we are not able to predict the stability or instability of the first critical point itself because at this state A_{11}^F is zero and we need to examine the stability in the light of higher-order terms, which is beyond the scope of the present analysis. If the load is between the first and second critical loads, A_{22}^F is greater than

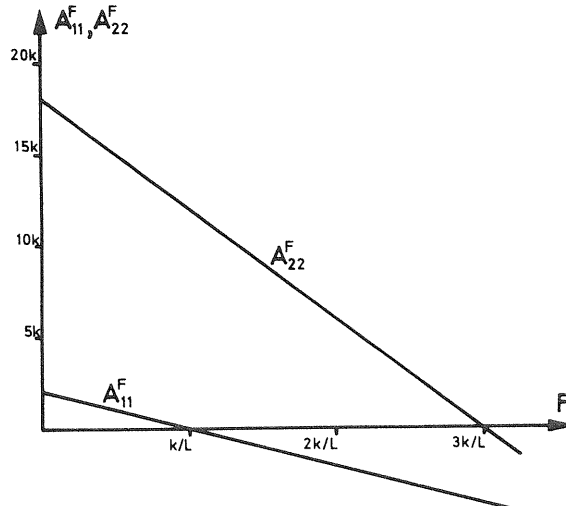


Figure 16 Variation of the stability coefficients along the fundamental path

zero but A_{11}^F is less than zero: this then generates a saddle-point in $A-u_1-u_2$ space at a fixed load level, the surface having a positive curvature in the u_2 direction and a negative curvature in the u_1 direction. We may therefore conclude that the fundamental path is unstable between the two critical points. We may also deduce that the second critical point itself is unstable due to the negative curvature in the u_1 direction, although we can say nothing about the stability of this state with respect to u_2 . Above the second critical load both stability coefficients are negative; we therefore obtain a maximum in $A-u_1-u_2$ space at a fixed load level and the fundamental equilibrium state is thus unstable. In conclusion, the fundamental path is stable below and unstable above the first critical point $u_1 = u_2 = 0$, $P^1 = k/L$, but we cannot predict the stability or instability of this point itself without looking at higher-order terms.

Having obtained the first critical load of the system it is also of interest to determine the mode into which the system buckles at this critical load. If we substitute $P = P^1 = k/L$ into the equilibrium equations we obtain

$$A_1 = k(\text{third-order terms and above}) = 0,$$

$$A_2 = k(12u_2 + \text{third-order terms and above}) = 0.$$

Thus, considering only the behaviour close to the critical point, the third-order terms and above become very small and the second equilibrium equation yields

$$u_2 = 0,$$

which also may be stated as

$$Q_1 = Q_2.$$

This indicates that the structure buckles initially in the u_1 mode for which $Q_1 = Q_2$. The information which has been obtained from this complete first-order analysis is summarized in Figure 17.

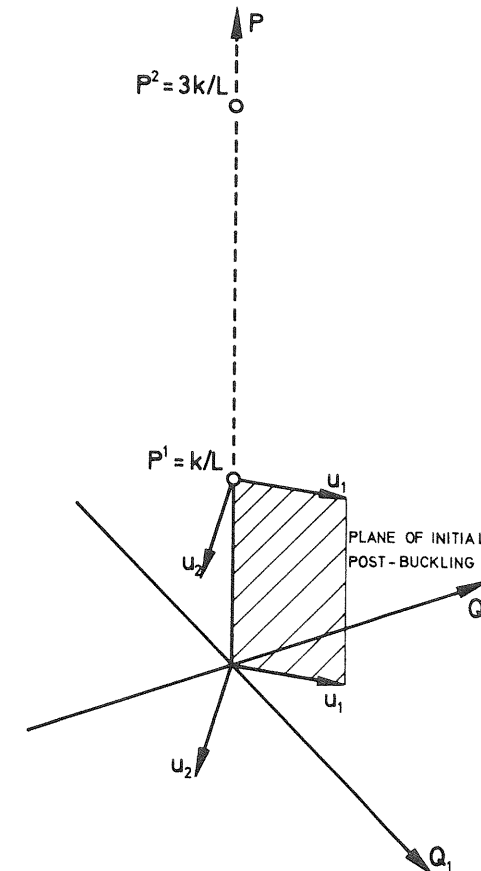


Figure 17 Information supplied by a linear eigenvalue analysis

We have made use of a method for finding the critical points of the system which resorts to a scheme of diagonalization, but such a scheme may be difficult to develop so we shall now indicate a method which includes no diagonalization. First we note that the determinant

$$|A_{ij}^F| = A_{11}^F A_{22}^F$$

is non-zero everywhere on the fundamental path except at the critical points where it vanishes. This determinant is related to the determinant of the non-diagonalized matrix V_{ij}^F by the relationship

$$|\alpha_{ij}|^2 \cdot |V_{ij}^F| = |A_{ij}^F|$$

where α_{ij} is the matrix of the linear coordinate transformation

$$Q_1 = \alpha_{11} u_1 + \alpha_{12} u_2,$$

$$Q_2 = \alpha_{21} u_1 + \alpha_{22} u_2.$$

Now α_{ij} is a non-singular matrix and hence $|\alpha_{ij}|$ is non-zero, so we may conclude that the determinant

$$|V_{ij}^F| = V_{11}^F V_{22}^F - V_{12}^F V_{21}^F$$

is only zero at the critical points. Any energy determinant will therefore be termed a *stability determinant* and we see that a vanishing stability determinant is an indication that we have encountered a critical equilibrium state; we note that this test holds for both diagonalized and non-diagonalized potential energy functions.

The analysis of this example has only included quadratic terms of potential energy. This has allowed us to predict critical loads and modes, but has not allowed us to find the slopes of the post-buckling paths. Such a treatment is termed a *linear eigenvalue analysis*.

1.3 The elastica

Introduction

The major concern of this book is the general theory of elastic stability for systems with a finite number of generalized coordinates, and so the simple link models considered so far are natural candidates for the application of this theory. The next vital step of this introductory chapter is to consider a problem with an infinite number of degrees of freedom, and to demonstrate how we can nevertheless deal with such a problem using the perturbation method which emerges from the general theory. This is set beside and compared with an alternative perturbation approach to such problems in which the system is not rendered discrete but is treated as a continuum. These two approaches, discrete and continuum, are similar in essence but often appear quite distinct due to the different formalisms employed in their development.

The particular example which we have chosen for this introductory role is the classical problem of the elastica for a pin-ended strut. This is found to be a rewarding choice since the nonlinear formulation of the problem is relatively simple and we have an exact solution presented by Timoshenko and Gere.¹⁹⁹ Also, we are able to continue the perturbation schemes past the first-order solution and thus gain some experience of continuing analyses. We first write

down an exact energy formulation for the strut. Using the calculus of variations this may then be used to generate the Euler equation for the problem which can then lead into a nonlinear continuum perturbation analysis. Alternatively we may substitute a modal expansion into the energy expression and thus generate a nonlinear discrete perturbation analysis. Here we shall present a continuum approach and two discrete approaches, harmonic and finite-element; we shall take the three schemes as far as the fifth-order perturbation equation thereby obtaining expressions for the post-buckling path derivatives as far as the fourth-order terms.

As we develop these analyses several distinctive features become apparent. In the continuum analysis we generate an ordered series of linear *differential* equations and we see that the r th-order post-buckling path derivative is obtained from the $r+1$ th perturbation equation by the ‘suppression of secular terms’ without solving the equation directly. The discrete analyses generate ordered series of linear *algebraic* equations and display a process which we refer to as the ‘contraction’ mechanism and which is observed to play precisely the same role as the suppression of secular terms in the continuum analysis. In the harmonic approach the modal waves represent the buckling modes of the strut so the analysis is greatly simplified. First the basic matrix which arises in each of the series of linear problems has a diagonal form and thus these problems are readily solved. Furthermore the infinite series of the general theory are truncated by certain further orthogonality conditions and so exact solutions for the path derivatives are obtained which naturally agree with those of the continuum analysis. The finite-element approach however contains no such diagonalizations or orthogonalities so we are obliged to turn to a digital computer to solve the equations and perform the necessary series summations. We shall observe the convergence of the resulting approximate path derivatives to the known exact values as the number of elements of the strut is successively increased. Finally we shall use the exact path derivatives to construct an approximate post-buckling equilibrium path as a series expansion in terms of a perturbation parameter, and compare this path with the known exact path.

Energy formulation

Consider the strut of Figure 18 of length l , simply supported as shown, and loaded by the axial force P which retains its magnitude and direction as the strut deflects. The strut is assumed to be axially inextensible, and the relevant bending stiffness is denoted by B .

Point A of the strut originally distance x from the left-hand support is displaced to A' and this displacement is resolved into an unspecified horizontal component and a vertical component w as shown. The centre-line being inextensible, the arc length SA' is equal to x , and the deflected form of the

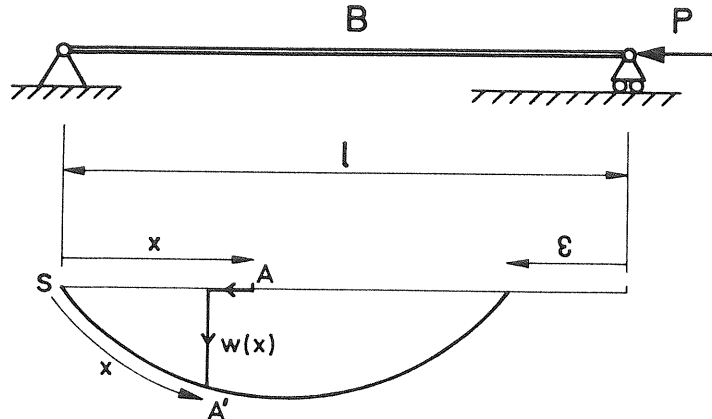


Figure 18 The pin-ended Euler strut

strut is totally specified by the mathematical function $w(x)$ where x ranges from 0 to l .

The curvature of an element is given by

$$\chi = \frac{d}{dx} \sin^{-1} \dot{w} = \ddot{w}(1 - \dot{w}^2)^{-\frac{1}{2}},$$

where a dot denotes differentiation with respect to x , so we have the strain energy functional

$$\begin{aligned} U &= \frac{1}{2}B \int_0^l \chi^2 dx \\ &= \frac{1}{2}B \int_0^l \ddot{w}^2(1 - \dot{w}^2)^{-1} dx \\ &= \frac{1}{2}B \int_0^l (\ddot{w}^2 + \ddot{w}^2 \dot{w}^2 + \ddot{w}^2 \dot{w}^4 + \dots) dx. \end{aligned} \quad (1.1)$$

The corresponding deflection of the axial load P is given by

$$\begin{aligned} \mathcal{E} &= l - \int_0^l (1 - \dot{w}^2)^{\frac{1}{2}} dx \\ &= \int_0^l (\frac{1}{2}\dot{w}^2 + \frac{1}{8}\dot{w}^4 + \frac{1}{16}\dot{w}^6 + \dots) dx \end{aligned} \quad (1.2)$$

so the total potential energy of the system is given by

$$\begin{aligned} V &= U - P\mathcal{E} \\ &= \frac{1}{2}B \int_0^l \ddot{w}^2(1 - \dot{w}^2)^{-1} dx - P \int_0^l [1 - (1 - \dot{w}^2)^{\frac{1}{2}}] dx \\ &= \frac{1}{2}B \int_0^l (\ddot{w}^2 + \ddot{w}^2 \dot{w}^2 + \ddot{w}^2 \dot{w}^4 + \dots) dx - P \int_0^l (\frac{1}{2}\dot{w}^2 + \frac{1}{8}\dot{w}^4 + \frac{1}{16}\dot{w}^6 + \dots) dx. \end{aligned}$$

Continuum analysis

We see that the total potential energy has the form

$$V = \int_0^l F(\ddot{w}, \dot{w}) dx.$$

We now apply the calculus of variations by taking a small increment of V ,

$$\delta V = \int_0^l \left(\frac{\partial F}{\partial \ddot{w}} \delta \ddot{w} + \frac{\partial F}{\partial \dot{w}} \delta \dot{w} \right) dx.$$

The order of differentiation may be reversed so the second term may be written

$$\int_0^l \frac{\partial F}{\partial \dot{w}} \delta \dot{w} dx = \int_0^l \frac{\partial F}{\partial \dot{w}} \frac{d}{dx} \delta w dx.$$

Integration by parts now yields

$$\int_0^l \frac{\partial F}{\partial \dot{w}} \delta \dot{w} dx = \left[\frac{\partial F}{\partial \dot{w}} \delta w \right]_0^l - \int_0^l \frac{d}{dx} \frac{\partial F}{\partial \dot{w}} \delta w dx.$$

Similarly

$$\begin{aligned} \int_0^l \frac{\partial F}{\partial \ddot{w}} \delta \ddot{w} dx &= \int_0^l \frac{\partial F}{\partial \ddot{w}} \frac{d}{dx} \delta \dot{w} dx \\ &= \left[\frac{\partial F}{\partial \ddot{w}} \delta \dot{w} \right]_0^l - \int_0^l \frac{d}{dx} \frac{\partial F}{\partial \ddot{w}} \delta \dot{w} dx \\ &= \left[\frac{\partial F}{\partial \ddot{w}} \delta \dot{w} \right]_0^l - \int_0^l \frac{d}{dx} \frac{d}{dx} \frac{\partial F}{\partial \ddot{w}} \delta w dx \\ &= \left[\frac{\partial F}{\partial \ddot{w}} \delta \dot{w} \right]_0^l - \left[\frac{d}{dx} \frac{\partial F}{\partial \ddot{w}} \delta w \right]_0^l + \int_0^l \frac{d^2}{dx^2} \frac{\partial F}{\partial \ddot{w}} \delta w dx. \end{aligned}$$

Thus the increment of V becomes

$$\delta V = \left[\frac{\partial F}{\partial \dot{w}} \delta w \right]_0^l + \left[\frac{\partial F}{\partial \ddot{w}} \delta \dot{w} \right]_0^l - \left[\frac{d}{dx} \frac{\partial F}{\partial \ddot{w}} \delta w \right]_0^l + \int_0^l \left(\frac{d^2}{dx^2} \frac{\partial F}{\partial \ddot{w}} - \frac{d}{dx} \frac{\partial F}{\partial \dot{w}} \right) \delta w dx.$$

Hence we may say that for δV to be zero under any δw we must have

$$\frac{d^2}{dx^2} \frac{\partial F}{\partial \ddot{w}} - \frac{d}{dx} \frac{\partial F}{\partial \dot{w}} = 0$$

and the square brackets must be eliminated by appropriate boundary conditions. The above equation is therefore the Euler equation for the strut. The physical boundary conditions are first

$$w(0) = w(l) = 0$$

and secondly that the bending moment is zero at $x = 0$ and $x = l$. The curvature at the ends of the strut is therefore zero and from the large-deflection curvature relationship we obtain

$$\ddot{w}(0) = \ddot{w}(l) = 0.$$

The first and third terms in the square brackets above can be seen to vanish by virtue of the conditions $w(0) = w(l) = 0$. For the second term we write

$$F = \frac{1}{2}B\ddot{w}^2(1 - \dot{w}^2)^{-1} - P[1 - (1 - \dot{w}^2)^{\frac{1}{2}}].$$

Thus

$$\frac{\partial F}{\partial \dot{w}} = B\ddot{w}(1 - \dot{w}^2)^{-1}$$

and we see that the second square bracket vanishes by virtue of the conditions $\ddot{w}(0) = \ddot{w}(l) = 0$. This analysis has therefore found the Euler equation for the pin-ended strut and justified the physical boundary conditions of the problem.

Performing the differentiations, the Euler equation becomes

$$\ddot{w}(1 - \dot{w}^2)^{-1} + 4\ddot{w}\dot{w}\dot{w}(1 - \dot{w}^2)^{-2} + \dot{w}^3(1 + 3\dot{w}^2)(1 - \dot{w}^2)^{-3} + \frac{P}{B}\dot{w}(1 - \dot{w}^2)^{-\frac{1}{2}} = 0,$$

which can be written in the expanded form

$$\begin{aligned} & \ddot{w}[1 + \dot{w}^2 + \dot{w}^4 + \dots] + 4\ddot{w}\dot{w}\dot{w}[1 + 2\dot{w}^2 + 3\dot{w}^4 + \dots] \\ & + \dot{w}^3[1 + 6\dot{w}^2 + 15\dot{w}^4 + \dots] + \frac{P}{B}\dot{w}[1 + \frac{3}{2}\dot{w}^2 + \frac{15}{8}\dot{w}^4 + \dots] = 0. \end{aligned}$$

The associated boundary conditions remain

$$\begin{aligned} w(0) &= \dot{w}(0) = 0, \\ w(l) &= \dot{w}(l) = 0. \end{aligned}$$

We are interested in the initial post-buckling of the strut and so, utilizing a perturbation approach, we write

$$w(x) = sw_1(x) + s^2 w_2(x) + s^3 w_3(x) + \dots$$

where s is some perturbation parameter, as yet unspecified. Thus

$$\dot{w}(x) = s\dot{w}_1(x) + s^2 \dot{w}_2(x) + s^3 \dot{w}_3(x) + \dots$$

etc., and we may also write

$$P = P^C + sP^{(1)} + \frac{1}{2}s^2 P^{(2)} + \dots$$

in which a bracketed superscript on P denotes differentiation with respect to s . The boundary conditions of the problem now become

$$\begin{aligned} w_i(0) &= \dot{w}_i(0) = 0, \\ w_i(l) &= \dot{w}_i(l) = 0, \end{aligned}$$

for all i , and if we now equate the perturbation parameter s to the central deflection of the strut b we obtain

$$b = w\left(\frac{l}{2}\right) = bw_1\left(\frac{l}{2}\right) + b^2 w_2\left(\frac{l}{2}\right) + \dots$$

This equation leads to the further normality conditions

$$w_1\left(\frac{l}{2}\right) = 1,$$

$$w_s\left(\frac{l}{2}\right) = 0 \quad \text{for } s \neq 1,$$

which, because of their role in the analysis, shall be referred to as the 'false' boundary conditions.

If the above expansions are substituted into the Euler equation and this equation is written as a power series in s we see that all coefficients of this power series must equal zero. This will generate an ordered series of differential equilibrium equations which are sequentially linear and are thus readily solved for the functions $w_i(x)$ using the above boundary conditions. We see that the coefficient of s in the power series expansion gives the first-order equilibrium equation

$$\ddot{w}_1 + \frac{P^C}{B}\dot{w}_1 = 0,$$

the complete solution of which can be written as

$$w_1(x) = A_1 \sin \sqrt{\left(\frac{P^C}{B}\right)x} + B_1 \cos \sqrt{\left(\frac{P^C}{B}\right)x} + C_1 x + D_1.$$

The true boundary conditions show that $B_1 = D_1 = 0$, and we find that if

$$\sin \sqrt{\left(\frac{P^C}{B}\right)}l \neq 0$$

we obtain the trivial solution $A_1 = C_1 = 0$. Therefore for a non-trivial solution

$$\sin \sqrt{\left(\frac{P^C}{B}\right)}l = 0$$

and hence $C_1 = 0$. Restricting attention to the first critical load we set

$$\sqrt{\left(\frac{P^C}{B}\right)}l = \pi,$$

giving

$$P^C = \left(\frac{\pi}{l}\right)^2 B$$

which is the well known Euler buckling load. This permits a solution with A_1 indeterminate and so applying now the ‘false’ boundary condition $w_1(l/2) = 1$, we find $A_1 = 1$. Thus the solution of the first-order equilibrium equation is

$$w_1(x) = \sin \frac{\pi x}{l}.$$

The first-order equilibrium equation is of course recognized as that of a conventional linear eigenvalue analysis that one encounters in engineering texts. It is instructive to observe how it arises naturally within a nonlinear perturbation scheme.

We now interrupt the flow of analysis and introduce a general differential equation expressed by

$$\ddot{w}_s + \left(\frac{\pi}{l}\right)^2 \ddot{w}_s = k_s \sin \frac{\pi x}{l} + l_s \sin \frac{3\pi x}{l} + m_s \sin \frac{5\pi x}{l} + \dots$$

with the true boundary conditions

$$\begin{aligned} w_s(0) &= \dot{w}_s(0) = 0, \\ w_s(l) &= \dot{w}_s(l) = 0, \end{aligned}$$

and the ‘false’ boundary condition

$$w_s\left(\frac{l}{2}\right) = 0.$$

The solution of this equation is the sum of the *complementary function*

$$w_s = A_s \sin \frac{\pi x}{l} + B_s \cos \frac{\pi x}{l} + C_s x + D_s$$

and the *particular integral*

$$w_s = K_s x \cos \frac{\pi x}{l} + L_s \sin \frac{3\pi x}{l} + M_s \sin \frac{5\pi x}{l} + \dots,$$

where

$$K_s = \frac{k_s}{2(\pi/l)^3},$$

$$L_s = \frac{l_s}{(\pi/l)^4 (3^4 - 3^2)} = \frac{l_s}{72(\pi/l)^4},$$

$$M_s = \frac{m_s}{(\pi/l)^4 (5^4 - 5^2)} = \frac{m_s}{600(\pi/l)^4}.$$

The true boundary conditions yield

$$B_s = C_s = D_s = 0$$

and ‘suppress the secular term’ by demanding that

$$K_s = k_s = 0.$$

The ‘false’ boundary condition gives

$$A_s - L_s + M_s - \dots = 0$$

and thus fixes the magnitude of A_s as

$$A_s = L_s - M_s + \dots.$$

The general solution of this differential equation can therefore be written as

$$w_s = (L_s - M_s + \dots) \sin \frac{\pi x}{l} + L_s \sin \frac{3\pi x}{l} + M_s \sin \frac{5\pi x}{l} + \dots$$

The suppression of the secular term arises naturally out of the true boundary conditions of the problem and we shall see it plays an important role in the determination of the required path derivatives.

We now return to the perturbation analysis and find that the coefficient of s^2 in the series expansion of the Euler equation gives the second-order equilibrium equation as

$$\ddot{w}_2 + \left(\frac{\pi}{l}\right)^2 \ddot{w}_2 + \frac{P^{(1)}}{B} \ddot{w}_1 = 0,$$

which on substitution for \ddot{w}_1 reduces to

$$\ddot{w}_2 + \left(\frac{\pi}{l}\right)^2 \ddot{w}_2 = k_2 \sin \frac{\pi x}{l},$$

where

$$k_2 = \frac{P^{(1)}}{B} \left(\frac{\pi}{l}\right)^2.$$

This equation is of the general form discussed above with $l_2 = m_2 = \dots = 0$ and so we know its solution. The secular term k_2 is suppressed by the true boundary conditions so

$$P^{(1)} = 0,$$

and the solution is, as we would expect from the symmetrical properties of the strut,

$$w_2(x) = 0.$$

The coefficient of s^3 in the series expansion of the Euler equation now gives the third-order equilibrium equation as

$$\ddot{w}_3 + \left(\frac{\pi}{l}\right)^2 \ddot{w}_3 + \left[\ddot{w}_1 \dot{w}_1^2 + 4\ddot{w}_1 \dot{w}_1 \dot{w}_1 + \dot{w}_1^3 + \frac{3}{2} \left(\frac{\pi}{l}\right)^2 \ddot{w}_1 \dot{w}_1^2 \right] + \frac{\frac{1}{2} P^{(2)}}{B} \ddot{w}_1 = 0,$$

which on substitution for the known derivatives of $w_1(x)$ reduces to

$$\ddot{w}_3 + \left(\frac{\pi}{l}\right)^2 \dot{w}_3 = k_3 \sin \frac{\pi x}{l} + l_3 \sin \frac{3\pi x}{l},$$

where

$$k_3 = \left(\frac{\pi}{l}\right)^2 \left[\frac{\frac{1}{2}P^{(2)}}{B} - \frac{1}{8} \left(\frac{\pi}{l}\right)^4 \right],$$

$$l_3 = -\frac{9}{8} \left(\frac{\pi}{l}\right)^6.$$

This equation is of the general form discussed above with $m_3 = n_3 = \dots = 0$ and so we know its solution. Suppression of the secular term k_3 leads to

$$P^{(2)} = \frac{1}{4}B \left(\frac{\pi}{l}\right)^4,$$

and we can write the solution of the third-order equation as

$$w_3(x) = -\frac{1}{64} \left(\frac{\pi}{l}\right)^2 \left(\sin \frac{\pi x}{l} + \sin \frac{3\pi x}{l} \right).$$

The coefficient of s^4 in the series expansion yields a fourth-order equilibrium equation with the expected results

$$P^{(3)} = 0,$$

$$w_4(x) = 0,$$

and the coefficient of s^5 gives the fifth-order equilibrium equation which may be written in the form

$$\ddot{w}_5 + \left(\frac{\pi}{l}\right)^2 \dot{w}_5 = k_5 \sin \frac{\pi x}{l} + l_5 \sin \frac{3\pi x}{l} + m_5 \sin \frac{5\pi x}{l},$$

where

$$k_5 = \left(\frac{\pi}{l}\right)^2 \left[\frac{\frac{1}{24}P^{(4)}}{B} - \frac{19}{512} \left(\frac{\pi}{l}\right)^6 \right].$$

Again this is of the general form discussed above but with $n_5 = \dots = 0$ and we see that the suppression of the secular term gives

$$P^{(4)} = \frac{57}{64}B \left(\frac{\pi}{l}\right)^6.$$

This is the stage at which we leave the analysis, the solution of the fifth-order equation not being pursued. We note that the fourth-order path derivative arises *directly* from the suppression of the secular term in this equation without demanding its solution.

General theory for discrete systems

The two discrete analyses which follow are best developed in terms of the general theory of elastic stability as presented in the main body of the book. Consequently we shall now introduce as much general theory as we need for this particular problem. Let us therefore consider a conservative structural system described by the total potential energy function $V(Q_i, \Lambda)$, where Q_i represents a set of n generalized coordinates and Λ is a loading parameter, and suppose that in the region of interest the n equilibrium equations $V_i = 0$ yield a single-valued *fundamental* solution $Q_i = Q_i^F(\Lambda)$. Here a subscript on V denotes partial differentiation with respect to the corresponding generalized coordinate. A *sliding* set of incremental coordinates q_i is then defined by the n equations

$$Q_i = Q_i^F(\Lambda) + q_i$$

and we introduce the new energy function

$$W(q_i, \Lambda) \equiv V[Q_i^F(\Lambda) + q_i, \Lambda].$$

The normal equilibrium and stability conditions hold good for this transformed energy function which has the properties

$$W_i(0, \Lambda) = 0,$$

$$W'_i(0, \Lambda) = 0,$$

$$W''_i(0, \Lambda) = 0,$$

etc., a subscript again denoting partial differentiation with respect to the corresponding generalized coordinate and a prime denoting partial differentiation with respect to Λ . We see that we have a valid mapping from the original $\Lambda-Q_i$ space to the new $\Lambda-q_i$ space in which the fundamental equilibrium path is given by $q_i = 0$.

We suppose now that a distinct critical point C lies on the fundamental path at $\Lambda = \Lambda^C$, the determinant of W_{ij} vanishing at this point so that we can write

$$|W_{ij}(0, \Lambda^C)| = 0.$$

We now seek to express any *post-buckling* equilibrium path emerging from this critical equilibrium state in the parametric form

$$q_j = q_j(q_1), \quad \Lambda = \Lambda(q_1),$$

assuming without any essential loss of generality that the *first* generalized coordinate is a suitable expansion parameter. Here as elsewhere in this analysis it is convenient to write q_1 as $q_1(q_1)$.

These parametric equations can be substituted into the equilibrium equations $W_i = 0$ to give the identity

$$W_i[q_j(q_1), \Lambda(q_1)] \equiv 0.$$

Here the left-hand side is simply a function of the independent variable q_1 , so we can differentiate the equations with respect to q_1 as many times as we please. Thus, differentiating repeatedly, we can generate the ordered equilibrium equations

$$W_{ij}q_j^{(1)} + W'_i\Lambda^{(1)} = 0,$$

$$(W_{ijk}q_k^{(1)} + W'_{ij}\Lambda^{(1)})q_j^{(1)} + W_{ij}q_j^{(2)} + (W'_{ij}q_j^{(1)} + W''_i\Lambda^{(1)})\Lambda^{(1)} + W'_i\Lambda^{(2)} = 0,$$

etc. Here a bracketed superscript denotes differentiation with respect to q_1 , and we must remember that

$$q_1^{(1)} \equiv \frac{dq_1}{dq_1} = 1,$$

$$q_1^{(2)} \equiv \frac{d^2 q_1}{dq_1^2} = 0,$$

etc. The dummy-suffix summation convention is employed with all summations ranging from 1 to n .

If we evaluate the equilibrium equations at the critical point C where $q_i = 0$, $\Lambda = \Lambda^C$ and $W_i = W'_i = W''_i = \dots = 0$, we have

$$W_{ij}q_j^{(1)}|^C = 0,$$

$$W_{ijk}q_j^{(1)}q_k^{(1)} + 2W'_{ij}q_j^{(1)}\Lambda^{(1)} + W_{ij}q_j^{(2)}|^C = 0,$$

etc. Since $q_1^{(1)} = 1$ we can solve the first equation for the rates $q_j^{(1)C}$. We now introduce the ‘contraction’ mechanism in which the i th equation of the second order is multiplied by $q_i^{(1)C}$ and the set of equations is added. The final term vanishes by virtue of the first equation and we obtain

$$\Lambda^{(1)C} = -\frac{W_{ijk}q_i^{(1)}q_j^{(1)}q_k^{(1)}}{2W'_{ij}q_i^{(1)}q_j^{(1)}}|^C.$$

Here we have assumed the critical point to be *simple* in the sense that $W'_{ij}q_i^{(1)}q_j^{(1)}|^C$ which clearly plays a key role in the analysis is non-zero. Since $q_1^{(2)} = 0$ we can now substitute for $q_j^{(1)C}$ and $\Lambda^{(1)C}$ into the second-order equations and solve for the further path derivatives $q_j^{(2)C}$. Clearly we can continue this ordered perturbation scheme as far as necessary.

Harmonic analysis

We perform now a harmonic analysis of the strut, writing the change in deflection from the purely trivial fundamental path as

$$w(x) = \sum_i^\infty u_i \sin \frac{i\pi x}{l},$$

the incremental generalized coordinates being here written as u_i , rather than q_i , in anticipation of the fact that the Fourier harmonics represent the buckling modes of the problem. Substituting this into the energy functional and expanding about the unloaded state gives us an algebraic energy function of the form

$$V = W = U - P\mathcal{E}$$

$$= \frac{1}{2}U_{ij}(0)u_i u_j + \frac{1}{24}U_{iklm}(0)u_i u_j u_k u_m + \dots$$

$$- P[\frac{1}{2}\mathcal{E}_{ij}(0)u_i u_j + \frac{1}{24}\mathcal{E}_{iklm}(0)u_i u_j u_k u_m + \dots],$$

where

$$U_{ij}(0) = 0 \quad \text{for } i \neq j,$$

$$U_{ii}(0) = \frac{Bl}{2} \left(\frac{i\pi}{l}\right)^4,$$

$$\mathcal{E}_{ij}(0) = 0 \quad \text{for } i \neq j,$$

$$\mathcal{E}_{ii}(0) = \frac{l}{2} \left(\frac{i\pi}{l}\right)^2,$$

$$U_{iklm}(0)u_i u_j u_k u_m = 12B \left(\frac{\pi}{l}\right)^6 \sum_i \sum_j \sum_k \sum_m i^2 j^2 k m u_i u_j u_k u_m \int_0^l \sin \frac{i\pi x}{l}$$

$$\times \sin \frac{j\pi x}{l} \cos \frac{k\pi x}{l} \cos \frac{m\pi x}{l} dx,$$

$$\mathcal{E}_{iklm}(0) = 3ijkm \left(\frac{\pi}{l}\right)^4 \int_0^l \cos \frac{i\pi x}{l} \cos \frac{j\pi x}{l} \cos \frac{k\pi x}{l} \cos \frac{m\pi x}{l} dx,$$

$$U_{ijklmn}(0)u_i u_j u_k u_m u_n u_o = 360B \left(\frac{\pi}{l}\right)^8 \sum_i \sum_j \sum_k \sum_m \sum_n \sum_o i^2 j^2 k m n o$$

$$\times u_i u_j u_k u_m u_n u_o \int_0^l \sin \frac{i\pi x}{l} \sin \frac{j\pi x}{l} \cos \frac{k\pi x}{l}$$

$$\times \cos \frac{m\pi x}{l} \cos \frac{n\pi x}{l} \cos \frac{o\pi x}{l} dx,$$

$$\mathcal{E}_{ijklmn}(0) = 45 \left(\frac{\pi}{l}\right)^6 ijkmno \int_0^l \cos \frac{i\pi x}{l} \cos \frac{j\pi x}{l} \cos \frac{k\pi x}{l}$$

$$\times \cos \frac{m\pi x}{l} \cos \frac{n\pi x}{l} \cos \frac{o\pi x}{l} dx,$$

etc. Here it has been necessary to include summations in the equalities associated with U_{ijkm} and U_{ijkmno} since the U derivatives are necessarily symmetric while the integrals are not: this fact presents no real difficulty, although some care must naturally be exercised.

We see that both U_{ij} and \mathcal{E}_{ij} are diagonal forms, the Fourier harmonics thus representing the buckling modes of the strut, while the first critical load is given by

$$P^C = \frac{U_{11}(0)}{\mathcal{E}_{11}(0)} = B \left(\frac{\pi}{l} \right)^2.$$

Expanding now about the critical equilibrium state $(0, P^C)$ we have

$$\begin{aligned} W &= \frac{1}{2}(U_{ii} - P^C \mathcal{E}_{ii}) u_i^2 + \frac{1}{24}(U_{ijkm} - P^C \mathcal{E}_{ijkm}) u_i u_j u_k u_m + \dots \\ &\quad - p[\frac{1}{2}\mathcal{E}_{ii} u_i^2 + \frac{1}{24}\mathcal{E}_{ijkm} u_i u_j u_k u_m + \dots], \end{aligned}$$

where $p = P - P^C$, so we can write the required W derivatives as

$$W_{ij}^C = U_{ij}(0) - P^C \mathcal{E}_{ij}(0) = 0 \quad \text{for } i \neq j,$$

$$W_{11}^C = U_{11}(0) - P^C \mathcal{E}_{11}(0) = 0,$$

$$W_{ss}^C = U_{ss}(0) - P^C \mathcal{E}_{ss}(0) = \frac{Bl}{2} \left(\frac{\pi}{l} \right)^4 s^2(s^2 - 1) \quad \text{for } s \neq 1,$$

$$W'_{ij}^C = -\mathcal{E}_{ij}(0) = 0 \quad \text{for } i \neq j,$$

$$W'_{11}^C = -\mathcal{E}_{11}(0) = -\frac{l}{2} \left(\frac{\pi}{l} \right)^2,$$

$$W_{1111}^C = \frac{3}{8} Bl \left(\frac{\pi}{l} \right)^6,$$

$$W_{s111}^C = 0 \quad \text{for } s \neq 3,$$

$$W_{3111}^C = \frac{27}{8} Bl \left(\frac{\pi}{l} \right)^6,$$

$$W'_{1111}^C = -\frac{9}{8} l \left(\frac{\pi}{l} \right)^4,$$

$$W_{111111}^C = \frac{135}{16} Bl \left(\frac{\pi}{l} \right)^8.$$

Substituting these into the general perturbation scheme, the diagonal nature of W_{ij}^C renders the linear equations trivial and the solutions can immediately be written

$$u_s^{(1)C} = P^{(1)C} = u_s^{(2)C} = 0,$$

$$P^{(2)C} = \frac{B}{4} \left(\frac{\pi}{l} \right)^4,$$

$$u_s^{(3)C} = 0 \quad \text{for } s \neq 3,$$

$$u_3^{(3)C} = -\frac{3}{32} \left(\frac{\pi}{l} \right)^2,$$

$$P^{(3)C} = u_s^{(4)C} = 0,$$

$$P^{(4)C} = \frac{63}{64} B \left(\frac{\pi}{l} \right)^6.$$

We see that we have

$$u_s(u_1) = \frac{1}{6} u_s^{(3)} u_1^3 + \text{order } u_1^5$$

so the central deflection b can be written as

$$\begin{aligned} b &= w \left(\frac{l}{2} \right) = u_1 - u_3 + u_5 - u_7 + \dots \\ &= u_1 - \frac{1}{6} u_3^{(3)} u_1^3 + \text{order } u_1^5, \end{aligned}$$

and inverting this series we have

$$u_1 = b + \frac{1}{6} u_3^{(3)} b^3 + \text{order } b^5.$$

Thus writing

$$P(b) = P[u_1(b)]$$

so that

$$\frac{dP}{db} = P^{(1)} \frac{du_1}{db},$$

$$\frac{d^2 P}{db^2} = P^{(2)} \left(\frac{du_1}{db} \right)^2 + P^{(1)} \frac{d^2 u_1}{db^2},$$

etc., we can obtain the post-buckling derivatives of P with respect to the central deflection b as

$$\begin{aligned}\frac{dP}{db}^C &= 0, \\ \frac{d^2P}{db^2}^C &= P^{(2)C} = \frac{B}{4} \left(\frac{\pi}{l}\right)^4, \\ \frac{d^3P}{db^3}^C &= 0, \\ \frac{d^4P}{db^4}^C &= P^{(4)C} + 4P^{(2)C} u_3^{(3)C} = \frac{57}{64} B \left(\frac{\pi}{l}\right)^6.\end{aligned}$$

Finite-element analysis

As an illustration of the non-diagonalized perturbation scheme we shall now analyse the strut using the kinematically-admissible finite-element procedure, utilizing the physical symmetry of the post-buckled form by adopting twice the energy of the half-strut as the complete energy expression.

The energy functional for the strut has already been derived, so it remains to fabricate a kinematically-admissible form for the *mathematical function* $w(x)$ which we might note does not represent the *physical shape* of the strut if it is simply plotted in rectangular coordinates. Thus considering the function $w(x)$ with x ranging from 0 to l we divide the x -domain into n equal 'elements' by introducing $n+1$ equally spaced stations along the axis, one station being at the mid-point. Each internal station is given an arbitrary displacement w and an arbitrary first derivative \dot{w} , while in accordance with the boundary conditions of the problem the terminal stations are given an arbitrary first derivative but no displacement. The totality of the arbitrary displacements and first derivatives represent the generalized coordinates of the strut and are denoted by Q_i , the assumed symmetry reducing the number of independent coordinates to n . The ordering of these n independent coordinates is shown in Figure 19 for the right-hand half of the strut.

A third-order polynomial is now fitted in each region giving an overall deflection, which is continuous in displacement and first derivative but which admits discontinuities in its second derivative at the stations. Considering the general h th region with its local independent variable \bar{x} (Figure 19) this third-order polynomial is

$$\begin{aligned}w^h &= Q_{2h-2} \left[\bar{x} - 2\left(\frac{n}{l}\right) \bar{x}^2 + \left(\frac{n}{l}\right)^2 \bar{x}^3 \right] + Q_{2h-1} \left[1 - 3\left(\frac{n}{l}\right)^2 \bar{x}^2 + 2\left(\frac{n}{l}\right)^3 \bar{x}^3 \right] \\ &\quad + Q_{2h} \left[-\left(\frac{n}{l}\right) \bar{x}^2 + \left(\frac{n}{l}\right)^2 \bar{x}^3 \right] + Q_{2h+1} \left[3\left(\frac{n}{l}\right)^2 \bar{x}^2 - 2\left(\frac{n}{l}\right)^3 \bar{x}^3 \right],\end{aligned}$$

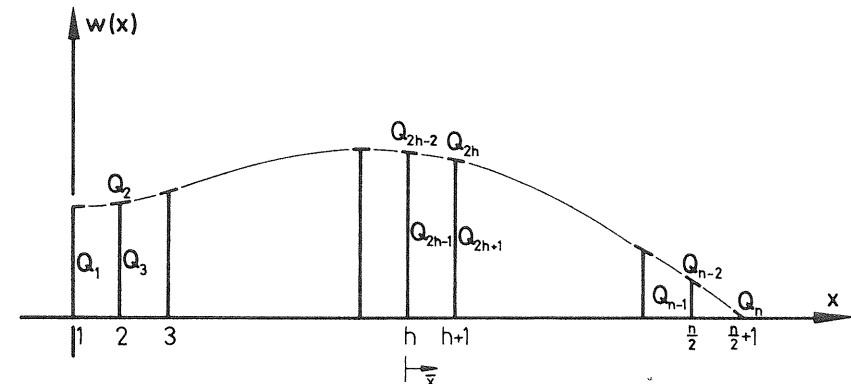


Figure 19 The finite-element fabrication of the mathematical function $w(x)$

which after substitution into the energy functional for the region,

$$\begin{aligned}V^h &= \frac{1}{2} B \int_0^{l/n} [(\ddot{w}^h)^2 + (\dot{w}^h)^2 (\dot{w}^h)^2 + (\dot{w}^h)^2 (\ddot{w}^h)^4 + \dots] d\bar{x} \\ &\quad - P \int_0^{l/n} [\frac{1}{2}(\dot{w}^h)^2 + \frac{1}{8}(\dot{w}^h)^4 + \frac{1}{16}(\dot{w}^h)^6 + \dots] d\bar{x},\end{aligned}$$

gives V^h in terms of the generalized coordinates bounding the region. The complete energy functional for the strut may now be obtained from the equation

$$V = 2 \sum_{h=1}^{n/2} V^h,$$

the summation ranging over the half-strut of Figure 19.

In this way we obtain an algebraic energy function with the form of the expansion about the unloaded state of the harmonic analysis; the quadratic forms associated with U_{ij} and \mathcal{E}_{ij} are now, however, not diagonal. As with the harmonic analysis, care must be taken to obtain the energy coefficients in a symmetrical form.

Before we may utilize the general perturbation scheme it is necessary to evaluate the first critical load of the finite-element model. The fundamental equilibrium path is known to be trivial and we may thus calculate the critical load from the energy requirement

$$|W_{ij}^C| = |U_{ij}(0) - P^C \mathcal{E}_{ij}(0)| = 0.$$

Thus using a computer and varying the loading parameter systematically until the determinant approaches zero, the value of P^C can readily be found.

The sliding transformation of the general theory being here trivial so that $V = W$ and $Q_i = q_i$ we can now proceed with the general perturbation scheme

taking the central deflection q_1 as the independent path parameter and solving the sequence of linear problems on a computer. The first linear problem of the general theory is

$$W_{ij} q_j^{(1)C} = 0$$

and this was solved, not by treating it as an eigenvalue problem, but by simply noting that the identity $q_1^{(1)} = 1$ allows it to be rewritten as

$$W_{is}^C q_s^{(1)C} = -W_{i1}^C \quad (s \neq 1).$$

Here we have n equations in $n - 1$ unknowns and simply disregarding one of the equations the remaining non-singular set was solved on the computer by matrix inversion and multiplication.

The second-order equations before and after contraction yield the expected results

$$P^{(1)C} = q_j^{(2)C} = 0,$$

and in the light of the known derivatives the third contracted equation becomes

$$P^{(2)C} = -\frac{W_{ijkl} q_i^{(1)} q_j^{(1)} q_k^{(1)} q_l^{(1)}}{3 W'_{ij} q_i^{(1)} q_j^{(1)}} \Big|_C,$$

giving the first post-buckling derivative of interest.

Continuing the perturbation scheme the third-order equilibrium equation can now be written as

$$W_{ij} q_j^{(3)C} = -W_{ijkl} q_i^{(1)} q_j^{(1)} q_k^{(1)} q_l^{(1)} - 3 W'_{ij} q_i^{(1)} P^{(2)C} \Big|_C$$

and remembering that $q_1^{(3)C} = 0$ we see that we have a set of n equations in $n - 1$ unknowns. Thus disregarding the same equation as before, we see that the required matrix has already been inverted so the derivatives $q_s^{(3)C}$ are directly obtained by matrix multiplication. We can note at this point that summations and matrix multiplications are now the only operations required in a continued perturbation scheme of this kind.

The fourth-order equations before and after contraction yield the expected results

$$P^{(3)C} = q_j^{(4)C} = 0,$$

while the fifth contracted equation may be reduced to the form

$$\begin{aligned} P^{(4)C} = & -\frac{1}{5 W'_{ij} q_i^{(1)} q_j^{(1)}} [W_{ijklmn} q_i^{(1)} q_j^{(1)} q_k^{(1)} q_l^{(1)} q_m^{(1)} q_n^{(1)} + 10 W_{ijkl} q_i^{(1)} q_j^{(1)} q_k^{(1)} q_l^{(1)} q^{(3)} \\ & + 10 W'_{ijkl} q_i^{(1)} q_j^{(1)} q_k^{(1)} q_l^{(1)} P^{(2)C} + 10 W'_{ij} q_i^{(1)} q_j^{(3)} P^{(2)C}] \Big|_C, \end{aligned}$$

giving after the required summations the second load derivative of interest $P^{(4)C}$.

This finite-element analysis to determine, P^C , $P^{(2)C}$ and $P^{(4)C}$ has been repeated for values of n , which is both the number of independent generalized coordinates Q_i and the number of elements in the *whole* strut, equal to two,

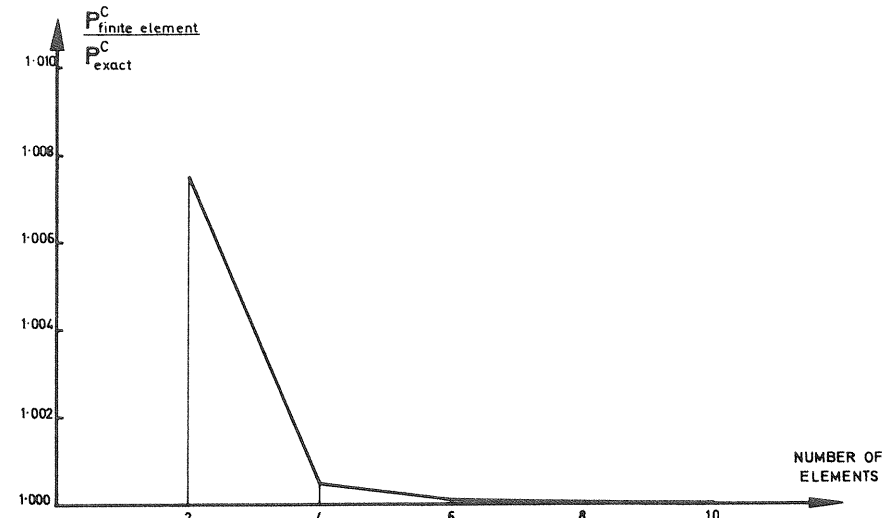


Figure 20 Convergence of the finite-element critical load

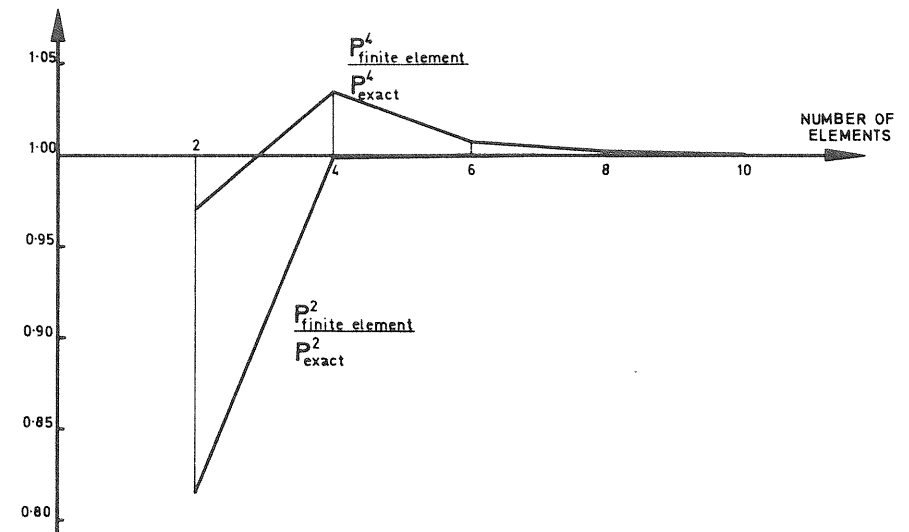


Figure 21 Convergence of the first two finite-element path derivatives

four, six, eight and ten. The answers were found to converge rapidly with increasing n to the known exact values and this convergence is shown in Figures 20 and 21.

Post-buckling solution

The continuum analysis has given us exact closed form solutions for the critical load P^c and the two post-buckling load derivatives $P^{(2)c}$ and $P^{(4)c}$. These are confirmed by the harmonic analysis which also gives closed form solutions due to the truncation of various series by certain orthogonality conditions related to the form of the continuum solution. The numerical finite-element analysis gives approximate values for these quantities which have been seen to converge rapidly to the exact values as the number of elements is increased.

The exact post-buckling derivatives can be used to construct the post-buckling equilibrium path of the strut by truncations of the series

$$P = P^c + \frac{1}{2}P^{(2)c}b^2 + \frac{1}{24}P^{(4)c}b^4 + \dots$$

and the solutions obtained are shown in Figure 22 together with the complete solution presented by Timoshenko and Gere.¹⁹⁹ The solution using only

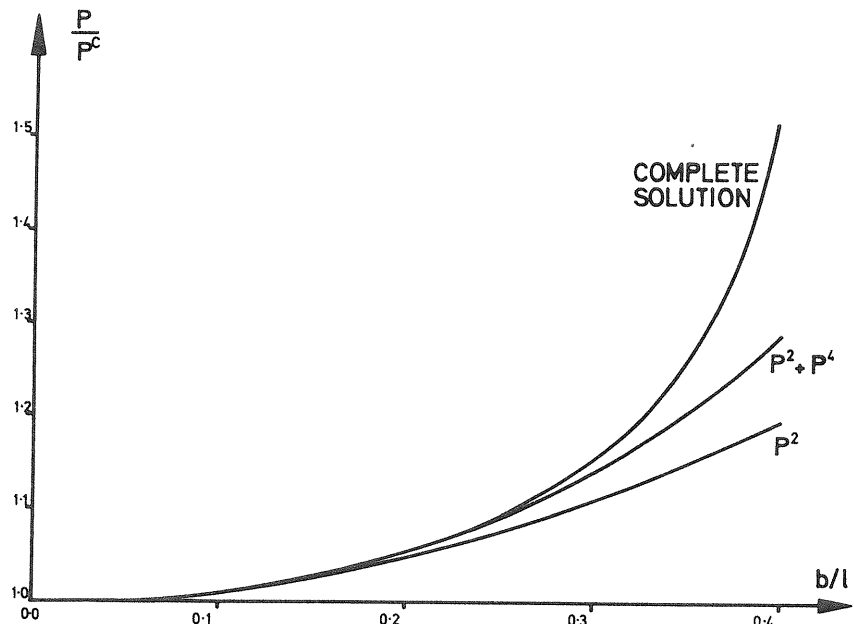


Figure 22 The complete and perturbation solutions for the post-buckling path

$P^{(2)c}$ is seen to represent a good approximation to the complete solution for values of b/l up to about 0.2, while the solution using $P^{(2)c}$ and $P^{(4)c}$ is seen to represent a good approximation for values of b/l up to about 0.3.

It is observed that the suppression of secular terms in the continuum theory plays precisely the same role as the contraction of the equilibrium equations in the discrete theory.

2

GENERAL INTRODUCTION

2.1 Introduction

The concept of the stability of equilibrium is a strongly intuitive one, and it consequently arises quite early in the development of classical mechanics. The work of Euler¹ appeared in 1744, and the contribution of Lagrange² in 1788. A century later a general bifurcation theory was sketched by Poincaré³ in 1885, and the definition of stability was given mathematical rigour in the treatise of Liapunov⁴ in 1892.

A nonlinear bifurcation theory for continuous elastic systems was presented by Koiter⁵ in 1945, and this has recently been further developed both by Koiter⁶⁻²² and by Budiansky and Hutchinson and their associates at Harvard.²³⁻⁴⁸ This development has been stimulated by shell-buckling problems of structural engineering, and has been linked with the rigorous formulation of adequate shell equations. Significant linear studies of conservative and non-conservative systems were made by Ziegler^{49, 50} in 1956 and more recently by Herrmann and his colleagues.⁵¹

A new line of study in the general nonlinear theory of elastic stability was initiated by Thompson in 1963 in terms of generalized coordinates,⁵² and this has been extensively developed at University College London.⁵³⁻¹³⁶ This activity forms an essential back-cloth to the present monograph, and will now be briefly reviewed.

The first significant contribution was that of Roorda, who examined the distinct branching points of elastic stability in general terms. His work included a careful experimental study of the bifurcation properties of frames, following Britvec and Chilver, which supplied the first experimental verification of Koiter's general conclusions. A general perturbation theory was subsequently developed, and a comprehensive review article embracing the four well known distinct critical points was published in 1969.¹⁰⁵

Interest turned next to the approach and coalescence of branching points, and Chilver showed that in the presence of nearly-coincident critical loads, post-buckling equilibrium paths can exhibit violent contortions, which however vanish when complete coincidence is achieved.⁷⁰ Branching analyses associated with nearly-coincident critical loads will thus experience severe difficulties which can perhaps be overcome by an analytical 'rudge' to sense

complete simultaneity. Supple focused attention on near-coincidence in symmetric systems, and showed that secondary branching from a primary post-buckling path can arise. This phenomenon can explain changes in the buckling modes of structures, and in particular the dynamic changes in waveform of compressed plates.¹¹⁶

More recent studies of completely simultaneous buckling by Chilver and Johns have enumerated the many post-buckling paths which can be generated at a compound branching point, and a corresponding perturbation theory employing a systematic elimination of passive coordinates has been presented by Thompson and Hunt both with and without a scheme of diagonalization. The great complexity of behaviour implied by these many paths may have a profound influence on the development of the subject of structural stability, and may necessitate a more experimental approach to stability problems.

The above stream of activity follows the classical assumptions that loading can be described by a single parameter, that all deflections are admissible and that the structures remain integral under load. Such assumptions occasionally break down, and a complementary stream of non-classical studies was also pursued at University College. Here we might mention the extensive work of Huseyin on problems of multiple loading, the work of Burgess on one-way buckling phenomena, and the recent studies of Hayman¹¹¹ on the behaviour of degenerating structures, such as heavily-cracked cooling towers. The early study of frames has been extended by Godley and Chilver, and some general statistical studies have been made.

A significant feature in the development of the general theory was the demonstration by Thompson and Walker¹⁰² that the perturbation branching studies could be developed without resort to a scheme of diagonalization, and this served to give the theory greater elegance and invariance. Of more importance, however, was the fact that the new theory could be used most advantageously with the kinematically-admissible finite-element procedure as a method of post-buckling analysis. This has been actively pursued by Walker and others,^{104, 106, et al.} the applications including structures with irregular geometry and loading which could not be treated by closed-form methods.

The relative merits of the finite-element and finite-difference approaches for the solution of practical structural problems have been examined by Croll and Walker, and a most useful unification of outlook was achieved.^{93, 109} This showed the finite-element and finite-difference methods to be but two examples of more general numerical procedures, and offered a basis for a comparison of their accuracy and convergence properties. For use in finite-difference studies, numerical solution algorithms based on the differential equations of equilibrium and compatibility have been developed by Croll for perturbation analyses about either normal or critical equilibrium states, in parallel with the methods developed for the finite-element procedure.

This activity at University College has proceeded in parallel with the fine

studies of Sewell at the University of Reading,^{137–141} and we are pleased to acknowledge our indebtedness to these articles for many fruitful ideas.

The core of the University College work is a systematic and complete elaboration of Poincaré's ideas for a general mechanical system described by a set of n generalized coordinates, and this forms the material of the present monograph.

The need for such a treatise is two-fold. On the one hand, the general theory can often be more fully and rigorously developed than the corresponding continuum theory, and so plays a significant and heuristic role in the formulation of new ideas and concepts. This has been the case with Ziegler's linear studies, and is emphasized by the continuing interest in general discrete theories typified for example by the constant repetition in hydrodynamic texts^{142, 143} of the now rather out-dated work of Poincaré.

On the other hand, the analytical value of the discrete coordinate general theory, which has been clearly established both by the University College activity and by recent papers in the United States (see, for example, reference 144), will become increasingly important in the field of practical engineering structures. Here the continuing trend towards lighter and thinner structures associated with the use of high-strength materials is bringing problems of elastic stability increasingly to the fore. This has long been the case in the aerospace field, but it is now rapidly extending to ships and to civil engineering structures such as bridges and high-rise buildings.

Thus elastic instability is now a subject of prime concern to all structural engineers, and as designs become even more efficient the engineer will be faced with ever more severe and complex instabilities demanding the sophisticated treatments presented in this book. This is because an optimum design is by its very nature prone to instability. Thus if a small perturbation carries an optimum structure into an adjacent, and therefore non-optimal, configuration the structure will be unable to sustain its load and failure will occur. A perfect spherical shell is for example an ideal shape for resisting uniform external pressure, but it exhibits an extreme sensitivity to initial imperfections and small dynamic disturbances.

The shallow elastic arch of Figure 43 is a further example. Here to support a central load a symmetric arch is clearly an optimum solution. Any deviation from symmetry, represented for simplicity in the tests by a small offset of the load, results in a dramatic reduction in load-carrying capacity as shown in the figure. In this context it is interesting to observe that the *addition* of material to one side of a symmetric arch of this type will cause a *lowering* of the failure load.

A further feature of structural optimization is that it often calls for simultaneity of various failure loads of the system, and a recent study of this by Thompson and Lewis is presented in Chapters 12 and 13. Here the simple optimization of a thin-walled column is shown to demand the coincidence of

local and overall buckling loads which Van der Neut has shown¹⁴⁵ will give rise to highly unstable post-buckling behaviour despite the fact that the two uncoupled modes of buckling are themselves quite stable in the post-buckling range.

The later chapters of this monograph concerning the nonlinear coupling which arises in problems of simultaneous buckling will thus take on a special relevance in design problems of this type, and in the last chapter we have presented some discussion of the impact of this coupling phenomenon on the important problem of structural optimization.

2.2 Structural System

We consider in this monograph a general conservative structural system, by which we mean the simple dynamical system of Synge and Griffith,¹⁴⁶ described by the total potential energy function $V(Q_i, \Lambda)$ where Q_i represents a set of n generalized coordinates and Λ is a loading parameter. The work thus represents a contribution to the classical mechanics of discrete finite systems, although its most significant applications lie in conservative problems of nonlinear continuum elasticity. In this continuum field the theory is immediately valid for the discrete analytical systems generated in many practical studies by a *finite* and therefore approximate modal analysis, whether the mode-forms be continuous as in early Rayleigh–Ritz analyses, or localized and discontinuous as in the kinematically-admissible finite-element procedure (Fraeijs de Veubeke,¹⁴⁷ Thompson⁷⁷). Numerous applications indicate that the theory remains valid for the discrete systems generated in classical continuum studies by an *infinite* modal analysis associated with a complete set of functions.

Bearing in mind these two fields of application, the essential features of the work are developed in two complementary forms which together yield a deep insight into the structure of the general theory. Thus on the one hand the theory is presented using only the basic generalized coordinates without resort to a scheme of diagonalization, this development possessing a high degree of invariance and being readily applicable to the approximate finite analyses. On the other hand use is made of a set of principal coordinates generated by a scheme of diagonalization, and this development of the general theory yields explicit solutions which can be directly employed in many classical studies. The finite-element and harmonic analyses of the Euler strut presented in Chapter 1 are examples from these two fields of application, and more will be encountered later in the monograph.

As indicated, the total potential energy of the general theory is taken to be a function both of the generalized coordinates and of the distinct algebraic variable Λ , the equilibrium and stability of the system being discussed at different but constant values of this variable. Thus in specific applications this

loading parameter Λ can be equated to any controlled variable appearing in the energy function whose influence on the system we wish to discuss. Often Λ will be associated with the magnitude of prescribed forces acting on a system, but it might equally be identified as a mass, a dimension or an elastic modulus or as the magnitude of a prescribed displacement independent of the generalized coordinates.^{54, 148}

In many problems of practical interest the total potential energy will be a linear function of the chosen loading parameter, and since the class of systems for which this linearity holds exhibits some distinctive characteristics, it is treated in some detail as a specialization of the more general class previously discussed. In this treatment we shall, for purely semantic reasons, replace A by P and then write $V(Q_i, P) = U(Q_i) - P\mathcal{E}(Q_i)$, where P can be regarded as the magnitude of a generalized force acting through the generalized displacement $\mathcal{E}(Q_i)$.

For the general structural system described by the total potential energy function $V(Q_i, \Lambda)$ we shall be concerned with its statical equilibrium and its stability in the dynamical sense of Liapunov,⁴ and to make the work self-contained we start by introducing two basic axioms. The first states that a stationary value of the energy with respect to the coordinates is necessary and sufficient for the equilibrium of the system, while the second axiom states that a complete relative minimum of the energy is necessary and sufficient for the stability of an equilibrium state. The acceptability of these two axioms is discussed in Chapter 3 where the formal delineation of our structural system can also be found.

Associating the basic variables Q_i and Λ with rectangular axes in an $n + 1$ -dimensional Euclidean space we see that the n equilibrium equations specifying a stationary value of V with respect to the Q_i will define a series of equilibrium paths in this space, and it is the form and stability of these paths that will concern us in the present monograph. In particular we shall be interested in the initial loss of stability of a structural system as it is 'loaded' with increasing Λ from an initial stable equilibrium state which without any loss of generality we can take to be the origin $Q_i = \Lambda = 0$.

2.3 Some basic phenomena

Since both are related in a simple fashion to the form of the total potential energy, it is clear that there will be a close relationship between the equilibrium configurations and the stability of the system, and this has already been observed in the examples of Chapter 1. There we were introduced to four common modes of instability associated with *distinct* critical points (that is to say critical points characterized by the vanishing of only a single stability coefficient) and we shall now have a look at these four critical points in more general terms. They are shown schematically in Figures 23 to 27, where heavy

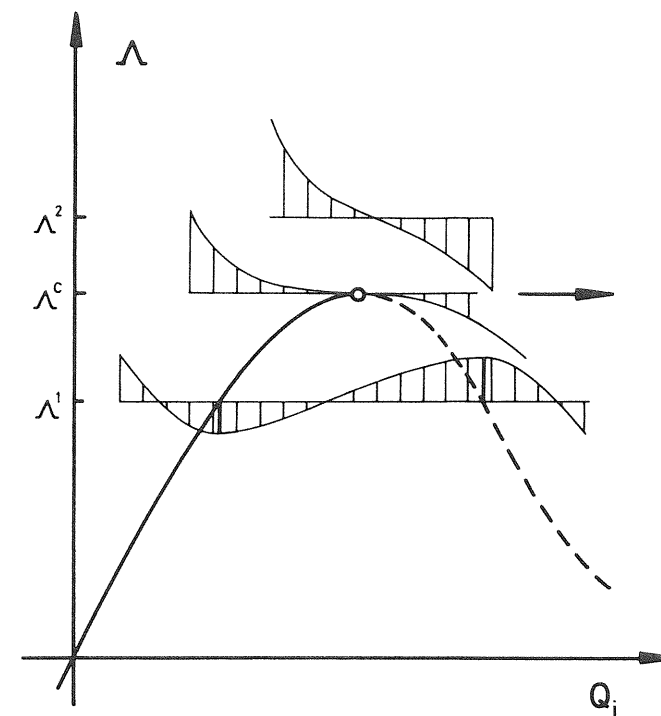


Figure 23 Energy transformation in the limit point

lines represent equilibrium paths, continuous lines denoting stable paths while broken lines denote unstable paths. Plots of the total potential energy at various prescribed values of A are shown in light lines.

Figure 23 shows the *limit point* and here the initially stable equilibrium path from the origin loses its stability on reaching the locally maximum value of the loading parameter Λ^c . This point arises in the mathematical treatment as the ‘most general’ stability phenomenon, and it is well-known to structural engineers in the response of shallow arches and domes. At a prescribed value of $\Lambda = \Lambda^1$ less than Λ^c the total potential energy $V(Q_t, \Lambda^1)$ has a minimum with respect to Q_t on the stable rising region of the path and a maximum on the unstable falling region. As the prescribed value of Λ is increased the maximum and minimum coalesce so that at $\Lambda = \Lambda^c$ the total potential energy $V(Q_t, \Lambda^c)$ has a horizontal point of inflexion at the critical equilibrium state. At the higher value of $\Lambda = \Lambda^2$ there are no local equilibrium states and the total potential energy $V(Q_t, \Lambda^2)$ has no local stationary point as shown. The critical equilibrium state is seen to be itself unstable, and the absence of local equilibrium states at values of Λ greater than Λ^c implies that a physical system under slowly

increasing Λ must snap dynamically from our field of vision as indicated by the heavy arrow.

The characteristics of the limit point have been illustrated schematically in two dimensions in Figure 23 on a plot of Λ against one of the Q_i and a more general schematic diagram is shown in three dimensions in Figure 24 on a plot

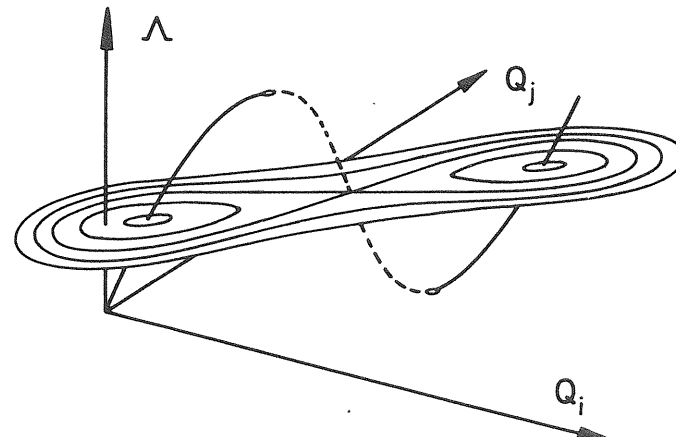


Figure 24 Energy contours in the limit point

of Λ against two of the Q_i . Here a remote rising region of the equilibrium path has been added since this is a feature often encountered with this type of phenomenon. Contours of equal total potential energy are drawn for a prescribed value of Λ less than the critical value. As Λ is increased through its critical value we see that for such a system the dynamic snap will initiate a large amplitude (nonlinear) vibration about the remote stable equilibrium path: and in the presence of some damping the system will eventually come to rest on this path.

These two figures yield considerable insight into the limiting phenomenon, but it must be remembered that we are dealing with a system with n degrees of freedom and care must be taken in drawing conclusions from these *schematic* figures. On an *actual* plot of Λ against one of the Q_i the limit point is for example *normally* seen as a smooth maximum, but it must be realized that for a *certain* choice of the coordinate Q_i the point *might* appear as a sharp cusp. The smooth maximum of a path in three-dimensional space can for example be seen as a cusp if the eye is directed along the horizontal tangent to the path. For the specialized (Q_i, P) system the limit point will however be seen as a smooth maximum on a plot of the generalized force P against its corresponding deflection $\mathcal{E}(Q_i)$ as shown in Figure 28.

After the limit point we come to the points of bifurcation, called synonymously bifurcation points or branching points, and the *asymmetric point of*

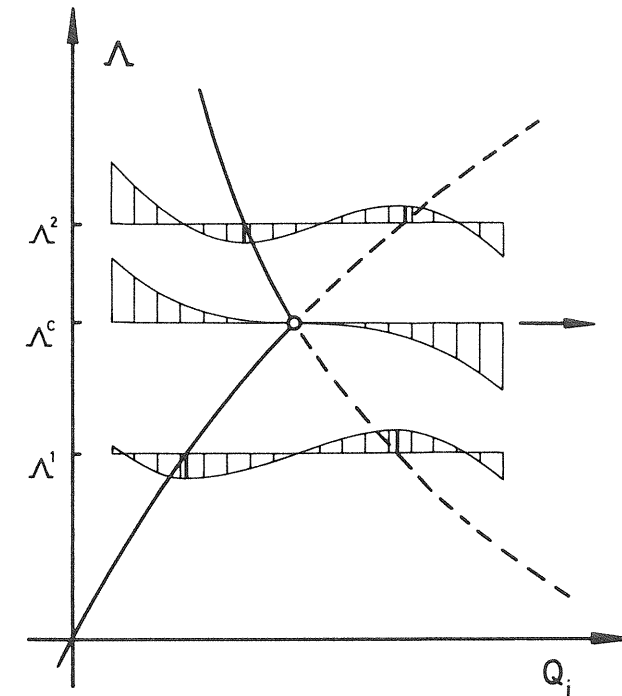


Figure 25 Energy transformation in the asymmetric point of bifurcation

bifurcation is shown schematically in Figure 25. Here the initially stable *fundamental* equilibrium path from the origin loses its stability on intersecting a distinct and continuous *post-buckling* equilibrium path. Both paths have a non-zero slope at the critical point, and with varying Λ the paths exhibit the *exchange of stability* discussed by Poincaré in 1885. For $\Lambda^1 < \Lambda^c$ the total potential energy $V(Q_i, \Lambda^1)$ has a minimum with respect to Q_i on the stable region of the fundamental path and a maximum with respect to Q_i on the unstable region of the post-buckling path. As Λ is increased the maximum and minimum coalesce so that at $\Lambda = \Lambda^c$ the total potential energy $V(Q_i, \Lambda^c)$ has a horizontal point of inflection at the critical equilibrium state, after which a maximum and a minimum reappear as shown. Thus the critical equilibrium state is again unstable, so in the presence of even infinitesimal disturbances a physical system under slowly increasing Λ would snap dynamically from this critical equilibrium state as indicated by the heavy arrow, despite the existence of stable equilibrium states at higher values of Λ .

As before we must remember that the system under consideration has n degrees of freedom, and we must exercise care in drawing conclusions from this

schematic figure. On a real plot of the loading parameter against one of the generalized coordinates the asymmetric point of bifurcation is usually seen as the *direct* intersection of two equilibrium paths, but for a certain choice of Q_i the two equilibrium paths might *touch* each other tangentially. This follows from the fact that the direct intersection of two paths in three-dimensional space can be seen as the touching of two paths if the eye is directed along the

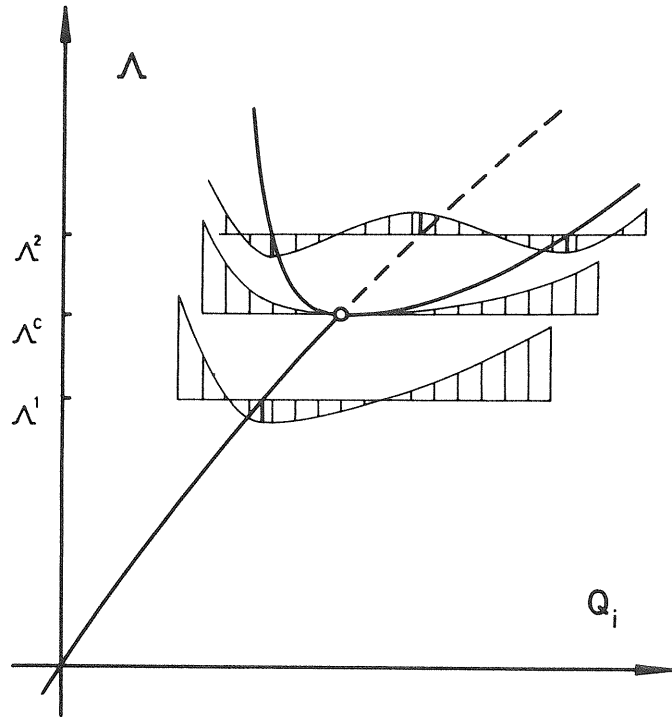


Figure 26 Energy transformation in the stable-symmetric point of bifurcation

limiting horizontal segment. Such a situation does indeed arise for the specialized system where the two paths of the asymmetric branching point are observed to touch tangentially on a plot of the generalized force P against its corresponding deflection $\mathcal{E}(Q_i)$ as shown in Figure 28.

Figure 26 shows schematically the third configuration of interest which has been called the *stable-symmetric* point of bifurcation or branching point. Here a fundamental equilibrium path rising monotonically from the origin is seen to lose its initial stability on intersecting a stable rising post-buckling path which passes smoothly through the critical equilibrium state with zero slope. The total potential energy $V(Q_i, \Lambda^1)$, where $\Lambda^1 < \Lambda^c$, has a single stationary value

with respect to Q_i , namely the minimum on the stable region of the fundamental equilibrium path, and as the value of Λ is increased this minimum is transformed into two minima and a maximum as shown. The critical equilibrium state is stable, so a physical system under slowly increasing Λ would exhibit no dynamic snap but would follow the stable rising post-buckling path, the direction taken depending on the small disturbances assumed to be present.

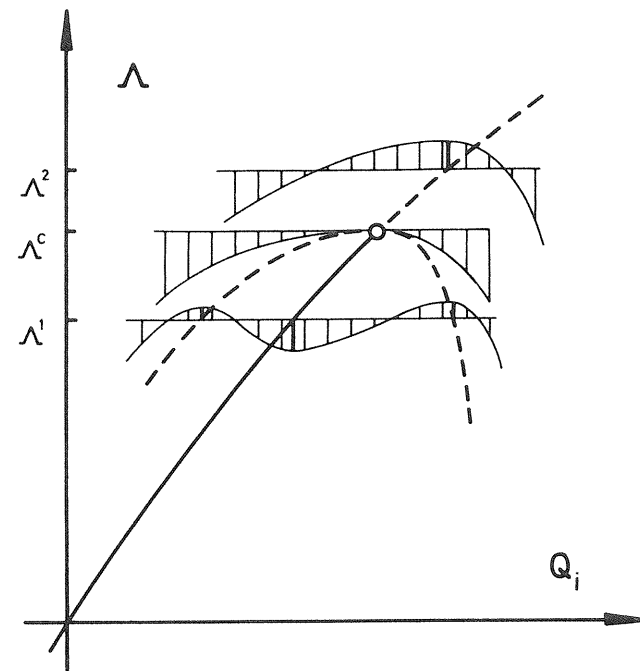


Figure 27 Energy transformation in the unstable-symmetric point of bifurcation

If Λ were actually plotted against one of the Q_i the picture would normally have the appearance of the drawn figure, but for a pathological choice of the coordinate Q_i the post-buckling path might appear as a cusp striking the fundamental equilibrium path. Such a cusp does in fact arise on a plot of P against $\mathcal{E}(Q_i)$ for the specialized system as shown in Figure 28.

The fourth configuration that we shall examine in detail is the *unstable-symmetric point of bifurcation* shown schematically in Figure 27. Here the fundamental path intersects an unstable falling post-buckling path which as in the previous case has a zero slope at the critical equilibrium state. At a prescribed value of $\Lambda = \Lambda^1$ less than the critical value the energy $V(Q_i, \Lambda^1)$ has

now three stationary values with respect to Q_i , namely two maxima on the unstable post-buckling path and a minimum on the stable region of the fundamental path. These three stationary points transform into a single maximum

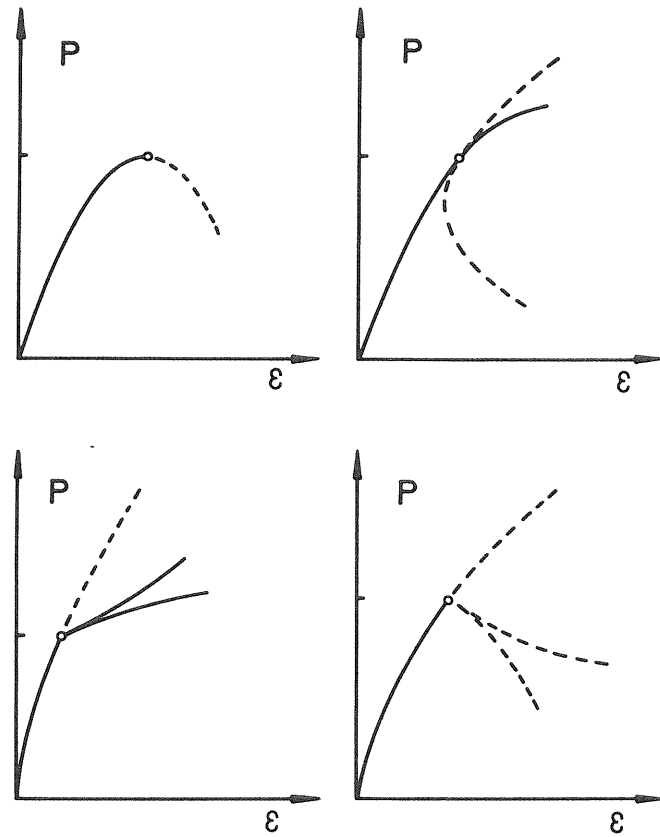


Figure 28 Load versus corresponding deflection in the limit point, the asymmetric and the two symmetric points of bifurcation

with increasing Λ as shown. The critical equilibrium state is seen to be unstable, so a physical system would snap dynamically from the critical equilibrium state, the direction taken depending on the postulated small disturbances. An actual plot of Λ against one of the Q_i would normally have the appearance of the figure, but it could happen that the post-buckling path might appear as a cusp striking the fundamental path at the critical equilibrium state. The plot of P against $\epsilon(Q_i)$ for the specialized system does indeed exhibit such a cusp as shown in Figure 28.

The definition of the two symmetric points of bifurcation requires a word of explanation at this stage. For generality of treatment the terms stable-symmetric and unstable-symmetric are applied when the post-buckling path has a zero slope, that is a zero first derivative, at the point of intersection, the former being used when the second derivative of this path is positive and the latter when it is negative. There is thus *no overall symmetry requirement*, and the third derivative will in general be non-zero at the point of bifurcation. In many practical problems these symmetric points of bifurcation do however arise under conditions of overall symmetry and the general discussion is then of course still applicable, certain terms (such as the odd derivatives) simply vanishing identically. A common consequence of some overall symmetry

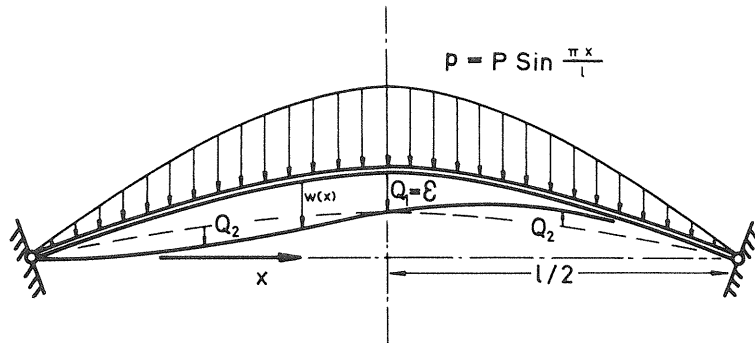


Figure 29 A shallow sinusoidal arch

arises for example for either of these two symmetric points of bifurcation in the $P-\epsilon$ plots of Figure 28, the two limbs of the post-buckling path being often completely superimposed so that they appear as one curve.

In the three critical configurations from which the system exhibits a finite dynamic snap, namely the limit point, the asymmetric point of bifurcation and the unstable-symmetric point of bifurcation, we see that for values of Λ just less than Λ^c the system is initially in a state of *metastability*, being stable for small disturbances but unstable for large disturbances. This fact must always be borne in mind and may of course render such states unusable in a practical situation.

It will be useful to elaborate a little on the general discussions of this section by considering a specific example, and we choose for this the moderately shallow arch of Figure 29 which is discussed by Ashwell.¹⁴⁹ Here a shallow sinusoidal elastic arch, pinned to rigid abutments, is loaded by a sinusoidally varying distributed load of amplitude P , and it will be adequate for our discussion to suppose that the arch has only two degrees of freedom represented by the harmonic amplitudes Q_1 and Q_2 . We have then an example of our

special $P-Q_i$ system with the generalized corresponding deflection $\mathcal{E}(Q_i)$ given by Q_1 . Equilibrium paths of the system can be represented in the three-dimensional load-coordinate space of Figure 30, and for a suitably chosen arch the response of the system is as shown in the figure. We see that in the $P-Q_1$ plane we have the well known limiting behaviour, but that before the corresponding instability with respect to Q_1 is encountered we have a bifurcation of equilibrium into the Q_2 mode at point A.

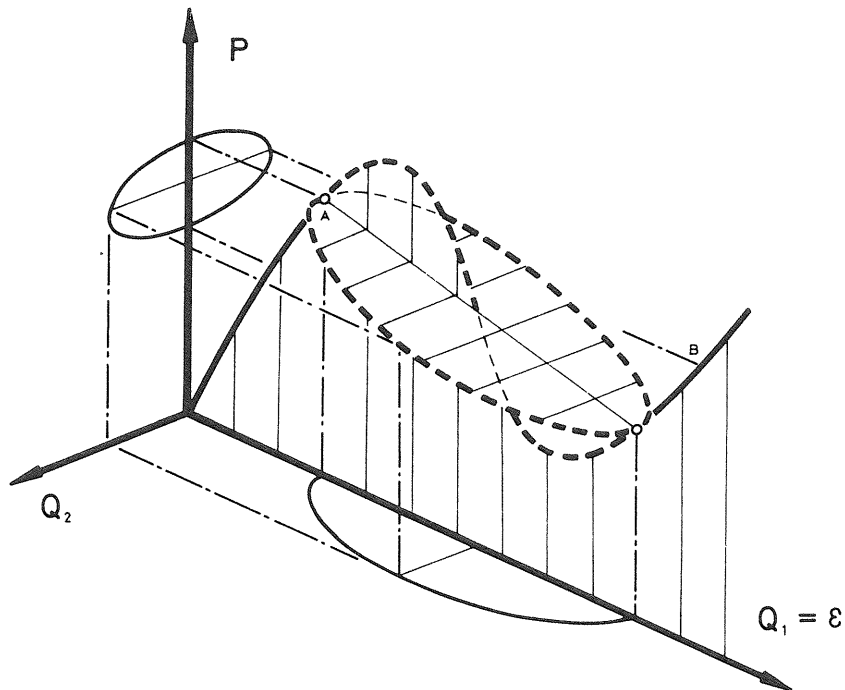


Figure 30 Equilibrium paths of the arch

The physical response of the arch can now be traced. As we load from the origin of coordinates the arch deflects symmetrically about its centre-line with Q_1 increasing nonlinearly with P and Q_2 equal to zero. At point A we hit an unstable-symmetric point of bifurcation and the arch will then snap dynamically through non-symmetric states typified by $Q_2 \neq 0$. In the presence of some damping this motion will come to rest in the stable equilibrium state represented by point B on the figure.

Two points which are of common occurrence in the field of structural stability are worthy of special mention. The first is that the *symmetric* point of bifurcation is associated with the development of deformations which are physically *non-symmetric*. Indeed it is the very physical asymmetry of the buckling mode

that guarantees a (completely) symmetric point of bifurcation. The second point to note is that states A and B are both physically symmetric about the centre-line of the arch. It might then be thought (on the basis of superficial experimental observation for example) that the failure of the arch could be predicted by an analysis using the Q_1 mode alone. Actually this conclusion is false, as we have seen, and the dynamic inversion of the arch is possible at P^A only by the use of deformations that are physically non-symmetric. That is to say, that Q_2 is most definitely non-zero during the dynamic motion to the symmetric inverted state B. We see further that due to the overall symmetry of the problem the two limbs of the post-buckling path (for which $Q_2 \neq 0$) will be coincident on a two-dimensional plot of P against Q_1 , while the only stable equilibrium states of the system lie on the extremities of the fundamental path as indicated by the solid lines.

We present now a brief synopsis of the occurrence of these four distinct critical points in the fields of structural engineering and classical mechanics.

The limit point, as we have indicated, is familiar to the structural engineer in the response of laterally-loaded arches and domes. Here the physical inversion of a shallow structure is associated simply with a limit point on the initial loading path, while for deeper structures the failure may be associated with a point of bifurcation lying on this path before its maximum, as we have just seen. Limit points are, moreover, generated by imperfections in structures which fail nominally at a point of bifurcation, and an experimental study of this is reported by Thompson.¹⁵⁰

In comparison with the symmetric points of bifurcation the asymmetric point is relatively rare, and the reason for this is not hard to find: bifurcations are usually generated by some degree of physical symmetry, and this symmetry is frequently sufficient to guarantee a symmetric point of bifurcation. The asymmetric point of bifurcation does, however, arise in the *rotationally-symmetric* buckling of a complete spherical shell under external pressure⁵⁷ and in the buckling of oblate spheroidal shells under external pressure.³⁸

It also arises in the buckling of braced⁵³ and unbraced⁷² rigid-jointed frames, and some of Roorda's experiments on the former will shortly be presented. A fairly extensive discussion of the buckling of frames was given by Britvec¹⁵¹ in 1965, and a simple frame exhibiting an asymmetric point of bifurcation is analysed by Haftka and Nachbar.¹⁵²

The distinct symmetric points of bifurcation, whether stable or unstable, arise throughout the spectrum of structural stability problems.

Simple struts and rings¹⁵³ normally yield stable-symmetric points of bifurcation, while a strut on an elastic foundation¹⁵⁴ can yield either a stable or an unstable symmetric point of bifurcation, as we shall show later in the monograph. Laterally-loaded arches frequently yield an unstable-symmetric point of bifurcation before the limiting maximum of a nonlinear fundamental equilibrium path,⁵⁵ as we have just seen.

Simply-stiff pin-jointed frames yield stable and unstable symmetric points of bifurcation as shown by Britvec.^{156, 157}

Plates loaded in their plane normally yield stable-symmetric points of bifurcation^{158–161} while axially compressed panels^{6, 162} exhibit both stable and unstable points of bifurcation, approaching the stable behaviour of plates and the unstable behaviour of cylindrical shells as the curvature parameter is varied.

Conical shells yield both stable-symmetric and unstable-symmetric branching behaviour, as demonstrated by Akkas and Bauld.¹⁶³

The initial post-buckling behaviour of a wide variety of thin elastic shells has recently been studied by Budiansky and Hutchinson and their associates at Harvard, and by virtue of their physical symmetry most of the shells considered were observed to exhibit symmetric points of bifurcation. Thus cylindrical shells under torsion²⁹ and external pressure,³⁴ toroidal shell segments,³¹ eccentrically-stiffened cylindrical shells³² and oval cylindrical shells under axial compression³⁶ all exhibit distinct symmetric points of bifurcation, both stable and unstable depending on the parameters of the shell. The study of the oval cylindrical shell is particularly worthy of note in demonstrating the value of bifurcation studies: previous large-deflection analyses were seen to have completely missed significant local behaviour close to the point of bifurcation.

Shallow spherical domes under lateral load exhibit distinct symmetric bifurcations from a nonlinear fundamental path, the branching points being stable for a point load³⁵ but unstable for a uniformly distributed pressure load.⁴³ Similar work, including a study of sandwich shells, is reported by Akkas and Bauld.^{164–166}

We see that the four distinct critical points that we have been considering are central to the field of elastic stability, and a substantial part of the monograph is devoted to them. Coincident branching points associated with the simultaneous vanishing of two or more stability coefficients are discussed in later chapters, and can give rise to a great diversity of branching phenomena.

The two notorious (simultaneous) buckling problems are of course the complete spherical shell under uniform external pressure and the long axially-compressed cylindrical shell, and these have been extensively studied over the years in view of the original large discrepancy between theoretical and experimental results. On the theoretical side, the branching studies of Koiter on the cylinder¹¹ and Koiter²¹ and Hutchinson³⁰ on the sphere are particularly relevant to our general viewpoint.

On the experimental side, carefully controlled tests have been performed on cylindrical shells by workers at Lockheed¹⁶⁷ and on complete spherical shells by workers at Stanford,^{168, 169} these workers manufacturing accurate electroplated specimens following Thompson.¹⁷⁰ Other relevant tests are reported by Evensen¹⁷¹ and Tennyson.¹⁷²

The workers at Lockheed used a mandrel inside their specimens to minimize plasticity and obtained different but repeatable buckling loads for the various specimens, the loads lying roughly between one half and three-quarters of the bifurcation loads of the corresponding perfect cylinders. They concluded that initial imperfections in the specimens, rather than dynamic disturbances from the (laboratory) environment were the cause of the discrepancy between the experimental results and the (theoretical) bifurcation loads. They thus confirm the view of Koiter, the Harvard group and the present writers that *the notorious discrepancies in the buckling of thin shells are largely attributable to initial imperfections in the test specimens*. The high-speed photographs taken during the buckling process (without a mandrel) are of further interest in showing that the initiation of buckling is associated with short-wavelength ripples which transform into the well known large-amplitude diamond pattern during the dynamic snap.

The buckling of cylinders is complicated by the fact that 'weak' boundary conditions can lower the theoretical bifurcation load by a factor of almost three, as demonstrated by Hoff and his associates.^{173–175} Meanwhile the search for a 'lower buckling load' in the advanced post-buckling range may be completely meaningless,¹⁷⁶ and the interested reader is referred to the excellent review article by Hutchinson and Koiter⁴⁴ for a more detailed discussion of these two complex buckling problems.

We might finally look at some examples from related fields of classical mechanics. Here limit points under tensile stress conditions arise in the inflation of spherical and cylindrical balloons made of certain types of rubber^{177, 178} while inflated spherical membranes may actually bifurcate into a non-spherical shape.¹⁷⁹ A further instability under tensile conditions is the necking of an inelastic tensile specimen, where a plastic point of bifurcation coincides with a maximum of the fundamental path.^{180–182}

In cosmology, limit points and stable and unstable-symmetric points of bifurcation arise in the mathematical study of the stability of stars and planetary masses as discussed by Lyttleton¹⁴² and Ledoux.¹⁴³

In crystallography the rupture of an atomic bond is a straightforward example of a limit point, and it has recently been shown that a point of bifurcation arises in the fracture of certain crystal lattices.†

2.4 Two fundamental theorems

The critical points that we have just examined hint at the existence of two basic theorems which were first delineated by Thompson¹¹⁸ in 1970. These allow stability predictions to be made on the basis of purely equilibrium

† N. H. Macmillan and A. Kelly, The mechanical properties of perfect crystals, *Proc. R. Soc., Series A*, 330, 251 (1972).

studies. The first theorem focuses attention on points of bifurcation and can be stated formally as follows.

Theorem 1. *An initially-stable (primary) equilibrium path rising monotonically with the loading parameter cannot become unstable without intersecting a further distinct (secondary) equilibrium path.*

The three branching points of the previous section clearly conform with this statement and the circumstances ruled out by the theorem are illustrated in Figure 31. The second theorem, which is written here to embrace both branching and limit points, can be expressed as follows.

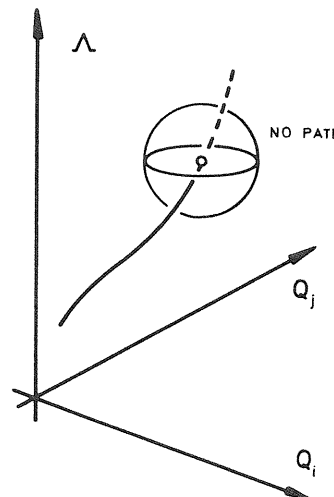


Figure 31 Response denied by Theorem 1

Theorem 2. *An initially-stable equilibrium path rising with the loading parameter cannot approach an unstable equilibrium state from which the system would exhibit a finite dynamic snap without the approach of an equilibrium path (which may or may not be an extension of the original path) at values of the loading parameter less than that of the unstable state.*

The circumstances ruled out by this theorem are illustrated in Figure 32, and we see that the limit point and the asymmetric and unstable-symmetric points of bifurcation are in conformity with it.

These theorems relating to the actual nonlinear world concern real equilibrium paths of finite length and are thus more broadly based than the usual linear (eigenvalue) theorems relating to the existence of a so-called aman-

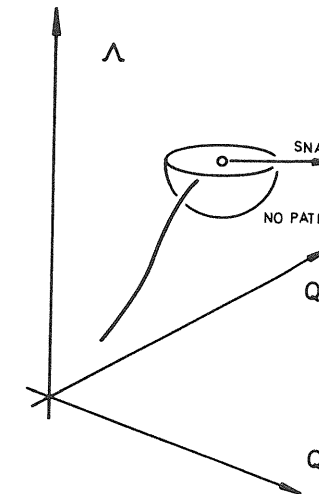


Figure 32 Response denied by Theorem 2

position of equilibrium which may or may not be associated with a real finite path. They allow stability predictions to be made once all equilibrium paths of a system are known, a circumstance that might arise in numerical studies.

As one might surmise from their global nonlinear character, the theorems are not readily proven, and only limited proofs are available at the present time. The evidence of many specific structural examples and experience in the general theory of elastic stability do nevertheless lend strong support to the total validity of the theorems: further evidence is afforded by the significant lack of counter examples, which have been earnestly sought.

For a general one-degree-of-freedom system described by $V(Q_1, \Lambda)$ topological and analytical proofs were presented in the original paper by Thompson. Of these two approaches the topological is by far the more powerful and is here used to sharpen the theorems, which were originally presented in a rather blunt form necessitated by the analytical approach.

The nature of this sharpening needs some further comment, and the original wording of the theorems is given for reference in Appendix I. There it can be seen for Theorem 1 that the loss of stability of the primary path was associated, by the insertion of the word 'thoroughly', with the passage through zero of a stability coefficient (V_{11}). Most problems of physical interest will fall within this assumption, but in presenting a global theorem it must be admitted that a stability coefficient could be zero everywhere on the primary path: the whole path would then be critical, but a loss of stability could still arise by, for example, the passage through zero of a fourth derivative (V_{1111}) under the condition that the third derivative (V_{111}) be everywhere zero. Such pathological

circumstances are fully covered by the topological proofs which are given here. Theorem 2 has likewise been sharpened to include the possibility of an everywhere critical path, and has further been reworded to embrace limiting as well as branching phenomena.

To prove Theorem 1 for a one-degree-of-freedom system we consider the monotonically rising primary path shown in Figure 33, which becomes unstable

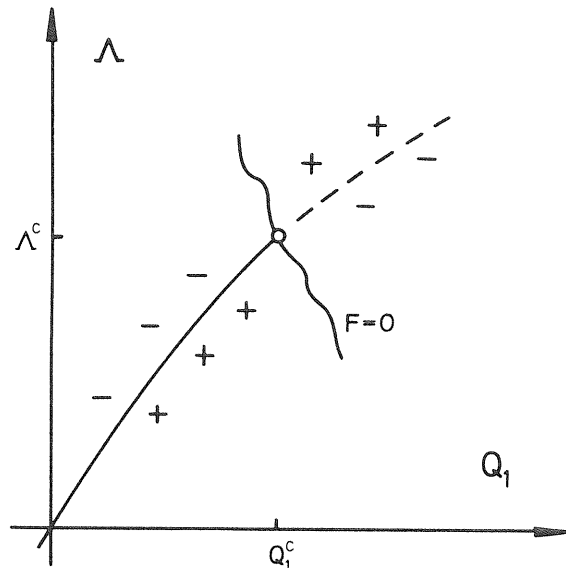


Figure 33 Geometric proof of Theorem 1

as indicated by the broken line. Now since V is a minimum on the lower region of the path, the function $F(Q_1, \Lambda) \equiv V_1(Q_1, \Lambda)$ which vanishes on the path must be positive to the right-hand side of the path and negative to the left-hand side as indicated. Further, since V is stationary but not a minimum on the path for the higher values of Λ , this function must be either negative on the right of the path or positive on the left: normally it will be both as shown on the figure. Assuming continuity of the function F it is then clear that a second equilibrium path given by $F(Q_1, \Lambda) = 0$ must intersect the primary equilibrium path and the first theorem is proved.

For Theorem 2 we consider the rising path shown approaching an unstable equilibrium state in Figure 34. Once again F must be positive on the right-hand side of this path and negative on the left-hand side. Now the unstable equilibrium state is assumed to give rise to a *finite* dynamic snap, so at its fixed value of the loading parameter there must either be a finite domain of negative F on the right (as drawn) or a finite domain of positive F on the left. Thus by

again invoking the continuity of $F(Q_1, \Lambda)$ we see that a path must approach from below, and the second theorem is proved.

The original analytical proofs depending on the local vanishing of the single stability coefficient are presented for reference in Appendix I after the appropriate statements of the theorems. With similar restrictions, the proofs can be extended to our general n -degree-of-freedom system if attention is

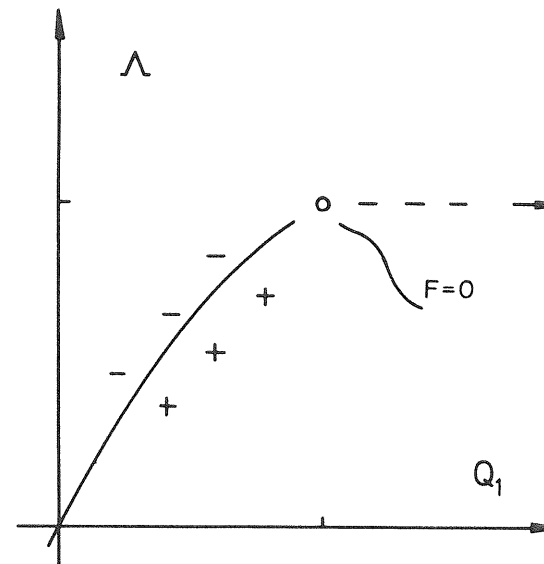


Figure 34 Geometric proof of Theorem 2

confined to *distinct* branching points since $n - 1$ passive coordinates can then be eliminated, as we shall show in Chapter 10. This extension was demonstrated by Hunt¹²⁷ in 1971.

It is not clear to the writers to what extent the recent work of Vozlinskii¹⁸³ contributes to a complete proof of these two theorems.

2.5 Initial imperfections

Structural systems can never be built precisely as planned and physical systems inevitably contain small *imperfections* associated with such things as geometrical errors and material defects. These imperfections can drastically change the response of the system, and an important feature of our general theory is concerned with the loss of stability of an imperfect system derived as a perturbation of the 'perfect' system of the previous discussions. In this study a family of systems is generated by introducing the perturbation or

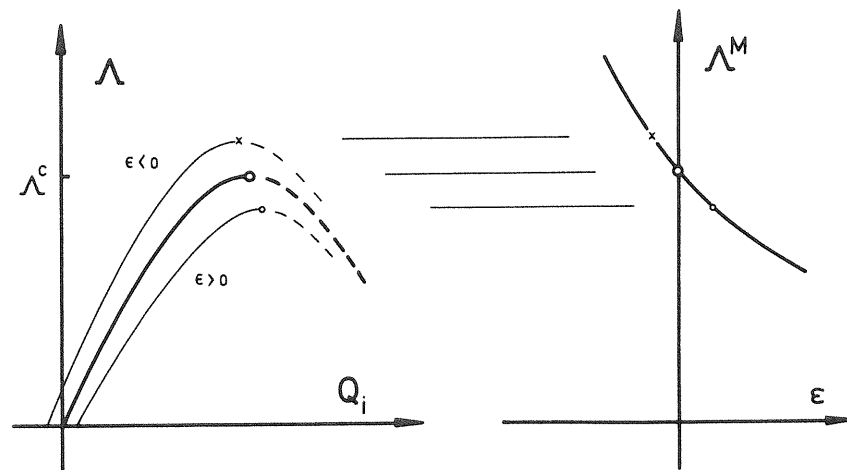


Figure 35 Initial imperfections in the limit point

imperfection parameter ϵ into the total potential energy function to give us the algebraic function $V(Q_i, \Lambda, \epsilon)$. The system corresponding to $\epsilon = 0$ is described as the *perfect system*, it being understood that this was the system of our earlier discussion, and systems corresponding to non-zero values of ϵ are described as *imperfect systems*.

Considering then the four distinct critical points in turn, *typical* equilibrium path configurations are shown on a plot of Λ against one of the Q_i in Figures 35 to 38. Here heavy lines represent the equilibrium paths of the perfect

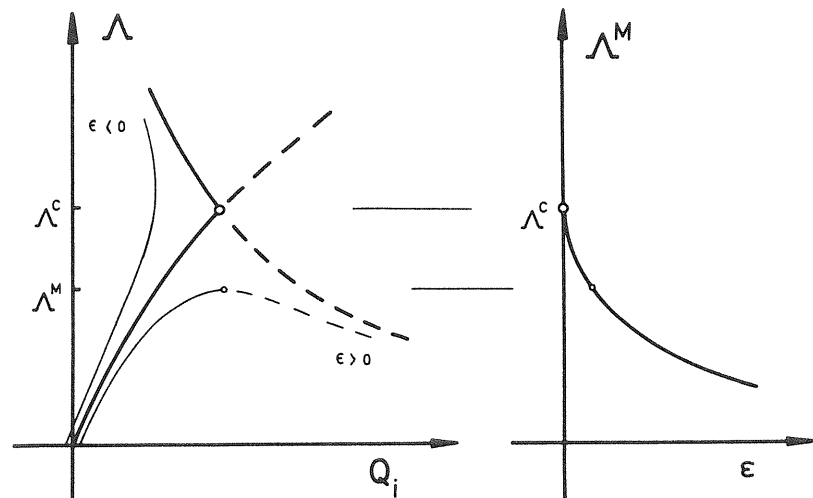


Figure 36 Initial imperfections in the asymmetric point of bifurcation

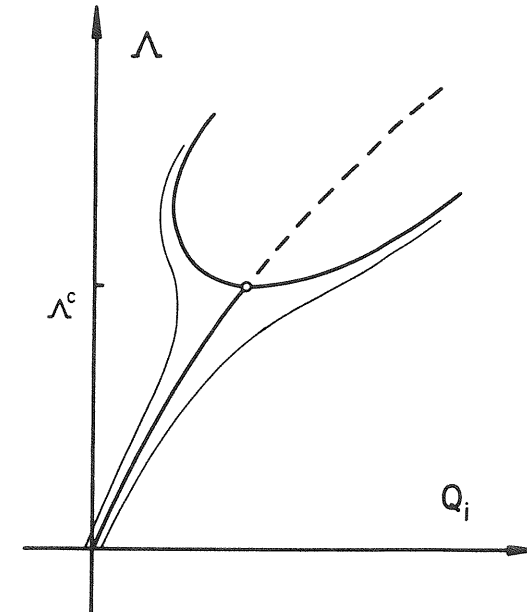


Figure 37 Initial imperfections in the stable-symmetric point of bifurcation

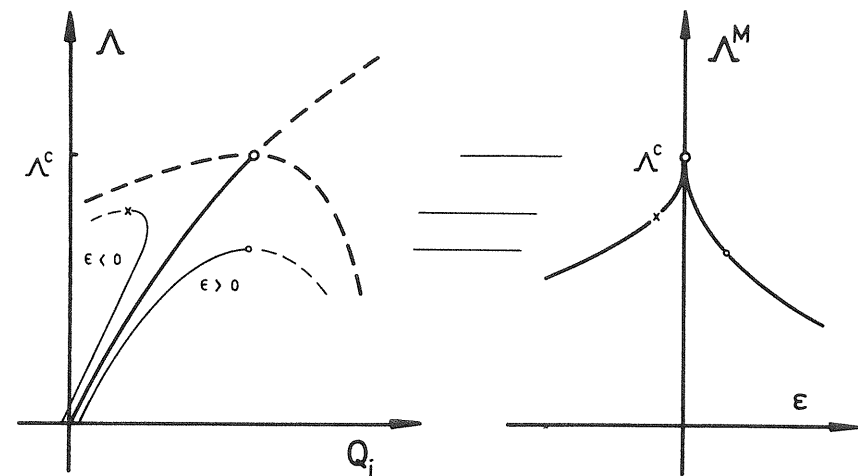


Figure 38 Initial imperfections in the unstable-symmetric point of bifurcation

system while light lines represent the equilibrium paths of the imperfect systems, continuous lines representing stable equilibrium paths and broken lines representing unstable equilibrium paths.

Figure 35 relates to the limit point, and we see that the response of an imperfect system is here not dissimilar from that of the corresponding perfect system. The peak or *failure load* Λ^M naturally varies with the imperfection parameter ϵ , and this variation is shown in the right-hand diagram of the figure, the function $\Lambda^M(\epsilon)$ having normally a finite and non-zero slope and no singularity at the critical point.

Typical pictures for the asymmetric point of bifurcation are shown in Figure 36 and we see that imperfections now play a significant role in changing the response of the system. For a small positive value of ϵ the system loses its stability at a limit point at a considerably reduced value of the loading parameter, while a system with a small negative value of ϵ exhibits no instability in the vicinity of the critical point and follows a rising stable path. We might note however that this continuously rising path traverses a region of metastability, and so may not be reliable in the presence of small dynamic disturbances. The variation of the failure load Λ^M with the imperfection parameter ϵ is now of considerable interest and is shown in the right-hand diagram. For positive imperfections the function $\Lambda^M(\epsilon)$ is locally parabolic, having no singularity at the critical point but having an infinite slope as shown; there is thus an *extreme sensitivity* to initial positive imperfections. Systems with negative imperfections having no local failure loads, their 'buckling' is simply characterized by a more rapid growth of the deflections as the critical load of the perfect system is approached. Thus there is no local branch of the $\Lambda^M(\epsilon)$ curve for negative values of ϵ .

Figure 37 shows a typical picture for the stable-symmetric point of bifurcation, and we see that here imperfections play a less significant role in changing the response of the system. Small positive and small negative imperfections have similar effects, each yielding a continuously stable and rising equilibrium path as shown. Thus imperfect systems have no failure load, 'buckling' being simply characterized by a more rapid growth of the deflections as the critical load of the perfect system is approached.

Finally the unstable-symmetric point of bifurcation is depicted in Figure 38, and we see that imperfections are here playing a significant role in modifying the behaviour of the system. Small positive and small negative imperfections again have similar effects, each now inducing failure at a limit point at a considerably reduced value of Λ . The variation of Λ^M with ϵ is shown in the right-hand diagram. For both positive and negative imperfections the function $\Lambda^M(\epsilon)$ now follows locally a two-thirds power law which yields a sharp cusp as shown, there being thus an extreme sensitivity to both positive and negative initial imperfections.

Many specific analyses of imperfection-sensitivity can be found in the work

associated with Delft and Harvard, great complexity of behaviour naturally arising when initial imperfections modify a compound rather than a distinct branching point.

The above mentioned two-thirds power law for the imperfection-sensitivity of an unstable-symmetric point of bifurcation which is established in our general theory carries over to continuous systems if the geometric imperfection is there assumed to have the shape of the buckling mode. If this common assumption is not made, new power laws may emerge from the continuum theories, as in the work of Amazigo, Budiansky and Carrier⁴² on elastically-supported columns. Here, in addition to the two-thirds law, a linear law is derived for a local dimple-type imperfection, and a four-fifths power law for a random stochastic imperfection.

2.6 A criterion for classification

Koiter has stressed that the response of a family of imperfect structural systems in the vicinity of a branching point of a perfect system is dependent on the stability or instability of this branching point itself, and we shall here make some commentary on this important observation which we shall use as a means of classifying critical points.

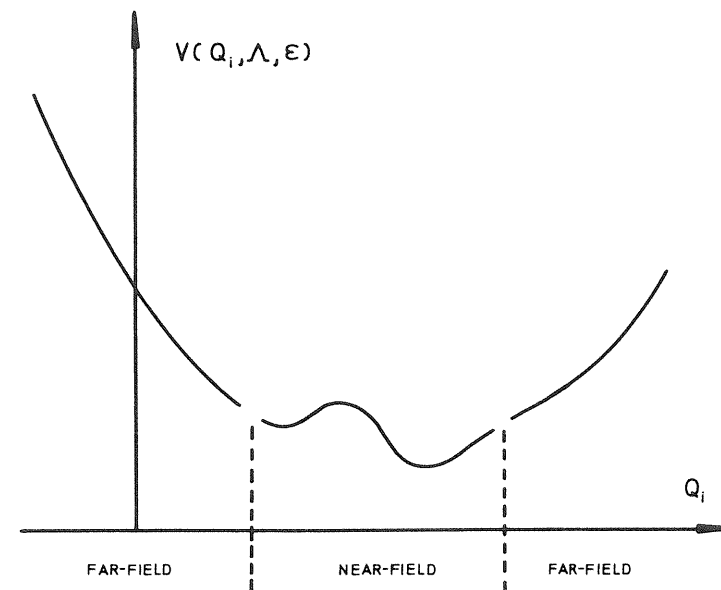


Figure 39 Stability in the large: a schematic diagram showing a stable far field

Suppose that we are considering the behaviour of a near-perfect system at a load close to a critical load of the perfect system. To see whether there is any danger of a violent dynamic snap, we must examine the overall form of the total potential energy function $V(Q_i, \Lambda, \varepsilon)$.

If in the ‘far-field’ the energy $V(Q_i, \Lambda, \varepsilon)$ is a complete relative minimum with respect to the Q_i , as shown schematically in Figure 39, the situation is clearly ‘safe’ and we might say that the structure is ‘stable in the large’. Under the influence of a small change in the loading or a small dynamic disturbance,

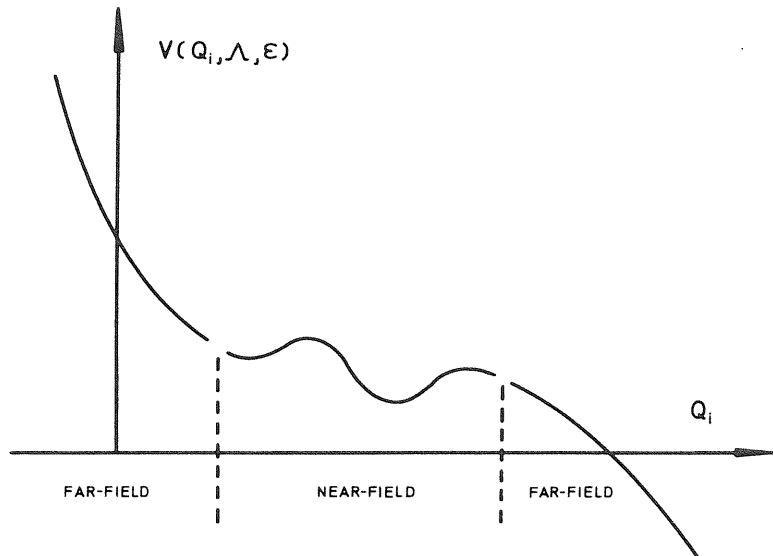


Figure 40 Instability in the large: a schematic diagram showing an unstable far field

small dynamic snaps may occur but nothing drastic can happen. If on the other hand the energy $V(Q_i, \Lambda, \varepsilon)$ is not a complete relative minimum in the far-field, as shown schematically in Figure 40, there is clearly some danger of a violent dynamic response, and we might say that the structure is ‘unstable in the large’. The behaviour of V in the far-field is thus of crucial importance, and the question arises as to how this behaviour is to be assessed.

The answer to this question is not hard to find. Clearly we must look at V when there is essentially *no near-field contribution*, namely when the quadratic energy terms vanish at the critical equilibrium state C of the perfect system. If $V(Q_i, \Lambda^c, 0)$ is a complete relative minimum at C we can expect there to be a stable far-field even when the form of V is slightly perturbed by a small change in the loading or imperfection parameter. Conversely if $V(Q_i, \Lambda^c, 0)$ is not a

complete minimum at this critical equilibrium state we can expect an unstable far-field when V is perturbed.

This argument will first be illustrated for the four distinct critical points that we have been considering. In Figures 23 and 35 the energy function $V(Q_i, \Lambda^c, 0)$ for the limit point is seen to be locally cubic and a potential far-field instability exists. Correspondingly, perfect and near-perfect systems under either infinitesimal or small-but-finite dynamic disturbances will fail dynamically at loads close to Λ^c .

For the asymmetric point of bifurcation shown in Figures 25 and 36, the energy function $V(Q_i, \Lambda^c, 0)$ is also locally cubic so a potential far-field instability again exists. Dramatic dynamic snaps can again be expected but are here not inevitable since a system with negative ε under *sufficiently-small* dynamic disturbances can pursue a stable rising path.

For the stable-symmetric point of bifurcation shown in Figures 26 and 37, the energy function $V(Q_i, \Lambda^c, 0)$ is locally quartic and positive so there is now no potential far-field instability. Consequently, perfect and imperfect systems under either infinitesimal or small-but-finite dynamic disturbances cannot exhibit a violent dynamic snap, but will pursue one or other limb of the stable rising post-buckling path.

In Figures 27 and 38 the function $V(Q_i, \Lambda^c, 0)$ for the unstable-symmetric point of bifurcation is seen to be locally quartic but negative so there is here a potential far-field instability. Both perfect and imperfect systems under either infinitesimal or small-but-finite dynamic disturbances will now fail dynamically by violent snapping action.

These distinct critical points are readily analysed in their entirety and the proposed far-field stability test is not therefore of great importance. It is, however, of very real value when dealing with problems involving coincident critical points which may well be too complex to analyse in full detail, and which can thus be usefully classified as either stable in the large or unstable in the large.

2.7 Experimental study

The three distinct *branching* points were first studied experimentally by Roorda⁶⁰ at University College, and some of his fine experimental results are reproduced in Figures 41 to 44. A fairly ‘rigid’ loading system¹⁴⁸ was employed throughout the experiments, so that equilibrium states which would have been unstable under dead loading were easily studied.

The asymmetric branching behaviour of a simple rigid-jointed frame, made from high-tensile steel strip to ensure elastic behaviour throughout, is shown in Figure 41. The load P is applied nominally at the rigid joint, and a family of imperfect systems is generated by displacing its point of application a small distance y along the horizontal member as shown.

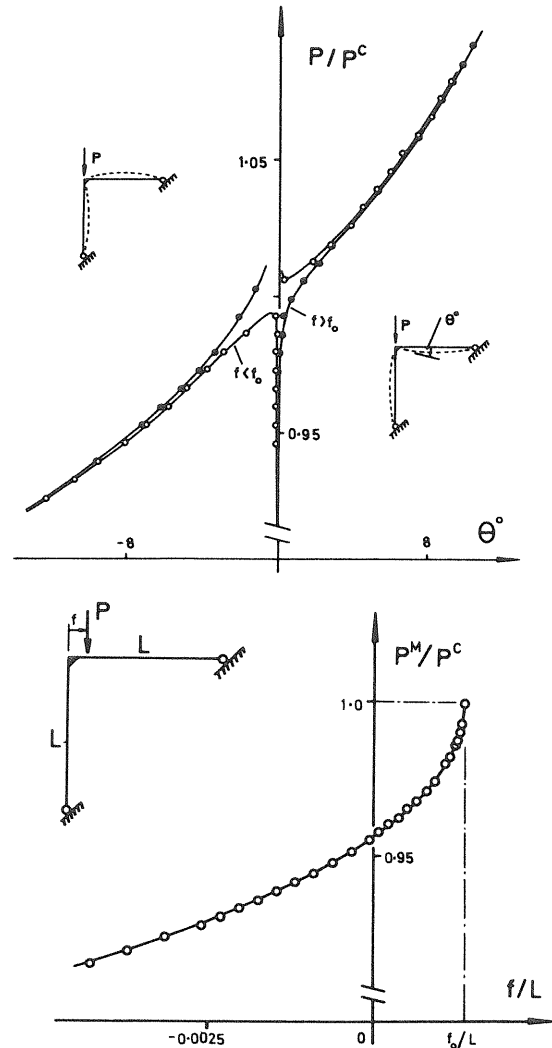


Figure 41 First experimental study of the asymmetric point of bifurcation (after Roorda 1965)

In the tests it was found that a small positive value of $f = f_0$ was needed to cancel the effect of unavoidable geometrical and other imperfections in the frame, so we can identify $\varepsilon = f - f_0$ as an appropriate imperfection parameter when viewing the results within the framework of the present general theory. The equilibrium paths, shown on a plot of P/P^c against the rotation θ , represent the response of two imperfect systems, the solid circles corresponding to an

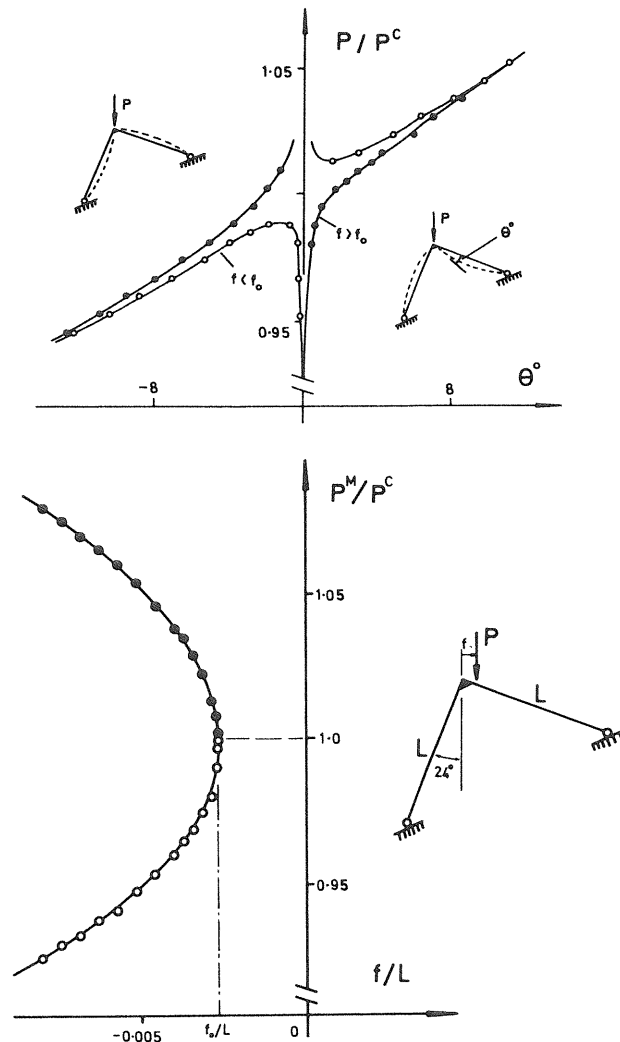


Figure 42 Second experimental study of the asymmetric point of bifurcation (after Roorda 1965)

imperfection with $f > f_0$ and the open circles corresponding to an imperfect system with $f < f_0$. For each of these two imperfect systems the *natural* equilibrium path rising from the origin of coordinates is shown, together with the *complementary* equilibrium path which would not be encountered in a natural loading sequence but which can be readily located experimentally by manually reversing the deformation mode at high values of the load P . The curves of

these two imperfect systems can be seen to band the response of the idealized perfect system for which f is precisely equal to f_0 . The imperfection-sensitivity of the system was studied experimentally and is shown in the plot of P^M/P^C against f/L . The predicted initial parabolic variation is clearly seen, and a theoretical analysis of the imperfection-sensitivity of this simple frame by Koiter¹⁷ has been shown to be in excellent agreement with these experimental results. A further theoretical study of this frame due to Hunt is given in Chapter 9.

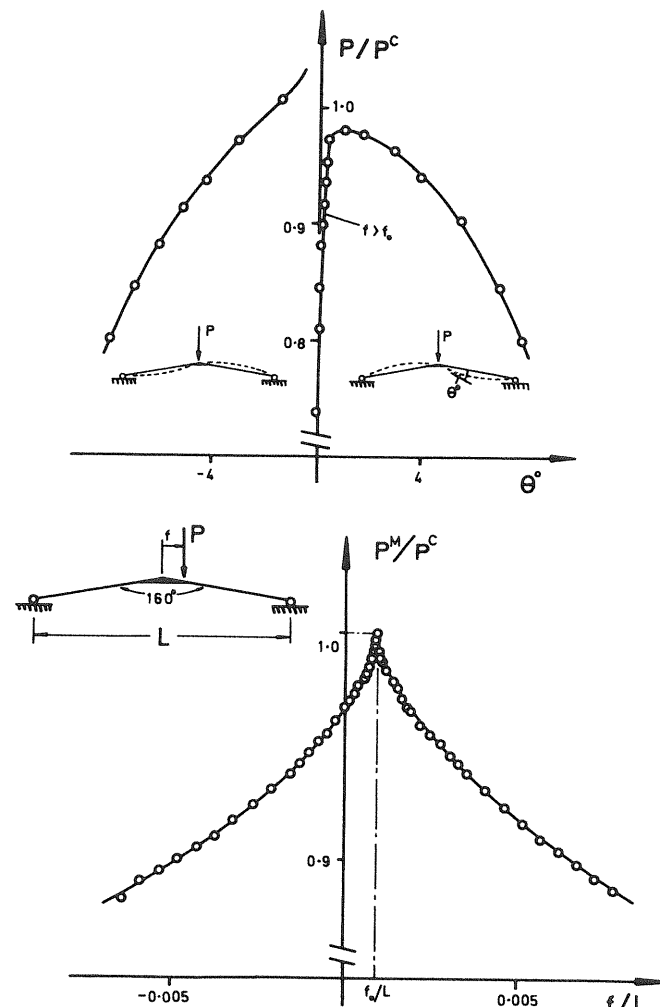


Figure 43 First experimental study of the unstable-symmetric point of bifurcation (after Roorda 1965)

Further pictures of an asymmetric point of bifurcation are shown in Figure 42 for a similar rigid-jointed frame, the plot of P^M/P^C against f/L being here extended above the critical value of unity by generalizing P^M to include the minima of the complementary equilibrium paths.

Figure 43 shows the unstable-symmetric branching behaviour of a simple rigid-jointed arch made of high-tensile steel strip. Once again the load P is applied nominally at the rigid joint, and a family of imperfect systems is generated by displacing its point of application a small distance f as shown. A small positive value of $f=f_0$ was needed to cancel the effect of unavoidable imperfections in the frame, and we can again identify $\varepsilon=f-f_0$ as an appropriate imperfection parameter. The equilibrium paths on a plot of P/P^C against θ here represent the response of a single imperfect system with $f>f_0$, the natural and the complementary paths being both located. The imperfection-sensitivity of the system is shown in the plot of P^M/P^C against f/L , and the expected two-thirds power law is clearly seen.

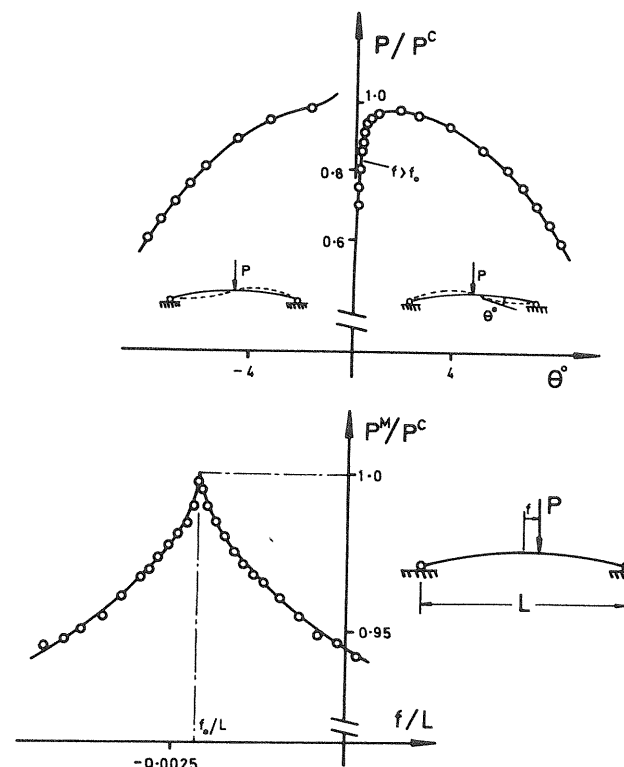


Figure 44 Second experimental study of the unstable-symmetric point of bifurcation (after Roorda 1965)

Similar pictures for another unstable-symmetric point of bifurcation are shown in Figure 44 for the shallow arch formed by a buckled strut.

2.8 Theoretical developments

We shall conclude this introductory chapter with an outline of the theoretical developments of the monograph.

Chapter 3 is concerned with the stability of an equilibrium state and the appropriate generalization, namely the stability of an equilibrium path. The structural system is first defined and the two basic axioms introduced. The total potential energy function V is then expanded as a *Taylor* or power series about an equilibrium state of interest E , and a linear transformation of coordinates is employed to diagonalize the quadratic form of V . A diagonalized energy function D is thus obtained in terms of the fixed principal coordinates u_i . The coefficients of u_i^2 in the Taylor expansion of this new energy function, namely $D_{ii}^E \equiv \partial^2 D / \partial u_i^2|_E$, represent a set of n stability coefficients and are denoted by C_i . With these we can discuss the stability of the system *with respect to* each of the principal coordinates. The number of negative stability coefficients is termed the *degree of instability*, and we see that this can only change at a *critical* equilibrium state at which the determinants of V_{ij} and D_{ij} must vanish.

If the second variation of the total potential energy is positive definite we say that the equilibrium state is *thoroughly stable*. If the second variation admits negative values we say that the equilibrium state is *thoroughly unstable*. If the second variation is positive semi-definite we have no immediate decision about the stability of the equilibrium state and higher terms of the Taylor expansion must be examined.

This higher-order examination is then made for a *distinct* critical point C involving a single zero stability coefficient, C_1 say. The examination is pursued in the basic coordinates Q_i as far as the cubic term in the Taylor expansion and finally in the principal coordinates u_i as far as the quartic terms. The key coefficients in this last examination are found to be D_{111}^C and

$$\tilde{D}_{1111}^C \equiv D_{1111}^C - 3 \sum_{s=2}^{s=n} (D_{s11}^C)^2 / D_{ss}^C.$$

For an equilibrium path a scheme of continuous diagonalization is introduced to diagonalize the quadratic form of the total potential energy at every point on the equilibrium path, the necessary transformation varying continuously with distance along the path. We thus generate a sliding and rotating set of (incremental) principal coordinates, and a set of stability coefficients that vary continuously along the path. We see that a change in the degree of instability, and in particular a loss of initial stability, can only occur at a critical equilibrium state at which the stability determinants vanish.

Chapter 4 is concerned with the response of a system in the vicinity of a

normal, that is to say a non-critical, equilibrium state E . Anticipating the existence of an equilibrium path through this state, we write such a path in the parametric form $Q_j = Q_j(s)$, $\Lambda = \Lambda(s)$, where s is any suitable parameter defining progress along the path. Substituting this into the equilibrium equation $V_i = 0$ gives us the *characterizing equilibrium identity*

$$V_i[Q_j(s), \Lambda(s)] \equiv 0.$$

The left-hand side of each equation of this set is an implicit function of s , and if a function $F(s)$ of s is identically zero it follows that all the derivatives of this function with respect to s are zero, so that we can write $F_s = F_{ss} = F_{sss} = \dots = 0$. We can then differentiate the equations of the characterizing equilibrium identity with respect to s as many times as we please, so that we can write formally

$$\frac{d^m}{ds^m} V_i[Q_j(s), \Lambda(s)] = 0 \text{ for } m = 1, 2, 3, \dots$$

We can, moreover, evaluate these derived equations at the equilibrium state E , and for reasons that will become apparent we shall refer to the m th evaluated set of equations as the *mth-order equilibrium equation*, which can be written formally as

$$\frac{d^m}{ds^m} V_i[Q_j(s), \Lambda(s)]|_E = 0.$$

Written in full the first-order equilibrium equation is seen to be

$$V_{ij} \dot{Q}_j + V'_i \dot{\Lambda}|_E = 0.$$

Here a prime denotes differentiation with respect to Λ , a dot denotes differentiation with respect to s , and the dummy-suffix summation convention is employed with all summations ranging from one to n .

Allowing one of the basic variables, Q_j or Λ , to be independent by equating its increment, q_j or λ , to s , and correspondingly replacing its first derivative with respect to s by unity and its higher derivatives with respect to s by zero, we see that we have generated a series of linear problems which can be solved for the remaining path derivatives. The first-order equilibrium equations therefore represent a set of linear equations in the remaining first derivatives which can then be found. These first derivatives can be substituted into the second-order equilibrium equations, thus giving a set of linear equations in the remaining second derivatives which are readily obtained. The known first and second derivatives can be substituted into the third-order equilibrium equations giving a set of linear equations in the remaining third derivatives, which are likewise readily obtained. In principle all the path derivatives can be obtained sequentially in this manner, and we note that each set of linear equations has the same basic matrix. The first-order equilibrium equation is recognized as the well-known equation of small-deflection linear elasticity.

This intrinsic analysis in which an inherently nonlinear problem is reduced to a sequence of linear problems was identified as a perturbation approach by Sewell.¹³⁷ A very general treatment of perturbation analysis is presented in the book by Bellman,¹⁸⁴ while a discrete coordinate study very similar to the present developments is contained in the lecture notes of J. B. Keller.¹⁸⁵

If we equate s to the loading parameter λ the determinant of each set of linear equations is the non-zero stability determinant $|V_{ij}^E|$, so we see that there will be a unique solution for all the path derivatives $\dot{Q}_j(0)$, $\ddot{Q}_j(0)$, $\dddot{Q}_j(0)$, ... There will thus be a unique equilibrium path through the non-critical equilibrium state.

Once the path derivatives are known a series solution for the equilibrium path can be written as

$$q_j(s) \equiv Q_j(s) - Q_j^E = \dot{Q}_j(0)s + \frac{1}{2}\ddot{Q}_j(0)s^2 + \dots$$

$$\lambda(s) \equiv \Lambda(s) - \Lambda^E = \dot{\Lambda}(0)s + \frac{1}{2}\ddot{\Lambda}(0)s^2 + \dots$$

This form of analysis can be used advantageously in the nonlinear analysis of continuous structures by the kinematically-admissible finite-element procedure, and two early papers on this were presented.^{84, 87} Applications in the present work include a large-deflection analysis of a laterally-loaded beam.

The perturbation analysis is repeated using the diagonalized energy function D and solutions are written down for the case in which $s = u_1$, the first principal coordinate.

In the second part of Chapter 4 the specialized system for which $V = U - P\mathcal{E}$ is discussed using the previously developed perturbation analysis in the basic Q_i coordinates with $s = P$, the loading parameter. The variation of the corresponding deflection \mathcal{E} along the equilibrium path is discussed and it is shown that the unique equilibrium path passing through a thoroughly stable equilibrium state cannot have a negative slope on a plot of the generalized force against its corresponding deflection.

The curvature of the $P-\mathcal{E}$ plot is considered and it is shown that the curvature of the unique equilibrium path passing through a non-critical equilibrium state on a plot of the generalized force against its corresponding deflection is not dependent on the solution of the second-order equilibrium equations. A consequence of this result is shown to be that a one-degree-of-freedom nonlinear Rayleigh–Ritz analysis about a non-critical equilibrium state employing the correct incremental displacement pattern will yield the correct current slope and the correct current curvature at the equilibrium state on a plot of the generalized force against its corresponding deflection.

In Chapter 5 the responses of the system in the vicinity of a distinct critical point C are examined and classified following Thompson⁵² and Sewell.¹³⁸ The diagonalized energy function D associated with a fixed set of principal coordinates u_i is employed, and a distinct critical point is considered at which

the first stability coefficient D_{11}^C is zero. Assuming the existence of one or more equilibrium paths through the point a perturbation scheme along the lines of that of Chapter 4 is employed and the *critical principal coordinate* u_1 is chosen as the independent variable. The path variations of the stability determinant and the corresponding deflection of the specialized system are examined.

Key coefficients are seen to be $D_1'^C$ and D_{111}^C , a prime denoting differentiation with respect to Λ , and when these are both non-zero the system exhibits the previously discussed *limit point*. The spatial form of this point is then examined, and the tangent to the unique equilibrium path is found to be parallel to the u_1 axis at the critical equilibrium state. As the path passes through the critical equilibrium state its degree of instability changes by one.

When $D_1'^C$ is zero we obtain the points of bifurcation, the asymmetric point of bifurcation arising when $D_{111}^C \neq 0$ and the symmetric points of bifurcation when $D_{111}^C = 0$. The spatial form of the asymmetric point of bifurcation is examined and it is found that the limiting segment passing between the two intersecting equilibrium paths at constant Λ is parallel to the u_1 axis. The stable and unstable-symmetric points of bifurcation are distinguished by the sign of \tilde{D}_{1111}^C , which as we have seen determines the stability or instability of the critical equilibrium state itself. The spatial forms of the symmetric points of bifurcation are examined and the tangent to one path is found to be parallel to the u_1 axis in each case. The forms taken by the limit point and the three points of bifurcation on a plot of P against \mathcal{E} for the specialized system are examined and are shown in Figure 28.

A similar classification in terms of a fixed energy function is given by Sewell,¹³⁹ who treats both distinct and compound critical points with the introduction of passive and active coordinates.

Chapter 6 represents a more detailed study of the branching points using a sliding set of axes, first without and secondly with a scheme of diagonalization. Starting afresh with the total potential energy function $V(Q_i, \Lambda)$ we assume the existence of a single-valued *fundamental* equilibrium path $Q_i = Q_i^F(\Lambda)$ and introduce incremental *sliding* coordinates by the equations $Q_i = Q_i^F(\Lambda) + q_i$. The q_i axes slide along the fundamental path in the original space, and we can introduce a new $\Lambda-q_i$ space in which the fundamental path is given by $q_i = 0$: there is a valid mapping between the two spaces. A new energy function is then defined by the equation $W(q_i, \Lambda) \equiv V[Q_i^F(\Lambda) + q_i, \Lambda]$.

A distinct critical point C is assumed to lie on this fundamental path, the two stability determinants $|V_{ij}|$ and $|W_{ij}|$ vanishing at this point, and an anticipated *post-buckling* equilibrium path passing through the point is written in the parametric form $q_j = q_j(q_1)$, $\Lambda = \Lambda(q_1)$. Following the earlier perturbation scheme these can be substituted into the equilibrium equation $W_i = 0$ to give us the *characterizing equilibrium identity*

$$W_i[q_j(q_1), \Lambda(q_1)] \equiv 0,$$

and differentiating with respect to q_1 we have the ordered equilibrium equations

$$\frac{d^m}{dq_1^m} W_i [q_j(q_1), \Lambda(q_1)]^C = 0 \quad \text{for } m = 1, 2, 3, \dots$$

Written in full the first-order equation is

$$W_{ij} q_j^{(1)} + W'_i \Lambda^{(1)}|^C = 0,$$

while the second can be written as

$$(W_{ijk} q_k^{(1)} + W'_{ij} \Lambda^{(1)}) q_j^{(1)} + W_{ij} q_j^{(2)} + (W'_{ij} q_j^{(1)} + W''_{ij} \Lambda^{(1)}) \Lambda^{(1)} + W'_i \Lambda^{(2)}|^C = 0,$$

where a bracketed superscript denotes differentiation of the functions $q_j(q_1)$, $\Lambda(q_1)$ with respect to q_1 . But W has the property that $W'^C = W''^C = 0$ so these equations simplify to

$$W_{ij} q_j^{(1)}|^C = 0,$$

$$W_{ijk} q_j^{(1)} q_k^{(1)} + 2W'_{ij} q_j^{(1)} \Lambda^{(1)} + W_{ij} q_j^{(2)}|^C = 0.$$

Now $q_1^{(1)} = dq_1/dq_1 = 1$, and assuming that q_1 is a suitable independent variable we can solve the first-order equation for the rates $q_s^{(1)C}$, where $s \neq 1$.

We next introduce the contraction mechanism in which the i th equation of the second-order equilibrium set is multiplied by $q_i^{(1)C}$ and the n equations added to give

$$W_{ijk} q_i^{(1)} q_j^{(1)} q_k^{(1)} + 2W'_{ij} q_i^{(1)} q_j^{(1)} \Lambda^{(1)} + W_{ij} q_i^{(1)} q_j^{(2)}|^C = 0,$$

Observing that the last term vanishes by virtue of the first-order equilibrium equation we find

$$\Lambda^{(1)C} = \frac{d\Lambda}{dq_1} \Bigg|_C = - \frac{W_{ijk} q_i^{(1)} q_j^{(1)} q_k^{(1)}}{2W'_{ij} q_i^{(1)} q_j^{(1)}} \Bigg|_C.$$

We see that by this manipulation we have obtained the slope $\Lambda^{(1)C}$ of the post-buckling path in terms of the rates $q_j^{(1)C}$, the second derivatives $q_j^{(2)C}$ having been eliminated. We can thus write the general result:

The slope of the post-buckling path passing through a simple distinct critical point on a plot of the loading parameter against a (suitable) generalized coordinate is not dependent on the solution of the second-order equilibrium equations.

A consequence of this result is that a one-degree-of-freedom nonlinear Rayleigh–Ritz analysis employing the linear buckling mode will yield the correct value for this slope.⁵⁸

Returning to the analysis, knowing $\Lambda^{(1)C}$ and remembering that $q_1^{(2)C} = d^2 q_1/dq_1^2 = 0$, we can now solve the second-order equations for the second

derivatives $q_s^{(2)C}$ ($s \neq 1$) if more information is needed. This sequence can be repeated as many times as we please.

General forms for the r th-order equilibrium equations before and after contraction are derived and used to prove the general result:

For the post-buckling path passing through a simple distinct critical point the r th derivative of the loading parameter with respect to a (suitable) generalized coordinate is not dependent on the solution of the $r+1$ th-order equilibrium equations.

The analysis so far is applicable whether or not the slope $\Lambda^{(1)C}$ is zero. When $\Lambda^{(1)C}$ is non-zero we have the previously discussed asymmetric point of bifurcation and when $\Lambda^{(1)C} = 0$ we have the symmetric points of bifurcation, the initial curvature being then given by

$$\Lambda^{(2)C} = - \frac{\tilde{W}_4}{3W'_{ij} q_i^{(1)} q_j^{(1)}} \Bigg|_C \quad (\Lambda^{(1)C} = 0),$$

where

$$\tilde{W}_4^C = W_{ijkl} q_j^{(1)} q_k^{(1)} q_l^{(1)} + 3W_{ijk} q_i^{(1)} q_j^{(1)} q_k^{(2)}|^C.$$

Obtaining the path derivatives sequentially in this way we can finally construct a series solution for the post-buckling equilibrium path as

$$q_j(q_1) = q_j^{(1)C} q_1 + \frac{1}{2} q_j^{(2)C} q_1^2 + \dots,$$

$$\lambda(q_1) = \Lambda^{(1)C} q_1 + \frac{1}{2} \Lambda^{(2)C} q_1^2 + \dots,$$

where $\lambda(q_1) \equiv \Lambda(q_1) - \Lambda^C$. The $P - \mathcal{E}$ response of the specialized system is finally examined.

This general W -analysis presented by Thompson and Walker¹⁰² is invaluable in studying the post-buckling of continuous structures by the kinematically-admissible finite-element procedure and two applications were presented in companion papers;^{86, 106} present applications include studies of the elastica (see in Chapter 1) and the post-buckling of uniformly compressed circular plates.

In the second part of Chapter 6 the branching points are examined in more detail using a scheme of continuous diagonalization following Thompson.⁶² After the diagonalizing transformation to a new energy function denoted by A the analysis follows the established perturbation pattern. The path variation of the stability determinant $|A_{ij}|$ is studied and the stability of the paths is examined. The stability of the critical equilibrium state itself is discussed and its relationship to the post-buckling response is noted.

Chapter 7 is entirely devoted to a substantial illustration of the preceding W -analysis following the work of Thompson and Lewis¹³⁵ on comparative branching studies of a uniformly compressed circular plate. A finite-element

formulation using a kinematically-admissible displacement field is employed and the analysis is performed for both simply-supported and clamped boundaries. Corresponding continuum analyses are also included, and these provide not only an interesting comparison with the discrete approach but also the exact solutions upon which the finite-element results are seen to converge; this convergence is found to be encouragingly good, as few as twelve elements being needed to obtain accurate numerical solutions.

In Chapter 8 the response of imperfect systems is discussed. A family of systems is generated by introducing the *imperfection parameter* ε into the total potential energy function to give $V(Q_i, \Lambda, \varepsilon)$. The ‘perfect’ system for which $\varepsilon = 0$ is understood to be the one previously discussed.

Consideration is first given to the response of imperfect systems in the vicinity of the distinct limit point of Chapter 5. The fixed principal axes of the earlier work are employed and the analysis starts by writing

$$D(u_i, \Lambda, \varepsilon) \equiv V[Q_i^C + \alpha_{ij} u_j, \Lambda, \varepsilon].$$

The critical points of the imperfect systems are written as $u_j = u_j^M(\varepsilon)$, $\Lambda = \Lambda^M(\varepsilon)$, and since these critical points are characterized by the vanishing of the D_i and the stability determinant $\Delta(u_k, \Lambda, \varepsilon) \equiv |D_{ij}|$ we have the *characterizing identities*

$$D_i[u_j^M(\varepsilon), \Lambda^M(\varepsilon), \varepsilon] \equiv 0,$$

$$\Delta[u_j^M(\varepsilon), \Lambda^M(\varepsilon), \varepsilon] \equiv 0.$$

A perturbation scheme is now generated by differentiation with respect to ε and the derivatives of the functions $u_j^M(\varepsilon)$, $\Lambda^M(\varepsilon)$ are obtained. In this way the equation of imperfection-sensitivity is derived, the limit point exhibiting the modest degree of imperfection-sensitivity shown in Figure 35.

Consideration is next given to the response of imperfect systems in the vicinity of the distinct branching point C of Chapter 6 to determine asymptotic equations of imperfection-sensitivity. The A -transformation is first employed following Thompson⁶² and the analysis starts by writing

$$A(u_i, \Lambda, \varepsilon) \equiv V[Q_i^F(\Lambda) + \alpha_{ij}(\Lambda) u_j, \Lambda, \varepsilon].$$

The natural functions of imperfection-sensitivity are $u_j = u_j^M(\varepsilon)$, $\Lambda = \Lambda^M(\varepsilon)$, a point in $\Lambda - u_i$ space corresponding to the critical equilibrium state of a given imperfect system. For the purposes of analysis these functions must however be written in the inverted form $u_j^M = u_j^M(u_1^M)$, $\Lambda^M = \Lambda^M(u_1^M)$, $\varepsilon = \varepsilon^M(u_1^M)$. Characterizing identities are now written and a perturbation scheme is generated for the derivatives of these inverted functions.

For the asymmetric point of bifurcation the initial parabolic variation of Λ^M with ε is finally obtained entirely in terms of the *post-buckling rates of the perfect*

system. Similarly, for the symmetric points of bifurcation the initial two-thirds power relationship between Λ^M and ε is obtained entirely in terms of the *post-buckling derivatives of the perfect system*.

The imperfection-sensitivity at branching points is finally studied in a more general form suitable for numerical analysis in terms of the nondiagonalized W -analysis following Thompson.¹⁰¹ Characterizing identities for critical points of imperfect systems are written down and a perturbation scheme developed using the first generalized coordinate q_1 as the independent variable. The initial interrelationships between ‘perfect’ and ‘imperfect’ perturbation analyses are here fully investigated, and general forms of the r th-order perturbation equations are developed which allow us to compare the patterns of solutions of the two schemes. Finally the first three terms of the full asymptotic equations of imperfection-sensitivity are explicitly derived for both asymmetric and symmetric points of bifurcation.

In Chapter 9 the general theory for imperfect systems is fully illustrated in two worked examples. First we perform an analysis of the strut on an elastic foundation using an expansion in orthogonal harmonic functions for the deflected shape of the system, thereby generating a diagonalized energy function. Secondly a finite-element analysis of a two-bar frame is presented to illustrate the more general W -analysis. Here we introduce a slight extension of the general theory which with the finite-element formulation neatly overcomes the difficult problem of nonlinear compatibility relationships at the knee of the frame.

We might note at this stage that examples of the mathematical treatment of continuum branching problems, with examples drawn from the whole spectrum of the physical sciences and including detailed discussions of the existence and uniqueness of solutions, can be found in the excellent collection of papers edited by Keller and Antman¹⁸⁶ and in the recent IUTAM conference of reference 103, edited by Leipholz.

Chapter 10 is concerned with the general theory for m coincident branching points giving rise to a single m -fold compound branching point on the fundamental path; here m stability coefficients are simultaneously zero. The analysis is first presented in diagonalized form and we thus have m active principal coordinates u_i associated with the vanishing stability coefficients and $n - m$ passive principal coordinates u_α associated with the non-vanishing stability coefficients.

We start with a perturbation scheme to eliminate the passive coordinates. Thus writing the parametric forms $u_\beta = u_\beta(u_i, \Lambda)$ we substitute these into $n - m$ of the equilibrium equations to obtain the *characterizing identity*

$$A_\alpha[u_i, u_\beta(u_i, \Lambda), \Lambda] \equiv 0.$$

Differentiating this identity with respect to the $m + 1$ independent variables

u_i and Λ as many times as we please, we generate the ordered equilibrium equations

$$\begin{aligned}\frac{\partial}{\partial u_i} A_\alpha &= A_{\alpha i} + A_{\alpha\beta} u_{\beta i} = 0, \\ \frac{\partial}{\partial \Lambda} A_\alpha &= A'_\alpha + A_{\alpha\beta} u'_{\beta} = 0,\end{aligned}$$

etc. We still employ the dummy-suffix summation convention but with summation over Greek subscripts ranging over the $n - m$ passive values and summation over Latin subscripts ranging over the m active values. Further subscripts on u_β denote differentiation with respect to the appropriate active coordinate and primes denote differentiation with respect to Λ . The equations are evaluated on the fundamental path F and sequentially solved to find the derivatives $u_{\alpha i}^F, u'_\alpha^F, u_{\alpha i j}^F, u_{\alpha l}^F$, etc.

The series expansions $u_\alpha(u_i, \Lambda)$ which are obtained from the above derivatives lead to a new energy function with m degrees of freedom defined by

$$\mathcal{A}(u_i, \Lambda) \equiv A[u_i, u_\alpha(u_i, \Lambda), \Lambda].$$

The derivatives of this new energy function are directly obtained by differentiation as follows

$$\begin{aligned}\mathcal{A}_i &= A_i + A_\alpha u_{\alpha i}, \\ \mathcal{A}'_i &= A_{\alpha i} u'_\alpha + A'_i + A_{\alpha\beta} u_{\alpha i} u'_\beta + A'_\alpha u_{\alpha i} + A_\alpha u'_{\alpha i},\end{aligned}$$

etc. Finally evaluation on the fundamental path gives the coefficients $\mathcal{A}_i^F, \mathcal{A}'^F, \mathcal{A}_{ij}^F, \mathcal{A}'^F$, etc. in terms of the known derivatives of u_α .

Before we can use the new \mathcal{A} -function in a post-buckling analysis it is necessary to show that the normal equilibrium and stability conditions are preserved over the transformation. The equilibrium condition is easily dealt with analytically, and we include some heuristic reasoning which suggests that the stability condition is likewise fully preserved. The post-buckling paths emerging from the compound critical point C are now written in the parametric form $u_j = u_j(s), \Lambda = \Lambda(s)$ and these substituted into the equilibrium equations $\mathcal{A}_i = 0$ to give the characterizing identity of a new perturbation scheme

$$\mathcal{A}_i[u_j(s), \Lambda(s)] \equiv 0,$$

where the perturbation parameter s remains unspecified. Successive differentiation with respect to s now leads to ordered equilibrium equations as before, the first non-vanishing equation evaluated at C becoming

$$\mathcal{A}_{ijk} \dot{u}_j \dot{u}_k + 2\mathcal{A}'_{ii} \dot{u}_i \dot{\Lambda}|^C = 0, \text{ no summation over } i,$$

where a dot denotes differentiation with respect to s .

These equations constitute m homogeneous quadratics and following Sewell^{139, 141} we find by the theorem of Bezout¹⁸⁷ that the maximum number of

solutions and hence post-buckling paths passing through the critical point is $2^m - 1$. Having an unspecified perturbation parameter, the post-buckling solutions are generated in the rate space $\dot{\Lambda} - \dot{u}_i$, but these become the path tangents when mapped directly into the coordinate space $\Lambda - u_i$. The convergence of an analysis of this type has been discussed by Sewell,¹⁴⁰ who also examines the difficulties associated with near coincidence. Some specific solutions which might arise in practical systems are presented for the case of $m = 2$.

The stability of the compound critical point itself is next examined in terms of the new \mathcal{A} -function and we should note that a similar study has been presented by Sewell¹³⁹ using some order of contact ideas. This stability relates to the far-field response of the system which is discussed in Section 2.6 and it is suggested that this provides a useful classification for problems involving coincident critical points which may well be too complex to analyse in detail.

In the second part of Chapter 10 a similar pattern of solution is followed in terms of the W -function. Again we consider an m -fold compound branching point on the fundamental path and $n - m$ passive coordinates are eliminated from the analysis using a perturbation scheme. Here, however, separation of the incremental coordinates into the active coordinates q_i and the passive coordinates q_α is not necessarily immediately obvious, but it is shown that a valid segregation can always be found by insisting that $|W_{\alpha\beta}^C| \neq 0$. The elimination of the passive coordinates leads to a new potential energy function with m degrees of freedom which is then used to find the post-buckling solutions in the rate space $\dot{\Lambda} - \dot{q}_i$. It is suggested that this method is the most useful for numerical work involving, for example, the kinematically-admissible finite-element procedure.

Chapter 11 is devoted to a study of the two-fold branching point that can arise in the problem of a spherical shell buckling under an external pressure. The general theory is applied to this continuum by the introduction of an expansion in Legendre functions, giving rise to a potential energy function that is in a near-diagonal form. The problem is first tackled by adopting a diagonalizing transformation, and the A -analysis of the general theory is followed closely, the post-buckling solutions finally being obtained from an appeal to one of the specific cases given in the earlier work. An alternative method of analysis is also included, which does not appeal to the diagonalizing transformation and therefore follows the W -analysis of the general theory.

In Chapters 12 and 13 we finish on a divergent note, drawing on problems both from the field of elastic stability and from outside it to point out some of the dangers of structural optimization. Chapter 12 deals specifically with three types of compound failure of columns, and Chapter 13 includes a number of examples in which a criterion of optimization might seem of value, but is particularly concerned with the sometimes hidden dangers which can arise in such a scheme.

3

STABILITY OF EQUILIBRIUM

3.1 Structural system

We consider a conservative mechanical system, spatial configurations of which are described by a set of n generalized coordinates Q_i . There is assumed to be a unique one-to-one correspondence between sets of the Q_i and the spatial configurations of the system, and the coordinates and their variation are subjected to no constraints. Thus if we associate the Q_i with a set of rectangular axes in an n -dimensional Euclidean space we can be sure that any point in this *coordinate space* corresponds to a unique admissible spatial configuration of the system, while any trajectory in this space corresponds to a unique admissible spatial motion of the system.

The system is assumed to have the single-valued total potential energy function $V(Q_i, \Lambda)$ and the single-valued kinetic energy function $T(Q_i, \dot{Q}_j, \Lambda) = \frac{1}{2}T^{ij}(Q_k, \Lambda)\dot{Q}_i\dot{Q}_j$, each of which is assumed to be continuous and well behaved. The parameter Λ , subsequently referred to as a *loading parameter*, is essentially any basic parameter of the system whose influence we wish to study, and we shall be concerned with the equilibrium and stability of the system under different but constant values of this parameter. With Λ prescribed, the dynamic response of the system is assumed to be determined by the equations of Lagrange and Hamilton.

Such energy functions might arise directly from a discrete mechanical system, or indirectly from a continuous system rendered discrete by a modal analysis, and introductory examples from these two classes have been presented in Chapter 1. Since there are no constraints on the variations of the coordinates the general system under consideration is *holonomic* in the terminology of classical mechanics. The system is moreover *scleronomous*, since time does not appear explicitly in either V or T , and we shall introduce the term *structural* to embrace these two criteria. We are thus concerned with a conservative structural system, namely the *simple* dynamical system defined by Synge and Griffith.¹⁴⁶

The concept of statical equilibrium is well understood, and we adopt the classical definition of stability due to Liapunov.⁴ This relates to the $2n$ -dimensional phase space of the system and states that an equilibrium state is stable if and only if all motions of the system starting close to the equilibrium

state remain close to this state for all time. A most readable introduction to this classical definition of stability is contained in the book by La Salle and Lefschetz¹⁸⁸ and we might also mention the book by Chetayev.¹⁸⁹

To make the work self-contained, we now introduce two basic axioms for the system.

Axiom 1. *A stationary value of the total potential energy with respect to the generalized coordinates is necessary and sufficient for the equilibrium of the system.*

This axiom can of course be easily proved.

Axiom 2. *A complete relative minimum of the total potential energy with respect to the generalized coordinates is necessary and sufficient for the stability of an equilibrium state of the system.*

This axiom cannot be proved in *complete* generality for our simple dynamical system (the proof sketched by La Salle and Lefschetz cannot be made universally valid), and a recent appraisal of the situation is presented by Koiter.¹⁴ It seems clear, however, that a complete proof will eventually be found, and in the meantime we follow Koiter by expressing our complete faith in the axiom.

We notice that the kinetic energy function $T(Q_i, \dot{Q}_j, \Lambda)$ makes no appearance in these axioms, and will thus play no part whatsoever in the monograph. We can thus forget about it completely, but before doing so we shall here present a brief discussion of the situation. That the form of the kinetic energy has no effect on the statical equilibrium states of the system is quite expected, but since stability is a dynamical concept concerning motions of the system we might express some surprise that a change in the disposition of inertial mass can effect neither a stabilization nor a destabilization of a system. That this is indeed the case has quite an important consequence in our treatment of structural loadings.

We have in the simple models of Chapter 1 glibly postulated the existence of a dead vertical load P , assumed to retain its magnitude and direction as the systems deflect, and it is pertinent to inquire how such a load might arise in practice. In such cases, structural engineers will usually have in mind a mass m hanging in a uniform gravitational field g , where mg is equal to P . This is fine under static conditions, but we see that under dynamic conditions this gravity loading does not quite fit the bill: during motion of the system the hanging mass will experience vertical accelerations, so the tension in the wire will not be equal to $mg = P$.

In the variational mechanics formulation the two systems shown in Figure 45 will have identical V -functions, but the T -functions will differ by an additive factor $\frac{1}{2}m\omega^2\delta^2$ where δ is the vertical displacement of the mass, and herein lies

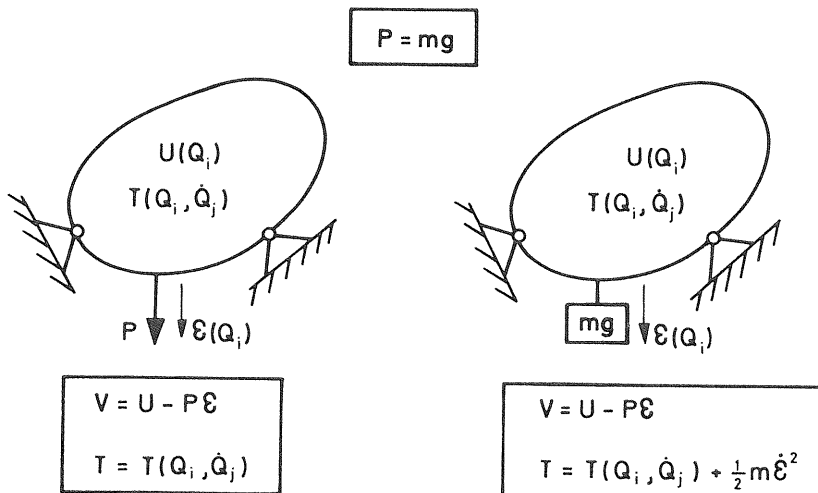


Figure 45 Two systems with different dynamic responses but identical static responses

the key. By virtue of our two axioms the two systems will have the *same response* as far as their equilibrium and stability are concerned, and so the distinction between the systems need be of no concern to us in this monograph.

Suffice it to say that in structural loading situations of any complexity it is usually much safer and more elegant to enlarge the system under consideration to embrace the loading feature and then to associate Λ with a fundamental parameter of the enlarged system such as a mass or even a gravitational constant: we prefer the hanging mass to the nebulous force P . By doing this we can be sure that we are indeed dealing with a conservative system: non-conservative systems, such as arise with the so-called ‘follower force,’ are out of the scope of the present study.

Associating the basic variables Q_i and Λ with rectangular axes in an $n + 1$ -dimensional Euclidean space, we see that the n equilibrium equations specifying a stationary value of V with respect to the Q_i will define a series of equilibrium paths in this space, and it is the form and stability of these paths that will concern us in the present work. The previously defined n -dimensional coordinate space is of course a subspace of this $n + 1$ -dimensional *load-coordinate space*.

We consider finally an important specialization of the preceding general system which can be made when the original total potential energy function $V(Q_i, \Lambda)$ is linear in the loading parameter Λ . When this linearity holds we shall, for purely semantic reasons, replace Λ by P and then write

$$V(Q_i, P) \equiv U(Q_i) - P\mathcal{E}(Q_i).$$

Here the function $U(Q_i)$ can be regarded as a *generalized strain energy*, while P can be regarded as the magnitude of a *generalized force* acting through the *generalized displacement* $\mathcal{E}(Q_i)$.

3.2 Stability of an equilibrium state

We consider now the stability of an equilibrium state

$$Q_i = Q_i^E, \quad \Lambda = \Lambda^E,$$

satisfying the n equilibrium equations

$$V_i(Q_j^E, \Lambda^E) = 0,$$

a subscript on V denoting partial differentiation with respect to the corresponding generalized coordinate. Considering the increments from this state defined by

$$Q_i = Q_i^E + q_i,$$

$$V = V^E + v,$$

where

$$V^E = V(Q_i^E, \Lambda^E),$$

we first write the Taylor expansion with respect to the generalized coordinates

$$v = \frac{1}{2}V_{ij}^E q_i q_j + \frac{1}{6}V_{ijk}^E q_i q_j q_k + \dots,$$

where

$$V_{ij}^E \equiv V_{ij}(Q_k^E, \Lambda^E),$$

etc. The basic state being one of equilibrium, there is no linear term in this expansion. The dummy-suffix summation convention is employed, with all summations ranging from one to n .

The stability of the equilibrium state will depend in the first instance on the quadratic form

$$v^2 = \frac{1}{2}V_{ij}^E q_i q_j$$

in which the superscript 2 denotes a quadratic form and not, as at first glance might be supposed, the square of v . We start by reducing this to a diagonal form by means of a non-singular linear coordinate transformation

$$q_i = \alpha_{ij} u_j, \quad \text{where } |\alpha_{ij}| \neq 0,$$

with the inverse

$$u_i = \beta_{ij} q_j, \quad \text{where } |\beta_{ij}| \neq 0.$$

We note that if we plot the u_i coordinates in q_i space we do not necessarily obtain a set of rectangular axes. In the new coordinates we can write

$$v^2 = \frac{1}{2} C_i u_i^2$$

where the C_i are constants.

We now define a new energy function

$$D(u_i, A) \equiv V(Q_i^E + \alpha_{ij} u_j, A)$$

and writing

$$D = D^E + d,$$

where

$$D^E \equiv D(0, A^E),$$

we expand D about the equilibrium state to give

$$d = \frac{1}{2} D_{ii}^E u_i^2 + \frac{1}{6} D_{ijk}^E u_i u_j u_k + \dots$$

Here subscripts on D denote partial differentiation with respect to the corresponding u_i , and the superscript E denotes evaluation at the equilibrium state. We see that

$$C_i = D_{ii}^E = D_{ii}(0, A^E),$$

and¹⁹⁰

$$|\alpha_{ij}|^2 \cdot |V_{ij}^E| = |D_{ij}^E| = C_1 C_2 C_3 C_4 \dots C_n.$$

The quadratic form v^2 can be diagonalized in an infinite number of ways, and we shall suppose that one such way has been chosen, noting that the invariant properties of v^2 manifest themselves as invariant properties of the C_i . The number of positive C_i , the number of negative C_i and the number of zero C_i are independent of the choice of the diagonalizing transformation.¹⁹⁰

The coordinates u_i and the coefficients C_i play an important role in the following theory, and we shall call the u_i a set of *principal coordinates* and the C_i a set of *stability coefficients*.

We use these to make *qualified* statements about the stability of the equilibrium state. Thus if a particular stability coefficient C_r is positive we shall say that the equilibrium state is stable *with respect to* the corresponding principal coordinate u_r . If a particular stability coefficient C_s is negative we shall say that the equilibrium state is unstable *with respect to* the corresponding principal coordinate u_s . If a particular stability coefficient C_t is zero we shall say that the equilibrium state is *critical with respect to* the corresponding principal coordinate u_t .

The number of negative stability coefficients is called the *degree of instability*.

An equilibrium state is called *critical* without qualification if it is critical with respect to one or more of the principal coordinates, and we see that the two determinants $|V_{ij}|$ and $|D_{ij}|$ will vanish in a critical equilibrium state.

If the lowest stability coefficient is positive the equilibrium state is stable with respect to all of the principal coordinates and v^2 is *positive definite*. The equilibrium state is then clearly stable, and in contrast to critically stable equilibrium states whose stability depends on higher variations of V , we might say that the state is *thoroughly stable*.

If the lowest stability coefficient is negative the equilibrium state is unstable with respect to one or more of the principal coordinates and v^2 *admits negative values*. The equilibrium state is then clearly unstable, and in contrast to the critically unstable equilibrium states whose instability depends on higher variations of V , we might say that the state is *thoroughly unstable*.

If the lowest stability coefficient is zero, the equilibrium state is critical with respect to one or more of the principal coordinates and stable with respect to the rest. The quadratic form v^2 is then *positive semi-definite* and supplies no decision about the stability of the equilibrium state. Higher-order terms in the expansion of v must then be examined, and we shall pursue this for a distinct critical point denoted by C at which a single stability coefficient is zero.

In the following type of discussion it is useful to be able to visualize the variation of potential energy in coordinate space, so we now demonstrate the two ways of visualizing V by means of schematic diagrams. First for 2 degrees of freedom it is possible to envisage a V -surface in $V-u_i$ space as shown in Figure 46; this is clearly drawn in the region of an equilibrium state which is

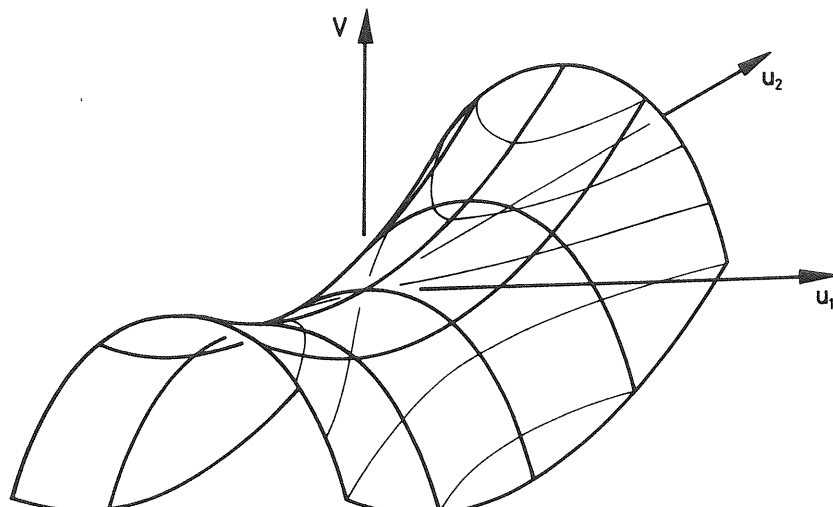


Figure 46 A total potential energy surface showing stability with respect to u_2 but instability with respect to u_1 . Such a surface is called a saddle point

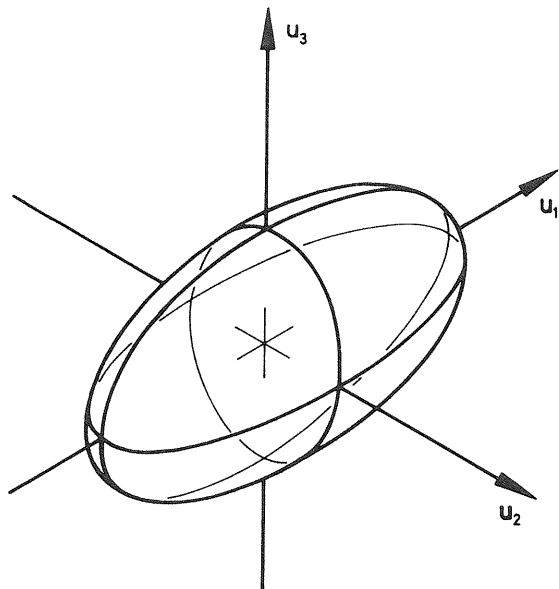


Figure 47 Contour of constant total potential energy about a stable equilibrium state

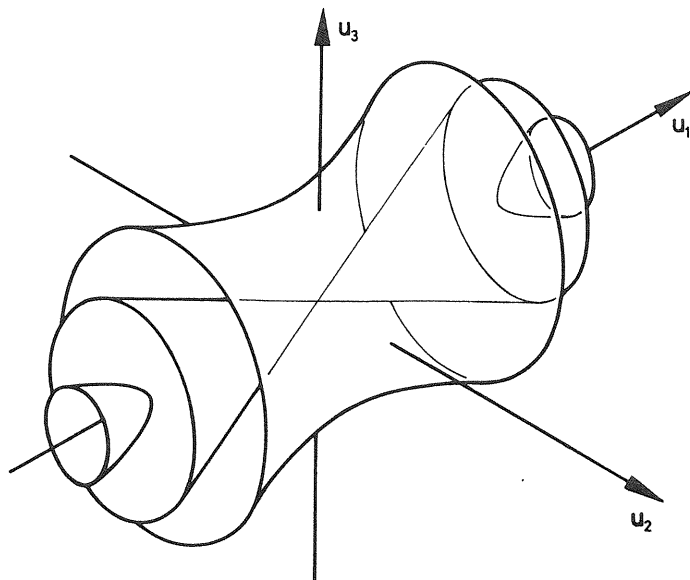


Figure 48 Contours of constant total potential energy showing stability with respect to u_2 and u_3 but instability with respect to u_1 .

unstable with respect to one principal coordinate u_1 and stable with respect to the second principal coordinate u_2 , and thus takes the form of a saddle point. Secondly for 3 degrees of freedom we can draw V -contours in u_i space as shown in Figures 47 and 48; these show stable and unstable equilibrium states respectively. For the stable state of Figure 47, V always increases as we emerge from the equilibrium state, while in Figure 48 we see that V decreases as we emerge from the equilibrium state in the direction u_1 but rises as we proceed in the u_2 or u_3 directions.

Returning to the distinct critical point, we consider the case in which $C_1 = 0$ while $C_s > 0$ for $s \neq 1$. The quadratic form v^2 is thus positive semi-definite, being zero in the *critical direction* defined by

$$u_s = \beta_{sj} q_j = 0 \quad (\text{all } s \neq 1).$$

We employ first the basic coordinates Q_i , and keeping Λ fixed at the value Λ^C we shall examine the variation of V along *all* coordinate paths (not equilibrium paths) leading from the equilibrium state. To do this we write a general path from the equilibrium state in the parametric form

$$Q_i = Q_i(s)$$

where s is some suitable parameter, vanishing at C , which we need not specify.

The variation of V along this path is then given by the defining equality

$$v(s) \equiv V[Q_i(s), \Lambda^C] - V^C$$

and we expand this variation as a function of s as follows

$$v(s) = \dot{v}^C s + \frac{1}{2}\ddot{v}^C s^2 + \frac{1}{6}\dddot{v}^C s^3 + \dots$$

where a dot denotes differentiation with respect to s .

The coefficients of this series are readily obtained by the differentiation of the defining equality with respect to s . Thus

$$\dot{v} \equiv \frac{dv}{ds} = V_i \dot{Q}_i$$

and evaluating at the critical equilibrium state C we have the expected result

$$\dot{v}^C = 0.$$

Differentiating a second time gives

$$\ddot{v} = V_{ij} \dot{Q}_i \dot{Q}_j + V_i \ddot{Q}_i$$

and evaluating we have

$$\ddot{v}^C = V_{ij}^C \dot{Q}_i^C \dot{Q}_j^C.$$

We see that \ddot{v}^c is a positive semi-definite function of the n rates \dot{Q}_j^c , taking a (non-trivial) minimum value of zero for the set of rates associated with the critical direction, which is given by the equations

$$\frac{\partial \ddot{v}^c}{\partial \dot{Q}_r^c} = 2V_{rj}^c \dot{Q}_j^c = 0$$

i.e.

$$V_{ij}^c \dot{Q}_j^c = 0.$$

Paths not starting in the critical direction yield positive values for \ddot{v}^c , and it remains to study higher variations of $v(s)$ along paths starting in the critical direction.

The third differentiation of the defining equality yields

$$\ddot{v} = V_{ijk} \dot{Q}_i \dot{Q}_j \dot{Q}_k + 3V_{ij} \dot{Q}_i \dot{Q}_j + V_i \ddot{Q}_i$$

giving on evaluation for the *critical set of rates*

$$\ddot{v}^c = V_{ijk}^c \dot{Q}_i^c \dot{Q}_j^c \dot{Q}_k^c.$$

If this is non-zero, the critical equilibrium state is clearly unstable. We observe that \ddot{v}^c depends only on the rates and a third variation instability can thus be found by a test along a straight path. Since V is assumed to be well behaved we shall assume that it is adequate to consider only well behaved escape paths: it is unreasonable to suppose that for a well behaved V the most critical escape path should be singular. If \ddot{v}^c is zero we have no decision about the stability of the critical equilibrium state, and higher variations of $v(s)$ must be considered. We shall not pursue this any further in the basic coordinates Q_i , but we now consider the problem afresh in the principal coordinates u_i .

Proceeding as before we write a general coordinate path from the critical equilibrium state C in parametric form, choosing now u_1 (the critical principal coordinate) as the independent variable as follows

$$u_i = u_i(u_1).$$

Here it is understood that $u_1(u_1) = u_1$, and we write

$$u_i^{(1)} = \frac{du_i}{du_1}, \quad u_i^{(2)} = \frac{d^2 u_i}{du_1^2},$$

etc., it again being understood that

$$u_1^{(1)} \equiv \frac{du_1}{du_1} = 1,$$

$$u_1^{(2)} \equiv \frac{d^2 u_1}{du_1^2} = 0,$$

etc., which can be written more neatly as

$$u_1^{(r)} = \delta_{1r},$$

where δ_{ij} denotes the Kronecker delta. Here the bracketed superscript r denotes differentiation r times with respect to u_1 .

The variation of the total potential energy along this path is given by the defining equality

$$d(u_1) \equiv D[u_i(u_1), A^c] - D^c$$

and we expand this variation as a function of u_1 as follows

$$d(u_1) = d_1^c u_1 + \frac{1}{2} d_{11}^c u_1^2 + \frac{1}{6} d_{111}^c u_1^3 + \dots,$$

where

$$d_1^c \equiv \left. \frac{dd}{du_1} \right|_1^c,$$

etc.

The coefficients of this series are readily obtained by the differentiation of the defining equality with respect to u_1 . Thus

$$d_1 = D_i u_i^{(1)}$$

giving at the critical equilibrium state

$$d_1^c = 0.$$

Differentiating a second time we have

$$d_{11} = D_{ij} u_i^{(1)} u_j^{(1)} + D_i u_i^{(2)}$$

giving on evaluation, since D_{ij} is a diagonal form with $D_{11}^c = 0$,

$$d_{11}^c = D_{ss}^c (u_s^{(1)c})^2,$$

with a summation over s from two to n .

We see that d_{11}^c is a positive semi-definite function of the rates, being zero for

$$u_s^{(1)c} = 0 \quad (\text{for all } s \neq 1),$$

and we proceed to study higher variations of $d(u_1)$ under this condition.

Differentiating a third time we have

$$d_{111} = D_{ijk} u_i^{(1)} u_j^{(1)} u_k^{(1)} + 3D_{ij} u_i^{(2)} u_j^{(1)} + D_i u_i^{(3)}$$

giving

$$d_{111}^c = D_{111}^c.$$

If this is non-zero the critical equilibrium state C is clearly unstable, while if this is zero we have no decision. We thus proceed to examine the fourth variation of $d(u_1)$ under the condition that $D_{111}^C = 0$.

Differentiating the defining equality a fourth time we have

$$\begin{aligned} d_{1111} &= D_{ijkl} u_i^{(1)} u_j^{(1)} u_k^{(1)} u_l^{(1)} + 6D_{ijk} u_i^{(2)} u_j^{(1)} u_k^{(1)} \\ &\quad + 4D_{ij} u_i^{(3)} u_j^{(1)} + 3D_{ij} u_i^{(2)} u_j^{(2)} + D_{ii} u_i^{(4)} \end{aligned}$$

giving on evaluation

$$d_{1111}^C = D_{1111}^C + 6D_{s11}^C u_s^{(2)c} + 3D_{ss}^C (u_s^{(2)c})^2,$$

summations on s ranging from two to n . This can be written as

$$d_{1111}^C = D_{1111}^C - 3 \frac{(D_{s11}^C)^2}{D_{ss}^C} + 3D_{ss}^C \left[u_s^{(2)c} + \frac{D_{s11}^C}{D_{ss}^C} \right]^2$$

and we see that we now have d_{1111}^C as a function of the $n - 1$ second derivatives $u_s^{(2)c}$ ($s \neq 1$). This function clearly takes a *minimum* value of

$$\begin{aligned} d_{1111}^C &= D_{1111}^C - 3 \sum_{s=2}^{s=n} \frac{(D_{s11}^C)^2}{D_{ss}^C}, \\ &\equiv \tilde{D}_{1111}^C \quad \text{say,} \end{aligned}$$

when

$$u_s^{(2)c} = -D_{s11}^C / D_{ss}^C \quad (s \neq 1).$$

We see that if \tilde{D}_{1111}^C is positive the critical equilibrium state is stable, while if \tilde{D}_{1111}^C is negative the equilibrium state is unstable. This criterion takes account of the possibility that although the potential energy may increase as we emerge from the critical equilibrium state along all straight coordinate paths, it may in fact decrease along a curved coordinate path, as we shall see in the following example.

Consider the simple diagonalized potential energy function

$$D = 0 \cdot u_1^2 + u_2^2 + u_1^2 u_2 + c u_1^4.$$

Naively we might expect the condition for stability to be that $c > 0$. However by completing a square we may write

$$D = [u_2 + \frac{1}{2}u_1^2]^2 + (c - \frac{1}{4})u_1^4$$

and we see that the first term becomes zero along the curved ray

$$u_2 = -\frac{1}{2}u_1^2.$$

Thus D can take negative values along this curve if $c < \frac{1}{4}$, and so the true condition for stability is that $c > \frac{1}{4}$. A schematic representation of the potential energy for $0 < c < \frac{1}{4}$ is given in Figure 49, and we see that whereas D increases

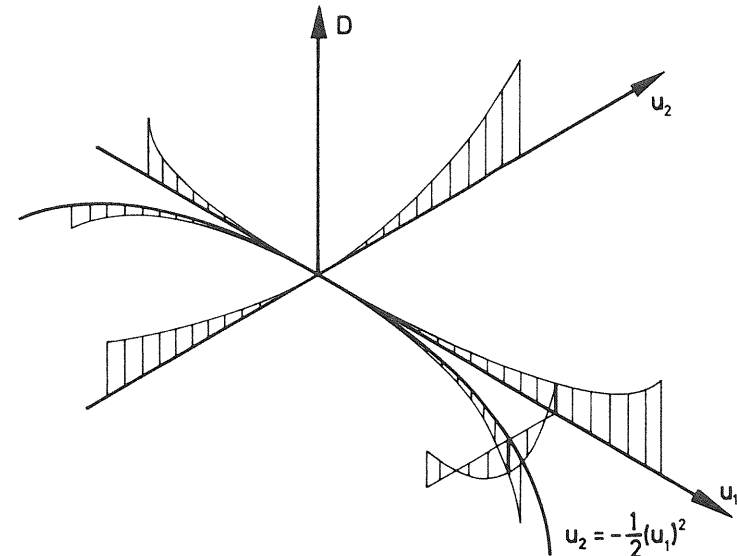


Figure 49 Schematic representation of D for $0 < c < \frac{1}{4}$

as we emerge from C along the u_1 and u_2 axes it decreases along the curved ray $u_2 = -\frac{1}{2}u_1^2$. Applying now the general theory we write

$$D_{11}^C = 0, \quad D_{22}^C = 2,$$

$$D_{1111}^C = 24c, \quad D_{112}^C = 2.$$

Thus

$$\tilde{D}_{1111}^C = 24c - 3 \cdot \frac{4}{2} > 0$$

for stability, and so according to the general theory the true criterion for stability is confirmed to be

$$c > \frac{1}{4}.$$

If the coefficient \tilde{D}_{1111}^C is zero we have no decision and must examine higher variations of $d(u_1)$, but we shall not pursue this problem any further here. The more complex problem of the *compound* critical point, in which more than one stability coefficient is simultaneously zero, is dealt with in general terms in

later chapters. We note that as indicated earlier it is an inherent assumption of this analysis that the expressions $u_i(u_1)$ are analytic functions. A similar, but not identical, treatment of the stability of critical points is given by Sewell.¹³⁹

3.3 Stability of an equilibrium path

Having studied the stability of an equilibrium state we shall now consider the appropriate generalization of the preceding analysis that will allow us to study the stability of an equilibrium path.

We start by writing an equilibrium path of interest in the single-valued parametric form

$$Q_i = Q_i^P(s), \quad \Lambda = \Lambda^P(s),$$

where s is any suitable parameter specifying uniquely the position on the path: one suitable choice of s would of course be the distance along the path. We now introduce a ‘sliding’ set of axes q_i by means of the transformation

$$Q_i = Q_i^P(s) + q_i.$$

We further change coordinates by means of the transformation

$$q_i = \alpha_{ij}(s) u_j, \quad \text{where } |\alpha_{ij}(s)| \neq 0,$$

chosen to diagonalize the quadratic coordinate form of V at every point on the path.

As we have seen before, this diagonalization can be accomplished in an infinite number of ways and we shall suppose that one such way has been chosen, merely insisting that α_{ij} is a continuous and single-valued function of s . In the Λ - Q_i space the u_i -axes will thus slide along the path and in general rotate both as a set and relative to each other to give the axes varying orientation and obliquity.

Substituting these coordinate transformations into the potential energy function we can now obtain a new potential energy function of the principal coordinates u_i , the loading parameter Λ and the path parameter s , which has certain properties arising from its derivation. If the path is single-valued with respect to Λ in the region of interest, we can set $s = \Lambda$ to obtain the Λ -transformation. This transformation has proved invaluable in the discussion of branching points⁶² and will be employed in the later chapters. It is defined with reference to the fundamental path F by the equation

$$A(u_i, \Lambda) \equiv V[Q_i^F(\Lambda) + \alpha_{ij}(\Lambda) u_j, \Lambda]$$

and it thus has the properties arising from its derivation

$$A_i(0, \Lambda) = A'_i(0, \Lambda) = A''_i(0, \Lambda) = \dots = 0,$$

$$A_{ij}(0, \Lambda) = A'_{ij}(0, \Lambda) = A''_{ij}(0, \Lambda) = \dots = 0 \quad \text{for } i \neq j$$

where a prime denotes differentiation with respect to Λ . The stability of any point on the path is now determined by the function

$$A(u_i, \Lambda)$$

and we can write

$$A_{ii}(0, \Lambda) = C_i(\Lambda)$$

to obtain a set of stability coefficients which vary continuously along the path. We see that the degree of instability of a path can only change at a critical equilibrium state for which at least one stability coefficient is equal to zero. A change in the degree of instability, and in particular a loss of initial stability, will thus be characterized by the vanishing of the stability determinants $|V_{ij}|$ and $|A_{ij}|$.

We finally apply a transformation of this type to each equilibrium path, matching the transformations at any point of intersection (bifurcation) so that at the intersection of two or more paths there will be a unique set of u_i -axes. Difficulties may conceivably arise in this scheme, particularly if the equilibrium paths contain closed loops, and we shall simply assume that the scheme can be accomplished in the immediate neighbourhood of any equilibrium state of interest, including those associated with a point of bifurcation.

The concepts developed here will be used in the later chapters to discuss the stability changes that occur in the equilibrium paths passing through a critical equilibrium state. We have in fact intuitively made use of these concepts in the harmonic analysis of the elastica of Chapter 1. Here we have a diagonal quadratic form of potential energy and so the stability coefficients may be written

$$\begin{aligned} C_i(P) &= U_{ii}(0) - P \mathcal{E}_{ii}(0) \\ &= \frac{Bl}{2} \left(\frac{i\pi}{l} \right)^4 - P \frac{l}{2} \left(\frac{i\pi}{l} \right)^2. \end{aligned}$$

Thus the lowest critical load can immediately be found by the vanishing of the first stability coefficient

$$C_1(P) = U_{11}(0) - P^c \mathcal{E}_{11}(0) = 0.$$

Furthermore, in the non-diagonalized finite-element analysis the first critical load is characterized by the vanishing of the stability determinant

$$|W_{ij}^c| = |U_{ij}(0) - P^c \mathcal{E}_{ij}(0)| = 0.$$

3.4 Multi-link model

The concepts developed above are further illustrated in the following analysis of a multi-degree-of-freedom system. Let us therefore consider the

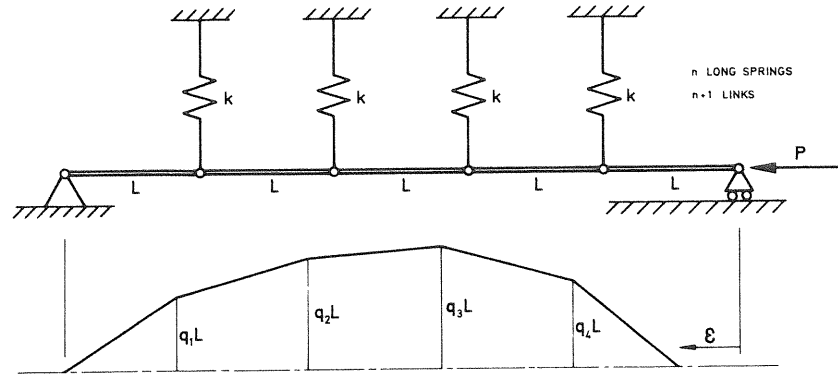


Figure 50 The multi-link model

multi-link model of Figure 50 comprising $n + 1$ rigid links of length L , pinned at their joints, and restrained by the long extensional springs of stiffness k as shown. The load P is assumed to retain its magnitude and direction as the system deflects. The vertical deflections of the internal joints are denoted by q_1L, q_2L, \dots, q_nL as shown, so the total deflected form may be fully represented by specifying the n non-dimensional generalized coordinates q_i . The model is assumed to be perfect in the sense that the springs are unstrained when $q_i = 0$.

The strain energy of the system is

$$U = \frac{1}{2}kL^2(q_1^2 + q_2^2 + \cdots + q_n^2)$$

and the corresponding deflection of the dead load P becomes

$$\begin{aligned} \mathcal{E} &= (n+1)L - L[1 - q_1^2]^{\frac{1}{2}} - L[1 - (q_2 - q_1)^2]^{\frac{1}{2}} - \cdots \\ &\quad - L[1 - (q_{n-1} - q_n)^2]^{\frac{1}{2}} - L[1 - q_n^2]^{\frac{1}{2}} \end{aligned}$$

which may be written

$$\begin{aligned} \mathcal{E} &= \frac{1}{2}L[2q_1^2 + 2q_2^2 + \cdots + 2q_n^2 - 2q_1q_2 \\ &\quad - 2q_2q_3 - \cdots - 2q_{n-1}q_n] + \text{higher-order terms.} \end{aligned}$$

Thus the total potential energy of the system becomes

$$\begin{aligned} V &= \frac{1}{2}kL^2[q_1^2 + q_2^2 + \cdots + q_n^2] \\ &\quad - \frac{PL}{2}[2q_1^2 + 2q_2^2 + \cdots + 2q_n^2 - 2q_1q_2 \\ &\quad - 2q_2q_3 - \cdots - 2q_{n-1}q_n] + \text{higher-order terms.} \end{aligned}$$

We now introduce the diagonalizing transformation

$$q_i = \alpha_{ij} u_j, \quad \text{where } \alpha_{ij} = \sin \frac{ij\pi}{n+1}.$$

The strain energy can now be written

$$U = \frac{1}{2}kL^2 \sum_{i=1}^n q_i^2 = \frac{1}{2}kL^2 \sum_{i=1}^n (\alpha_{ij} u_j)^2,$$

and so the coefficient of $u_l u_m$ becomes

$$\begin{aligned} \frac{1}{2}kL^2 \sum_{i=1}^n \sin \frac{il\pi}{n+1} \sin \frac{im\pi}{n+1} &= 0 \quad \text{if } l \neq m, \\ &= \frac{kL^2(n+1)}{4} \quad \text{if } l = m. \end{aligned}$$

Treating the corresponding deflection of the load in the same way we write

$$\begin{aligned} \mathcal{E} &= \frac{1}{2}L \sum_{i=1}^n 2q_i^2 - \frac{1}{2}L \sum_{i=1}^{n-1} 2q_i q_{i+1} \\ &= \frac{1}{2}L \sum_{i=1}^n 2(\alpha_{ij} u_j)^2 - \frac{1}{2}L \sum_{i=1}^{n-1} 2(\alpha_{ij} u_j)(\alpha_{i+1j} u_j), \end{aligned}$$

and the coefficient of $u_l u_m$ may thus be written as

$$\frac{1}{2}L \sum_{i=1}^n 2\alpha_{il} \alpha_{im} - \frac{1}{2}L \sum_{i=1}^{n-1} 2\alpha_{il} \alpha_{i+1m}.$$

After some algebra we find that this coefficient vanishes if $l \neq m$ and furthermore that the coefficient of u_l^2 becomes

$$L(n+1) \sin^2 \frac{l\pi}{2(n+1)}.$$

The evaluation of these coefficients allows us to write the stability coefficients immediately as

$$C_i(P) = V_{ii} = \frac{kL^2(n+1)}{2} - 2PL(n+1) \sin^2 \frac{i\pi}{2(n+1)}.$$

The critical load P_r^c associated with the r th principal coordinate u_r can therefore be written as

$$P_r^c = \frac{kL}{4 \sin^2 [r\pi/2(n+1)]}.$$

The corresponding buckling mode is given by $u_t = 0$ ($t \neq r$) and hence

$$q_i = \alpha_{ir} u_r = \sin \frac{ir\pi}{n+1} u_r.$$

The buckling modes are thus polygons inscribed within the sin curve

$$\sin \frac{r\pi}{n+1}.$$

The lowest critical load is of course given by

$$P_n^C = \frac{kL}{4 \sin^2 [n\pi/2(n+1)]}$$

and we note that whereas in the case of the Euler strut the lowest critical load is associated with the lowest sin form, in this example the lowest critical load is associated with the highest sin form.

4

NORMAL BEHAVIOUR

4.1 The general system

We now consider equilibrium solutions in the neighbourhood of a normal, that is to say a non-critical, equilibrium state (Q_j^E, Λ^E) . The n equilibrium equations are

$$V_i(Q_j, \Lambda) = 0,$$

and anticipating the existence of an equilibrium path passing through the equilibrium state we write

$$Q_j = Q_j(s), \quad \Lambda = \Lambda(s),$$

with a view to constructing the parametric series solution

$$\begin{aligned} q_j(s) &\equiv Q_j(s) - Q_j^E = \dot{Q}_j(0)s + \frac{1}{2}\ddot{Q}_j(0)s^2 + \dots, \\ \lambda(s) &\equiv \Lambda(s) - \Lambda^E = \dot{\Lambda}(0)s + \frac{1}{2}\ddot{\Lambda}(0)s^2 + \dots. \end{aligned}$$

Here s might represent any suitable parameter defining progress along the path, but we shall in fact assume that s is to be equated to one of the basic variables $q_j = Q_j - Q_j^E$ or $\lambda = \Lambda - \Lambda^E$, the formulation naturally taking a particularly simple and symmetric form if s is equated to the loading parameter λ . A dot is used to denote differentiation with respect to s .

Performing the substitutions, the equilibrium equations must be satisfied at every point on the equilibrium path, so we can write the characterizing equilibrium identity

$$V_i(Q_j(s), \Lambda(s)) \equiv 0.$$

The left-hand side of each equation is now an implicit function of s , so we can differentiate each equation with respect to s as many times as we please. Differentiating once we have

$$V_{ij} \dot{Q}_j + V'_i \dot{\Lambda} = 0,$$

where a prime denotes differentiation with respect to Λ and the dummy-suffix summation convention is employed with all summations ranging from one to n . Differentiating a second time we have

$$(V_{ij} \ddot{Q}_j + V'_{ij} \dot{\Lambda}) \dot{Q}_j + V_{ij} \ddot{\Lambda} + (V'_{ij} \dot{Q}_j + V''_{ij} \dot{\Lambda}) \dot{\Lambda} + V'_i \ddot{\Lambda} = 0,$$

and a third time

$$\begin{aligned} & \{(V_{ijk} Q_i + V'_{ijk} \Lambda) \dot{Q}_k + V_{ijk} \ddot{Q}_k + (V'_{ijk} \dot{Q}_k + V''_{ijk} \Lambda) \dot{\Lambda} + V'_{ij} \ddot{\Lambda}\} \dot{Q}_j \\ & + (V_{ijk} \dot{Q}_k + V'_{ij} \Lambda) \ddot{Q}_j + (V_{ijk} \dot{Q}_k + V'_{ij} \Lambda) \dot{Q}_j + V_{ij} \ddot{Q}_j \\ & + \{(V'_{ijk} \dot{Q}_k + V''_{ijk} \Lambda) \dot{Q}_j + V'_{ij} \ddot{Q}_j + (V''_{ij} \dot{Q}_j + V'''_{ij} \Lambda) \dot{\Lambda} + V'''_{ij} \ddot{\Lambda}\} \dot{\Lambda} \\ & + (V'_{ij} \dot{Q}_j + V''_{ij} \Lambda) \ddot{\Lambda} + (V'_{ij} \dot{Q}_j + V''_{ij} \Lambda) \ddot{\Lambda} + V'_{ij} \ddot{\Lambda} = 0, \end{aligned}$$

etc.

These equations can be evaluated at the equilibrium state (Q^E, Λ^E) , and we shall refer to the *evaluated* equation obtained from the m th differentiation as the m th-order equilibrium equation: in this equation all path derivatives are evaluated at the equilibrium state E . Allowing one of the basic variables, Q_j or Λ , to be independent by equating its increment, q_j or λ , to s , and correspondingly replacing its first derivative with respect to s by unity and its higher derivatives with respect to s by zero, we see that we have generated a series of linear problems which can in principle be solved for the remaining path derivatives.

The first-order equilibrium equations therefore represent a set of linear equations in the remaining first derivatives which can thus be found. These first derivatives can be substituted into the second-order equilibrium equations thereby giving a set of linear equations in the remaining second derivatives which are now readily obtained. The known first and second derivatives can be substituted into the third-order equilibrium equations, thereby giving a set of linear equations in the remaining third derivatives which are likewise readily obtained. In principle all the path derivatives can be obtained sequentially in this manner, and we note that each set of linear equations has the same basic matrix.

Equating s to the loading parameter λ we obtain the more symmetric equations

$$\begin{aligned} V_{ij} Q'_j + V'_i &= 0, \\ (V_{ijk} Q'_k + V'_{ij}) Q'_j + V_{ij} Q''_j + (V'_{ij} Q'_j + V''_i) &= 0, \end{aligned}$$

etc., a prime on the Q_j reminding us that s is now replaced by λ . The determinant of each set of the evaluated equations is now the non-zero stability determinant $|V_{ij}^E|$, so we see that there will be a unique solution for all the path derivatives $Q'_j(0), Q''_j(0), Q'''_j(0), \dots$. There will thus be a *unique* equilibrium path through the non-critical equilibrium state. This corresponds to the well known Kirchhoff uniqueness theorem of small-deflection elasticity.

The variation of the stability determinant $\Delta(Q_k, \Lambda) \equiv |V_{ij}(Q_k, \Lambda)|$ along the equilibrium path can be written as

$$\mathcal{D}(s) \equiv \Delta[Q_i(s), \Lambda(s)]$$

so that we have

$$\dot{\mathcal{D}}(s) = \Delta_i \dot{Q}_i + \Delta' \dot{\Lambda},$$

etc., and this variation can be used to estimate the lowest critical load of a system.^{78,191}

Having evaluated the path derivatives, we can finally construct the parametric equations of the equilibrium path in a series form as indicated earlier. A change in the independent variable is now readily effected, so the independent variable employed in the analysis itself has no lasting significance. The variable can be chosen for purely analytical convenience, and the final results can be readily recast in terms of any other suitable variable. The analysis itself thus has some desirable flexibility, but in the subsequent recasting the choice of independent variable becomes important.

Consider for example the series expansion

$$y(x) = \frac{dy}{dx} \Big|_0^0 x + \frac{1}{2} \frac{d^2 y}{dx^2} \Big|_0^0 x^2 + \frac{1}{6} \frac{d^3 y}{dx^3} \Big|_0^0 x^3 + \dots,$$

which is readily inverted to give

$$x(y) = \frac{dx}{dy} \Big|_0^0 y + \frac{1}{2} \frac{d^2 x}{dy^2} \Big|_0^0 y^2 + \frac{1}{6} \frac{d^3 x}{dy^3} \Big|_0^0 y^3 + \dots,$$

the first m derivatives of x with respect to y depending on the first m derivatives of y with respect to x . If we wish to plot a graph of y against x the first m terms of the $y(x)$ expansion will naturally not yield the same curve as the first m terms of the $x(y)$ expansion. Both curves will normally differ from the true curve represented by $y(x)$ or $x(y)$ although they will both have correct values for the first m derivatives at the origin. The two power series may, moreover, have quite different ranges of convergence. It thus follows that the choice of the independent variable acquires a real significance when an approximate solution is finally constructed from the path derivatives.

The normal behaviour of the system is more readily examined if we employ a diagonalizing transformation, and we shall now repeat the preceding analysis using the D -transformation of the stability analysis. A new energy function is therefore defined as before by the equation

$$D(u_i, \Lambda) \equiv V(Q_i^E + \alpha_{ij} u_j, \Lambda),$$

the matrix α_{ij} diagonalizing the quadratic coordinate form of the potential energy at the equilibrium state E . The n equilibrium equations are now

$$D_i(u_j, \Lambda) = 0,$$

and we write

$$u_j = u_j(s), \quad \Lambda = \Lambda(s),$$

with a view to constructing a parametric series solution as before. Substituting into the equilibrium equations we have the characterizing equilibrium identity

$$D_i[u_j(s), A(s)] \equiv 0,$$

and differentiating repeatedly with respect to s we have

$$\begin{aligned} D_{ij}\dot{u}_j + D'_i\dot{A} &= 0, \\ (D_{ijk}\dot{u}_k + D'_{ij}\dot{A})\dot{u}_j + D_{ij}\ddot{u}_j + (D'_{ij}\dot{u}_j + D''_i\dot{A})\dot{A} + D'_i\ddot{A} &= 0, \end{aligned}$$

etc., as before.

If we evaluate at the equilibrium state E , the equations now take a particularly simple form, since D_{ij}^E is diagonal. Thus the first-order equilibrium equations are simply

$$D_{ii}\dot{u}_i + D'_i\dot{A}|^E = 0 \quad (i = 1, 2, \dots, n),$$

there being now no summations involved, while the second-order equilibrium equations can be written as

$$D_{ijk}\dot{u}_j\dot{u}_k + 2D'_{ij}\dot{u}_j\dot{A} + D_{ii}\ddot{u}_i + D''_i(\dot{A})^2 + D'_i\ddot{A}|^E = 0 \quad (i = 1, 2, \dots, n).$$

These equations are readily solved once s is prescribed, and setting $s = u_1$ for example, we can immediately write down the corresponding rates. Thus setting $i = 1$ in the first-order equilibrium equation we have

$$A^{(1)E} \equiv \frac{dA}{du_1} \Big|_E = -\frac{D_{11}}{D'_1}$$

while setting $i = s \neq 1$ and using this first result we have

$$u_s^{(1)E} \equiv \frac{du_s}{du_1} \Big|_E = \frac{D_{11}D_s}{D_{ss}D'_1} \Big|_E \quad (s = 2, 3, \dots, n).$$

The second derivatives are also readily written down, and we see that the unique equilibrium path passes through the non-critical equilibrium state in a simple fashion. The form of perturbation technique employed in this section is similar to that outlined by Sewell.¹³⁷

4.2 The specialized system

We now consider an important specialization of the preceding general theory in which V is linear in the loading parameter and is written as

$$V(Q_i, P) \equiv U(Q_i) - P\mathcal{E}(Q_i).$$

The normal response of this specialized system exhibits a number of significant features and will now be examined. The preceding general developments

are of course immediately applicable, and we shall employ the original Q_i coordinate system taking the loading parameter, denoted now by P , as the independent variable. Thus equating to zero all energy derivatives involving more than one differentiation with respect to the loading parameter (such as V''_i), we have from the earlier work the ordered equilibrium equations

$$\begin{aligned} V_{ij}Q'_j + V'_i|^E &= 0, \\ V_{ijk}Q'_jQ'_k + 2V'_{ij}Q'_j + V_{ij}Q''_j|^E &= 0, \end{aligned}$$

etc. In these equations a prime now denotes differentiation with respect to P . Alternatively, if we observe that the n equilibrium equations may be written

$$U_i(Q_j) = P\mathcal{E}_i(Q_j),$$

the above equations become

$$\begin{aligned} U_{ij}Q'_j|^E &= \mathcal{E}_i + P\mathcal{E}_{ij}Q'_j|^E, \\ U_{ijk}Q'_jQ'_k + U_{ij}Q''_j|^E &= 2\mathcal{E}_{ij}Q'_j + P\mathcal{E}_{ijk}Q'_jQ'_k + P\mathcal{E}_{ij}Q''_j|^E. \end{aligned}$$

These equations yield three equalities which will be required in the subsequent analysis. Multiplying each equation of the first set by the corresponding rate $Q'_i|^E$ and summing the equations of this set we have the *first equality*

$$V_{ij}Q'_iQ'_j + V'_iQ'_i|^E = 0.$$

Repeating this operation, again on the first set of equations, but now multiplying by the corresponding second derivatives $Q''_i|^E$ we have the *second equality*

$$V_{ij}Q''_iQ'_j + V'_iQ''_i|^E = 0.$$

Multiplying each equation of the second set by the corresponding rate $Q'_i|^E$ and summing the equations of this set we have the *third equality*

$$V_{ijk}Q'_iQ'_jQ'_k + 2V'_{ij}Q'_iQ'_j + V_{ij}Q'_iQ''_j|^E = 0.$$

We consider now the variation of the corresponding deflection, $\mathcal{E}(Q_i)$, along the equilibrium path, writing

$$e(P) \equiv \mathcal{E}[Q_i(P)] - \mathcal{E}^E.$$

The first derivative of e is given by

$$e' = \mathcal{E}'_i Q'_i = -V'_i Q'_i,$$

while the second derivative is given by

$$\begin{aligned} e'' &= \mathcal{E}_{ij}Q'_iQ'_j + \mathcal{E}'_iQ''_i \\ &= -V'_{ij}Q'_iQ'_j - V'_iQ''_i. \end{aligned}$$

Evaluating at the equilibrium state E and using the first equality we find that

$$e'^E \equiv \frac{de}{dP} \Big|_E = V_{ij} Q'_i Q'_j |_E,$$

the first result of interest.

Clearly, if the non-critical equilibrium state E is stable, so that V_{ij}^E is positive definite, the slope e'^E cannot be negative. We thus have the well known result for the specialized system:

The unique equilibrium path passing through a thoroughly stable equilibrium state cannot have a negative slope on a plot of the generalized force against its corresponding deflection.

If we evaluate the second derivative of e at the equilibrium state E and use the second and third equalities we have

$$e''^E \equiv \frac{d^2 e}{dP^2} \Big|_E = -V_{ijk} Q'_i Q'_j Q'_k - 3V'_{ij} Q'_i Q'_j |_E,$$

the second result of interest. We see that we have obtained the second derivative e''^E in terms of the rates Q'_i^E , the second derivatives Q''_i^E having been eliminated. We can thus write for the specialized system:

The curvature of the unique equilibrium path passing through a non-critical equilibrium state on a plot of the generalized force against its corresponding deflection is not dependent on the solution of the second-order equilibrium equations.

A consequence of this result, which will now be proved, is that a one-degree-of-freedom nonlinear Rayleigh–Ritz analysis employing the *current incremental displacement pattern*, will yield the correct path curvature on a plot of P against \mathcal{E} . Considering then such an analysis, the assumed displacement pattern will be given by

$$Q_i = Q_i^E + AK_i,$$

where the K_i are constants related to the true *current rates* by the equations

$$K_i = KQ'_i |_E.$$

Here A is the single free amplitude parameter, and K is an unknown factor. The Rayleigh–Ritz energy function can be written as

$$V(A, P) \equiv V(Q_i^E + AK_i, P),$$

$$U(A) - P\mathcal{E}(A) \equiv U(Q_i^E + AK_i) - P\mathcal{E}(Q_i^E + AK_i)$$

and we have the relations

$$\begin{aligned} V_A &= V_i K_i, & V'_A &= V'_i K_i, \\ V_{AA} &= V_{ij} K_i K_j, & V'_{AA} &= V'_{ij} K_i K_j, \\ V_{AAA} &= V_{ijk} K_i K_j K_k, \end{aligned}$$

a subscript A denoting differentiation with respect to A .

Now the one-degree-of-freedom *analytical model* generated by the nonlinear Rayleigh–Ritz procedure is described by the energy function

$$V(A, P) = U(A) - P\mathcal{E}(A),$$

and we see that this model is itself a member of the class of specialized systems under consideration. The previous results of this section can thus be used to obtain the required Rayleigh–Ritz solutions. The first-order equilibrium equation of the analytical model is therefore

$$V_{AA} A' + V'_A |_E = 0$$

giving

$$V_{ij} K_i K_j A' + V'_i K_i |_E = 0.$$

Remembering that $K_i = KQ'_i |_E$, a comparison with the first equality shows that

$$A'^E = \frac{1}{K}$$

as we would expect.

Employing again the preceding results, the Rayleigh–Ritz prediction for e'^E is

$$\begin{aligned} e'^E &= -V'_A A' |_E \\ &= -\frac{V'_i K_i}{K} |_E \\ &= -V'_i Q'_i |_E, \end{aligned}$$

which agrees with the exact solution, while the Rayleigh–Ritz prediction for the second derivative is

$$\begin{aligned} e''^E &= -V_{AAA}(A')^3 - 3V'_{AA}(A')^2 |_E \\ &= -V_{ijk} Q'_i Q'_j Q'_k - 3V'_{ij} Q'_i Q'_j |_E, \end{aligned}$$

which likewise agrees with the exact solution. We thus have the required result:

A one-degree-of-freedom nonlinear Rayleigh–Ritz analysis about a non-critical equilibrium state employing the correct incremental displacement pattern will yield the correct current slope and the correct current curvature at the equilibrium state on a plot of the generalized force against its corresponding deflection.

A number of similar theorems can be proved for systems exhibiting various forms of symmetry, but these systems will not be considered here.

4.3 The finite-element method

Introduction

It is well known^{77, 147} that the finite-element method using a kinematically-admissible displacement field may be viewed advantageously as an application of the Rayleigh–Ritz procedure with localized rather than overall Rayleigh functions. Bound theorems can be used, and since the Rayleigh amplitudes represent a set of generalized coordinates the results of our general theory can be employed directly. We have chosen to illustrate the finite-element method first via a simple stress analysis problem: the exact solution of the n -degree-of-freedom Rayleigh problem is obtained and is shown to converge uniformly to the continuum solution as n tends to infinity. In this problem we shall emphasize the Rayleigh–Ritz aspect of the finite-element method while in our other illustrative examples involving beams and plates the alternative view is presented and the method is seen as a curve-fitting procedure.

Continuum formulation

The example chosen to illustrate the proposed method of analysis is that of a uniform elastic bar hanging vertically under its own weight, as shown in Figure 51: this will be treated as a small-deflection linear problem so that in a perturbation analysis only the first-order equilibrium equation will give non-trivial results. The bar has the constant cross-sectional area A , Young's Modulus E and density ρ . The original length of the bar is L , and a cross-section originally at a distance x from the support moves down a distance $u(x)$.

The strain energy of the bar can be written as

$$U = \frac{EA}{2} \int_0^L u_x^2 dx$$

where a subscript x denotes differentiation with respect to x . The potential energy of the distributed mass of the bar is

$$J = -\rho A \int_0^L u dx$$

and we write

$$P \equiv \rho A$$

so that P can be regarded as the magnitude of a generalized force acting through the generalized displacement

$$\mathcal{E} \equiv \int_0^L u dx.$$

Setting for convenience $EA = 1$, the total potential energy of the system can be written as

$$V = U - P\mathcal{E}$$

$$= \frac{1}{2} \int_0^L u_x^2 dx - P \int_0^L u dx.$$

We see that V has the form

$$V = \int_0^L F(u_x, u) dx$$

and we now apply the calculus of variations by taking a small increment of V ,

$$\delta V = \int_0^L \left(\frac{\partial F}{\partial u} \delta u + \frac{\partial F}{\partial u_x} \delta u_x \right) dx.$$

We now reverse the order of differentiation of the second term and integrate by parts to obtain

$$\int_0^L \frac{\partial F}{\partial u_x} \delta u_x dx = \int_0^L \frac{\partial F}{\partial u_x} \frac{d}{dx} \delta u dx$$

$$= \left[\frac{\partial F}{\partial u_x} \delta u \right]_0^L - \int_0^L \frac{d}{dx} \frac{\partial F}{\partial u_x} \delta u dx,$$

and so the variation of V becomes

$$\delta V = \left[\frac{\partial F}{\partial u_x} \delta u \right]_0^L + \int_0^L \left(\frac{\partial F}{\partial u} - \frac{d}{dx} \frac{\partial F}{\partial u_x} \right) \delta u dx.$$

Hence we can say that for δV to be zero under any δu we must have

$$\frac{\partial F}{\partial u} - \frac{d}{dx} \frac{\partial F}{\partial u_x} = 0,$$

and the square bracket must be eliminated by the appropriate choice of boundary conditions. The above equation is therefore the Euler equation of the problem and the physical boundary conditions

$$u(0) = 0,$$

$$u_x(L) = 0,$$

ensure that the square bracket vanishes. Performing the differentiations, the exact solution to the Euler equation is readily found to be

$$u = Px(L - \frac{1}{2}x)$$

and is shown in Figure 51.

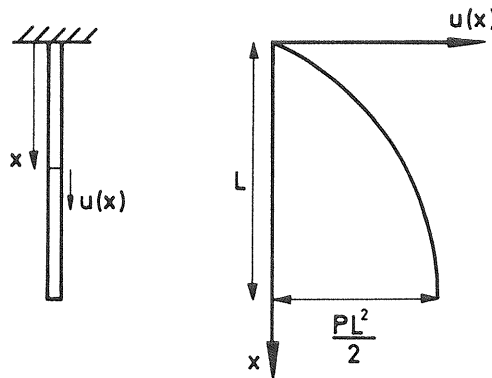


Figure 51 Continuum solution for the hanging bar

Localized Ritz formulation

To obtain an approximate solution of the problem by the conventional Rayleigh–Ritz procedure it would be necessary to write the function $u(x)$ in the form

$$u(x) = \sum_i Q_i f_i(x),$$

the functions $f_i(x)$ satisfying the geometrical boundary conditions of the problem, so that the amplitudes Q_i can be regarded as a set of generalized coordinates. In a classical Rayleigh–Ritz analysis each $f_i(x)$ would be a continuous function running from $x = 0$ to $x = L$, but it is the essence of the finite-element method of analysis to choose discontinuous functions each of which is non-zero only in the region of an associated station. We thus introduce n numbered stations along the bar as shown in Figure 52, making $f_i(x)$, the localized Rayleigh function associated with a typical station i , non-zero only in the region between the neighbouring stations $i - 1$ and $i + 1$.

Since the energy functional contains u and u_x but no higher derivatives, we must clearly make each localized Rayleigh function continuous in x but can tolerate discontinuities in the first- and higher-order derivatives. Further, we need give each station only one degree of freedom corresponding to a free choice of the displacement u . The simplest localized Rayleigh functions that we can choose will then be piecewise linear as shown in Figure 52.

These can be contrasted with the functions which must be used for the normal displacement $w(x)$ of a beam under bending. The energy integral for the beam will contain the second derivative w_{xx} , so that we can no longer tolerate discontinuities in the first derivative w_x . We must then apparently give each station

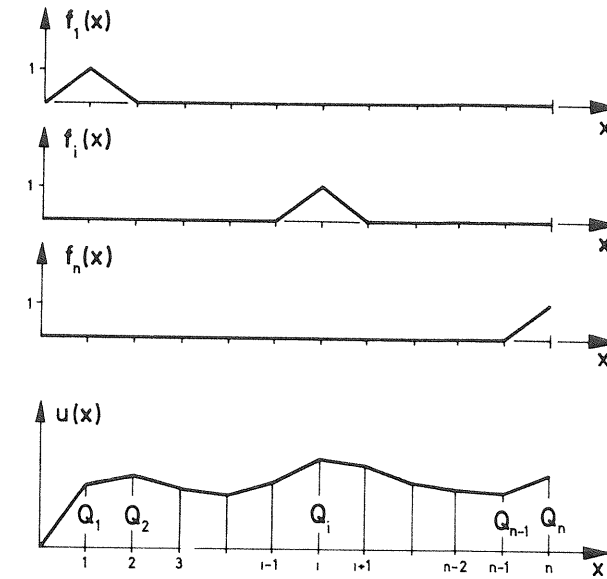


Figure 52 Localized Rayleigh functions for the hanging bar

two degrees of freedom corresponding to a free choice of both the displacement w and its first derivative w_x . That is to say we must associate two localized Rayleigh functions $f_i^0(x)$ and $f_i^x(x)$ with a typical station i , these functions having the forms of those shown in Figure 53. Simple polynomials are normally used to generate these functions, which can be allowed to have discontinuities in

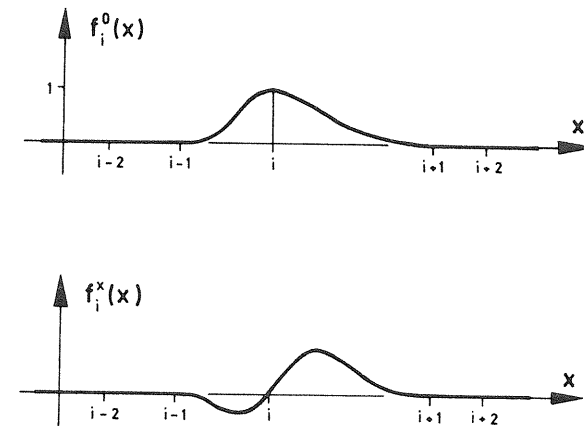


Figure 53 Localized Rayleigh functions for a beam or strut

their second derivatives at the stations. We note that equivalent polynomial functions have in fact been employed in the finite-element study of the elastica presented in Chapter 1.

We have so far restricted our attention to localized Rayleigh functions for one displacement function (u for the bar, w for the beam) in one variable (x), and so we shall now briefly discuss the extension to more complex problems. In a two-dimensional plane stress problem in the rectangular coordinates

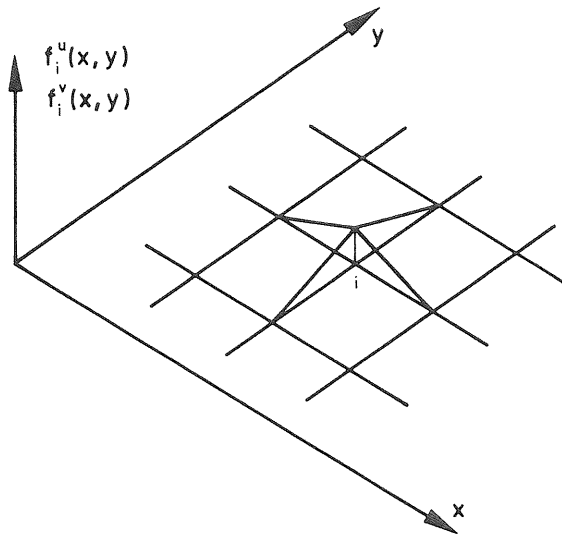


Figure 54 Localized Rayleigh functions for a plane stress problem

(x, y) we might for example draw a rectangular mesh to give us a rectangular array of stations as shown in Figure 54. We can then introduce two sets of localized Rayleigh functions for the two in-plane displacements $u(x, y)$ and $v(x, y)$. We can tolerate discontinuities in the first derivatives, and for a given displacement (u say) we need perhaps give a station only a single degree of freedom corresponding to a free choice of that displacement. The two sets could then be composed of localized Rayleigh functions with the form of that shown in Figure 54.

Considering secondly the choice of the normal displacement function $w(x, y)$ for the bending of a plate, we might again introduce a rectangular array of stations as shown in Figure 55. Clearly we cannot here tolerate discontinuities in the first derivatives, and it seems that we must give each station at least four degrees of freedom corresponding to a free choice of the displacement w , its first derivatives w_x and w_y , and the cross-derivative w_{xy} , as shown in Figure 55.

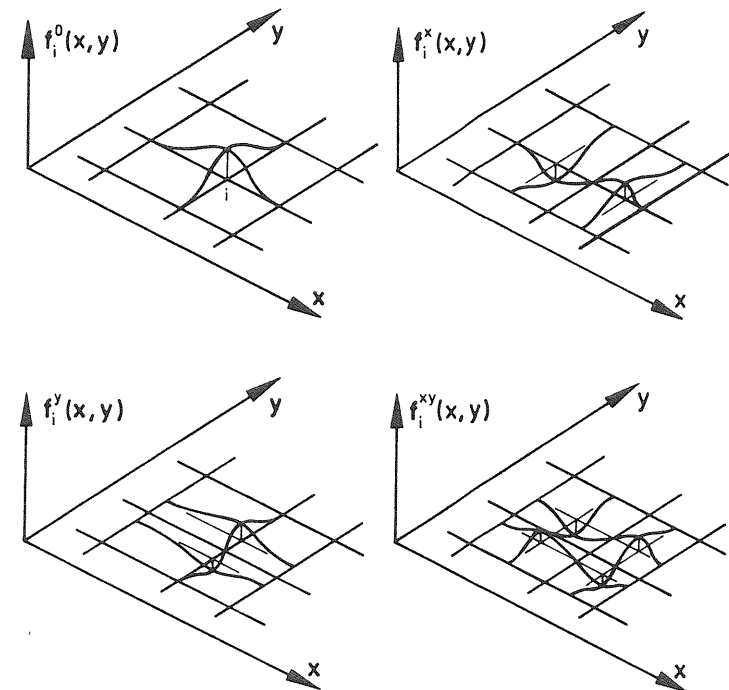


Figure 55 Localized Rayleigh functions for a plate in bending

Finite-element solution

Returning to the bar, and having chosen a set of n Rayleigh functions $f_i(x)$, we can now follow the normal Rayleigh–Ritz procedure. Thus substituting our assumed form for $u(x)$ into the energy integral we obtain

$$V(Q_i, P) = U(Q_i) - P\mathcal{E}(Q_i)$$

and since U will be a quadratic and \mathcal{E} a linear function of the Q_i we can write

$$V(Q_i, P) = \frac{1}{2}U_{ij}Q_iQ_j - P\mathcal{E}_iQ_i.$$

Here the dummy-suffix summation convention is employed with all summations ranging from one to n , and a subscript i denotes differentiation with respect to Q_i . We note that this energy function has the typical form for a small-deflection linear analysis of continuum elasticity. The n equilibrium equations are now

$$V_i(Q_j, P) = U_{ij}Q_j - P\mathcal{E}_i = 0$$

or in matrix form

$$[U_{ij}][Q_j] = P[\mathcal{E}_i].$$

We now proceed to solve these equations for the problem in hand. For convenience we specify that the stations be equally spaced, so that each local region of the bar has length L/n . Then, identifying a local region by the number of its right-hand station, we see that the potential energy associated with a typical region i is

$$V^i = \frac{1}{2} \frac{n}{L} (Q_i^2 - 2Q_i Q_{i-1} + Q_{i-1}^2) - \frac{1}{2} P \frac{L}{n} (Q_i + Q_{i-1})$$

so that

$$V = \sum_{i=1}^{i=n} V^i$$

where Q_0 is to be identified as zero. Thus the equilibrium equations become

and we see that these equations are satisfied by the values of u predicted to exist at the stations by the exact continuum solution. That is to say the equations are satisfied if we write

$$u\left(\frac{iL}{n}\right) = P \frac{iL}{n} \left(L - \frac{iL}{2n}\right) = Q_i.$$

It follows that the Rayleigh–Ritz solutions have the character of inscribed polygons, as shown in Figure 56, and we see that the solutions will thus converge to the continuum solution as n tends to infinity. Considering the solutions for $n = 1, 2, 4, 8, \dots$, we see that this convergence satisfies the well known bound theorem, the value of the generalized deflection

$$\mathcal{E} \equiv \int_a^L u \, dx$$

increasing monotonically with n for a given value of its generalized force P .

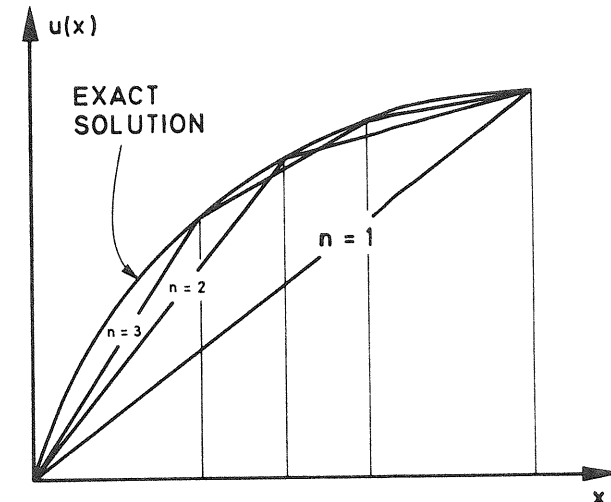


Figure 56 Continuum and finite-element solutions for the hanging bar

4.4 The laterally-loaded beam

Introduction

To conclude this treatment of the normal behaviour of structural systems we shall illustrate the perturbation method of the general theory: we shall present harmonic and finite-element analyses of a simply-supported beam suffering large bending deflections under a lateral point load at its centre. An exact beam formulation is employed, and a *continuum* perturbation analysis is presented for comparison. The first seven path derivatives are evaluated and are observed to converge rapidly in each case to the continuum values, which are then used to construct the load-deflection curve of the beam. The curve obtained depends on the independent variable employed in this final construction, and two curves are drawn using the load and its corresponding deflection respectively. Both curves are shown to be in good agreement with the known nonlinear solution for central deflections up to about one-fifth of the length of the beam.

It is concluded that the perturbation analysis will be a useful tool in problems of moderate nonlinearity.

Energy formulation

Consider the beam of Figure 57, of length l , simply-supported as shown, and loaded by the lateral force P which retains its magnitude and direction as the beam deflects. The beam is assumed to be axially inextensional, and the relevant bending stiffness is denoted by B .

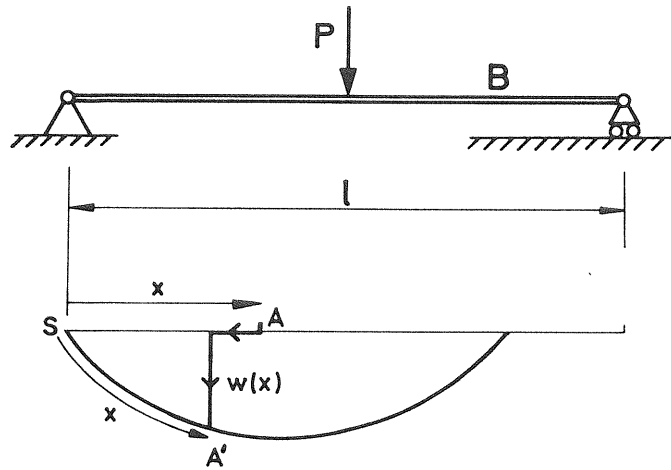


Figure 57 The laterally-loaded beam

The exact large-deflection strain energy formulation for the beam is identical to the elastica expression of Chapter 1 given by equation (1.1), and so we can write the strain energy directly as

$$U = \frac{1}{2}B \int_0^l (\ddot{w}^2 + \dot{w}^2 \dot{w}^2 + \dot{w}^2 \dot{w}^4 + \dots) dx,$$

while the corresponding deflection of the dead load P is

$$\mathcal{E} = w \left(\frac{l}{2} \right).$$

The total potential energy of the beam is thus

$$\begin{aligned} V &= U - P\mathcal{E} \\ &= \frac{1}{2}B \int_0^l (\ddot{w}^2 + \dot{w}^2 \dot{w}^2 + \dot{w}^2 \dot{w}^4 + \dots) dx - Pw \left(\frac{l}{2} \right), \end{aligned}$$

and taking advantage of the symmetry of the beam this may alternatively be written

$$V = B \int_0^{l/2} (\ddot{w}^2 + \dot{w}^2 \dot{w}^2 + \dot{w}^2 \dot{w}^4 + \dots) dx - Pw \left(\frac{l}{2} \right)$$

Continuum analysis

We see that the total potential energy has the form

$$V = B \int_0^{l/2} F(\ddot{w}, \dot{w}) dx - Pw \left(\frac{l}{2} \right).$$

We now apply the calculus of variations by taking a small increment of V ,

$$\delta V = B \int_0^{l/2} \left(\frac{\partial F}{\partial \ddot{w}} \delta \ddot{w} + \frac{\partial F}{\partial \dot{w}} \delta \dot{w} \right) dx - P \delta w \left(\frac{l}{2} \right).$$

Reversing the order of differentiation and integrating by parts, as with the analysis of the elastica, the second term of the integral may be written

$$\int_0^{l/2} \frac{\partial F}{\partial \dot{w}} \delta \dot{w} dx = \left[\frac{\partial F}{\partial \dot{w}} \delta w \right]_0^{l/2} - \int_0^{l/2} \frac{d}{dx} \frac{\partial F}{\partial \dot{w}} \delta w dx.$$

Similarly, the first term becomes

$$\int_0^{l/2} \frac{\partial F}{\partial \ddot{w}} \delta \ddot{w} dx = \left[\frac{\partial F}{\partial \ddot{w}} \delta \dot{w} \right]_0^{l/2} - \left[\frac{d}{dx} \frac{\partial F}{\partial \ddot{w}} \delta w \right]_0^{l/2} + \int_0^{l/2} \frac{d^2}{dx^2} \frac{\partial F}{\partial \ddot{w}} \delta w dx.$$

Thus the increment of V becomes

$$\begin{aligned} \delta V &= B \left[\frac{\partial F}{\partial \ddot{w}} \delta w \right]_0^{l/2} + B \left[\frac{\partial F}{\partial \dot{w}} \delta \dot{w} \right]_0^{l/2} - B \left[\frac{d}{dx} \frac{\partial F}{\partial \ddot{w}} \delta w \right]_0^{l/2} \\ &\quad + B \int_0^{l/2} \left(\frac{d^2}{dx^2} \frac{\partial F}{\partial \ddot{w}} - \frac{d}{dx} \frac{\partial F}{\partial \dot{w}} \right) \delta w dx - P \delta w \left(\frac{l}{2} \right). \end{aligned}$$

Hence we may say that for δV to be zero under any δw we must have

$$\frac{d^2}{dx^2} \frac{\partial F}{\partial \ddot{w}} - \frac{d}{dx} \frac{\partial F}{\partial \dot{w}} = 0,$$

and the remaining terms must be eliminated by appropriate boundary conditions. The above equation is therefore the Euler equation for the beam. The physical boundary conditions are first

$$w(0) = \dot{w} \left(\frac{l}{2} \right) = 0$$

and secondly that the bending moment is zero at $x = 0$. The curvature at $x = 0$ is thus zero and from the large-deflection curvature relationship we obtain

$$\ddot{w}(0) = 0.$$

The first two terms in square brackets vanish by virtue of these physical boundary conditions. For the remaining term we write

$$-B \left[\frac{d}{dx} \frac{\partial F}{\partial \dot{w}} \delta w \right]_0^{l/2} - P \delta w \left(\frac{l}{2} \right) = 0.$$

Performing the differentiations, whilst bearing in mind that $\delta w = 0$ at $x = 0$ and $\dot{w} = 0$ at $x = l/2$, this may be written

$$P = -2B\ddot{w}\left(\frac{l}{2}\right).$$

We note that this is the only expression involving P that we will require in the following analysis; we can therefore solve the problem without mention of P and then use the above expression to evaluate the coefficients of the power series expansions

$$\begin{aligned} P(\mathcal{E}) &= C_1 \mathcal{E} + C_2 \mathcal{E}^2 + C_3 \mathcal{E}^3 + \dots, \\ \mathcal{E}(P) &= D_1 P + D_2 P^2 + D_3 P^3 + \dots. \end{aligned}$$

Making use of the calculus of variations we have thus found the Euler equation of the beam and justified the physical boundary conditions of the problem.

Performing the differentiations and expanding the resulting expressions as power series, the Euler equation becomes

$$\begin{aligned} \ddot{w}[1 + \dot{w}^2 + \dot{w}^4 + \dots] \\ + 4\ddot{w}\dot{w}\dot{w}[1 + 2\dot{w}^2 + 3\dot{w}^4 + \dots] \\ + \dot{w}^3[1 + 6\dot{w}^2 + 15\dot{w}^4 + \dots] = 0. \end{aligned}$$

The associated boundary conditions remain

$$w(0) = \dot{w}(0) = \ddot{w}\left(\frac{l}{2}\right) = 0,$$

$$P = -2B\ddot{w}\left(\frac{l}{2}\right).$$

To start a continuum perturbation analysis we write

$$w(x) = w_1(x)s + w_2(x)s^2 + w_3(x)s^3 + \dots,$$

so that

$$\dot{w}(x) = \dot{w}_1(x)s + \dot{w}_2(x)s^2 + \dot{w}_3(x)s^3 + \dots,$$

etc. Here s is some suitable perturbation parameter, as yet undefined. The boundary conditions now become

$$\begin{aligned} w_i(0) = \dot{w}_i(0) = \ddot{w}_i\left(\frac{l}{2}\right) &= 0, \\ P &= -2B[\dot{w}_1(x)s + \dot{w}_2(x)s^2 + \dot{w}_3(x)s^3 + \dots]^{l/2}. \end{aligned}$$

Setting $s = \mathcal{E}$, the central deflection of the beam, we obtain the 'false' boundary condition

$$\begin{aligned} w_1\left(\frac{l}{2}\right) &= 1, \\ w_s\left(\frac{l}{2}\right) &= 0 \quad \text{for } s \neq 1. \end{aligned}$$

If we substitute the series forms for the w derivatives into the Euler equation and write this equation as a power series in s , we see that we can equate the coefficients to zero to generate an ordered series of equilibrium equations. These equilibrium equations are sequentially linear and are readily solved for the $w_i(x)$, the first five of these functions being determined in the present work.

Thus equating the coefficient of s to zero gives us the first-order equilibrium equation

$$\ddot{w}_1 = 0$$

which is the well known small-deflection equation and yields with the boundary conditions the solution

$$w_1(x) = -\frac{1}{2(l/2)^3} x^3 + \frac{3}{2(l/2)} x.$$

Equating the coefficient of s^2 to zero gives us the second-order equilibrium equation $\ddot{w}_2 = 0$ which with the boundary conditions gives the expected result $w_2(x) = 0$. The third-order equation is

$$\ddot{w}_3 + 4\ddot{w}_1 \dot{w}_1 \dot{w}_1 + \dot{w}_1^3 = 0$$

giving

$$w_3(x) = \frac{1}{280} \left[\frac{27}{(l/2)^9} x^7 - \frac{126}{(l/2)^7} x^5 + \frac{171}{(l/2)^5} x^3 + \frac{72}{(l/2)^3} x \right].$$

The fourth-order equation yields the expected result $w_4(x) = 0$, while the fifth-order problem yields

$$w_5(x) = -\frac{0.0184}{(l/2)^{15}} x^{11} + \frac{0.145}{(l/2)^{13}} x^9 - \frac{0.329}{(l/2)^{11}} x^7 + \frac{0.164}{(l/2)^9} x^5 + \frac{0.173}{(l/2)^7} x^3 - \frac{0.134}{(l/2)^5} x.$$

The coefficients of the power series $P(\mathcal{E})$ can be established directly from the fourth boundary condition

$$P = -2B \left[\ddot{w}_1 \left(\frac{l}{2} \right) s + \ddot{w}_2 \left(\frac{l}{2} \right) s^2 + \ddot{w}_3 \left(\frac{l}{2} \right) s^3 + \dots \right].$$

Remembering that $s = \mathcal{E}$ the coefficients of the $P(\mathcal{E})$ series are given by

$$C_i = -2B\ddot{w}_i \left(\frac{l}{2} \right),$$

and we note that the i th coefficient may be obtained directly from the i th equilibrium equation without its complete solution. To achieve this we multiply the equation by w_1 and integrate over the half-length of the beam. The recurring term \ddot{w}_i thus becomes

$$\int_0^{l/2} \ddot{w}_i w_1 dx$$

and integration by parts shows that this equals $\ddot{w}_i(l/2)$. This then gives $\ddot{w}_i(l/2)$ as the integral of an expression containing derivatives of $w_j(x)$, where $j < i$; C_i can thus be easily evaluated. For example C_3 can be written as

$$C_3 = -2B\ddot{w}_3 \left(\frac{l}{2} \right) = 2B \int_0^{l/2} (4\ddot{w}_1 \dot{w}_1 \dot{w}_1 w_1 + \ddot{w}_1^3 w_1) dx = 6.17 \frac{B}{(l/2)^5}$$

from the third-order equilibrium equation. We have here evaluated the first seven C_i on the basis of the first five $w_i(x)$ and the results are shown in Table 4.1 together with the readily derived inverse coefficients D_i .

Harmonic analysis

To perform a harmonic analysis of the beam we must first express $w(x)$ as a harmonic expansion. Employing the symmetry of the beam we thus write

$$w = \sum_{i=1,2}^{i=n} Q_i \sin \frac{I\pi x}{l}$$

where $I \equiv 2i - 1$, and substituting this form into the energy functional gives us an algebraic energy function of the form

$$\begin{aligned} V(Q_i, P) &= U(Q_i) - P\mathcal{E}(Q_i) \\ &= (\frac{1}{2} U_{ij}(0) Q_i Q_j + \frac{1}{24} U_{ijkl}(0) Q_i Q_j Q_k Q_l + \dots) - P\mathcal{E}_i(0) Q_i \end{aligned}$$

TABLE 4.1 Perturbation coefficients from the continuum analysis

C_1	C_3	C_5	C_7
$6 \frac{B}{(l/2)^3}$	$6.17 \frac{B}{(l/2)^5}$	$7.18 \frac{B}{(l/2)^7}$	$8.65 \frac{B}{(l/2)^9}$
D_1	D_3	D_5	D_7
$\frac{(l/2)^3}{6B}$	$-4.76 \times 10^{-3} \frac{(l/2)^7}{B^3}$	$2.54 \times 10^{-4} \frac{(l/2)^{11}}{B^5}$	$-1.66 \times 10^{-5} \frac{(l/2)^{15}}{B^7}$

The coefficients of this function are given by

$$\begin{aligned} \mathcal{E}_i(0) &= \sin \frac{I\pi}{2} = (-1)^{i+1}, \\ U_{ij}(0) &= BI^2 J^2 \left(\frac{\pi}{l} \right)^4 \int_0^l \sin \frac{I\pi x}{l} \sin \frac{J\pi x}{l} dx \\ &= 0 \quad \text{for } i \neq j \\ &= \frac{Bl}{2} \left(\frac{I\pi}{l} \right)^4 \text{ for } i = j, \\ U_{ijkl}(0) Q_i Q_j Q_k Q_l &= 12B \left(\frac{\pi}{l} \right)^6 \sum_i \sum_j \sum_k \sum_l I^2 J^2 K L Q_i Q_j Q_k Q_l \\ &\quad \times \int_0^l \sin \frac{I\pi x}{l} \sin \frac{J\pi x}{l} \cos \frac{K\pi x}{l} \cos \frac{L\pi x}{l} dx, \end{aligned}$$

etc. Here, as in the elastica analysis, it has been necessary to include summations in the equality associated with $U_{ijkl}(0)$, since the U derivatives are necessarily symmetric while the integrals are not; again this fact presents no real difficulty, although some care must naturally be exercised.

We now have an energy function with the form of the specialized system of Section 4.2, so the general theory of this chapter can be directly employed. Taking P as the independent variable, and evaluating the equilibrium equations at the unloaded state 0, we see that the diagonalization of $U_{ij}(0)$ allows the direct solution of each of the ordered series of equilibrium equations. The first equilibrium equation thus gives

$$\frac{Bl}{2} \left(\frac{I\pi}{l} \right)^4 Q'_i|_0 = (-1)^{i+1}$$

so that

$$Q'_i|_0 = \frac{2(-1)^{i+1}}{Bl(I\pi/l)^4}$$

and

$$\begin{aligned}\mathcal{E}'^0 = \mathcal{E}_i Q_i'^0 = D_1 &= \frac{2}{Bl(\pi/l)^4} \sum_{i=1}^{l=n} I^{-4} \\ &= \frac{2}{Bl(\pi/l)^4} \left\{ 1 + \frac{1}{3^4} + \frac{1}{5^4} + \dots \right\} \\ &= \frac{l^3}{48B}.\end{aligned}$$

The second evaluated equilibrium equation gives $Q_i''^0 = \mathcal{E}''^0 = 0$, and the third equation yields

$$\begin{aligned}\mathcal{E}'''^0 &= 6D_3 \\ &= -\frac{192l^7}{B^3\pi^{10}} \sum_i \sum_j \sum_k \sum_l \frac{(-1)^{i+j+k+l}}{I^2 J^2 K^3 L^3} \int_0^l \sin \frac{I\pi x}{l} \sin \frac{J\pi x}{l} \cos \frac{K\pi x}{l} \cos \frac{L\pi x}{l} dx.\end{aligned}$$

Higher derivatives are readily written down, and the first seven have been evaluated on a computer, the corresponding series converging rapidly to the continuum solutions with increasing n .

Finite-element analysis

As a second illustration of the general perturbation theory of Section 4.1 we shall now outline a finite-element analysis of the laterally-loaded beam using a kinematically-admissible displacement field. As we have seen, such an analysis can be viewed advantageously as a straightforward application of the Rayleigh–Ritz energy procedure with localized rather than with overall Rayleigh functions. The analysis will thus follow closely the harmonic Rayleigh–Ritz analysis with localized functions replacing the overall functions.

Considering then the displacement function $w(x)$ for the whole beam, we introduce stations along the x -axis as shown in Figure 58, one station being at the loaded mid-point. Each internal station is given an arbitrary displacement w and an arbitrary first derivative \dot{w} , while corresponding to the boundary conditions of the problem the terminal stations are given an arbitrary first derivative but no displacement. The totality of the arbitrary displacements and derivatives represent the generalized coordinates of the beam and are denoted by Q_i . A third-order polynomial is now fitted in each region, giving an overall deflected form which is continuous in displacement and first derivative, but which admits discontinuities in its second derivative at the stations.

Substituting this expression for $w(x)$ into the energy functional gives us an algebraic energy function with the form of that of the harmonic analysis, so the general theory of the specialized system can again be directly employed.

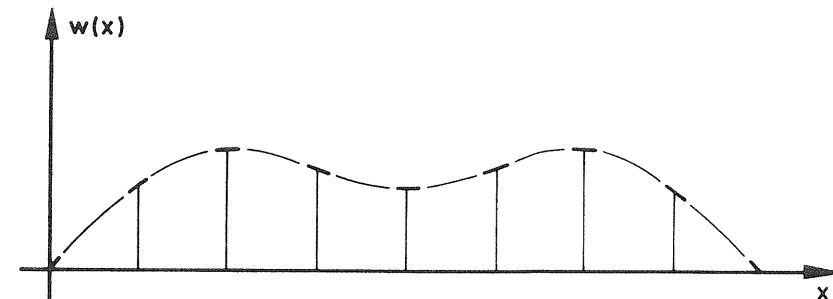


Figure 58 Finite-element fabrication of $w(x)$

Now, however, the quadratic form associated with $U_{ij}(0)$ is not diagonal, so the series of linear problems must be solved on a computer. The first seven have been solved in the present study, the displacement of the central station being used as the independent variable. The first two path derivatives were found to agree with the continuum values for a single internal station, while the higher path derivatives were observed to converge rapidly to the continuum values with increasing number of stations.

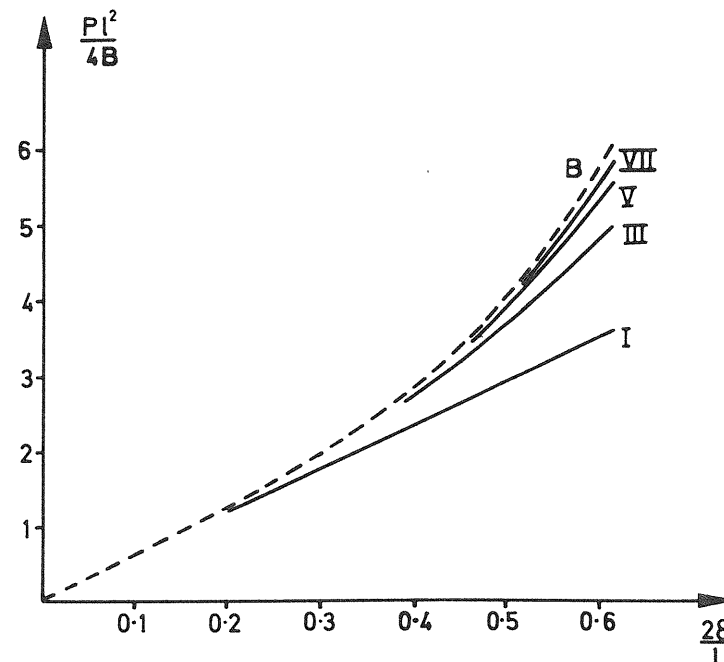


Figure 59 Perturbation solutions with ϵ as the independent variable

Perturbation solutions

The two Rayleigh-Ritz analyses, namely the harmonic analysis and the finite-element analysis, yield perturbation coefficients C_i and D_i which converge rapidly to those of the continuum analysis, so we shall here focus attention on the latter which are recorded in Table 4.1. If we first take \mathcal{E} as our independent variable and truncate the $P(\mathcal{E})$ expansion after one, three, five and seven terms we obtain the curves I, III, V and VII of Figure 59, in which B represents the known nonlinear beam solution.¹⁹² The perturbation solutions are seen to approach this exact solution monotonically, the seventh-order solution yielding close agreement with B for central deflections up to one quarter of the length of the beam.

Secondly, taking P as our independent variable and truncating the $\mathcal{E}(P)$ expansion after one, three, five and seven terms, we obtain the curves I, III, V and VII of Figure 60, in which B again represents the known nonlinear solution. The perturbation solutions are now seen to band this exact solution in an oscillatory fashion with an apparent divergence at large deflections.

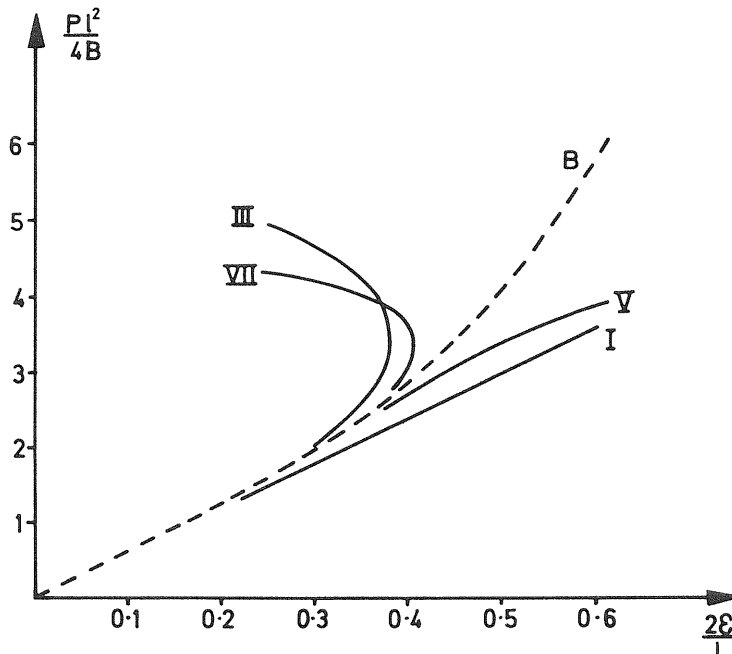


Figure 60 Perturbation solutions with P as the independent variable

Remembering that these two figures represent the results of the same perturbation analysis, the contrast is surprising indeed, and emphasizes the key role of the final expansion.

5

CRITICAL BEHAVIOUR

5.1 Introduction

In the previous chapter we have examined the equilibrium solutions around a non-critical equilibrium state, and we have seen that there will always be a unique path through such a state. We must now turn our attention to critical equilibrium states, and the examples of Chapters 1 and 2 show that uniqueness will not now be ensured.

More specifically the contribution of this chapter is to examine the limit point and the three basic branching points in a single analysis using a principal coordinate frame tied to the critical equilibrium state. Such a treatment will spotlight the interrelationships between these four distinct critical points and will allow us to classify them in a systematic manner. We shall see that the limit point is in a mathematical sense the most usual way for a structural system to lose its stability.

The chapter is thus concerned with the *delineation of phenomena*, and it must be emphasized that the forms of analysis used here are not appropriate for the structural analyst. The use of coordinates measured from a limit point is hardly appropriate if it is the limit point that we are trying to find: and for a branching point the use of a fixed set of axes is not usually the best analytical approach. This having been said, the busy analyst may prefer to skip this chapter on first reading, but it is hoped that he might return to it at a later stage to gain some insight into the basic phenomena of elastic stability.

5.2 Perturbation equations

We shall examine now the equilibrium solutions in the vicinity of a distinct critical equilibrium state (Q_i^C, Λ^C) , this being defined by the vanishing of a single stability coefficient: the more complex critical behaviour arising at a compound critical point at which *more than one* stability coefficient is zero will be examined towards the end of the book. Here we shall employ the diagonalized energy function D defined as before by the equation

$$D(u_i, \Lambda) \equiv V(Q_i^C + \alpha_{ij} u_j, \Lambda)$$

and we shall suppose that $D_{11}^C = 0$ while $D_{ss}^C \neq 0$ for $s \neq 1$.

We now seek to express any equilibrium paths emanating from the critical point C in parametric form, and we shall take the critical principal coordinate u_1 as the independent variable, writing the paths as

$$u_j = u_j(u_1), \quad \Lambda = \Lambda(u_1).$$

Substituting these into the equilibrium equation $D_i = 0$ and differentiating repeatedly with respect to u_1 as before, we have the ordered equilibrium equations

$$D_{ii} u_i^{(1)} + D'_i \Lambda^{(1)}|^C = 0,$$

$$D_{ijk} u_k^{(1)} u_j^{(1)} + 2D'_{ij} u_j^{(1)} \Lambda^{(1)} + D_{ii} u_i^{(2)} + D''_i (\Lambda^{(1)})^2 + D'_i \Lambda^{(2)}|^C = 0,$$

etc., where $i = 1, 2, \dots, n$. Here, as earlier,

$$u_j^{(1)} \equiv \frac{du_j}{du_1}, \quad u_j^{(2)} \equiv \frac{d^2 u_j}{du_1^2},$$

so that

$$u_1^{(1)} = 1, \quad u_1^{(2)} = 0.$$

The stability determinant

$$\Delta(u_k, \Lambda) \equiv |D_{ij}(u_k, \Lambda)|$$

will vary along any equilibrium path, and substituting our parametric forms we write

$$\mathcal{D}(u_1) \equiv \Delta[u_i(u_1), \Lambda(u_1)].$$

The first variation of \mathcal{D} is therefore given by

$$\mathcal{D}'^{(1)} \equiv \frac{d\mathcal{D}}{du_1} = \Delta_i u_i^{(1)} + \Delta' \Lambda^{(1)}.$$

Now D_{ij} is diagonal at C with $D_{11}^C = 0$; thus differentiating Δ by columns with respect to either u_i or Λ and evaluating at C , only the leading determinant remains and we have

$$\Delta_i^C = D_{111} D_{22} D_{33} \cdots D_{nn}|^C,$$

$$\Delta'^C = D'_{11} D_{22} D_{33} \cdots D_{nn}|^C,$$

giving

$$\mathcal{D}'^{(1)C} = (D_{111} u_1^{(1)} + D'_{11} \Lambda^{(1)}) D_{22} D_{33} \cdots D_{nn}|^C.$$

This expression will subsequently allow us to examine the stability of the corresponding equilibrium path.

For the specialized P -system the D -transformation can be written out in full as

$$\begin{aligned} D(u_i, P) &\equiv V(Q_i^C + \alpha_{ij} u_j, P) \\ &\equiv U(Q_i^C + \alpha_{ij} u_j) - P \mathcal{E}(Q_i^C + \alpha_{ij} u_j) \\ &\equiv \bar{U}(u_i) - P \bar{\mathcal{E}}(u_i) \end{aligned}$$

and we write the path variation of the corresponding deflection in the form

$$e(u_1) \equiv \bar{\mathcal{E}}[u_i(u_1)] - \mathcal{E}^C.$$

The first derivative of e can thus be written down as follows

$$e^{(1)} \equiv \frac{de}{du_1} = \bar{\mathcal{E}}_i u_i^{(1)} = -D'_i u_i^{(1)}.$$

5.3 The limit point

The equations of normal behaviour

$$D_{ii} \dot{u}_i + D'_i \dot{\Lambda}|^E = 0$$

indicate that a key coefficient in the critical behaviour will be $D_1^{(1)C}$, and we shall see that this coefficient differentiates the limiting and branching phenomena, the former arising when $D_1^{(1)C}$ is non-zero (Figure 61). Thus to investigate the nature of the limit point we first specify that $D_1^{(1)C}$ is non-zero, and proceed to examine the equilibrium solutions in the vicinity of the critical equilibrium state C for which $D_{11}^C = 0$ while $D_{ss}^C \neq 0$ when $s \neq 1$.

Under these conditions the first-order equilibrium equations yield

$$\begin{aligned} \Lambda^{(1)C} &= 0, \\ u_s^{(1)C} &= 0 \quad \text{for } s \neq 1, \end{aligned}$$

and using these results the second-order equations give

$$\Lambda^{(2)C} = -\left. \frac{D_{111}}{D'_1} \right|^C,$$

and

$$u_s^{(2)C} = \left. \frac{D_{111} D'_s - D_{s11} D'_1}{D_{ss} D'_1} \right|^C \quad \text{for } s \neq 1.$$

The first derivative of $\mathcal{D}(u_1)$ becomes

$$\mathcal{D}'^{(1)C} = D_{111} D_{22} D_{33} \cdots D_{nn}|^C$$

and for the specialized system we have

$$e^{(1)C} = -D_1^{(1)C}.$$

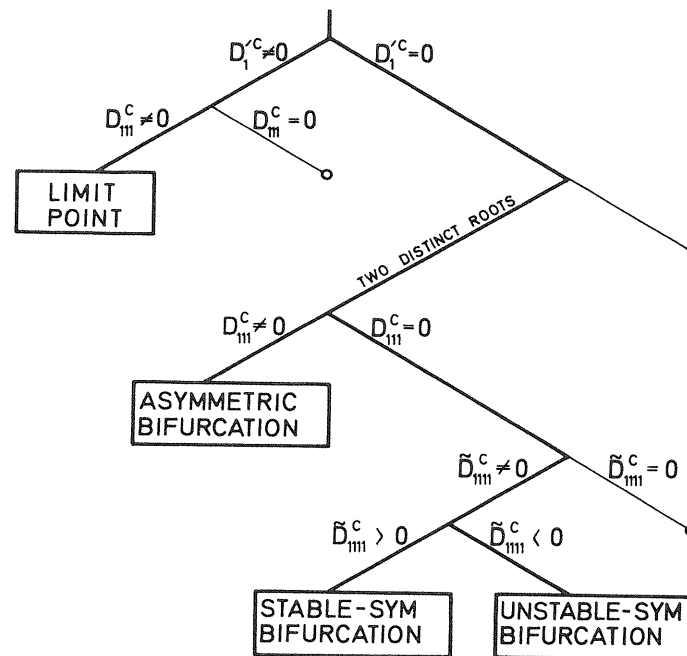


Figure 61 Classification of distinct critical points

When $D_{111}^c \neq 0$ these solutions correspond to the well known *limit* or snapping point. A single equilibrium path passes through the critical equilibrium state yielding a locally maximum or minimum value of Λ . The tangent to the path at point C is parallel to the u_1 axis, as shown in Figure 62. On a plot of the loading parameter Λ against the critical principal coordinate u_1 or against the corresponding deflection of the specialized system \mathcal{E} , the path exhibits a smooth maximum or minimum, while on a plot of Λ against any non-critical principal coordinate u_s ($s \neq 1$) the path exhibits a sharp cusp.⁵²

To examine the stability of the equilibrium path we now consider a set of sliding and rotating principal axes as outlined in Chapter 3; these axes vary in orientation and obliquity and thus in general rotate both as a set and relative to one another, and in the following analysis we take the *fixed* u_1 as the independent variable. The new axes are chosen to match the fixed principal axes when the fixed u_1 equals zero, so we have a set of stability coefficients $C_i(u_1)$ with the properties

$$C_1(0) = D_{11}^c = 0,$$

$$C_s(0) = D_{ss}^c \neq 0 \quad \text{for } s \neq 1.$$

Now we see from the perturbation analysis that the stability determinant $\mathcal{D}(u_1)$ passes *through* zero at the critical point C , and it follows that the single stability coefficient $C_1(u_1)$ must pass *through* zero at this point; the degree of instability of the path thus changes by one at point C . This is shown in Figure 62 in which a solid line denotes equilibrium states that are stable with respect to

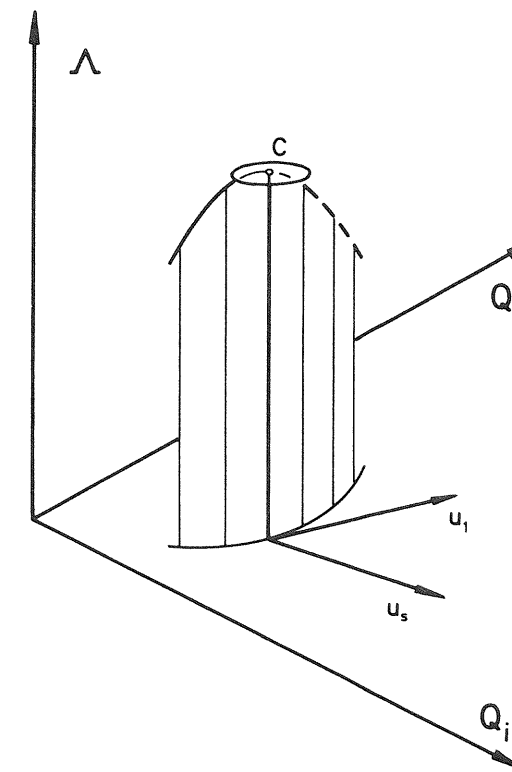


Figure 62 The spatial form of the limit point

the sliding and rotating principal coordinate u_1 , while a broken line denotes equilibrium states that are unstable with respect to this coordinate. We can finally note that the critical equilibrium state is itself always unstable due to the non-zero cubic coefficient D_{111}^c .

The approximate location of a limit point by supposing it to arise as the ‘imperfect approach’ to a fictitious branching point is presented by Haftka, Marrett and Nachbar.¹⁹³

5.4 Simple arch

At the present stage of development we have concerned ourselves with the normal behaviour of a non-critical equilibrium state and the critical behaviour arising at a limit point, so perhaps before moving on to the points of bifurcation it would be useful to introduce a simple example which illustrates the preceding general theory. The one-degree-of-freedom arch of Chapter 1 is perhaps best suited to this role since the nonlinear analysis is relatively uncomplicated and thus does not serve to obscure the important phenomena. The interested reader can of course refer back to the beginning of Chapter 1 for the necessary formulation but for our present purposes we need merely rewrite the potential energy function

$$\begin{aligned} V(Q_1, P) &= U(Q_1) - P \mathcal{E}(Q_1) \\ &= \frac{1}{4}kR^2(\alpha^4 - 2\alpha^2 Q_1^2 + Q_1^4) - PR(\alpha - Q_1), \end{aligned}$$

the geometry and notation being fully explained with reference to Figure 1: this potential energy function is based on the assumption that the angles α and Q_1 are small. The complete response of this system is shown in Figures 2 and 3, and it is our intention here to investigate first the normal behaviour of the system by the introduction of a set of incremental coordinate axes at a non-critical equilibrium state and secondly the critical limiting behaviour by a similar set of axes positioned at a critical point.

Let us therefore first investigate the behaviour at a typical non-critical equilibrium state E , say that which is defined by $Q_1^E = \alpha/2\sqrt{3}$. We introduce the incremental generalized coordinate q_1 given by

$$Q_1 = Q_1^E + q_1$$

and which on substitution into the V -function leads to the new potential energy function

$$\begin{aligned} D(q_1, P) &\equiv V(Q_1^E + q_1, P) \\ &= \frac{1}{4}kR^2 \left(\frac{121\alpha^4}{144} - \frac{11\alpha^3}{6\sqrt{3}} q_1 - \frac{3\alpha^2}{2} q_1^2 + \frac{2\alpha}{\sqrt{3}} q_1^3 + q_1^4 \right) \\ &\quad - PR \left(\frac{2\sqrt{3}-1}{2\sqrt{3}} \alpha - q_1 \right). \end{aligned}$$

It is of course not necessary to diagonalize this function, since the system has a single degree of freedom. Differentiation of the energy function once with respect to q_1 now gives the equilibrium equation

$$D_1 = \frac{1}{4}kR^2 \left(-\frac{11\alpha^3}{6\sqrt{3}} - 3\alpha^2 q_1 + \frac{6\alpha}{\sqrt{3}} q_1^2 + 4q_1^3 \right) + PR = 0.$$

We see that the value of the load at E may be obtained directly from this relationship by evaluation

$$P^E = \frac{11kR\alpha^3}{24\sqrt{3}}.$$

To perform a perturbation analysis about E we first write the load in the parametric form $P = P(q_1)$ and substitute this into the equilibrium equation to give the identity

$$\frac{1}{4}kR^2 \left(-\frac{11\alpha^3}{6\sqrt{3}} - 3\alpha^2 q_1 + \frac{6\alpha}{\sqrt{3}} q_1^2 + 4q_1^3 \right) + P(q_1) R \equiv 0.$$

Differentiation of this identity once with respect to q_1 leads to the first-order equilibrium equation

$$\frac{1}{4}kR^2 \left(-3\alpha^2 + \frac{12\alpha}{\sqrt{3}} q_1 + 12q_1^2 \right) + P^{(1)} R = 0,$$

and the subsequent evaluation of this equation at E gives the slope of the equilibrium path through E ,

$$P^{(1)E} = \frac{3kR\alpha^2}{4}.$$

We note that this slope could have been obtained directly using the general result

$$A^{(1)E} = - \left. \frac{D_{11}}{D'_1} \right|_E$$

if we had observed that

$$\begin{aligned} D_{11}^E &= - \frac{3kR^2 \alpha^2}{4}, \\ D'_1{}^E &= R. \end{aligned}$$

We can of course continue this differentiation and evaluation process to obtain the higher-order path derivatives. These lead us to conclude that there is a unique equilibrium path through this normal equilibrium state as we would expect.

We now move on to the critical behaviour of this system at the limit point C defined by $Q_1^C = \alpha/\sqrt{3}$. We introduce a new incremental coordinate q_1 given by

$$Q_1 = Q_1^C + q_1$$

and which leads to the new D -function

$$D(q_1, P) \equiv V(Q_1^C + q_1, P)$$

$$= \frac{1}{4}kR^2 \left(\frac{4\alpha^4}{9} - \frac{8\alpha^3}{3\sqrt{3}} q_1 + \frac{4\alpha}{\sqrt{3}} q_1^2 + 4q_1^3 \right) - PR \left(\frac{\sqrt{3}-1}{\sqrt{3}} \alpha - q_1 \right).$$

The equilibrium equation now becomes

$$D_1 = \frac{1}{4}kR^2 \left(-\frac{8\alpha^3}{3\sqrt{3}} + \frac{12\alpha}{\sqrt{3}} q_1^2 + 4q_1^3 \right) + PR = 0,$$

giving

$$P^C = \frac{2\alpha^3}{3\sqrt{3}} kR$$

on evaluation.

For a perturbation analysis we express P in the parametric form $P = P(q_1)$ as before and substitute this into the equilibrium equation to obtain the identity

$$\frac{1}{4}kR^2 \left(-\frac{8\alpha^3}{3\sqrt{3}} + \frac{12\alpha}{\sqrt{3}} q_1^2 + 4q_1^3 \right) + P(q_1) R \equiv 0.$$

Differentiating this once with respect to q_1 and evaluating at C we obtain the expected result

$$P^{(1)C} = 0.$$

A second differentiation and evaluation yields the curvature of the equilibrium path at C ,

$$P^{(2)C} = -\frac{6kR\alpha}{\sqrt{3}}.$$

Finally we note that this curvature could have been obtained directly using the general result

$$A^{(2)C} = -\frac{D_{111}}{D'_1} \Big|_C$$

if we had observed that

$$D_{111}^C = \frac{6kR^2\alpha}{\sqrt{3}},$$

$$D'_1 C = R.$$

5.5 Branching points

Returning to our classification of the distinct critical points, we have seen that a non-zero value of the coefficient $D'_1 C$ defines a limit point, so we shall now investigate the branching behaviour which arises when this coefficient vanishes. Let us therefore consider the distinct critical point C at which $D'_1 C = 0$, $D_{111}^C = 0$ and $D_{ss}^C \neq 0$ for $s \neq 1$.

If we set $i = 1$ in the first-order equilibrium equation it now gives no information, but setting $i = s \neq 1$ we obtain

$$u_s^{(1)C} = -\frac{D'_s}{D_{ss}} A^{(1)} \Big|_C.$$

For $i = 1$ the second-order equilibrium equation yields

$$D_{111} + 2 \sum_{s=2}^{s=n} D_{11s} u_s^{(1)} + \sum_{s=2}^{s=n} \sum_{k=2}^{k=n} D_{1ks} u_k^{(1)} u_s^{(1)} + 2D'_{11} A^{(1)} \\ + 2A^{(1)} \sum_{s=2}^{s=n} D'_{1s} u_s^{(1)} + D''_1 (A^{(1)})^2 |_C = 0,$$

and substituting for $u_s^{(1)C}$ we have finally

$$A(A^{(1)})^2 + BA^{(1)} + C |_C = 0,$$

where

$$A \equiv D''_1 - 2 \sum_{s=2}^{s=n} \frac{D'_{1s} D'_s}{D_{ss}} + \sum_{s=2}^{s=n} \sum_{k=2}^{k=n} \frac{D_{1ks} D'_s D'_k}{D_{ss} D_{kk}} \Big|_C, \\ B \equiv 2D'_{11} - 2 \sum_{s=2}^{s=n} \frac{D_{11s} D'_s}{D_{ss}} \Big|_C, \\ C \equiv D_{111}^C.$$

The variation of the corresponding deflection of the specialized system is given by

$$e^{(1)C} = P^{(1)} \sum_{s=2}^{s=n} \frac{(D'_s)^2}{D_{ss}} \Big|_C.$$

If we restrict attention to the case in which the quadratic equation for $A^{(1)C}$ yields *two real and distinct roots* (including the special circumstance in which A vanishes so that we have the degenerate solutions $A^{(1)C} = \infty$ or $-C/B$) we see that we now have a point of bifurcation involving the intersection of two distinct equilibrium paths. Further restricting our attention to the initial loss of stability of a system under increasing A , such points of bifurcation can be classified as indicated in the diagram of Figure 61. When $C = D_{111}^C$ is not identically zero the quadratic equation is not satisfied by $A^{(1)C} = 0$, so the two equilibrium paths have distinct and non-zero slopes; we shall call such an intersection an *asymmetric* point of bifurcation or branching point.

Let us now consider the variation of any u_s ($s \neq 1$) with A . We can write

$$u_s(u_1) \equiv u_s[A(u_1)]$$

giving on differentiation with respect to u_1

$$u_s^{(1)} = u'_s A^{(1)}.$$

Now $\Lambda^{(1)c} \neq 0$ for either path, so we can invert this to obtain

$$u_s'{}^c = \frac{u_s^{(1)}}{\Lambda^{(1)}} \Big| {}^c,$$

and using the earlier result we have

$$u_s'{}^c = -\frac{D'_s}{D_{ss}} \Big| {}^c.$$

This holds for *either* path, so we see that the point of bifurcation has the characteristics shown in Figure 63: a segment drawn between the two equilibrium paths at a constant value of Λ has the direction of u_1 as this value of Λ tends to Λ^c . Thus on a plot of the loading parameter Λ against the critical principal coordinate u_1 the two equilibrium paths have a direct intersection, while the two equilibrium paths *touch* each other on a plot of Λ against any non-critical principal coordinate u_s .⁵²

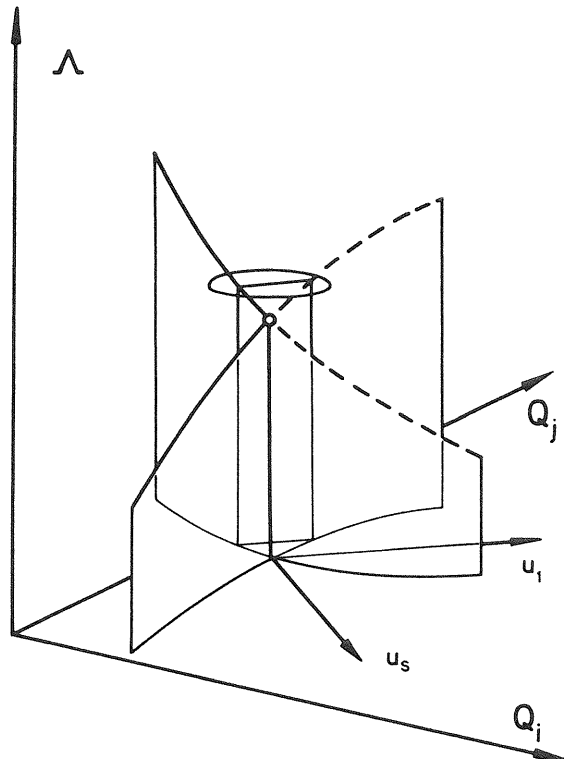


Figure 63 The spatial form of the asymmetric point of bifurcation

Let us next consider the variation of the corresponding deflection of the specialized system \mathcal{E} with the magnitude of the generalized force P . Here we write

$$e(u_1) \equiv e[P(u_1)]$$

giving on differentiation with respect to u_1

$$e'{}^c = e' P^{(1)}.$$

Now $P^{(1)c} \neq 0$ for either path, so we invert this to obtain

$$e'{}^c = \frac{e^{(1)}}{P^{(1)}} \Big| {}^c,$$

and using the earlier result we have

$$e'{}^c = \sum_{s=2}^{s=n} \frac{(D'_s)^2}{D_{ss}} \Big| {}^c.$$

This holds for *either* path, so the two paths of the asymmetric point of bifurcation are seen to *touch*⁵² on a plot of the load P against its corresponding deflection \mathcal{E} as shown in Figure 28.

The stability of the two intersecting equilibrium paths of the asymmetric point of bifurcation is discussed later in Chapter 6 which makes use of a more sophisticated analysis; we shall see that this exhibits the *exchange of stabilities* described by Poincaré.³ Thus considering two matching sets of sliding and rotating principal axes we see that only one stability coefficient, namely that associated with the critical principal coordinate u_1 , is involved. Moving along one path with increasing Λ this stability coefficient changes in sign from positive to negative on passing through the critical equilibrium state, while moving along the other path with increasing Λ the corresponding stability coefficient changes in sign from negative to positive. This is shown in Figure 63 in which a solid curve denotes equilibrium states which are stable with respect to the sliding and rotating critical principal coordinate u_1 while a broken curve denotes equilibrium states which are unstable with respect to this coordinate. Since we have earlier restricted attention to systems losing their initial stability it follows that each of the two paths is everywhere stable with respect to the other sliding principal coordinates, so the solid curves represent equilibrium states that are stable without qualification.

As with the limit point, the critical state of an asymmetric point of bifurcation is itself unstable due to the non-zero cubic coefficient D_{111}^c .

Finally we consider the case when $C \equiv D_{111}^c$ is identically zero; here one solution of the quadratic equation is given by $\Lambda^{(1)c} = 0$, the other solution being non-zero, since we have earlier assumed the solutions to be distinct. Thus one of the intersecting equilibrium paths, path A say, has a non-zero initial

slope while the other, path B say, has a zero initial slope. We shall call such a point of intersection a *symmetric* point of bifurcation or branching point. Since $u_s^{(1)c}$ is still given for $s \neq 1$ by the equation

$$u_s^{(1)c} = -\frac{D'_s}{D_{ss}} A^{(1)} \Big|_c,$$

we see that the rate of change with u_1 of any non-critical principal coordinate u_s is now zero for the path which is associated with $A^{(1)c} = 0$ (path B). The tangent at the critical point to path B is thus parallel to the u_1 -axis.

Assuming that the initial loss of stability of the system under increasing A is associated with path A we shall see in Chapter 6 that the precise path configurations depend on the sign of the coefficient \tilde{D}_{1111}^c , defined in Chapter 3, which determines the stability of the critical equilibrium state itself. Thus if \tilde{D}_{1111}^c is positive the critical equilibrium state and the path B are both stable and the path B curves upwards as shown in Figure 64; the intersection is then called a *stable-symmetric* point of bifurcation. Proceeding with increasing A along the

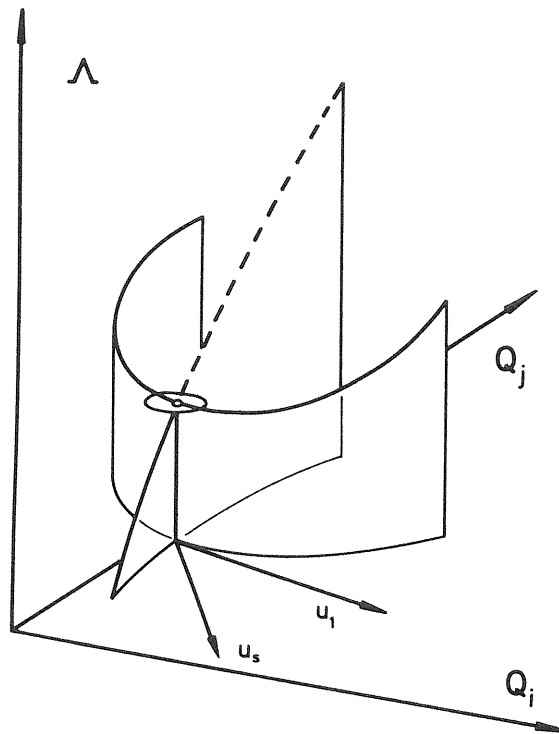


Figure 64 The spatial form of the stable-symmetric point of bifurcation

path A the stability coefficient associated with a sliding and rotating critical principal coordinate u_1 changes from positive to negative at the critical equilibrium state, while along the initially-horizontal path B the corresponding stability coefficient is never negative but touches zero at the critical equilibrium state.

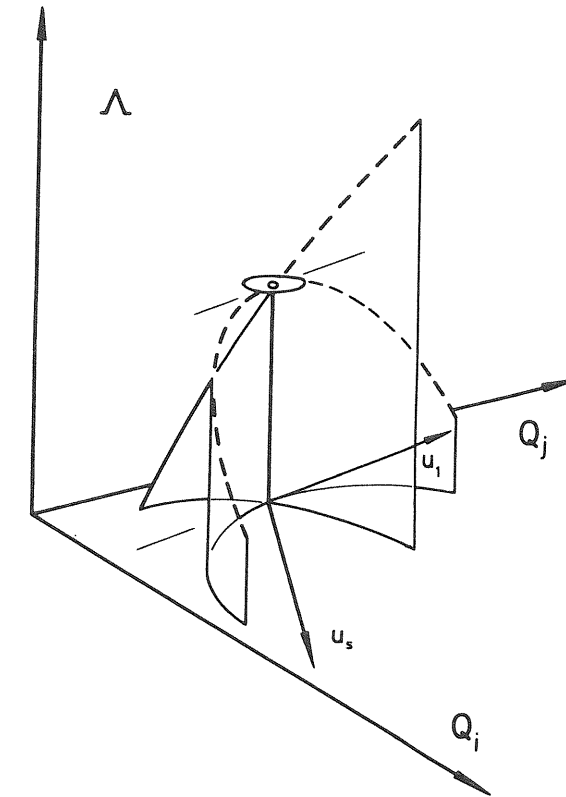


Figure 65 The spatial form of the unstable-symmetric point of bifurcation

Secondly if \tilde{D}_{1111}^c is negative the critical equilibrium state and the path B are both unstable and the path B curves downwards as shown in Figure 65; the intersection is then called an *unstable-symmetric* point of bifurcation. Proceeding with increasing A along the path A the stability coefficient associated with a sliding and rotating critical principal coordinate u_1 changes from positive to negative at the critical equilibrium state, while along the initially-horizontal path B the corresponding stability coefficient is never positive but touches zero at the critical equilibrium state.

Finally if \tilde{D}_{111}^c is zero more complex points of bifurcation are generated as indicated in the diagram of Figure 61.

For both the symmetric points of bifurcation a plot of Λ against the fixed u_1 will be characterized by the direct intersection of two equilibrium paths, one path exhibiting a local maximum or minimum at the critical equilibrium state. On a plot of the loading parameter against any non-critical principal coordinate u_s or against the corresponding deflection of the specialized system \mathcal{E} (Figure 28) the degeneration of the equations indicates that this local maximum or minimum will appear as a cusp striking the other equilibrium path.

We conclude by noting that this treatment of branching points is very restricted because of the ‘primitive’ set of coordinates used in the analysis. In the following chapter we shall be able to examine these in greater detail by the use of a sliding and rotating set of incremental principal coordinates.

6

DISTINCT BRANCHING POINTS

6.1 Introduction

In this chapter we focus our attention on the branching points alone, and we are therefore able to make use of the properties which are common to all points of bifurcation to generate a more sophisticated analysis. In particular the branching behaviour exhibits a single-valued *fundamental* equilibrium path which is assumed to emerge from the origin in $\Lambda-Q_i$ space and pass through the critical point. We make use of this presumably known path by the introduction of a set of incremental coordinates representing changes in the generalized coordinates from the path: these are referred to as a set of *sliding* coordinates, since they are defined at every value of the loading parameter—not merely at the critical load as in the previous chapter—and thus have the appearance of sliding along the fundamental path with varying load.

We start with a general analysis which makes no resort to a scheme of diagonalization; the incremental coordinates then slide along the fundamental path but retain the directions of the original generalized coordinates. This is perhaps the most useful formulation for numerical analysis, since in general a scheme of diagonalization is difficult to follow numerically. The perturbation equations are written down in full to the fifth order and some general results are obtained from a detailed study of the general r th-order perturbation equation.

The branching phenomena are finally examined in greater detail in a special analysis which involves a scheme of continuous diagonalization. The incremental coordinates still slide along the fundamental path but now in general vary in orientation and obliquity as they slide, thus rotating both as a set and relative to one another.

6.2 General analysis

Let us consider the general system described by the total potential energy function $V(Q_i, \Lambda)$. We start the general analysis by supposing that in the region of interest the n equilibrium equations $V_i = 0$ yield a single-valued *fundamental*

solution $Q_i = Q_i^f(\Lambda)$. A *sliding* set of incremental coordinates is defined by the n equations

$$Q_i = Q_i^f(\Lambda) + q_i$$

and we introduce the new energy function

$$W(q_i, \Lambda) \equiv V[Q_i^f(\Lambda) + q_i, \Lambda].$$

This V to W transformation does have some physical significance. Consider for example the potential energy function in two generalized coordinates A and B and a loading parameter Λ

$$V = \frac{1}{2}A^2 + \frac{1}{2}B^2 - \frac{1}{2}AB^2 - \Lambda A.$$

The equilibrium equations $\partial V/\partial A = 0$ and $\partial V/\partial B = 0$ yield the fundamental path solution

$$A = A,$$

$$B = 0,$$

and we define two incremental coordinates a and b emerging from the fundamental path as follows

$$A = A + a,$$

$$B = 0 + b.$$

Substituting into V we obtain the transformed energy function

$$W = \frac{1}{2}a^2 + \frac{1}{2}b^2 - \frac{1}{2}ab^2 - \frac{1}{2}\Lambda b^2 + (-\frac{1}{2}\Lambda^2).$$

It is of course possible to neglect the bracketed Λ^2 term of this function, since it vanishes identically on differentiation of W with respect to a or b . The V to W transformation can thus be seen as a standard mechanism by which an axial force acting on a linear displacement form (A) is transformed to act on a quadratic form involving displacements out of the loading plane (b^2). Such an instability mechanism arises in the buckling of plates as we shall see in the circular plate analysis of Chapter 7. We note that a V to W transformation will normally destroy a linearity in Λ .

Let us now return to the general W -analysis. The normal equilibrium and stability conditions hold good for the transformed energy function W which has the properties

$$W_i[0, \Lambda] = 0,$$

$$W'_i[0, \Lambda] = 0,$$

$$W''_i[0, \Lambda] = 0,$$

etc. We have a valid mapping from the original Λ - Q_i space to the new Λ - q_i space in which the fundamental equilibrium path is given by $q_i = 0$. We now suppose that a distinct critical point C lies on the fundamental equilibrium

path at $\Lambda = \Lambda^C$. We know that the determinant of W_{ij} will vanish at this point so we can write

$$|W_{ij}(0, \Lambda^C)| = 0.$$

We now utilize a perturbation approach and seek to express any post-buckling equilibrium path emerging from this critical equilibrium state in the parametric form

$$q_j = q_j(q_1), \quad \Lambda = \Lambda(q_1),$$

assuming without any essential loss of generality that the *first* generalized coordinate is a suitable expansion parameter. More specifically we insist that the minor of W_{11}^C is non-zero; there must of course be a non-zero first minor of W_{ij} at a distinct critical point, since this matrix is of rank $n - 1$ so the condition can always be satisfied by a suitable choice of q_1 . We note that the above includes writing q_1 as $q_1(q_1)$ as before and this must be borne in mind throughout the analysis. These parametric forms may now be substituted into the equilibrium equations $W_i = 0$ to give the identity

$$W_i[q_j(q_1), \Lambda(q_1)] \equiv 0,$$

and we see that the left-hand side is now simply a function of the independent variable q_1 so we may differentiate the equations with respect to q_1 as many times as we please. Thus, differentiating repeatedly, we can generate the ordered equilibrium equations

$$W_{ij}q_j^{(1)} + W'_i\Lambda^{(1)} = 0,$$

$$(W_{ijk}q_k^{(1)} + W'_{ij}\Lambda^{(1)})q_j^{(1)} + W_{ij}q_j^{(2)} + (W'_{ij}q_j^{(1)} + W''_i\Lambda^{(1)})\Lambda^{(1)} + W'_i\Lambda^{(2)} = 0,$$

etc. Here bracketed superscripts denote differentiation with respect to q_1 as before, and remembering the expression of q_1 as $q_1(q_1)$ we may write

$$q_1^{(r)} \equiv \frac{dq_1}{dq_1^r} = \delta_{1r},$$

where δ_{ij} denotes the Kronecker delta. The perturbation analyses based on this formulation (e.g. the elastica analysis of Chapter 1) sometimes require these equations derived as far as the fifth order, so collecting like terms we now present these explicitly

$$W_{ij}q_j^{(1)} + W'_i\Lambda^{(1)} = 0,$$

$$W_{ijk}q_k^{(1)}q_j^{(1)} + W_{ij}q_j^{(2)} + 2W'_{ij}q_j^{(1)}\Lambda^{(1)} + W'_i\Lambda^{(2)} + W''_i(\Lambda^{(1)})^2 = 0,$$

$$\begin{aligned} & W_{ijkl}q_l^{(1)}q_k^{(1)}q_j^{(1)} + 3W_{ijk}q_j^{(1)}q_k^{(2)} + W_{ij}q_j^{(3)} + 3W'_{ijk}q_j^{(1)}q_k^{(1)}\Lambda^{(1)} \\ & + 3W'_{ij}q_j^{(2)}\Lambda^{(1)} + 3W'_{ij}q_j^{(1)}\Lambda^{(2)} + W'_i\Lambda^{(3)} + 3W''_{ij}q_j^{(1)}(\Lambda^{(1)})^2 \\ & + 3W_{ij}q_j^{(1)}\Lambda^{(2)} + W''_i(\Lambda^{(1)})^3 = 0, \end{aligned}$$

$$\begin{aligned}
& W_{ijklm} q_j^{(1)} q_k^{(1)} q_l^{(1)} q_m^{(1)} + 6W_{ijkl} q_j^{(1)} q_k^{(1)} q_l^{(2)} + 3W_{ijk} q_j^{(2)} q_k^{(2)} + 4W_{ijk} q_j^{(1)} q_k^{(3)} \\
& + W_{ij} q_j^{(4)} + 4W'_{ijk} q_j^{(1)} q_k^{(1)} q_l^{(1)} \Lambda^{(1)} + 12W'_{ijk} q_j^{(1)} q_k^{(2)} \Lambda^{(1)} \\
& + 6W'_{ijk} q_j^{(1)} q_k^{(1)} \Lambda^{(2)} + 4W'_{ij} q_j^{(3)} \Lambda^{(1)} + 6W'_{ij} q_j^{(2)} \Lambda^{(2)} + 4W'_{ij} q_j^{(1)} \Lambda^{(3)} \\
& + W'_{ij} \Lambda^{(4)} + 6W''_{ijk} q_j^{(1)} q_k^{(1)} (\Lambda^{(1)})^2 + 12W''_{ij} q_j^{(1)} \Lambda^{(1)} \Lambda^{(2)} \\
& + 6W''_{ij} q_j^{(2)} (\Lambda^{(1)})^2 + 4W''_{ij} \Lambda^{(1)} \Lambda^{(3)} + 3W''_{ij} (\Lambda^{(2)})^2 + 4W''_{ij} q_j^{(1)} (\Lambda^{(1)})^3 \\
& + 6W''_{ij} (\Lambda^{(1)})^2 \Lambda^{(2)} + W'''_{ij} (\Lambda^{(1)})^4 = 0,
\end{aligned}$$

$$\begin{aligned}
& W_{ijklmn} q_j^{(1)} q_k^{(1)} q_l^{(1)} q_m^{(1)} q_n^{(1)} + 10W_{ijklm} q_j^{(1)} q_k^{(1)} q_l^{(1)} q_m^{(1)} q_n^{(1)} + 15W_{ijkl} q_j^{(1)} q_k^{(2)} q_l^{(2)} q_n^{(2)} \\
& + 10W_{ijkl} q_j^{(1)} q_k^{(1)} q_l^{(3)} + 10W_{ijk} q_j^{(2)} q_k^{(3)} + 5W_{ijk} q_j^{(1)} q_k^{(4)} + W_{ij} q_j^{(5)} \\
& + 5W'_{ijklm} q_j^{(1)} q_k^{(1)} q_l^{(1)} q_m^{(1)} \Lambda^{(1)} + 30W'_{ijkl} q_j^{(1)} q_k^{(1)} q_l^{(2)} \Lambda^{(1)} \\
& + 10W'_{ijkl} q_j^{(1)} q_k^{(1)} q_l^{(1)} \Lambda^{(2)} + 15W'_{ijk} q_j^{(2)} q_k^{(2)} \Lambda^{(1)} + 20W'_{ijk} q_j^{(1)} q_k^{(3)} \Lambda^{(1)} \\
& + 30W'_{ijk} q_j^{(1)} q_k^{(2)} \Lambda^{(2)} + 10W'_{ijk} q_j^{(1)} q_k^{(1)} \Lambda^{(3)} + 5W'_{ij} q_j^{(4)} \Lambda^{(1)} \\
& + 10W'_{ij} q_j^{(3)} \Lambda^{(2)} + 10W'_{ij} q_j^{(2)} \Lambda^{(3)} + 5W'_{ij} q_j^{(1)} \Lambda^{(4)} + W_i \Lambda^{(5)} \\
& + 10W''_{ijkl} q_j^{(1)} q_k^{(1)} q_l^{(1)} (\Lambda^{(1)})^2 + 30W''_{ijk} q_j^{(1)} q_k^{(2)} (\Lambda^{(1)})^2 \\
& + 30W''_{ijk} q_j^{(1)} q_k^{(1)} \Lambda^{(1)} \Lambda^{(2)} + 10W''_{ij} q_j^{(3)} (\Lambda^{(1)})^2 + 30W''_{ij} q_j^{(2)} \Lambda^{(1)} \Lambda^{(2)} \\
& + 20W''_{ij} q_j^{(1)} \Lambda^{(3)} + 15W''_{ij} q_j^{(1)} (\Lambda^{(2)})^2 + 5W''_{ij} \Lambda^{(1)} \Lambda^{(4)} + 10W''_{ij} \Lambda^{(2)} \Lambda^{(3)} \\
& + 10W''_{ij} q_j^{(1)} q_k^{(1)} (\Lambda^{(1)})^3 + 30W''_{ij} q_j^{(1)} (\Lambda^{(1)})^2 \Lambda^{(2)} + 10W''_{ij} q_j^{(2)} (\Lambda^{(1)})^3 \\
& + 10W''_{ij} (\Lambda^{(1)})^2 \Lambda^{(3)} + 15W''_{ij} \Lambda^{(1)} (\Lambda^{(2)})^2 + 5W'''_{ij} q_j^{(1)} (\Lambda^{(1)})^4 \\
& + 10W'''_{ij} (\Lambda^{(1)})^3 \Lambda^{(2)} + W''''_{ij} (\Lambda^{(1)})^5 = 0.
\end{aligned}$$

We now diverge slightly from the mainstream analysis to study a general form of these equations. The numerical analyst should note that these r th-order results are not of immediate analytical value and thus could be omitted on first reading, but it is hoped that he might return to them at a later date to obtain a deeper understanding of the perturbation scheme: a condensed version of this scheme which excludes the general results is given in the general introduction of Chapter 2. The r th-order equilibrium equation which is written formally as

$$\frac{d^r}{dq_1^r} W_i[q_j(q_1), \Lambda(q_1)] = 0,$$

can be seen, by the following inductive reasoning, to have the structure

$$\begin{aligned}
\frac{d^r}{dq_1^r} W_i &= W_{ij} q_j^{(r)} + F_i(q_j^{(r-1)}, q_j^{(r-2)}, \dots, q_j^{(1)}, \Lambda^{(r-2)}, \Lambda^{(r-3)}, \dots, \Lambda^{(1)}) \\
& + r(W'_{ij} q_j^{(1)} + W''_{ij} \Lambda^{(1)}) \Lambda^{(r-1)} + W'_i \Lambda^{(r)} = 0,
\end{aligned}$$

for $r \geq 3$. Let us therefore assume that this is the structure of the r th equation.

Differentiation of this equation with respect to q_1 leads to the $r+1$ th equilibrium equation, where

$$W_{ij} q_j^{(r)} \text{ becomes } \begin{cases} (W_{ij} q_j^{(1)} + W'_{ij} \Lambda^{(1)}) q_j^{(r)} & (\text{included in } F_i^{r+1}) \\ W_{ij} q_j^{(r+1)}, \end{cases}$$

$$\begin{aligned}
& F_i \text{ all included in } F_i^{r+1}, \\
& r(W'_{ij} q_j^{(1)} + W''_{ij} \Lambda^{(1)}) \Lambda^{(r-1)}
\end{aligned}$$

$$\begin{aligned}
& \text{becomes } \begin{cases} r[(W'_{ij} q_j^{(1)} + W''_{ij} \Lambda^{(1)}) q_j^{(1)} + W'_{ij} q_j^{(2)} \\ \quad + (W''_{ij} q_j^{(1)} + W''_{ij} \Lambda^{(1)}) \Lambda^{(1)} \\ \quad + W''_{ij} \Lambda^{(2)}] \Lambda^{(r-1)} & (\text{all included in } F_i^{r+1}) \\ r(W'_{ij} q_j^{(1)} + W''_{ij} \Lambda^{(1)}) \Lambda^{(r)}, \end{cases} \\
& W'_i \Lambda^{(r)} \text{ becomes } \begin{cases} ((W'_{ij} q_j^{(1)} + W''_{ij} \Lambda^{(1)}) \Lambda^{(r)}) \\ W'_i \Lambda^{(r+1)}. \end{cases} (r+1)(W'_{ij} q_j^{(1)} + W''_{ij} \Lambda^{(1)}) \Lambda^{(r)}
\end{aligned}$$

This process shows that if the structure is correct for the r th equation it is likewise correct for the $r+1$ th equation: but by inspection we can see it to hold for $r=3$, and therefore by the well known induction mechanism it follows that it is valid for $r \geq 3$.

If we evaluate the equilibrium equations at the critical point C , where $q_1 = 0$, $\Lambda = \Lambda^C$ and $W_i = W'_i = W''_i = \dots = 0$, we have

$$\begin{aligned}
W_{ij} q_j^{(1)}|_C &= 0, \\
W_{ijk} q_j^{(1)} q_k^{(1)} + 2W'_{ij} q_j^{(1)} \Lambda^{(1)} + W_{ij} q_j^{(2)}|_C &= 0,
\end{aligned}$$

etc. and we see that the r th evaluated equation can be written as

$$\frac{d^r}{dq_1^r} W_i|_C = W_{ij} q_j^{(r)} + rW'_{ij} q_j^{(1)} \Lambda^{(r-1)} + R_i^r (\text{lower derivatives})|_C = 0,$$

this equation holding for all $r \geq 1$ if we interpret Λ^0 as zero.

Since $q_1^{(1)} = 1$ we can solve the first equation for the rates $q_j^{(1)C}$. We now introduce the ‘contraction’ mechanism in which the i th equation of the second order is multiplied by $q_i^{(1)C}$ and the set of equations is added. The final term vanishes by virtue of the first equation and we obtain

$$\Lambda^{(1)C} = -\left. \frac{W_{ijk} q_j^{(1)} q_k^{(1)} q_i^{(1)}}{2W'_{ij} q_i^{(1)} q_j^{(1)}} \right|_C.$$

Here we have assumed the critical point to be ‘simple’ in the sense that $W'_{ij} q_i^{(1)} q_j^{(1)}|_C$, which clearly plays a key role in the analysis, is non-zero. The non-vanishing of this expression is related to the direct passage through zero

of the corresponding stability coefficient, as will become more apparent in the diagonalized A -analysis which follows; it would for example vanish if the fundamental path were to remain stable above the critical point, so that the stability coefficient simply touched zero. We next substitute for $q_j^{(1)c}$ and $A^{(1)c}$ into the second-order equations, and since $q_1^{(2)} = 0$ we can solve these equations for the further path derivatives $q_j^{(2)c}$. Clearly, we can continue this ordered perturbation scheme as far as is necessary.

We see that by applying the contraction mechanism to the second-order equilibrium equations we have obtained the slope $A^{(1)c}$ in terms of the rates $q_j^{(1)c}$, the second derivatives $q_j^{(2)c}$ having been eliminated. We can thus write the general result:

The slope of the post-buckling path passing through a simple distinct critical point on a plot of the loading parameter against a (suitable) generalized coordinate is not dependent on the solution of the second-order equilibrium equations.

A consequence of this result is that a one-degree-of-freedom nonlinear Rayleigh–Ritz analysis employing the linear buckling mode will yield the correct value for this slope.^{58, 194} A formal proof of this is readily written down following the corresponding proof of Chapter 4.

Let us now contract the r th-order equilibrium equations by multiplying the i th equation by $q_i^{(1)c}$ and adding the set to obtain

$$\left[\frac{d^r}{dq_1^r} W_i \right] q_i^{(1)c} = W_{ij} q_i^{(1)} q_j^{(r)} + r W'_{ij} q_i^{(1)} q_j^{(1)} A^{(r-1)} + R_i q_i^{(1)c} = 0.$$

We see that the first term vanishes by virtue of the first-order equilibrium equation and so we can write the r th contracted equation as

$$A^{(r-1)c} = - \frac{R_i q_i^{(1)}}{r W'_{ij} q_i^{(1)} q_j^{(1)}} \Big|_c \quad (r = 1, 2, \dots).$$

Since $q_1^{(r)} = 0$ for $r \neq 1$, $A^{(r-1)c}$ may now be substituted into the set of evaluated equations, and they may then be solved for the path derivatives $q_j^{(r)c}$.

The ordered evaluated equations are *sequentially linear* with the same basic matrix and are thus readily solved, the r th equations yielding on solution the mode derivatives $q_j^{(r)c}$ while the $r+1$ th contracted equation yields directly the load derivative $A^{(r)c}$. The perturbation process thus proceeds as indicated in Figure 66, the scheme of solution not depending on the type of branching point (asymmetric or symmetric) under consideration. We can summarize this schematic diagram in the general statement:

For the post-buckling path passing through a simple distinct critical point the r th derivative of the loading parameter with respect to a (suitable) generalized coordinate is not dependent on the solution of the $r+1$ th-order equilibrium equations.

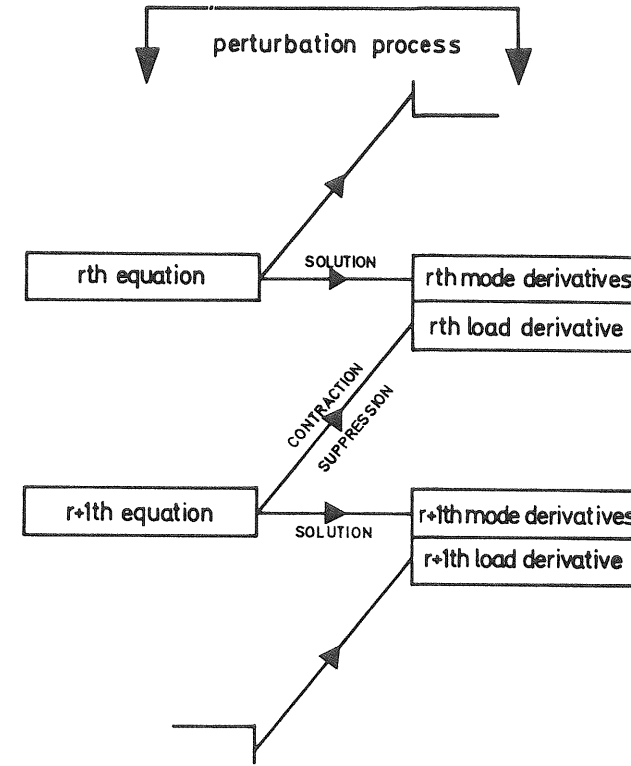


Figure 66 Perturbation patterns of continuum and discrete theories

The work so far is applicable whether or not the slope $A^{(1)c}$ is zero. When $A^{(1)c}$ is non-zero we have the previously discussed asymmetric point of bifurcation, and we shall now set $A^{(1)c} = 0$ to study the symmetric points of bifurcation in more detail. Thus with $A^{(1)c} = 0$, the third-order equilibrium equations evaluated at the critical point can be written after contraction as

$$W_{ijkl} q_i^{(1)} q_j^{(1)} q_k^{(1)} q_l^{(1)} + 3W_{ijk} q_i^{(1)} q_j^{(1)} q_k^{(2)} + 3W'_{ij} q_i^{(1)} q_j^{(1)} A^{(2)} + W_{ij} q_i^{(1)} q_j^{(3)} \Big|_c = 0.$$

As before the last term vanishes by virtue of the first-order equilibrium equation, and with our previous assumption that $W'_{ij} q_i^{(1)} q_j^{(1)} \neq 0$ we can now write the path curvature as

$$A^{(2)c} = - \frac{\tilde{W}_4}{3W'_{ij} q_i^{(1)} q_j^{(1)}} \Big|_c,$$

where

$$\tilde{W}_4^C \equiv W_{ijkl} q_i^{(1)} q_j^{(1)} q_k^{(1)} q_l^{(1)} + 3 W_{ijk} q_i^{(1)} q_j^{(1)} q_k^{(2)} |^C. \quad (6.1)$$

Let us consider now the post-buckling response of the specialized system on a plot of the load P against its corresponding deflection \mathcal{E} . The energy transformation of the general theory can first be written out in full as follows

$$\begin{aligned} W(q_i, P) &\equiv V[Q_i^F(P) + q_i, P] \\ &\equiv U[Q_i^F(P) + q_i] - P\mathcal{E}[Q_i^F(P) + q_i] \end{aligned}$$

and some required derivatives of W can be written down

$$\begin{aligned} W_i &= U_i - P\mathcal{E}_i, \\ W_{ij} &= U_{ij} - P\mathcal{E}_{ij}, \\ W' &= U_i Q_i^{F'} - \mathcal{E} - P\mathcal{E}_i Q_i^{F'}, \\ W'_j &= U_{ij} Q_i^{F'} - \mathcal{E}_j - P\mathcal{E}_{ij} Q_i^{F'}. \end{aligned}$$

Now $W'^C = 0$, so we have

$$\begin{aligned} \mathcal{E}_j^C &= (U_{ij} - P\mathcal{E}_{ij}) Q_i^{F'}|^C \\ &= W_{ij} Q_i^{F'}|^C, \end{aligned}$$

whereupon contracting these equations we find that

$$\mathcal{E}_j q_j^{(1)}|^C = W_{ij} Q_i^{F'} q_j^{(1)}|^C.$$

But the right-hand side of this last equation is zero by virtue of the first-order equilibrium equation, so we have the important result that

$$\mathcal{E}_j q_j^{(1)}|^C = 0.$$

This corresponds to the fact that at a point of bifurcation (as opposed to a limit point) the generalized load does no first-order work as the system moves through its buckling displacement.

We consider now the change in the corresponding deflection defined by the equation

$$e(q_i, P) \equiv \mathcal{E}[Q_i^F(P) + q_i] - \mathcal{E}^F[Q_i^F(P)],$$

and we write down some required derivatives as follows,

$$\begin{aligned} e_i &= \mathcal{E}_i, \quad e_{ij} = \mathcal{E}_{ij}, \\ e' &= \mathcal{E}_i Q_i^{F'} - \mathcal{E}_i^F Q_i^{F'}, \quad e'_j = \mathcal{E}_{jk} Q_k^{F'}, \\ e'' &= \mathcal{E}_{ij} Q_i^{F'} Q_j^{F'} + \mathcal{E}_i Q_i^{F''} - \mathcal{E}_{ij}^F Q_i^{F'} Q_j^{F'} - \mathcal{E}_i^F Q_i^{F''}, \\ e'^C &= 0, \quad e''^C = 0. \end{aligned}$$

The total variation of e with q_1 along the post-buckling equilibrium path is

$$e(q_1) \equiv e[q_j(q_1), P(q_1)]$$

giving on differentiation

$$\begin{aligned} \frac{de}{dq_1} &= e_j q_j^{(1)} + e' P^{(1)}, \\ \frac{d^2 e}{dq_1^2} &= (e_{jk} q_j^{(1)} + e'_j P^{(1)}) q_j^{(1)} + e_j q_j^{(2)} + (e'_j q_j^{(1)} + e'' P^{(1)}) P^{(1)} + e' P^{(2)}, \end{aligned}$$

so using the earlier results we have

$$\begin{aligned} \frac{de}{dq_1} \Big|_C &= 0, \\ \frac{d^2 e}{dq_1^2} \Big|_C &= \mathcal{E}_{jk} q_j^{(1)} q_k^{(1)} + 2P^{(1)} \mathcal{E}_{jk} Q_k^{F'} q_j^{(1)} + \mathcal{E}_j q_j^{(2)}|^C. \end{aligned}$$

For the asymmetric point of bifurcation in which $P^{(1)C} \neq 0$ the total post-buckling variation of e with P is well behaved and we can write

$$e(q_1) \equiv e[P(q_1)]$$

so that

$$\frac{de}{dq_1} = \frac{de}{dP} P^{(1)},$$

$$\frac{d^2 e}{dq_1^2} = \frac{d^2 e}{dP^2} (P^{(1)})^2 + \frac{de}{dP} P^{(2)}.$$

We thus obtain the required results

$$\begin{aligned} \frac{de}{dP} \Big|_C &= 0, \\ \frac{d^2 e}{dP^2} \Big|_C &= \frac{\mathcal{E}_{jk} q_j^{(1)} q_k^{(1)} + 2P^{(1)} \mathcal{E}_{jk} Q_k^{F'} q_j^{(1)} + \mathcal{E}_j q_j^{(2)}}{(P^{(1)})^2} \Big|_C. \end{aligned}$$

Thus for the asymmetric point of bifurcation we see that on a plot of P against \mathcal{E} the fundamental and post-buckling equilibrium paths touch each other at the critical equilibrium point C as discussed earlier and as shown in Figure 28.

For the symmetric points of bifurcation in which $P^{(1)C} = 0$ we see that the total post-buckling variation of e with P is associated with a singularity, but we can write

$$\frac{de}{dP} = \left(\frac{1}{2} \frac{d^2 e}{dq_1^2} q_1^2 + \dots \right) / \left(\frac{1}{2} P^{(2)} q_1^2 + \dots \right)$$

to obtain the limiting slope

$$\begin{aligned}\frac{\Delta e}{\Delta P} \Big|_C &= \frac{d^2 e}{dq_1^2} \Big|_{P^{(2)}} \Big|_C \\ &= \frac{\mathcal{E}_{jk} q_j^{(1)} q_k^{(1)} + \mathcal{E}_j q_j^{(2)}}{P^{(2)}} \Big|_C.\end{aligned}$$

Thus for the symmetric points of bifurcation we see that on a plot of P against \mathcal{E} the post-buckling equilibrium path exhibits a cusp striking the fundamental equilibrium path at the critical point C as discussed earlier and as shown in Figure 28.

Some general studies of the P - \mathcal{E} response of specialized systems have been made by Mansfield¹⁹⁵ and Pope¹⁹⁶ while the response of completely symmetric systems with some interesting large-deflection results has been examined by Masur.[†]

6.3 Analysis with diagonalization

We now employ a scheme of continuous diagonalization to make a more detailed study of these branching points. Having introduced the transformed energy function

$$W(q_i, \Lambda) \equiv V[Q_i^F(\Lambda) + q_i, \Lambda],$$

we make a further change of coordinates by means of a non-singular linear transformation of the form $q_i = \alpha_{ij}(\Lambda)u_j$ to diagonalize the quadratic form corresponding to $W_{ij}(0, \Lambda)$. This diagonalization can be accomplished in an infinite number of ways and we shall suppose that one such way has been chosen, merely insisting that α_{ij} is a continuous and single-valued function of Λ . We now introduce the transformed energy function

$$A(u_i, \Lambda) \equiv V[Q_i^F(\Lambda) + \alpha_{ij}(\Lambda)u_j, \Lambda]$$

with the properties arising from its derivation

$$\begin{aligned}A_i(0, \Lambda) &= A'_i(0, \Lambda) = A''_i(0, \Lambda) = \cdots = 0, \\ A_{ij}(0, \Lambda) &= A'_{ij}(0, \Lambda) = A''_{ij}(0, \Lambda) = \cdots = 0 \quad \text{for } i \neq j.\end{aligned}$$

Here again a prime denotes differentiation with respect to Λ .

In the original Λ - Q_i space the u_i axes are seen to slide along the fundamental path and in general rotate both as a set and relative to each other to give the axes varying orientation and obliquity. Since $Q_i^F(\Lambda)$ and $\alpha_{ij}(\Lambda)$ are continuous

[†] E. F. Masur, Buckling, post-buckling and limit analysis of completely symmetric elastic structures, *Int. J. Solids Structures*, **6**, 587 (1970).

and single-valued, we see that we have a valid mapping from the original Λ - Q_i space to the final Λ - u_i space in which the fundamental path is given by $u_i = 0$.

Two special cases of this coordinate transformation are worth noting. First, we might insist that $\alpha_{ij}(\Lambda)$ should be orthogonal, to give us the T -transformation used by Roorda:⁶¹ the u_i axes will then slide and in general rotate, but will remain rectangular in Λ - Q_i space. Secondly, although the V to W transformation in general eliminates a linearity in Λ , we sometimes find that $W(q_i, \Lambda) \equiv V[Q_i^F(\Lambda) + q_i, \Lambda]$ may be linearized with respect to Λ . We can then write

$$W(q_i, \Lambda) = W^0(q_i) + \Lambda W^1(q_i)$$

and, if $W_{ij}^0(0)$ is positive definite, we can simultaneously diagonalize $W_{ij}^0(0)$ and $W_{ij}^1(0)$ by means of linear transformation $q_i = \alpha_{ij}u_j$. This then gives rise to a special case of the A -transformation in which α_{ij} is not a function of Λ ; the u_i axes now slide, are in general oblique, but do not rotate with Λ .

We can now start the analysis with the transformed energy function $A(u_i, \Lambda)$, the only necessary properties of which have been presented above. The energy function being diagonalized, the derivatives $A_{ii}(0, \Lambda)$ represent a set of stability coefficients, and we again focus attention on a distinct critical point C lying on the fundamental path, at which a *single* stability coefficient is zero. Thus we can write

$$\begin{aligned}A_{11}^C &\equiv A_{11}(0, \Lambda^C) = 0, \\ A_{ss}^C &\equiv A_{ss}(0, \Lambda^C) \neq 0 \quad \text{for } s \neq 1,\end{aligned}$$

where Λ^C is the critical value of Λ . Having specified a single-valued fundamental equilibrium path, such a critical point will in general correspond to a point of bifurcation. Observing that $A'_{11}(0, \Lambda)$ is the rate of change of the critical stability coefficient along the fundamental path, we assume that the critical point is simple in the sense that

$$A'_{11}^C \neq 0,$$

the diagonalized version of our earlier condition $W'_{ij} q_i^{(1)} q_j^{(1)} \neq 0$; we now see how this relates to the direct passage through zero of a stability coefficient. The case in which A'_{11}^C is equal to zero has been discussed briefly by Poincaré.³

For future reference we now evaluate some derivatives of the stability determinant

$$\Delta(u_k, \Lambda) \equiv |A_{ij}(u_k, \Lambda)|.$$

Differentiating by columns with respect to either u_i or Λ , and evaluating at the critical point, only the leading determinant remains and we have finally

$$\Delta_i^C = A_{11} A_{22} A_{33} \cdots A_{nn} |^C,$$

$$\Delta'^C = A'_{11} A_{22} A_{33} \cdots A_{nn} |^C,$$

all derivatives being evaluated at the critical point. We observe that A'^C is, by previous assumption, non-zero.

We evaluate, further, the second derivative Δ_{11} for the special case in which $A_{111}^C = 0$. Differentiating twice by columns and evaluating at the critical point, only determinants with a differentiated first column remain, and we have after some algebra

$$\Delta_{11}^C = \left\{ A_{1111} - 2 \sum_{s=2}^{s=n} \frac{(A_{s11})^2}{A_{ss}} \right\} A_{22} A_{33} \dots A_{nn} |^C.$$

Following the now familiar established scheme, we first write the post-buckling equilibrium path of the system in the form

$$u_j = u_j(u_1), \quad \Lambda = \Lambda(u_1)$$

which after substitution into the equilibrium equation $A_i = 0$ yield the characterizing equilibrium identity

$$A_i[u_j(u_1), \Lambda(u_1)] \equiv 0.$$

It should be noted carefully at this point that throughout this analysis the u_i axes are free to rotate and slide along the fundamental path: they thus always refer to the current value of Λ , and are not fixed at the critical point C .

As before we now differentiate the characterizing equilibrium identity with respect to u_1 to obtain

$$A_{ij} u_j^{(1)} + A'_i \Lambda^{(1)} = 0,$$

the bracketed superscript denoting differentiation of the parametric post-buckling functions with respect to u_1 . Once again it should be noted that great simplicity and no possibility of confusion are achieved by consistently writing u_1 as $u_1(u_1)$, so that

$$u_1^{(r)} \equiv \frac{d^r u_1}{du_1^r} = \delta_{1r}.$$

Evaluating this first-order equilibrium equation at the critical point C we see that for $i = 1$ the equation is identically satisfied, while for $i = s \neq 1$ we obtain

$$u_s^{(1)C} = 0 \quad (s \neq 1),$$

the first derivative of interest. Differentiating now the characterizing equilibrium identity a second time with respect to u_1 we have

$$(A_{ijk} u_k^{(1)} + A'_{ij} \Lambda^{(1)}) u_j^{(1)} + A_{ij} u_j^{(2)} + (A'_{ij} u_j^{(1)} + A''_{ij} \Lambda^{(1)}) \Lambda^{(1)} + A \Lambda^{(2)} = 0.$$

giving at the critical point

$$A^{(1)C} = - \frac{A_{111}}{2A'_{11}} \Big|_C, \quad (6.2)$$

and

$$u_s^{(2)C} = - \frac{A_{s11}}{A_{ss}} \Big|_C \quad (s \neq 1),$$

the other two derivatives of immediate interest. We see that when $A_{111}^C \neq 0$ the post-buckling slope $A^{(1)C}$ is non-zero and we have the asymmetric point of bifurcation.

We next proceed to determine some higher derivatives for the special case in which A_{111}^C and (consequently) $A^{(1)C}$ are zero. Differentiating the characterizing equilibrium identity a third time with respect to u_1 and evaluating at the critical point we have after some algebra

$$A^{(2)C} = - \frac{\tilde{A}_{1111}}{3A'_{11}} \Big|_C, \quad (6.3)$$

where

$$\tilde{A}_{1111}^C \equiv A_{1111} - 3 \sum_{s=2}^{s=n} \frac{(A_{s11})^2}{A_{ss}} \Big|_C. \quad (6.4)$$

Clearly this special case gives us the symmetric points of bifurcation, the stable-symmetric point when $A^{(2)C}$ is positive and the unstable-symmetric point when $A^{(2)C}$ is negative. More complex points of bifurcation are of course generated if \tilde{A}_{1111}^C and (consequently) $A^{(2)C}$ are zero.

It can be seen that we have now determined the derivatives of primary interest for the post-buckling equilibrium paths of the three branching points under consideration, and it remains to examine the stability of the intersecting paths, and finally the stability of the critical equilibrium states themselves. Returning to the general case we therefore assume, as before, that we are considering the initial loss of stability of the fundamental equilibrium path of a system under increasing Λ ; all the non-critical stability coefficients are thus positive ($A_{ss}^C > 0$ for $s \neq 1$) while the non-zero coefficient A'_{11}^C is negative. If we follow the approach of Chapter 3 and consider a new set of sliding and rotating principal coordinates for the *post-buckling* equilibrium path it is clear that in the vicinity of the critical point C the stability of the post-buckling equilibrium path will be dependent on the sign of the stability determinant $\mathcal{D}(u_k, \Lambda) \equiv |A_{ij}|$. We thus proceed to examine the variation of this determinant along the post-buckling path, writing

$$\mathcal{D}(u_1) \equiv \mathcal{D}[u_j(u_1), \Lambda(u_1)]$$

so that

$$\mathcal{D}^{(1)} \equiv \frac{d\mathcal{D}}{du_1} = A_j u_j^{(1)} + A' A^{(1)}.$$

Now $u_s^{(1)c} = 0$ for $s \neq 1$, and using the previously determined derivatives of A we have

$$\mathcal{D}^{(1)c} = (A_{111} + A' A^{(1)}) A_{22} A_{33} \cdots A_{nn}|^c,$$

and substituting now for $A^{(1)c}$ we find that

$$\mathcal{D}^{(1)c} = \frac{1}{2} A_{111} A_{22} A_{33} \cdots A_{nn}|^c,$$

which clearly has the same sign as $A^{(1)c}$. Thus for the asymmetric point of bifurcation in which $A_{111}^c \neq 0$ we see that we have the exchange of stabilities discussed earlier and shown in Figures 25 and 63.

For the symmetric points of bifurcation A_{111}^c , $A^{(1)c}$ and $\mathcal{D}^{(1)c}$ vanish and we can write the second variation of \mathcal{D} as

$$\mathcal{D}^{(2)} \equiv \frac{d^2 \mathcal{D}}{du_1^2} = (A_{jk} u_k^{(1)} + A' A^{(1)}) u_j^{(1)} + A_j u_j^{(2)} + (A' u_j^{(1)} + A'' A^{(1)}) A^{(1)} + A' A^{(2)},$$

to give

$$\begin{aligned} \mathcal{D}^{(2)c} &= A_{11} + \sum_{s=2}^{s=n} A_s u_s^{(2)} + A' A^{(2)} \\ &= \frac{2}{3} \tilde{A}_{1111} A_{22} A_{33} \cdots A_{nn}|^c. \end{aligned}$$

Thus when \tilde{A}_{1111}^c and $A^{(2)c}$ are positive, $\mathcal{D}^{(2)c}$ is positive so the rising post-buckling path of the stable-symmetric point of bifurcation is stable (Figures 26 and 64), while when \tilde{A}_{1111}^c and $A^{(2)c}$ are negative, $\mathcal{D}^{(2)c}$ is also negative so the falling post-buckling path of the unstable-symmetric point of bifurcation is unstable (Figures 27 and 65).

Since the coordinate derivatives of A are equivalent to the coordinate derivatives of D in Chapter 3, the stability of the critical equilibrium state itself is readily tested. For the asymmetric point of bifurcation the critical equilibrium state C is therefore seen to be unstable by virtue of the non-zero cubic coefficient A_{111}^c . For the stable-symmetric point of bifurcation the positive coefficient \tilde{A}_{1111}^c shows that state C is stable, while for the unstable-symmetric point of bifurcation the negative coefficient \tilde{A}_{1111}^c shows that the critical equilibrium state is then unstable.

As Koiter has observed, the post-buckling behaviour of the system is obviously closely linked to the stability of the critical equilibrium state itself. This fact, although of no great value in the study of distinct critical points, takes on a very real significance when we come to consider the altogether more complex post-buckling behaviour at coincident critical points.

6.4 The elastic ring

As a brief illustration of the preceding general theory we now consider the buckling of a thin circular ring of radius R deforming in its plane under a uniform radial compressive force of P per unit length. The axial stiffness of the ring is EA and the relevant bending stiffness is EI .

As is the case with the spherical shell of Chapter 11 (Figure 102), points of the ring are located by the central angle θ measured from some reference radius. The total inwards normal displacement is written as $W_t(\theta)$ and the total tangential displacement as $U_t(\theta)$. The pre-buckling uniform contraction of the ring is denoted by W_0 , and we write

$$\begin{aligned} W_t(\theta) &= W_0 + W(\theta), \\ U_t(\theta) &= U(\theta), \end{aligned}$$

so that W and U represent the buckling displacements. Dividing by the radius R , we have the corresponding non-dimensional quantities

$$\begin{aligned} w_t(\theta) &= w_0 + w(\theta), \\ u_t(\theta) &= u(\theta). \end{aligned}$$

Denoting the middle-surface strain by $\epsilon(\theta)$ the extensional strain energy of the ring can be written as

$$J_M = \frac{1}{2} EA \int_0^{2\pi} \epsilon^2 R d\theta.$$

Similarly, denoting the middle-surface curvature change by $\chi(\theta)$ the bending strain energy can be written as

$$J_B = \frac{1}{2} EI \int_0^{2\pi} \chi^2 R d\theta.$$

The loading is assumed to be ‘dead’ in the sense that the force on an element is assumed to retain its magnitude and direction as the ring deflects. The potential energy of the load is then given by the simple expression

$$J_L = -P \int_0^{2\pi} W_t R d\theta.$$

A more complex expression would arise in the case of a fluid pressure in which the force on an element varies in magnitude with the compression of the element and rotates to be always normal to the element.

The total potential energy of the system comprising the ring and its load can thus be written

$$V = \frac{1}{2} EA \int_0^{2\pi} \epsilon^2 R d\theta + \frac{1}{2} EI \int_0^{2\pi} \chi^2 R d\theta - P \int_0^{2\pi} W_t R d\theta.$$

For the strain-displacement relationships we now write

$$\varepsilon = u' - w_t + \frac{1}{2}(w'_t + \Gamma u)^2,$$

$$\chi = \frac{1}{R}(w'' + \Gamma u'),$$

where a prime denotes differentiation with respect to θ . Here the symbol Γ can either denote zero or unity. If it is taken as zero we have the well known Donnell equations, and the strains are identical to those of the spherical shell analysis of Chapter 11. If on the other hand it is taken as unity, we have a well known improvement on the Donnell equations. We shall see that the solution of the ring eigenvalue analysis is in fact independent of Γ for this loading.

In terms of the buckling components we have now

$$\varepsilon = (u' - w) + \frac{1}{2}(w' + \Gamma u)^2 - w_0,$$

$$\chi = \frac{1}{R}(w'' + \Gamma u'),$$

giving

$$\begin{aligned} V(u, w, w_0, P) = & \frac{1}{2}EA \int_0^{2\pi} [(u' - w)^2 + \frac{1}{4}(w' + \Gamma u)^4 + w_0^2 + (u' - w)(w' + \Gamma u)^2 \\ & - 2w_0(u' - w) - w_0(w' + \Gamma u)^2] R d\theta \\ & + \frac{1}{2}EI \int_0^{2\pi} \frac{1}{R^2}(w'' + \Gamma u')^2 R d\theta - PR \int_0^{2\pi} (w_0 + w) R d\theta. \end{aligned}$$

Now the uniform contraction w_0 is given by

$$w_0 = \frac{PR}{EA}$$

and substituting for this we obtain the transformed energy functional $W(u, w, P)$ related to a sliding coordinate system. Expanding this as

$$W = W_0 + W_1(u, w) + W_2(u, w) + \dots,$$

where W_m is the sum of all terms of degree m , we can ignore the arbitrary constant W_0 and the vanishing linear term W_1 . We have then the three items

$$\begin{aligned} W_2 = & \frac{1}{2}EA \int_0^{2\pi} (u' - w)^2 R d\theta + \frac{1}{2}EI \int_0^{2\pi} \frac{1}{R^2}(w'' + \Gamma u')^2 R d\theta \\ & - \frac{1}{2}PR \int_0^{2\pi} (w' + \Gamma u)^2 R d\theta, \end{aligned}$$

$$W_3 = \frac{1}{2}EA \int_0^{2\pi} (u' - w)(w' + \Gamma u)^2 R d\theta,$$

$$W_4 = \frac{1}{2}EA \int_0^{2\pi} \frac{1}{4}(w' + \Gamma u)^4 R d\theta.$$

For reasons that will be explained later, we shall here be concerned exclusively with the linear buckling problem and so merely need to consider the quadratic terms $W_2(u, w)$.

Now if we were to introduce new displacement functions

$$f_1(\theta) = w'(\theta) + \Gamma u(\theta),$$

$$f_2(\theta) = u'(\theta) - w(\theta),$$

we see that in W_2 we should have f_2 in the EA term only. This term is a complete square, and so W_2 would take its lowest value for $f_2 = 0$. It follows that in any buckling mode we would have

$$u'(\theta) = w(\theta),$$

which means that the modes are quasi-inextensional and EA will not appear in the expression for the critical load P^c .

Returning to the problem in hand, we now write

$$w(\theta) = \sum_i^\infty a_i \cos i\theta,$$

$$u(\theta) = \sum_i^\infty b_i \sin i\theta,$$

and it will be adequate for our purposes to start the summations with $i = 2$. This will eliminate some tedious discussions about rigid-body motions, etc.

Differentiating, we have

$$w = a_i \cos i\theta,$$

$$w' = -ia_i \sin i\theta, \quad u = b_i \sin i\theta,$$

$$w'' = -i^2 a_i \cos i\theta, \quad u' = ib_i \cos i\theta,$$

so that

$$u' - w = (ib_i - a_i) \cos i\theta,$$

$$w'' + \Gamma u' = (\Gamma ib_i - i^2 a_i) \cos i\theta,$$

$$w' + \Gamma u = (\Gamma b_i - ia_i) \sin i\theta,$$

and with the well known orthogonality properties we find

$$\int_0^{2\pi} (u' - w)^2 R d\theta = (ib_i - a_i)^2 \int_0^{2\pi} \cos^2 i\theta R d\theta,$$

$$\int_0^{2\pi} (w'' + \Gamma u')^2 R d\theta = i^2 (\Gamma b_i - ia_i)^2 \int_0^{2\pi} \cos^2 i\theta R d\theta,$$

$$\int_0^{2\pi} (w' + \Gamma u)^2 R d\theta = (\Gamma b_i - ia_i)^2 \int_0^{2\pi} \cos^2 i\theta R d\theta.$$

Thus we can write W_2 as

$$W_2 = \left[\frac{EA}{2} (ib_i - a_i)^2 + \frac{EI}{2R^2} i^2 (\Gamma b_i - ia_i)^2 - \frac{1}{2} PR(\Gamma b_i - ia_i)^2 \right] \int_0^{2\pi} \cos^2 i\theta R d\theta.$$

We see that this quadratic form is not strictly diagonal due to the non-zero $a_i b_i$ terms. However, it is clear that if we write the non-singular transformation

$$\begin{aligned} u_i &\equiv \Gamma b_i - ia_i, \\ v_i &\equiv ib_i - a_i, \end{aligned}$$

we shall obtain the diagonal form

$$A_2(u_i, v_i, P) = \left[\frac{EA}{2} v_i^2 + \frac{EI}{2R^2} i^2 u_i^2 - \frac{1}{2} PR u_i^2 \right] \int_0^{2\pi} \cos^2 i\theta R d\theta.$$

The u_i are the amplitudes of the buckling modes, and the critical load associated with a particular u_i is given by

$$P_i = \frac{EI}{R^3} i^2.$$

The lowest critical load, corresponding to $i = 2$, is given by

$$P^c = 4 \frac{EI}{R^3}.$$

This is the well known result for a ring under 'dead' load as given by Pearson.[†] For fluid pressure the factor 4 is replaced by 3 showing that the precise nature of the loading is a significant factor in ring buckling.

The buckling mode is given by

$$\begin{aligned} u_s &= 0, & v_s &= 0, \quad \text{for } s \neq 2, \\ v_2 &= 0, \end{aligned}$$

and is thus expressed by

$$\begin{aligned} w(\theta) &= a \cos 2\theta, \\ u(\theta) &= \frac{1}{2} a \sin 2\theta. \end{aligned}$$

To see how we might have obtained these results using an alternative system of principal coordinates we write

$$W_2 = \left[\frac{EA}{2} (ib_i - a_i)^2 + F_i(\Gamma b_i - ia_i)^2 \right] \int_0^{2\pi} \cos^2 i\theta R d\theta,$$

where

$$F_i = \frac{EI}{2R^2} i^2 - \frac{1}{2} PR.$$

[†] C. E. Pearson, General theory of elastic stability, *Q. appl. Math.*, 14, 131 (1956).

Regrouping, we have

$$\begin{aligned} W_2 &= \{b_i^2 [\frac{1}{2} EA i^2 + F_i \Gamma^2] + a_i b_i [\frac{1}{2} EA (-2i) + F_i (-2i \Gamma)] \\ &\quad + a_i^2 [\frac{1}{2} EA + F_i i^2]\} \int_0^{2\pi} \cos^2 i\theta R d\theta. \end{aligned}$$

Now the completion of a square can be written as

$$Ra^2 + Sab + Tb^2 = \alpha a^2 + x^2,$$

where

$$\begin{aligned} \alpha &= R - \frac{S^2}{4T}, \\ x &= \frac{1}{2\sqrt{T}} (Sa + 2Tb), \end{aligned}$$

and we use this to change coordinates as follows

$$\begin{aligned} a_i &= a_i, \\ x_i &= \frac{(-EAi - F_i 2i\Gamma) a_i + 2(\frac{1}{2} EAi^2 + F_i \Gamma^2) b_i}{2(\frac{1}{2} EAi^2 + F_i \Gamma^2)}. \end{aligned}$$

For $\Gamma = 1$ this is a load-dependent diagonalization since F_i is a function of P , so the new coordinates (a_i, x_i) represent a set of sliding and rotating principal coordinates as discussed in the preceding general theory.

The stability coefficients of a_i are

$$\alpha_i = (\frac{1}{2} EA + F_i i^2) - \frac{(EAi + F_i 2i\Gamma)^2}{4(\frac{1}{2} EAi^2 + F_i \Gamma^2)},$$

and setting $\alpha_i = 0$ we obtain

$$2EA F_i (i^2 - \Gamma)^2 = 0,$$

and so retrieve the required solutions corresponding to $F_i = 0$.

The Donnell equations and the improvement considered here are appropriate for problems in which the middle-surface membrane stresses have a strong influence on the initial post-buckling behaviour, and we note that the forms for W_3 and W_4 are correspondingly proportional to EA . Such membrane action is absent in the behaviour of struts and rings and the use of the Donnell-type equations will therefore predict zero or near zero post-buckling curvature. For such problems there will of course be a rather weak post-buckling contribution, due to nonlinear bending action and therefore dependent on EI , but this could not be picked up by our present formulations since it requires an improvement on the $\chi-w$ relationship corresponding to that of the Euler strut analysis.

For this reason we shall not pursue the ring further, simply retaining the present eigenvalue analysis as an attractive illustration of our diagonalization schemes.

THE CIRCULAR PLATE

7.1 General outline

As a first and substantial application of the preceding general theory, we shall devote this chapter to discrete and continuum branching studies of a uniformly compressed circular plate, with both simply-supported and clamped boundaries, following the work of Thompson and Lewis.¹³⁵ We shall see that the discrete coordinate general theory can indeed be employed in association with the kinematically-admissible finite-element procedure as a most viable method of post-buckling analysis. The inclusion of the continuum analysis will allow us to compare the two approaches side by side, and will also supply us with exact solutions to which the finite-element results are observed to converge.

Since the aim is to delineate a broad method of analysis for use in more complex practical problems the analyses are developed in their most basic form. The two original displacement functions are retained as dependent variables with no introduction of a stress function, and analytical refinements which might well break down in more practical problems are kept to a minimum.

Attention is confined to moderately large displacements, and the strain-displacement relationships corresponding to the Kármán plate equations are used to yield the required strain energy integrals. The loading is assumed to be conservative and such that the force per unit length of the *original* circumference is a controlled quantity, the formulation being then only approximately true for the alternative mode of compression in which the force per unit length of the *current* circumference is prescribed. The total potential energy functional is written down and is then expressed in terms of the buckling increments from the uniformly compressed state. This corresponds to the sliding transformation of the discrete coordinate theory, and leaves the loading parameter acting on a quadratic rather than a linear form, in a manner that we have already indicated in Chapter 6.

For the continuum study the differential equations of equilibrium are derived from the transformed energy functional using the calculus of variations, and a perturbation analysis is developed. Here, in place of the straightforward

suppression of secular terms (which are not always easily identified) a continuum contraction mechanism delineated by Croll¹²³ is employed: this corresponds closely to the contraction employed in the discrete-coordinate general theory.

The finite-element analysis follows, and polynomial forms consistent with the structure of the energy functional are used to fabricate the deflection functions. Thus third-order polynomials are employed for the lateral deflection with two degrees of freedom at each internal station, while the incremental in-plane displacement is chosen to be piecewise linear with only a single degree of freedom at each internal station. The energy coefficients for an element are written down and the heavily banded total energy coefficients are obtained by summation.

The general *W*-analysis of Chapter 6 is then employed and the pattern of analysis is seen to correspond closely to that of the continuum analysis. The finite-element results are finally observed to converge rapidly to the exact continuum values as the number of elements is increased, twelve elements being needed to obtain accurate numerical solutions.

7.2 Formulation

We begin by formulating the problem in terms of the total potential energy of the system. The structure under consideration is a thin circular plate of radius R and thickness t deforming symmetrically with respect to its axis of revolution. The movement of a point on the middle-surface is decomposed into an in-plane displacement $u(r)$ and a normal displacement $w(r)$ as shown in Figure 67, where r is the original distance of the point from the axis of symmetry. The second independent variable θ representing rotation about this axis will make little appearance in the analysis due to the assumed symmetry. The material of the plate is assumed to be linearly elastic with Young's modulus E and Poisson's ratio v , and the bending rigidity of the plate is written as

$$D = \frac{Et^3}{12(1-v^2)}.$$

Adequate expressions for the middle-surface curvatures are

$$\chi_r = \frac{d^2 w}{dr^2} = \ddot{w}, \quad \chi_\theta = \frac{1}{r} \frac{dw}{dr} = \frac{\dot{w}}{r},$$

where a dot denotes differentiation with respect to r , so the strain energy of bending can be written as

$$J_B = \frac{1}{2} D \int (\chi_r^2 + 2v \chi_r \chi_\theta + \chi_\theta^2) dA \\ = \pi D \int_0^R \left[\ddot{w}^2 + 2v \ddot{w} \frac{\dot{w}}{r} + \left(\frac{\dot{w}}{r} \right)^2 \right] r dr.$$

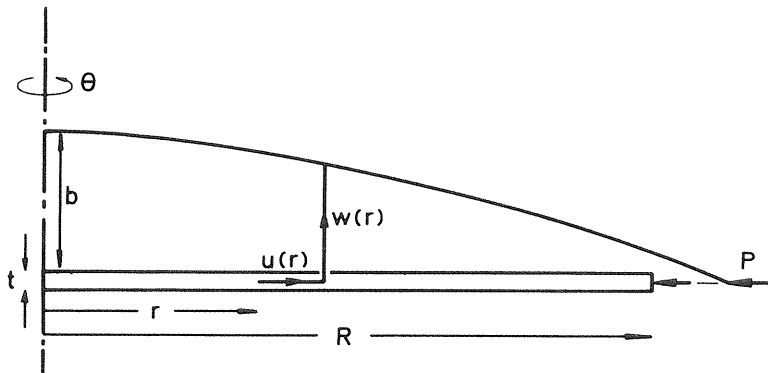


Figure 67 Notation for the circular plate

The middle-surface strains can likewise be written as

$$\epsilon_r = \dot{u} + \frac{1}{2}\dot{w}^2, \quad \epsilon_\theta = \frac{u}{r}$$

so the strain energy of stretching can be written

$$\begin{aligned} J_E &= \frac{Et}{2(1-v^2)} \int (\epsilon_r^2 + 2v\epsilon_r\epsilon_\theta + \epsilon_\theta^2) dA \\ &= \frac{\pi Et}{1-v^2} \int_0^R \left[(\dot{u} + \frac{1}{2}\dot{w}^2)^2 + 2v(\dot{u} + \frac{1}{2}\dot{w}^2)\frac{u}{r} + \left(\frac{u}{r}\right)^2 \right] r dr. \end{aligned}$$

In these expressions dA represents an element of area of the middle-surface.

The plate is assumed to be compressed symmetrically as indicated by a uniformly distributed force around the circumference. The loading is assumed to be conservative, and we shall consider two ways in which it might be realized.

Let us suppose first that we employ a fluid with the prescribed pressure p . The force per unit length of the *current* circumference is then a controlled quantity and the energy of the load is the product of the pressure and the volume change,

$$\begin{aligned} J_L &= pt \{ \pi[R + u(R)]^2 - \pi R^2 \} \\ &= 2\pi Rtp \left[u(R) + \frac{u(R)^2}{2R} \right]. \end{aligned}$$

Suppose secondly that we employ a large number of strings radiating from the axis of symmetry and tied to the circumference. With prescribed tensions, this will generate a controlled force per unit length of the *original* circumference, and the energy can be written as

$$J_L = 2\pi RPu(R),$$

where P is the force per unit length.

The different modes of loading do of course give rise to differing energy expressions, and in the present study we shall adopt the second expression which is exact for the string loading. This expression is approximately correct for the fluid pressure if we set $tp = P$, and would in fact be obtained if we were to linearize the first energy expression.

The total potential energy of the system embracing the plate and its loading device, can now be written as

$$\begin{aligned} V &= J_B + J_E + J_L \\ &= \pi D \int_0^R \left[\ddot{w}^2 + 2v\ddot{w}\frac{\dot{w}}{r} + \left(\frac{\dot{w}}{r}\right)^2 \right] r dr \\ &\quad + \frac{\pi Et}{1-v^2} \int_0^R \left[(\dot{u} + \frac{1}{2}\dot{w}^2)^2 + 2v(\dot{u} + \frac{1}{2}\dot{w}^2)\frac{u}{r} + \left(\frac{u}{r}\right)^2 \right] r dr + 2\pi RPu(R). \end{aligned}$$

Before buckling we have the simple fundamental response given by

$$w(r) = 0, \quad u(r) = u^F(r) = -\frac{P(1-v)}{Et}r,$$

and we now define changes in the displacements from this state by the equations

$$\begin{aligned} w(r) &= w(r), \\ u(r) &= u^F(r) + v(r). \end{aligned}$$

This corresponds to the sliding transformation of the discrete coordinate general theory, and we can now write the total potential energy of the system as a function of these incremental displacements,

$$\begin{aligned} W &= \pi D \int_0^R \left[\ddot{w}^2 + 2v\ddot{w}\frac{\dot{w}}{r} + \left(\frac{\dot{w}}{r}\right)^2 \right] r dr \\ &\quad + \frac{\pi Et}{1-v^2} \int_0^R \left[(\dot{u}^F + \dot{v} + \frac{1}{2}\dot{w}^2)^2 + 2v(\dot{u}^F + \dot{v} + \frac{1}{2}\dot{w}^2)\frac{u^F + v}{r} + \left(\frac{u^F + v}{r}\right)^2 \right] r dr \\ &\quad + 2\pi RP[u^F(R) + v(R)]. \end{aligned}$$

The constant term can be ignored, and observing that the linear terms vanish because the fundamental state is one of equilibrium, this can be simplified to

$$\begin{aligned} W(v, w, P) &= \pi D \int_0^R \left[\ddot{w}^2 + 2v\ddot{w}\frac{\dot{w}}{r} + \left(\frac{\dot{w}}{r}\right)^2 \right] r dr \\ &\quad + \frac{\pi Et}{1-v^2} \int_0^R \left[(\dot{v} + \frac{1}{2}\dot{w}^2)^2 + 2v(\dot{v} + \frac{1}{2}\dot{w}^2)\frac{v}{r} + \left(\frac{v}{r}\right)^2 \right] r dr \\ &\quad - \pi P \int_0^R \dot{w}^2 r dr. \end{aligned}$$

As we have discussed earlier, we notice that this has exactly the same form as $V[u, w, P]$ with the linear load term replaced by a quadratic load term.

The differential equations of equilibrium needed for the continuum perturbation analysis will now be derived using the calculus of variations. The first variation of W can be written immediately as

$$\delta W = \pi D \int_0^R \left[2\ddot{w}\delta\ddot{w} + 2v\delta\dot{w}\frac{\dot{w}}{r} + 2v\ddot{w}\frac{\delta\dot{w}}{r} + 2\frac{\dot{w}\delta\dot{w}}{r^2} \right] r dr \\ + \frac{\pi Et}{1-v^2} \int_0^R \left[2\ddot{v}\delta\ddot{v} + \delta\dot{v}\dot{w}^2 + \dot{v}2\ddot{w}\delta\dot{w} + \dot{w}^3\delta\dot{w} + 2v\delta\dot{v}\frac{v}{r} + 2v\dot{v}\frac{\delta v}{r} \right. \\ \left. + 2v\dot{w}\delta\dot{w}\frac{v}{r} + v\dot{w}^2\frac{\delta v}{r} + 2\frac{v\delta v}{r^2} \right] r dr - \pi P \int_0^R 2\dot{w}\delta\dot{w}r dr,$$

and using integration by parts we obtain the two differential equations

$$2r\ddot{w} + 4\ddot{w} - \frac{2\ddot{w}}{r} + \frac{2\dot{w}}{r^2} + \frac{12}{t^2}(-2\dot{v}\dot{r}\ddot{w} - 2\dot{w}\dot{r}\ddot{v} - 2\dot{w}\dot{v} - 3r\dot{w}^2\ddot{w} - \dot{w}^3 - 2vv\ddot{w} - 2v\dot{v}\dot{w}) \\ + \frac{P}{Et^3} 12(1-v^2)\{2\dot{w} + 2r\ddot{w}\} = 0, \\ \ddot{v} + \frac{\dot{v}}{r} - \frac{v}{r^2} + \dot{w}\ddot{w} + \frac{(1-v)\dot{w}^2}{2r} = 0,$$

together with the boundary requirements

$$2r\ddot{w}\delta\dot{w} - 2r\ddot{w}\delta w - 2\ddot{w}\delta w + 2v\dot{w}\delta\dot{w} + \frac{2\dot{w}}{r}\delta w \\ + \frac{12}{t^2}(2r\dot{v}\dot{w}\delta w + r\dot{w}^3\delta w + 2vv\dot{w}\delta w) - \frac{P}{Et^3} 12(1-v^2)\{2\dot{w}r\delta w\} \Big|_0^R = 0, \\ 2r\dot{v}\delta v + r\dot{w}^2\delta v + 2vv\delta v \Big|_0^R = 0.$$

Simplifying the out-of-plane equilibrium equation by integration, we are left with the two *Euler* equations

$$\ddot{w} + \frac{\dot{w}}{r} - \frac{\ddot{w}}{r^2} - \frac{12}{t^2} \left(\dot{v} + \frac{\dot{w}^2}{2} + \frac{v}{r} \right) \dot{w} + \frac{12P(1-v^2)}{Et^3} \dot{w} = 0, \\ \ddot{v} + \frac{\dot{v}}{r} - \frac{v}{r^2} + \dot{w}\ddot{w} + \frac{(1-v)\dot{w}^2}{2r} = 0.$$

We must now consider how the plate is to be supported, and we note that the variational process has supplied us with boundary requirements which must be met to ensure a well posed problem. In the present work we shall be concerned with both simply-supported and clamped plates, and it remains to observe how these will meet the requirements of the variational procedure.

The boundary conditions for the simply-supported plate are

$$w(R) = \delta w(R) = 0, \\ \dot{w}(0) = \delta \dot{w}(0) = 0, \\ v(0) = \delta v(0) = 0,$$

and to satisfy the written requirements we must add the further conditions

$$\dot{w} + v \frac{\dot{w}}{r} \Big|_0^R = 0, \\ \ddot{w} = \frac{\dot{w}}{r} \Big|_0^R, \\ \dot{v} + \frac{1}{2}\dot{w}^2 + v \frac{v}{r} \Big|_0^R = 0.$$

These are readily identified as appropriate boundary conditions on the edge bending moment, the centre curvatures and the edge direct stress. For the clamped plate we have the boundary conditions

$$w(R) = \delta w(R) = 0, \\ \dot{w}(0) = \delta \dot{w}(0) = 0, \\ v(0) = \delta v(0) = 0,$$

and now

$$\dot{w}(R) = \delta \dot{w}(R) = 0,$$

and to satisfy the written requirements we must add the further conditions

$$\ddot{w} = \frac{\dot{w}}{r} \Big|_0^R, \\ \dot{v} + \frac{1}{2}\dot{w}^2 + v \frac{v}{r} \Big|_0^R = 0,$$

which are again easily identified.

7.3 Continuum analyses

To start the continuum perturbation analysis of initial post-buckling we write

$$w(r) = sw_1(r) + s^2 w_2(r) + s^3 w_3(r) + \dots, \\ v(r) = sv_1(r) + s^2 v_2(r) + s^3 v_3(r) + \dots, \\ P = P^c + sP^{(1)} + \frac{1}{2}s^2 P^{(2)} + \dots,$$

where s is an independent expansion parameter defining progress along the post-buckling equilibrium path. Substituting these into the differential equations of equilibrium and writing them as power series in s we can equate the coefficients to zero to generate an ordered series of equilibrium equations. These are sequentially linear, and can be written as follows:

$$\begin{aligned}\ddot{w}_1 + \frac{\dot{w}_1}{r} - \frac{\dot{w}_1}{r^2} + \frac{12P^c(1-v^2)}{Et^3} \dot{w}_1 &= 0, \\ \ddot{w}_2 + \frac{\dot{w}_2}{r} - \frac{\dot{w}_2}{r^2} - \frac{12}{t^2} \left(\dot{w}_1 \dot{v}_1 + v \frac{\dot{w}_1 v_1}{r} \right) + \frac{12P^c(1-v^2)}{Et^3} \dot{w}_2 + \frac{12P^{(1)}(1-v^2)}{Et^3} \dot{w}_1 &= 0, \\ \ddot{w}_3 + \frac{\dot{w}_3}{r} - \frac{\dot{w}_3}{r^2} - \frac{12}{t^2} \left(\dot{w}_1 \dot{v}_2 + v \frac{\dot{w}_1 v_2}{r} + \frac{\dot{w}_1^3}{2} + \dot{w}_2 \dot{v}_1 + v \frac{\dot{w}_2 v_1}{r} \right) \\ + \frac{12(1-v^2)}{Et^3} (P^c \dot{w}_3 + P^{(1)} \dot{w}_2 + \frac{1}{2} P^{(2)} \dot{w}_1) &= 0,\end{aligned}$$

these being the first three out-of-plane equations, and

$$\begin{aligned}\ddot{v}_1 + \frac{\dot{v}_1}{r} - \frac{v_1}{r^2} &= 0, \\ \ddot{v}_2 + \frac{\dot{v}_2}{r} - \frac{v_2}{r^2} + \dot{w}_1 \dot{w}_1 + \frac{1}{2}(1-v) \frac{\dot{w}_1^2}{r} &= 0, \\ \ddot{v}_3 + \frac{\dot{v}_3}{r} - \frac{v^3}{r^2} + \dot{w}_1 \dot{w}_2 + \dot{w}_2 \dot{w}_1 + (1-v) \frac{\dot{w}_1 \dot{w}_2}{r} &= 0,\end{aligned}$$

these being the first three in-plane equations.

From now on in the continuum analysis we must consider the two support conditions separately, and we consider first the simply-supported plate. Substituting the expansions for $w(r)$ and $v(r)$ into the previously derived boundary conditions for simple supports we have

$$\begin{aligned}\dot{w}_i(0) = 0, \quad v_i(0) = 0 &\quad \text{for all } i, \\ w_i(R) = 0, \quad \dot{w}_i(R) + \frac{v}{R} \dot{w}_i(R) = 0 &\quad \text{for all } i,\end{aligned}$$

and

$$\begin{aligned}\dot{v}_1(R) + v \frac{v_1(R)}{R} &= 0, \\ \dot{v}_2(R) + \frac{1}{2} \dot{w}_1^2(R) + v \frac{v_2(R)}{R} &= 0, \\ \dot{v}_3(R) + \dot{w}_1(R) \dot{w}_2(R) + v \frac{v_3(R)}{R} &= 0.\end{aligned}$$

Equating now the progress parameter s to the central deflection of the plate $b = w(0)$ we obtain the ‘false’ boundary conditions

$$\begin{aligned}w_1(0) &= 1, \\ w_s(0) &= 0 \quad \text{for } s \neq 1.\end{aligned}$$

The first out-of-plane equation is seen to have the solution

$$\dot{w}_1(r) = A_1 J_1(\gamma r) + B_1 Y_1(\gamma r),$$

where J_1 and Y_1 are the Bessel functions of the first order and A_1 and B_1 are integration constants. Here

$$\gamma \equiv \sqrt{\frac{P^c}{D}}$$

where P^c is the as yet unknown critical load of the plate and D is the previously defined bending rigidity. For a plate without a central hole we must set $B_1 = 0$ and using the conditions $w_1(0) = 1$, $w_1(R) = 0$ we obtain

$$\dot{w}_1(r) = \frac{\gamma J_1(\gamma r)}{J_0(\gamma R) - 1}$$

giving

$$\ddot{w}_1(r) = \frac{\gamma^2}{J_0(\gamma R) - 1} \left\{ J_0(\gamma r) - \frac{J_1(\gamma r)}{\gamma r} \right\},$$

where J_0 is the Bessel function of zero order of the first kind.

Using the condition

$$\dot{w}_1(R) + v \frac{\dot{w}_1(R)}{R} = 0$$

we now obtain the equation

$$\gamma R J_0(\gamma R) - (1-v) J_1(\gamma R) = 0$$

which we must solve for γ and hence P^c . Setting Poisson’s ratio equal to 0.3, the equation is satisfied by $\gamma R = 2.049$, and hence we have

$$P^c = 4.198 \frac{D}{R^2},$$

the corresponding buckling mode being given by

$$w_1(r) = \frac{J_0(\gamma R) - J_0(\gamma r)}{J_0(\gamma R) - 1}.$$

The first in-plane equation and the second out-of-plane equation give us the expected results

$$v_1(r) = w_2(r) = P^{(1)} = 0,$$

and we proceed to the second in-plane equation which yields

$$v_2(r) = \frac{\gamma}{4[J_0(\gamma R) - 1]^2} \{(1 + \nu) J_0(\gamma r) J_1(\gamma r) + \nu \gamma r [J_0^2(\gamma R) - J_0^2(\gamma r) + J_1^2(\gamma R) - J_1^2(\gamma r)] - \gamma r J_1^2(\gamma R)\}.$$

The third-order equation for the lateral deflection can now be written as

$$\ddot{w}_3 + \frac{\dot{w}_3}{r} - \frac{\dot{w}_3}{r^2} + \frac{12(1 - \nu^2) P^C}{E t^3} \dot{w}_3 = \frac{12}{t^2} \left[\dot{v}_2 + \frac{\dot{w}_1^2}{2} + \nu \frac{v_2}{r} \right] \dot{w}_1 - \frac{12(1 - \nu^2) P^{(2)}}{2 E t^3} \dot{w}_1,$$

where the right-hand side is already known but for the required derivative $P^{(2)}$.

Experience with the elastica in Chapter 1 indicates that to find the second load derivative $P^{(2)}$ it will not be necessary to *solve* this equation for $w_3(r)$, and to extract $P^{(2)}$ we follow a manoeuvre of Croll.¹²³ This corresponds closely to the suppression of secular terms used in the strut analysis and proceeds as follows. Multiplying the differential equation by \dot{w}_1 and integrating from 0 to R using the differential $r dr$, the unknown left-hand side vanishes by virtue of the boundary conditions, and after some manipulation we retrieve the required derivative

$$P^{(2)} = \frac{2.269 D}{R^2 t^2}.$$

The leading terms of the series solution for the post-buckling load can then be written as

$$\frac{P}{P^C} = 1 + 0.2702 \left(\frac{b}{t} \right)^2 + \dots$$

This equation gives us the post-buckling path shown in Figure 68, which is seen to be in good agreement with the results of Friedrichs and Stoker.^{158–160}

The clamped plate analysis can be written down in a similar fashion. The boundary conditions are now

$$\begin{aligned} \dot{w}_i(0) &= 0, & v_i(0) &= 0, \\ w_i(R) &= 0, & \dot{w}_i(R) &= 0, \\ \dot{v}_i(R) + \frac{\nu}{R} v_i(R) &= 0, \end{aligned}$$

for all i , and the definition of the expansion parameter s gives us the additional conditions

$$w_1(0) = 1, \quad w_s(0) = 0 \quad \text{for } s \neq 1.$$

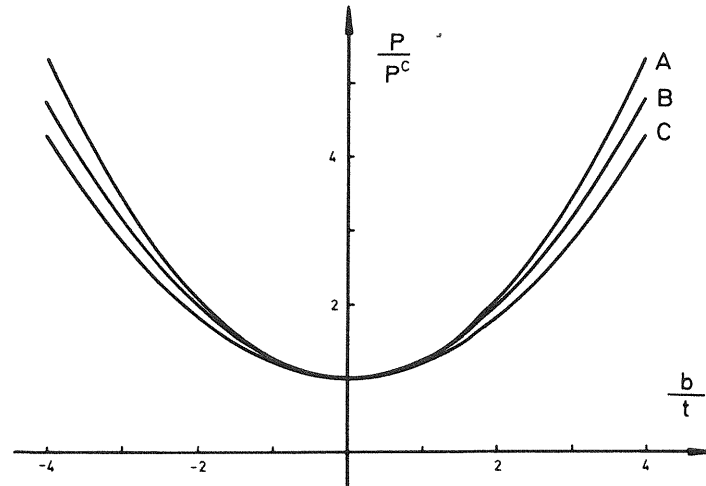


Figure 68 Post-buckling solutions: A, present work with simple supports; B, Friedrichs and Stoker with simple supports; C, present work with clamped boundary

For a solution of the first-order equation in the lateral deflection we must have

$$\frac{\gamma J_1(\gamma R)}{J_0(\gamma R) - 1} = 0, \quad \text{where } \gamma \equiv \sqrt{\frac{P^C}{D}},$$

and using the tabulated zeros of Bessel functions we obtain

$$\gamma R = 3.832, \quad P^C = 14.68 \frac{D}{R^2}.$$

The buckling mode is now

$$w_1(r) = \frac{J_0(\gamma R) - J_0(\gamma r)}{J_0(\gamma R) - 1},$$

where γ has of course a different value from that of the simply-supported plate.

Following the pattern of the simply-supported plate we again obtain the expected results

$$v_1(r) = w_2(r) = P^{(1)} = 0$$

and the second in-plane equation yields

$$\begin{aligned} v_2(r) &= \frac{\gamma}{4[J_0(\gamma R) - 1]^2} \{(1 + \nu) J_0(\gamma r) J_1(\gamma r) + \nu \gamma r [J_0^2(\gamma R) - J_0^2(\gamma r) + J_1^2(\gamma R) - J_1^2(\gamma r)] - \gamma r J_1^2(\gamma R)\}. \end{aligned}$$

The third equation for the lateral deflection has exactly the same form as for the simply-supported plate and treating it in like fashion we obtain, without solving the equation for $w_3(r)$,

$$P^{(2)} = \frac{6.017D}{R^2 t^2}$$

and

$$\frac{P}{P_c} = 1 + 0.2049 \left(\frac{b}{t} \right)^2 + \dots$$

This result is shown graphically in Figure 68.

7.4 Finite-element analyses

The plate will now be analysed afresh using the kinematically-admissible finite-element procedure.

We first divide the r domain into m equal elements as shown in Figures 69 and 70, the stations being numbered from 1 to $m + 1$, and we proceed to fabricate forms for the mathematical functions $w(r)$ and $v(r)$. For the out-of-plane function $w(r)$ each internal station is given an arbitrary displacement w and an arbitrary first derivative \dot{w} , both being denoted by the b_i coordinates. At the terminal station, $m + 1$, the freedom required clearly depends upon the problem under consideration: the simply-supported plate will have freedom of slope but no freedom of displacement, while the clamped plate will have no freedom at all. The first, central, station must be allowed displacement but no slope in

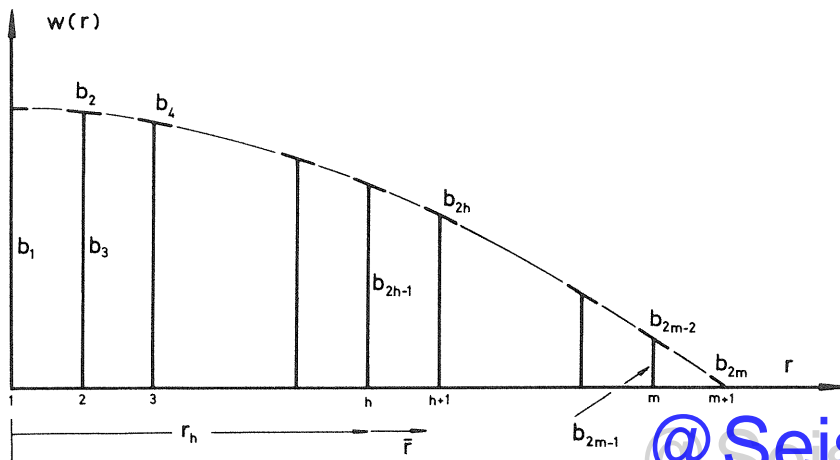


Figure 69 Fabrication of $w(r)$. For the clamped boundary $b_{2m} = 0$

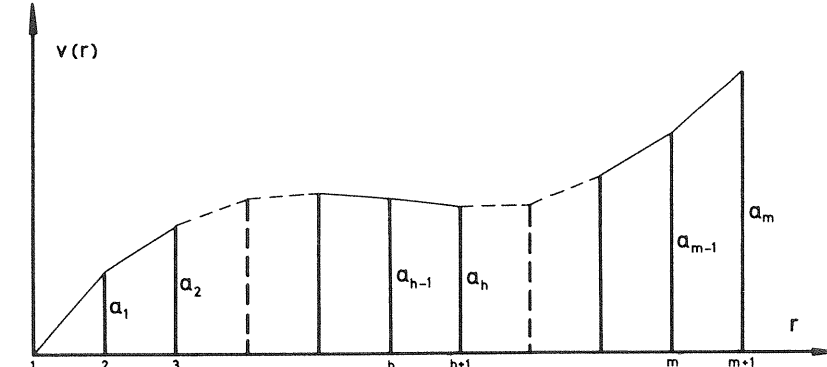


Figure 70 Fabrication of the mathematical function $v(r)$

either case. A third-order polynomial is now fitted in each region and can be written as

$$\begin{aligned} w\left(\frac{\bar{r}}{R}\right) &= b_{(2h-2)} R \left[\left(\frac{\bar{r}}{R}\right) - 2m \left(\frac{\bar{r}}{R}\right)^2 + m^2 \left(\frac{\bar{r}}{R}\right)^3 \right] \\ &\quad + b_{(2h-1)} R \left[1 - 3m^2 \left(\frac{\bar{r}}{R}\right)^2 + 2m^3 \left(\frac{\bar{r}}{R}\right)^3 \right] \\ &\quad + b_{2h} R \left[-m \left(\frac{\bar{r}}{R}\right)^2 + m^2 \left(\frac{\bar{r}}{R}\right)^3 \right] \\ &\quad + b_{(2h+1)} R \left[3m^2 \left(\frac{\bar{r}}{R}\right)^2 - 2m^3 \left(\frac{\bar{r}}{R}\right)^3 \right], \end{aligned}$$

where \bar{r} is the local independent variable defined by $\bar{r} = r - r_h$ as shown in the figures. The overall deflected shape will thus be continuous in displacement and first derivative, as demanded by the energy functional: there will, however, be discontinuities of second derivative at the internal stations.

Each internal station is next given an arbitrary displacement denoted by a_i for the in-plane function $v(r)$. The outer station can also be given an arbitrary displacement for either problem, but we must clearly allow no freedom at the first station as shown. The energy functional shows that discontinuities in v are allowable, so we can permit the form of v to be linear between stations as shown in Figure 70. The expression for a general region can thus be stated as

$$v\left(\frac{\bar{r}}{R}\right) = a_{(h-1)} R \left[1 - m \left(\frac{\bar{r}}{R}\right) \right] + a_h R \left[m \left(\frac{\bar{r}}{R}\right) \right].$$

Substituting these two functions into the energy functional for the general h th region we have

$$\begin{aligned} W^h = \pi D \int_0^{R/m} & \left[\ddot{w}^2 + 2v\dot{w}\frac{\dot{w}}{r_h + \bar{r}} + \left(\frac{\dot{w}}{r_h + \bar{r}} \right)^2 \right] (r_h + \bar{r}) d\bar{r} \\ & + \frac{\pi Et}{1 - v^2} \int_0^{R/m} \left[\dot{v}^2 + 2v\dot{v}\left(\frac{v}{r_h + \bar{r}} \right) + \left(\frac{v}{r_h + \bar{r}} \right)^2 + \dot{v}\dot{w}^2 + v\left(\frac{v}{r_h + \bar{r}} \right)\dot{w}^2 \right. \\ & \left. + \frac{1}{4}\dot{w}^4 \right] (r_h + \bar{r}) d\bar{r} - \pi P \int_0^{R/m} \dot{w}^2 (r_h + \bar{r}) d\bar{r} \end{aligned}$$

and considering a Taylor series expansion, this may be represented by

$$W^h = \frac{1}{2}J_{ij}^h b_i b_j + \frac{1}{2}K_{ij}^h a_i a_j + \frac{1}{2}L_{ijk}^h b_i b_j a_k + \frac{1}{24}M_{ijkl}^h b_i b_j b_k b_l - \frac{1}{2}PN_{ij}^h b_i b_j,$$

where the quadratic arrays, the quartic array and the quadratic $b_i b_j$ component of the cubic array are assumed to be symmetric. Finally using the summed identities

$$\begin{aligned} \frac{1}{2}J_{ij}^h b_i b_j &= \pi D \int_0^{R/m} \left[\ddot{w}^2 + 2v\dot{w}\frac{\dot{w}}{r_h + \bar{r}} + \left(\frac{\dot{w}}{r_h + \bar{r}} \right)^2 \right] (r_h + \bar{r}) d\bar{r}, \\ \frac{1}{2}K_{ij}^h a_i a_j &= \frac{\pi Et}{1 - v^2} \int_0^{R/m} \left[\dot{v}^2 + 2v\dot{v}\left(\frac{v}{r_h + \bar{r}} \right) + \left(\frac{v}{r_h + \bar{r}} \right)^2 \right] (r_h + \bar{r}) d\bar{r}, \\ \frac{1}{2}L_{ijk}^h b_i b_j a_k &= \frac{\pi Et}{1 - v^2} \int_0^{R/m} \left[\dot{v}\dot{w}^2 + v\left(\frac{v}{r_h + \bar{r}} \right)\dot{w}^2 \right] (r_h + \bar{r}) d\bar{r}, \\ \frac{1}{24}M_{ijkl}^h b_i b_j b_k b_l &= \frac{\pi Et}{1 - v^2} \int_0^{R/m} \frac{1}{4}\dot{w}^4 (r_h + \bar{r}) d\bar{r}, \\ \frac{1}{2}PN_{ij}^h b_i b_j &= \pi P \int_0^{R/m} \dot{w}^2 (r_h + \bar{r}) d\bar{r}, \end{aligned}$$

and enforcing the symmetry requirement when necessary, gives us the required energy coefficients, some of which are shown in Tables 7.1 to 7.3.

The in-plane quadratic form K^1 of the central element will only involve a_1 , and its dimensionless coefficient is $(1 + v)$ as shown in Table 7.1. For the general h th element this quadratic form will involve $a_{(h-1)}$ and a_h , and the coefficients are shown in Table 7.2. In a similar fashion the components of the out-of-plane quadratics J and N are readily written down for the central element and a general element respectively, while the components of L are shown in Table 7.3. Tables of all the energy coefficients can be found in the original paper by Thompson and Lewis.¹³⁵

TABLE 7.1 The coefficients of the array $(1 - v^2)/Et\pi R^2 \cdot \frac{1}{2}K_{ij}^1$

a_1	$(1 + v)$
-------	-----------

TABLE 7.2 The coefficients of the array $(1 - v^2)/Et\pi R^2 \cdot \frac{1}{2}K_{ij}^h$. Valid for $h > 1$

$a_{(h-1)}$	a_h
$\{[\ln(h) - \ln(h-1)]h^2 - v - 1\}$	$-[\ln(h) - \ln(h-1)]h(h-1)$
$-[\ln(h) - \ln(h-1)]h(h-1)$	$\{[\ln(h) - \ln(h-1)](h-1)^2 + v + 1\}$

TABLE 7.3 The coefficients of the array $(1 - v^2)/Et\pi R^2 \cdot \frac{1}{2}L_{ij}^h$. Valid for all h

$a_h\{1\} \times$	$b_{(2h-2)}$	$b_{(2h-1)}$	b_{2h}	$b_{(2h+1)}$
$b_{(2h-2)}$	$\left(\frac{4h-3+v}{30m} \right)$	$\left(\frac{h+v}{10} \right)$	$\left(\frac{1-2h-v}{60m} \right)$	$-\left(\frac{h+v}{10} \right)$
$b_{(2h-1)}$	$\left(\frac{h+v}{10} \right)$	$m\left(\frac{6h-3+3v}{5} \right)$	$\left(\frac{h-1}{10} \right)$	$-m\left(\frac{6h-3+3v}{5} \right)$
b_{2h}	$\left(\frac{1-2h-v}{60m} \right)$	$\left(\frac{h-1}{10} \right)$	$\left(\frac{4h-1+3v}{30m} \right)$	$-\left(\frac{h-1}{10} \right)$
$b_{(2h+1)}$	$-\left(\frac{h+v}{10} \right)$	$-m\left(\frac{6h-3+3v}{5} \right)$	$-\left(\frac{h-1}{10} \right)$	$m\left(\frac{6h-3+3v}{5} \right)$

$+a_{(h-1)}\{1\} \times$	$b_{(2h-2)}$	$b_{(2h-1)}$	b_{2h}	$b_{(2h+1)}$
$b_{(2h-2)}$	$\left(\frac{-4h+3+3v}{30m} \right)$	$-\left(\frac{h}{10} \right)$	$\left(\frac{2h-1-v}{60m} \right)$	$\left(\frac{h}{10} \right)$
$b_{(2h-1)}$	$-\left(\frac{h}{10} \right)$	$m\left(\frac{-6h+3+3v}{5} \right)$	$\left(\frac{-h+1+v}{10} \right)$	$-m\left(\frac{-6h+3+3v}{5} \right)$
b_{2h}	$\left(\frac{2h-1-v}{60m} \right)$	$\left(\frac{-h+1+v}{10} \right)$	$\left(\frac{-4h+1+v}{30m} \right)$	$-\left(\frac{-h+1+v}{10} \right)$
$b_{(2h+1)}$	$\left(\frac{h}{10} \right)$	$-m\left(\frac{-6h+3+3v}{5} \right)$	$-\left(\frac{-h+1+v}{10} \right)$	$m\left(\frac{-6h+3+3v}{5} \right)$

We can now add the contributions from the m elements of the plate to give us

$$W = \sum_{h=1}^{h=m} W^h = \frac{1}{2} J_{ij} b_i b_j + \frac{1}{2} K_{ij} a_i a_j + \frac{1}{2} L_{ijk} b_i b_j a_k + \frac{1}{24} M_{ijkl} b_i b_j b_k b_l - \frac{1}{2} P N_{ij} b_i b_j,$$

where we again demand appropriate symmetry in the arrays. Here

$$J_{ij} = \sum_1^m J_{ij}^h, \quad K_{ij} = \sum_1^m K_{ij}^h, \quad L_{ijk} = \sum_1^m L_{ijk}^h, \quad M_{ijkl} = \sum_1^m M_{ijkl}^h \quad \text{and} \quad N_{ij} = \sum_1^m N_{ij}^h,$$

and we obtain heavily banded arrays for the resulting coefficients. The mode of overlapping of the subarrays for the quadratic forms J and N is shown in Figure 71.

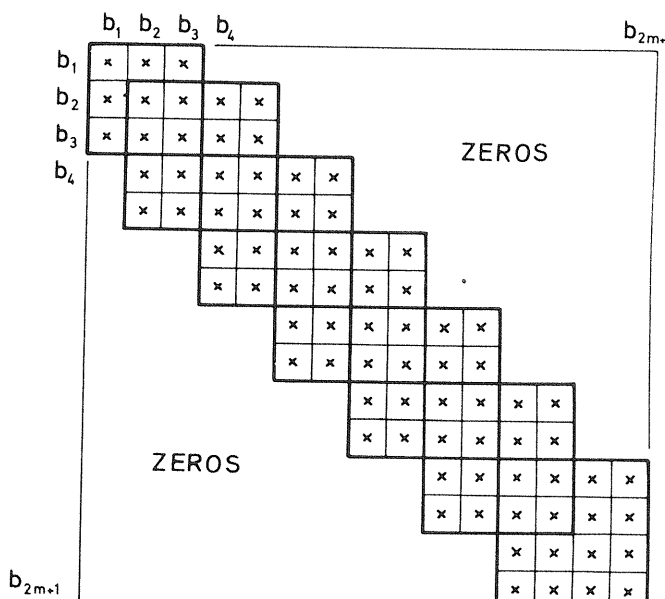


Figure 71 Overlapping of arrays

So far in the analysis we have employed the two sets of coordinates a_i and b_j , but in applying the results of the general branching theory it will be necessary to write q_i to denote the complete set of n generalized coordinates. For the simply-supported plate n will thus be equal to $3m$ and for the clamped plate $3m + 1$. Thus W_{ij} , the coefficient of $q_i q_j$, will embrace the J , K and N arrays, etc.

We see that we now have a discrete conservative structural system as envisaged in the preceding general theory defined by the transformed total potential energy function W . The system is in fact of the special P type, but this having been said we shall continue to write the loading parameter of the general theory as Λ so that we can set

$$\Lambda = \frac{PR^2}{D}.$$

Following the general theory, the first step in the analysis is the determination of the lowest critical load of the plate using the condition that $|W_{ij}| = 0$. Now from the partitioned nature of W_{ij} which corresponds to the forms

$$\frac{1}{2} J_{ij} b_i b_j + \frac{1}{2} K_{ij} a_i a_j - \frac{1}{2} P N_{ij} b_i b_j$$

we see that the in-plane coordinates will play no part in the eigenvalue analysis, and thus the determination of the critical load reduces to the location of the first zero of the subdeterminant of W_{ij} corresponding to $J_{ij} - P N_{ij}$. This was readily accomplished on a computer by systematically varying Λ , and the convergence of P^c with increasing number of elements is shown in Figure 72 for the two boundary conditions under consideration.

Now the first two evaluated equations of the general theory are

$$W_{ij} q_j^{(1)}|^c = 0, \\ W_{ijk} q_j^{(1)} q_k^{(1)} + 2 W'_{ij} \Lambda^{(1)} q_j^{(1)} + W_{ij} q_j^{(2)}|^c = 0,$$

and since $q_1^{(1)} = 1$ the first-order equation can be solved for the rates $q_s^{(1)c}$, where $s \neq 1$. This was done by crossing out the first equation of the set to give us the $n - 1$ linear equations

$$W_{ts} q_s^{(1)} = - W_{t1} |^c \quad (s \neq 1, t \neq 1)$$

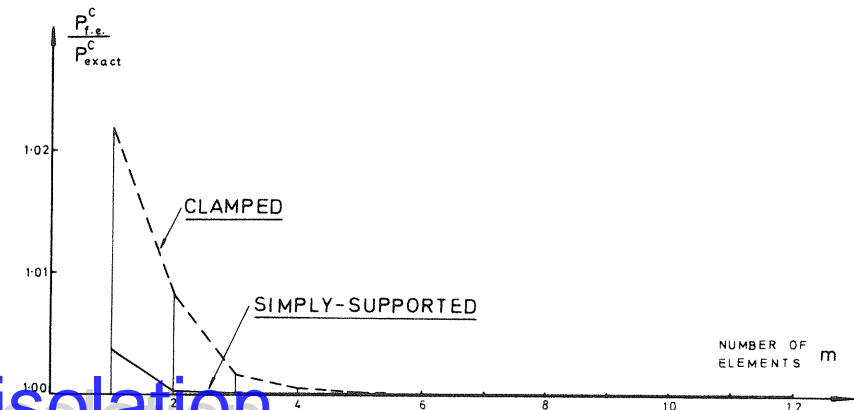


Figure 72 Convergence of the critical load P^c

for the $n - 1$ rates, the independent variable q_1 of the general theory being equated to b_1 the central deflection. Looking again at the structure of W_{ij} , we see that these equations will yield zero rates for the in-plane coordinates, so the problem reduces at once to the solution on a computer of the leading equations corresponding to $J_{ij} - PN_{ij}$. This is in direct analogy to the continuum analysis where the two first-order equations yielded $v_1 = 0$, $w_1 \neq 0$. The function $w_1(r)$ was observed to converge rapidly to that of the exact continuum analysis, the form of $w_1(r)$ for large numbers of elements being indistinguishable from the continuum form which is shown in Figure 73.

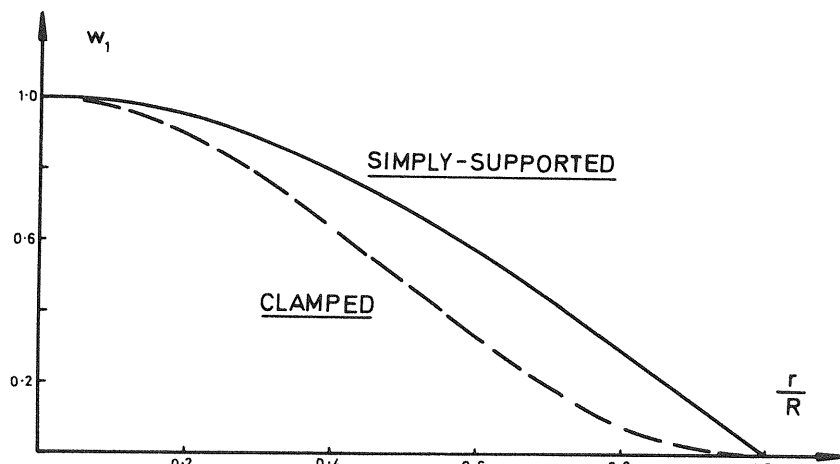


Figure 73 Form of the buckling mode $w_1(r)$

The general theory result for the post-buckling slope is

$$\Lambda^{(1)c} = - \frac{W_{ijk} q_i^{(1)} q_j^{(1)} q_k^{(1)}}{2 W'_{ij} q_i^{(1)} q_j^{(1)}} \Big|^c,$$

and since the only non-zero coefficients of the numerator involve the in-plane coordinates a_i whose rates we have seen to be zero, we have as expected

$$\Lambda^{(1)c} = 0,$$

irrespective of the support condition.

With $q_1^{(2)} = 0$ the uncontracted second-order equations must now be solved for the $q_s^{(2)c}$, where $s \neq 1$, and again deleting the first equation we are left with

$$W_{ts} q_s^{(2)} = - W_{tjk} q_j^{(1)} q_k^{(1)} \Big|^c \quad (s \neq 1, t \neq 1).$$

The matrix of the left-hand side is again W_{ts} , so remembering the partitioning of this and noting that the right-hand side will be zero for t corresponding to the

out-of-plane coordinates, we see that these equations yield zero solutions for the second b_i derivatives. Summing the remaining right-hand-side terms with the known rates we can solve the remaining equations for the second a_i derivatives on the computer. We see that there is again a complete correspondence between the continuum and finite-element perturbation schemes. The convergence of v_2 to the continuum values is indicated in the paper,¹³⁵ and the form of $v_2(r)$ for five elements is compared with the exact continuum solution in Figure 74.

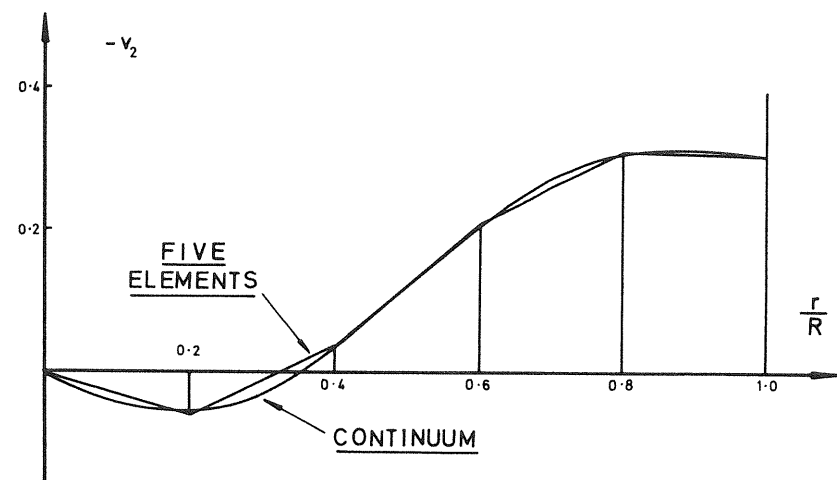


Figure 74 Continuum and five-element forms for $v_2(r)$

The general expression for the post-buckling path curvature is

$$\Lambda^{(2)c} = - \frac{W_{ijkl} q_i^{(1)} q_j^{(1)} q_k^{(1)} q_l^{(1)} + 3 W_{ijk} q_i^{(1)} q_j^{(1)} q_k^{(2)}}{3 W'_{ij} q_i^{(1)} q_j^{(1)}} \Big|^c$$

and performing the required summations on the computer with the known path derivatives gives us the required post-buckling path curvature $\Lambda^{(2)c} = R^2 P^{(2)c}/D$. The convergence of this curvature to the exact continuum value is shown in Figure 75.

The perturbation schemes have been seen to correspond closely to those observed for the post-buckling of an Euler strut in Chapter 1. The alternating sequence for $w_{(odd)}$ and $v_{(even)}$ has been observed, and in the finite-element analysis this is seen to be closely associated with the partitioning of the energy coefficients. The continuum contraction scheme of Croll¹²³ has been seen to correspond exactly to the contraction mechanism of the discrete coordinate general theory.

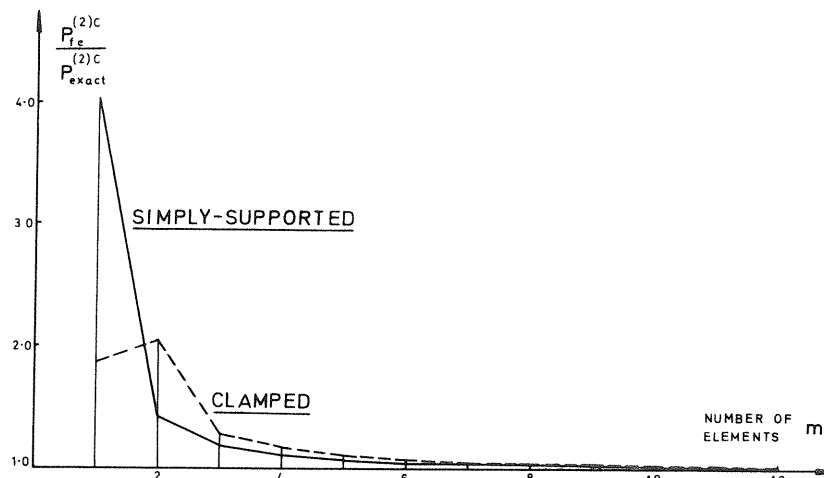


Figure 75 Convergence of the solution $P^{(2)C}$

The analysis of the plates has been continued as far as the second load derivative, so with the symmetry of the plates the final solutions have the form

$$P = P^C + \frac{1}{2}P^{(2)C}b^2,$$

where b is the central deflection. Exact solutions for P^C and $P^{(2)C}$ were obtained in the continuum analysis for both simply-supported and clamped boundaries, and the resulting post-buckling paths are compared with that of Friedrichs and Stoker¹⁵⁸⁻¹⁶⁰ in Figure 68. For the simply-supported plate for which we have a direct comparison we see that the perturbation solution gives good results for values of b/t up to about 3.

The convergence of the finite-element results to those of the continuum analysis was quite rapid, and was essentially complete with the use of twelve elements, which was therefore the maximum number employed. We might note that for the simply-supported plate this corresponds to a maximum of 36 degrees of freedom.

8

IMPERFECT SYSTEMS

8.1 Introduction

In most of the preceding chapters we have been concerned with the behaviour of a postulated *perfect* system, but practical structural systems of course carry inevitable small imperfections inherent in their manufacture. For this reason we shall now develop the general theory for a family of *imperfect* systems derived as perturbations from the perfect system of the previous work. Once again our major tool will be a perturbation approach and we shall throughout the chapter lay particular emphasis on establishing the important *imperfection-sensitivity* relationships. The limit point is considered first, and then two branching analyses are presented employing the diagonalized *A*-function and finally the general *W*-function.

In the case of the *A*-analysis the perturbation scheme is continued only until we have obtained a first-order estimate for each branching point of interest. However, as with the corresponding treatment of the perfect system, the *W*-analysis is developed in some depth and, apart from considering just the low-order equations of the scheme, some general results are obtained from the form of the r th-order perturbation equations. These allow us to set the patterns of solution of 'perfect' and 'imperfect' perturbation schemes side by side and to study the extent of the interplay which arises between the two schemes during the initial stages. However, we point out once more that these r th-order results need not be of immediate concern to the busy numerical analyst and can therefore be omitted on first reading, but again we hope he might return to them at a later stage for a deeper understanding of the subject.

The original formulation for each of the following analyses is the same, the family of systems being generated by introducing the perturbation or *imperfection parameter* ϵ into the energy function, giving us the single-valued function $V(Q_i, \Lambda, \epsilon)$. The system corresponding to $\epsilon = 0$ will thus be described as the *perfect system*, and it is to be understood that this was the system considered in the earlier chapters; we likewise describe systems corresponding to non-zero values of ϵ as *imperfect systems*.

8.2 The limit point

Let us first examine the response of imperfect systems in the vicinity of the distinct limit point treated analytically in Chapter 5. Deflections of all systems can be described by the same set of coordinates, so we are still able to use the fixed principal axes of the earlier work, and merely introduce the imperfection parameter ε into the potential energy function by writing

$$D(u_i, \Lambda, \varepsilon) \equiv V(Q_i^F + \alpha_{ij} u_j, \Lambda, \varepsilon).$$

The analysis therefore starts with this transformed energy function, the only necessary properties of which refer to the perfect system and can be written as

$$D_{ij}^F = 0 \quad \text{for } i \neq j,$$

$$D_{11}^C = 0,$$

$$D_{ss}^C \neq 0 \quad \text{for } s \neq 1,$$

$$D_1^C \neq 0,$$

$$D_{111}^C \neq 0.$$

We anticipate equilibrium paths with the form of those of Figure 35, in which a heavy line represents the equilibrium path of the perfect system while light lines represent the equilibrium paths of imperfect systems. We are naturally interested in the critical points of imperfect systems, so denoting a typical such point in load-coordinate space as (u_j^M, Λ^M) we express the locus of critical limit points in the parametric form $u_j = u_j^M(\varepsilon), \Lambda = \Lambda^M(\varepsilon)$.

Analytically the critical equilibrium states are characterized by the conditions $D_i = 0, \Delta = 0$, where $\Delta(u_i, \Lambda, \varepsilon) = |D_{ij}|$, so substituting our parametric forms into these equations we obtain the *characterizing identities*

$$D_i[u_j^M(\varepsilon), \Lambda^M(\varepsilon), \varepsilon] \equiv 0,$$

$$\Delta[u_j^M(\varepsilon), \Lambda^M(\varepsilon), \varepsilon] \equiv 0.$$

It is now possible to perform an intrinsic analysis, similar to those employed for the perfect systems, to determine initial derivatives of the functions $u_j^M(\varepsilon)$ and $\Lambda^M(\varepsilon)$; it is of course precisely determination of the important $\Lambda^M(\varepsilon)$ imperfection-sensitivity relationship which we seek in all these studies of imperfect systems.

Thus differentiating the characterizing identities with respect to ε we have

$$D_{ij} \dot{u}_j^M + D'_i \dot{\Lambda}^M + \dot{D}_i = 0,$$

$$\Delta_i \dot{u}_i^M + \Delta' \dot{\Lambda}^M + \dot{\Delta} = 0,$$

where a dot denotes differentiation with respect to ε . Evaluation of these two equations at the critical point of the perfect system, $u_i^M = 0, \Lambda^M = \Lambda^*, \varepsilon = 0$ gives the first derivatives $\dot{\Lambda}^{MC}$ and \dot{u}_i^{MC} . The former is of primary interest and

arises directly from the first of these equations if we are prepared to assume what is readily proved by the second equation, namely that $\dot{u}_i^{MC} \neq \infty$.

So setting $i = 1$ in the first equation we obtain

$$D'_1 \dot{\Lambda}^M + \dot{D}_1|_C = 0$$

and since $D'_1|_C \neq 0$ we can write

$$\dot{\Lambda}^{MC} = -\left. \frac{\dot{D}_1}{D'_1} \right|_C.$$

Thus, assuming that the imperfection has a direct action on the critical principal coordinate in the sense that $\dot{D}_1|_C \neq 0$, we see that the peak or failure load Λ^M varies initially linearly with the magnitude of the imperfection parameter ε as shown in Figure 35, and the imperfection-sensitivity is thus relatively modest compared with the results for the branching points of the next section.

8.3 Branching analysis with diagonalization

We now examine the response of imperfect systems in the vicinity of the branching points of Chapter 6, choosing first to operate in terms of the diagonalized A -function. Deflections of all systems can be described by the same set of coordinates, so we can still use the sliding and rotating set of principal axes u_i which emerge from the fundamental path of the perfect system, and write

$$A(u_i, \Lambda, \varepsilon) \equiv V[Q_i^F(\Lambda) + \alpha_{ij}(\Lambda) u_j, \Lambda, \varepsilon].$$

The analysis thus starts with this transformed energy function, the only necessary properties of which refer to the perfect system and are given in Chapter 6. We assume throughout that the imperfection parameter has a direct action on the critical principal coordinate in the sense that

$$\dot{A}_1^C \equiv \dot{A}_1(0, \Lambda^C, 0) \neq 0,$$

where a dot again denotes differentiation with respect to ε . The imperfection is then a major imperfection in the terminology of Roorda,⁶¹ who considers the action of both ‘major’ and ‘minor’ imperfections in an asymmetric point of bifurcation.

Introducing now the stability determinant

$$\Delta(u_k, \Lambda, \varepsilon) \equiv |A_{ij}(u_k, \Lambda, \varepsilon)|,$$

we can readily establish the result, analogous to those of Chapter 6, that

$$\dot{A}^C = A_{11} A_{22} A_{33} \cdots A_{nn}|_C.$$

The ‘imperfect’ perturbation scheme which is to be presented here seeks the locus of the critical limit points of imperfect systems and so anticipating

this result we write a critical equilibrium state as (u_j^M, Λ^M) in load-coordinate space. This will then differentiate between these parameters and those of the ‘perfect’ perturbation scheme of Chapter 6, which define the post-buckling path of the perfect system. Now the natural parametric representation for the locus of critical points would be

$$u_j = u_j^M(\varepsilon), \quad \Lambda = \Lambda^M(\varepsilon),$$

but, in line with the approach of Chapter 6, the analysis must be developed using the first generalized coordinate as expansion parameter. We thus write the above relationships in the inverted form

$$u_j^M = u_j^M(u_1^M), \quad \Lambda^M = \Lambda^M(u_1^M), \quad \varepsilon = \varepsilon^M(u_1^M). \quad (8.1)$$

As ε^M tends to zero, the behaviour of the corresponding imperfect system will approach that of the perfect system, so these relationships will clearly be satisfied by

$$u_j^M = 0, \quad \Lambda^M = \Lambda^C, \quad \varepsilon^M = 0. \quad (8.2)$$

The critical equilibrium states satisfying the conditions $A_i = 0$, $\Delta = 0$, we can now perform an intrinsic analysis to determine the initial derivatives of $u_j^M(u_1^M)$, $\Lambda^M(u_1^M)$, $\varepsilon^M(u_1^M)$. Thus, substituting these functions, we can write the characterizing identities

$$\begin{aligned} A_i[u_j^M(u_1^M), \Lambda^M(u_1^M), \varepsilon^M(u_1^M)] &\equiv 0, \\ A[u_j^M(u_1^M), \Lambda^M(u_1^M), \varepsilon^M(u_1^M)] &\equiv 0, \end{aligned}$$

and differentiating these functions of u_1^M with respect to u_1^M we have

$$\begin{aligned} A_{ij}u_j^{M(1)} + A_i\Lambda^{M(1)} + \dot{A}_i\varepsilon^{M(1)} &= 0, \\ A_ju_j^{M(1)} + \Delta'\Lambda^{M(1)} + \dot{\Delta}\varepsilon^{M(1)} &= 0. \end{aligned}$$

It will be seen that following the earlier work a bracketed superscript is used to denote differentiation of the functions (8.1) with respect to u_1^M and remembering that u_1^M is written as $u_1^M(u_1^M)$ we have

$$u_1^{M(r)} \equiv \frac{d^r u_1^M}{du_1^{Mr}} = \delta_{1r},$$

where δ_{ij} denotes the Kronecker delta.

Evaluating these equations at the critical point of the perfect system represented by equations (8.2) we find

$$\begin{aligned} \varepsilon^{M(1)C} &= 0, \\ u_s^{M(1)C} &= 0 \quad \text{for } s \neq 1, \\ \Lambda^{M(1)C} &= -\frac{A_1}{\Delta'} \Big|_1^C = -\frac{A_{111}}{A'_{11}} \Big|_1^C, \end{aligned}$$

the first derivatives of interest. A comparison with equation (6.2) of Chapter 6 shows that

$$\Lambda^{M(1)C} = 2\Lambda^{(1)C}.$$

Differentiating the characterizing identities a second time with respect to u_1^M we have

$$\begin{aligned} &(A_{ijk}u_k^{M(1)} + A'_{ij}\Lambda^{M(1)} + \dot{A}_{ij}\varepsilon^{M(1)})u_j^{M(1)} + A_{ij}u_j^{M(2)} \\ &+ (A'_{ij}u_j^{M(1)} + A''_i\Lambda^{M(1)} + \dot{A}'_i\varepsilon^{M(1)})\Lambda^{M(1)} + A'_i\Lambda^{M(2)} \\ &+ (A_{ij}u_j^{M(1)} + \dot{A}'_i\Lambda^{M(1)} + \ddot{A}_i\varepsilon^{M(1)})\varepsilon^{M(1)} + \dot{A}_i\varepsilon^{M(2)} = 0, \\ &(A_{jk}u_k^{M(1)} + A'_j\Lambda^{M(1)} + \dot{A}_j\varepsilon^{M(1)})u_j^{M(1)} + A_ju_j^{M(2)} \\ &+ (A'_ju_j^{M(1)} + A''_j\Lambda^{M(1)} + \dot{A}'_j\varepsilon^{M(1)})\Lambda^{M(1)} + A'\Lambda^{M(2)} \\ &+ (\dot{A}_ju_j^{M(1)} + \dot{A}'_j\Lambda^{M(1)} + \ddot{A}_j\varepsilon^{M(1)})\varepsilon^{M(1)} + \dot{A}\varepsilon^{M(2)} = 0, \end{aligned}$$

giving on evaluation

$$\begin{aligned} \varepsilon^{M(2)C} &= \frac{A_{111}}{A_1} \Big|_1^C, \\ u_s^{M(2)C} &= -\frac{A_{111}\dot{A}_s + A_{s11}\dot{A}_1}{A_{ss}\dot{A}_1} \Big|_1^C \quad \text{for } s \neq 1, \end{aligned}$$

and

$$\begin{aligned} \Lambda^{M(2)C} &= -\frac{1}{\Delta'} \left[A_{11} - 2A_1 \frac{A_{111}}{A'_{11}} - \sum_{s=2}^{s=n} A_s \frac{A_{111}\dot{A}_s + A_{s11}\dot{A}_1}{A_{ss}\dot{A}_1} \right. \\ &\quad \left. + \Delta'' \left(\frac{A_{111}}{A'_{11}} \right)^2 + \dot{\Delta} \frac{A_{111}}{A_1} \right] \Big|_1^C. \end{aligned}$$

The analysis so far applies whether or not $A_{111}^C = 0$. If this coefficient is non-zero we have the asymmetric point of bifurcation and we can stop the scheme here having obtained the required derivatives for a first-order imperfection-sensitivity estimate; these are tabulated in Table 8.1 together with the corresponding derivatives for the post-buckling path of the perfect system given in Chapter 6. Thus the important asymptotic variation of the peak or failure load Λ^M with the imperfection parameter ε becomes

$$\Lambda^M = \Lambda^C \pm (A_{111}^C)^{\frac{1}{2}} \frac{[2\dot{A}_1^C\varepsilon]^{\frac{1}{2}}}{A_{11}^C},$$

and provides the parabolic imperfection-sensitivity relationship of Figure 76 which is drawn for $A_{111}^C > 0$, $A_{11}^C < 0$, and $\dot{A}_1^C > 0$.

TABLE 8.1 Asymmetric point of bifurcation

Perfect derivatives

$$\begin{aligned} u_s^{(1)C} &= 0 & A^{(1)C} &= -\left. \frac{A_{111}}{2A'_{11}} \right|^c \end{aligned}$$

$$u_s^{(2)C} = -\left. \frac{A_{s11}}{A_{ss}} \right|^c$$

Imperfect derivatives

$$\begin{aligned} u_s^{M(1)C} &= 0 & A^{M(1)C} &= -\left. \frac{A_{111}}{A'_{11}} \right|^c & \varepsilon^{M(1)C} &= 0 \\ u_s^{M(2)C} &= -\left. \frac{A_{111}\dot{A}_s + A_{s11}\dot{A}_1}{A_{ss}\dot{A}_1} \right|^c & \varepsilon^{M(2)C} &= \left. \frac{A_{111}}{\dot{A}_1} \right|^c \end{aligned}$$

For the special case of symmetric points of bifurcation in which $A_{111}^C = 0$ we have from the above equations

$$\begin{aligned} A^{M(1)C} &= 0, \\ \varepsilon^{M(2)C} &= 0, \\ u_s^{M(2)C} &= -\left. \frac{A_{s11}}{A_{ss}} \right|^c \text{ for } s \neq 1, \end{aligned}$$

and, using the previously determined derivatives of A ,

$$A^{M(2)C} = -\left. \frac{\tilde{A}_{1111}}{A'_{11}} \right|^c,$$

where, as in equation (6.4) of Chapter 6,

$$\tilde{A}_{1111}^C \equiv A_{1111} - 3 \sum_{s=2}^{s=n} \left. \frac{(A_{s11})^2}{A_{ss}} \right|^c.$$

A comparison with equation (6.3) now shows that

$$A^{M(2)C} = 3A^{(2)C}.$$

We next proceed to evaluate the higher derivatives for this special case. Differentiating the characterizing identities a third time with respect to u_1^M , and evaluating, we have after some algebra,

$$\varepsilon^{M(3)C} = \left. \frac{2\tilde{A}_{1111}}{\dot{A}_1} \right|^c.$$

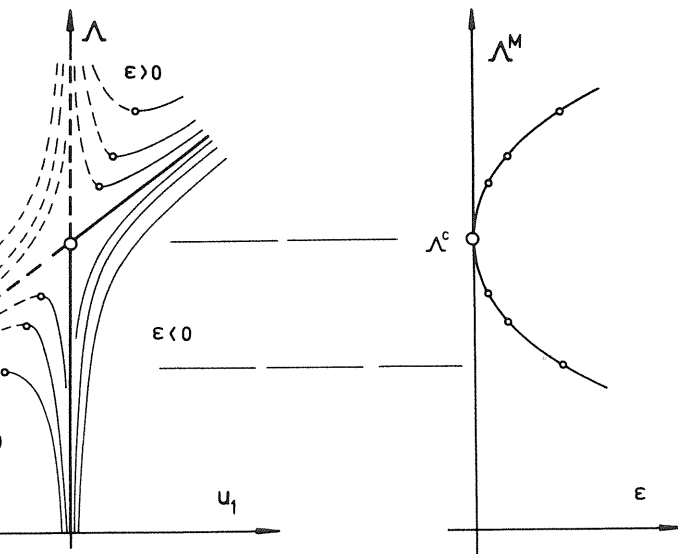


Figure 76 The asymmetric point of bifurcation

TABLE 8.2 Symmetric points of bifurcation

Perfect derivatives

$$\begin{aligned} u_s^{(1)C} &= 0 & A^{(1)C} &= 0 \\ u_s^{(2)C} &= -\left. \frac{A_{s11}}{A_{ss}} \right|^c & A^{(2)C} &= -\left. \frac{\tilde{A}_{1111}}{3A'_{11}} \right|^c \end{aligned}$$

Imperfect derivatives

$$\begin{aligned} u_s^{M(1)C} &= 0 & A^{M(1)C} &= 0 & \varepsilon^{M(1)C} &= 0 \\ u_s^{M(2)C} &= -\left. \frac{A_{s11}}{A_{ss}} \right|^c & A^{M(2)C} &= -\left. \frac{\tilde{A}_{1111}}{A'_{11}} \right|^c & \varepsilon^{M(2)C} &= 0 \\ \varepsilon^{M(3)C} &= \left. \frac{2\tilde{A}_{1111}}{\dot{A}_1} \right|^c & & & & \varepsilon^{M(3)C} = \left. \frac{2\tilde{A}_{1111}}{\dot{A}_1} \right|^c \end{aligned}$$

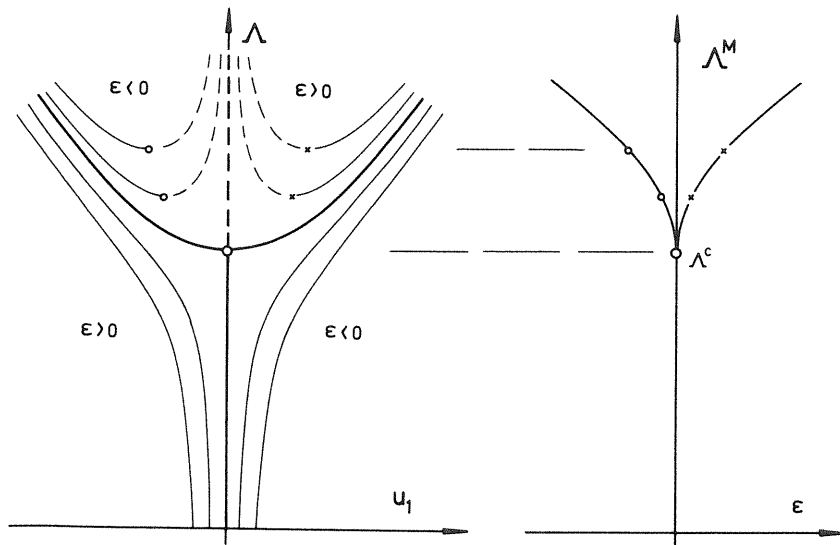


Figure 77 The stable-symmetric point of bifurcation

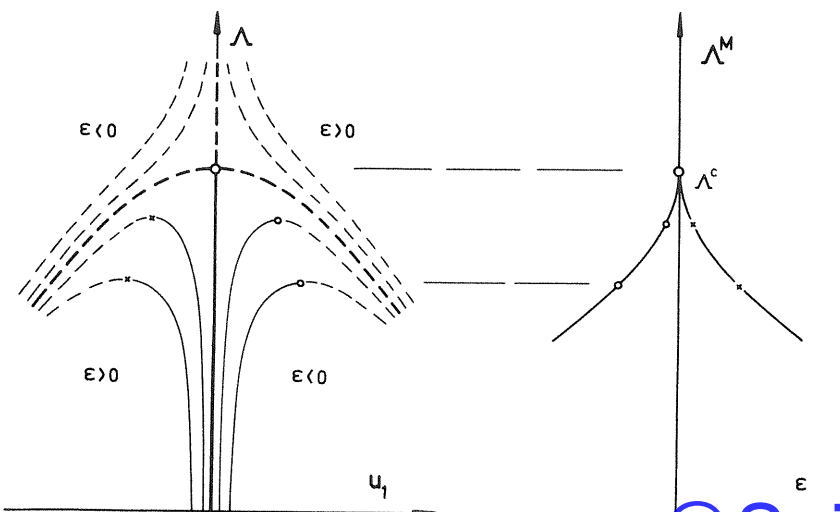


Figure 78 The unstable-symmetric point of bifurcation

We now have the required derivatives for the symmetric points of bifurcation, and these are tabulated in Table 8.2 together with the corresponding derivatives for the post-buckling path of the perfect system given in Chapter 6. Specifying that $\tilde{A}_{1111}^C \neq 0$, the asymptotic variation of the peak or failure load Λ^M with the imperfection parameter ϵ becomes

$$\Lambda^M = \Lambda^C - \frac{1}{2}(\tilde{A}_{1111}^C)^{\frac{1}{3}} \frac{[3\tilde{A}_1^C \epsilon]^{\frac{2}{3}}}{A_{11}^{1C}}. \quad (8.3)$$

This, then, provides the initial two-thirds power law imperfection-sensitivity relationship shown in Figures 77 and 78, which are drawn for $A_{11}^{1C} < 0$ and $\tilde{A}_1^C > 0$.

8.4 Two illustrative examples

To illustrate the preceding general theory for imperfect systems using the diagonalized A -analysis we shall now consider two models generating symmetric points of bifurcation; we refer back to the asymmetric model of Chapter 1, Section 1.2 for an example which can be similarly used to illustrate the application to an asymmetric point of bifurcation.

Stable-symmetric bifurcation

Since the non-critical principal coordinates can play a significant role in the symmetric points of bifurcation, it is of interest to consider a model having more than one degree of freedom. Such a model, demonstrating the effect a non-critical coordinate can have on the post-buckling curvature, consists of a rigid prismatic body floating in an infinite quasi-static ocean, as shown in Figure 79. The body is a right-angled prism of unit length and as a loading

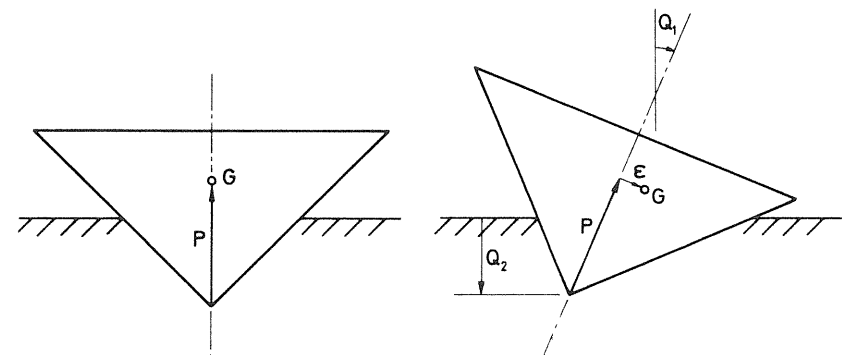


Figure 79 A boat model showing the undeflected perfect system and the deflected imperfect system

parameter we take the height of the centre of gravity above the apex, generating a family of systems by offsetting the centre of gravity a distance ε as shown.

Considering only movements in the plane of the paper and ignoring the arbitrary horizontal translation we have a conservative two-degree-of-freedom system, and we choose the rotation Q_1 and the depth of the apex Q_2 as our co-ordinates. The total potential energy of the ship and ocean can then be written as

$$\begin{aligned} V(Q_i, P, \varepsilon) = & m(P \cos Q_1 - \varepsilon \sin Q_1 - Q_2) \\ & + \frac{1}{6}\rho Q_2^3(\tan 45^\circ - Q_1 + \tan 45^\circ + Q_1), \end{aligned}$$

where m is the mass of the ship and ρ is the density of the ocean.

If we set $V_i = 0$ for $\varepsilon = 0$ we obtain the fundamental path of the perfect system

$$Q_1^F = 0, \quad Q_2^F = \left(\frac{m}{\rho}\right)^{\frac{1}{3}}.$$

Furthermore we see that on the fundamental path $V_{12} = 0$, so we can immediately write

$$Q_1 = u_1, \quad Q_2 = \left(\frac{m}{\rho}\right)^{\frac{1}{3}} + u_2,$$

to give

$$A(u_i, P, \varepsilon) = V \left[u_1, \left(\frac{m}{\rho}\right)^{\frac{1}{3}} + u_2, P, \varepsilon \right].$$

Differentiating we have

$$A_{11}^F = A_{11}(0, P, 0) = -mP + \frac{4}{3}\rho \left(\frac{m}{\rho}\right)^{\frac{1}{3}},$$

$$A_{22}^F = A_{22}(0, P, 0) = 2\rho \left(\frac{m}{\rho}\right)^{\frac{1}{3}},$$

giving the critical value of P ,

$$P^c = \frac{4}{3} \left(\frac{m}{\rho}\right)^{\frac{1}{3}}.$$

Finally, evaluating at this critical load, we obtain

$$\begin{aligned} A_1^C &= -m, \\ A_{11}^C &= -m, \\ A_{22}^C &= 2\rho \left(\frac{m}{\rho}\right)^{\frac{1}{3}}, \end{aligned}$$

$$\begin{aligned} A_{111}^C &= 0, \\ A_{211}^C &= 4\rho \left(\frac{m}{\rho}\right), \\ A_{1111}^C &= 28\rho \left(\frac{m}{\rho}\right)^{\frac{1}{3}}, \\ \tilde{A}_{1111}^C &= 4\rho \left(\frac{m}{\rho}\right)^{\frac{1}{3}}. \end{aligned}$$

The effect of a non-critical principal coordinate is here aptly demonstrated by the fact that $\tilde{A}_{1111}^C \neq A_{1111}^C$.

Now using equation (6.3) of Chapter 6 the initial curvature of the post-buckling path of the perfect system is given by

$$P^{(2)c} = \frac{4}{3} \left(\frac{m}{\rho}\right)^{\frac{1}{3}},$$

and finally, using equation (8.3), the asymptotic variation of the critical load with ε is given by

$$P^M = \frac{4}{3} \left(\frac{m}{\rho}\right)^{\frac{1}{3}} \left\{ 1 + \left[\frac{1}{2} \left(\frac{3}{2}\right)^{\frac{1}{3}} \left(\frac{\rho}{m}\right)^{\frac{1}{3}} \varepsilon \right]^{\frac{2}{3}} \right\}.$$

This two-thirds power law relationship of course relates to the limit points which arise in the complementary paths about the stable-symmetric point of bifurcation and are thus of no practical significance.

Unstable-symmetric bifurcation

Having studied a two-degree-of-freedom symmetric model we return to a one-degree-of-freedom model for the unstable-symmetric point of bifurcation. Three rigid links of length L are pinned together to form the arch of Figure 80, the two outer links being inclined initially at 45° and constrained

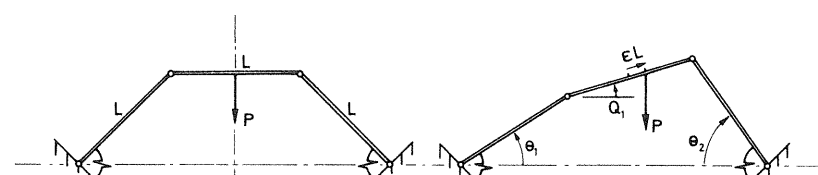


Figure 80 A four-pinned arch showing the undeflected perfect system and the deflected imperfect system

from rotation relative to the abutments by two linear rotational springs of stiffness k . A dead vertical load of magnitude P acts nominally at the centre of the central member, imperfect systems being generated by moving the point of application of the load a distance εL along the member.

Choosing Q_1 , the rotation of the central member, as the independent coordinate, and introducing also the rotations $\theta_1(Q_1)$ and $\theta_2(Q_1)$, we have the two compatibility equations

$$\begin{aligned}\cos \theta_1 + \cos Q_1 + \cos \theta_2 &= 1 + \sqrt{2}, \\ \sin \theta_1 + \sin Q_1 - \sin \theta_2 &= 0,\end{aligned}$$

and the total potential energy function

$$V = \frac{1}{2}k(\theta_1 - \frac{1}{4}\pi)^2 + \frac{1}{2}k(\theta_2 - \frac{1}{4}\pi)^2 + PL(\frac{1}{2}\sin \theta_1 + \frac{1}{2}\sin \theta_2 + \varepsilon \sin Q_1).$$

The fundamental equilibrium path of the perfect system being given by $Q_1 = 0$ and there being only one degree of freedom, we can write $Q_1 = u_1$ and equate V to the transformed energy function $A(u_1, P, \varepsilon)$.

Now, differentiating and using the compatibility equations, we find that

$$A_{11}^F = A_{11}(0, P, 0) = k - \frac{1}{2}PL(1 + \sqrt{2}),$$

giving the critical value of P ,

$$P^c = 2(\sqrt{2} - 1)\frac{k}{L},$$

and finally

$$\begin{aligned}A_1^c &= 2(\sqrt{2} - 1)k, \\ A_{11}^c &= -\frac{1}{2}(1 + \sqrt{2})L, \\ A_{111}^c &= 0, \\ \tilde{A}_{1111}^c &= A_{1111}^c = -\frac{5}{2}k.\end{aligned}$$

Thus using equation (6.3) of Chapter 6 the initial curvature of the post-buckling path of the perfect system is given by

$$P^{(2)c} = -\frac{5}{3}(\sqrt{2} - 1)\frac{k}{L},$$

and finally, using equation (8.3), the asymptotic variation of the critical load with the imperfection parameter is given by

$$P^M = 2(\sqrt{2} - 1)\frac{k}{L}\{1 - [\frac{3}{2}\sqrt{5}(\sqrt{2} - 1)\varepsilon]^{\frac{2}{3}}\}.$$

This two-thirds power law relationship is of very real practical significance since it represents a reduction of critical load in the presence of imperfections.

As well as illustrating the salient features of the general theory, these models also demonstrate its analytical value, since ad hoc analyses even of such simple

examples as these can be relatively lengthy and tedious. Further illustrative models are to be found in Chapter 1, and in the work of Koiter,⁹ Augusti¹⁹⁷ and Walker *et al.*¹³⁴ The behaviour of a bifurcating model in a centrifuge is discussed briefly by Thompson.¹³²

8.5 General branching analysis

It has been seen in the diagonalized A -analysis that a perturbation scheme seeking the locus of critical limit points associated with a family of imperfect systems is only of practical significance when the corresponding perfect system

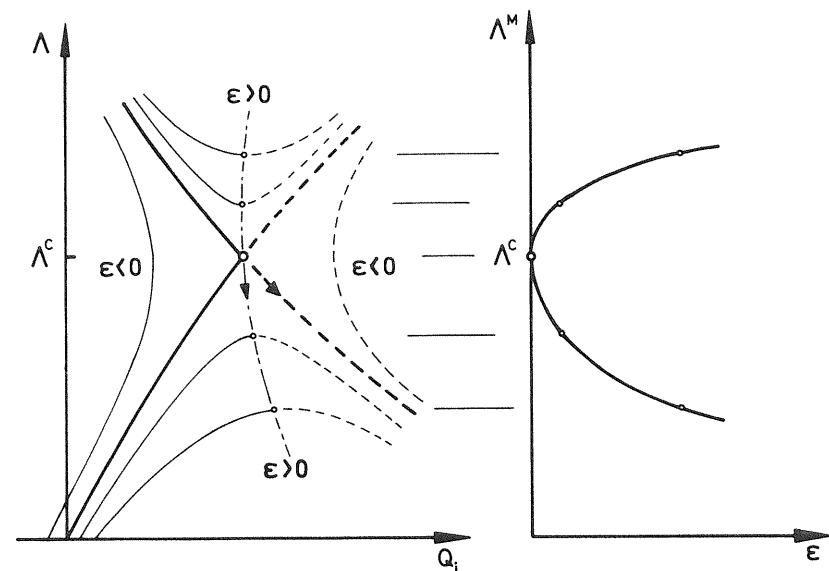


Figure 81 Perturbation paths in the asymmetric point of bifurcation

experiences either an asymmetric or an unstable-symmetric point of bifurcation. We therefore re-illustrate the equilibrium paths about these two critical points, along with the imperfection-sensitivity curves, in the two schematic representations of Figures 81 and 82. Here the two arrowheads on each diagram indicate the paths sought by the 'perfect' and 'imperfect' perturbation schemes, the former finding the post-buckling path of the perfect system and the latter the locus of critical limit points. In the following W -analysis we are not only concerned with first-order imperfection-sensitivity results but shall look at the continuing perturbation process and derive the first three terms of the full asymptotic equation for each critical point of interest. Thus, although we

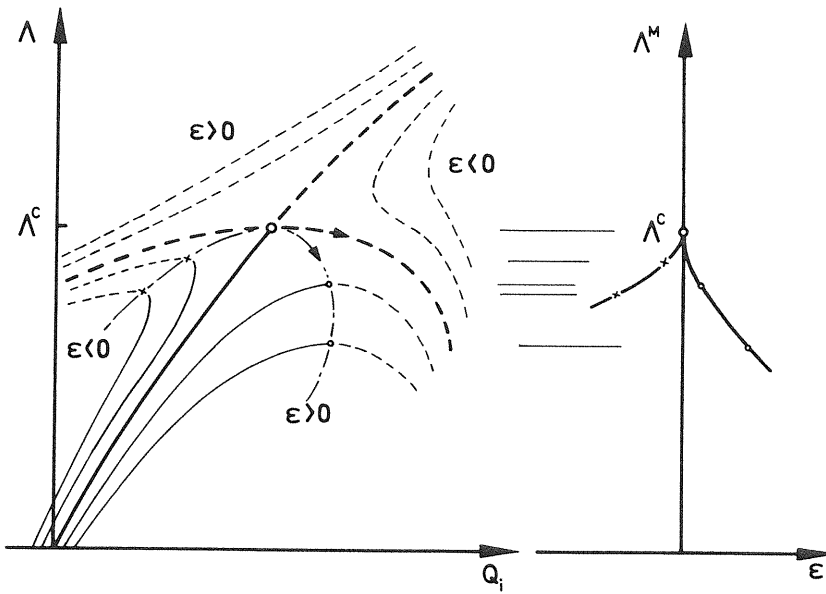


Figure 82 Perturbation paths in the unstable-symmetric point of bifurcation

remember that for the asymmetric point of bifurcation the imperfection-sensitivity curve approaches a parabolic variation at $\varepsilon = 0$, it is now seen to be contaminated by higher derivatives as ε increases. On the other hand, for the unstable-symmetric point of bifurcation the curve again approaches a two-thirds power law cusp at $\varepsilon = 0$ but also is subsequently contaminated by higher derivatives as ε increases, producing the noticeable asymmetry of the cusp. Both curves of course still exhibit an infinite slope at $\varepsilon = 0$.

As before, deflections of all systems can be described by the same set of coordinates, so we can still use the sliding set of incremental axes q_i which emerge from the fundamental path of the perfect system, and write

$$W(q_i, \Lambda, \varepsilon) \equiv V[Q_i^f(\Lambda) + q_i, \Lambda, \varepsilon].$$

The analysis thus starts with this transformed energy function, the only necessary properties of which refer to the perfect system and are given in Chapter 6.

Following the convention laid down in the A -analysis, we write a critical equilibrium state as (q_j^M, Λ^M) in load-coordinate space, thereby differentiating between these parameters and those of the ‘perfect’ perturbation scheme.

Now the natural parametric representation for the locus of critical points would be

$$q_j = q_j^M(\varepsilon), \quad \Lambda = \Lambda^M(\varepsilon),$$

but in line with the earlier work the analysis must be developed using the first generalized coordinate as expansion parameter. We thus write the above relationships in the inverted form

$$q_j^M = q_j^M(q_1^M), \quad \Lambda^M = \Lambda^M(q_1^M), \quad \varepsilon = \varepsilon^M(q_1^M). \quad (8.4)$$

As ε^M tends to zero, the behaviour of the corresponding imperfect system will approach that of the perfect system, so these relationships will clearly be satisfied by

$$q_j^M = 0, \quad \Lambda^M = \Lambda^C, \quad \varepsilon^M = 0.$$

The critical equilibrium states satisfy the conditions $W_i = 0, \Delta = 0$, where Δ is the stability determinant as before, and a direct analysis along the lines of the A -analysis is now possible using these conditions. The results of such a direct approach will, however, contain various derivatives of the determinant Δ and in a W -analysis vital comparisons with the post-buckling characteristics of the perfect system are not easily made. For this reason we introduce a local eigenvalue problem to define these critical points and this is written in the form

$$W_{ij} x_j = 0.$$

The eigenvector x_j is thus associated with the limit points of imperfect systems and is termed a spiralling eigenvector because of its varying orientation in load-coordinate space; it may also be written in the parametric form

$$x_j = x_j(q_1^M). \quad (8.5)$$

This spiralling eigenvector plays an important but transitory role in the following analysis and makes no appearance in the final results. The numerical analyst can thus use the results while giving no thought to this vector employed in their derivation.

We can now introduce our parametric forms into the equilibrium and critical state equations to obtain the characterizing identities

$$W_i[q_j^M(q_1^M), \quad \Lambda^M(q_1^M), \quad \varepsilon^M(q_1^M)] \equiv 0,$$

$$W_{ij}[q_j^M(q_1^M), \quad \Lambda^M(q_1^M), \quad \varepsilon^M(q_1^M)] x_j(q_1^M) \equiv 0.$$

If we introduce a normalizing condition on x_j such that $x_1 = 1$ we may differentiate these equations with respect to q_1^M as many times as we please to generate an ordered perturbation process.

First let us differentiate the equilibrium identity repeatedly with respect to q_1^M to obtain

$$\begin{aligned} W_{ij} q_j^{M(1)} + W'_i \Lambda^{M(1)} + \dot{W}_i \varepsilon^{M(1)} &= 0, \\ W_{ijk} q_j^{M(1)} q_k^{M(1)} + W_{ij} q_j^{M(2)} + 2W'_{ij} q_j^{M(1)} \Lambda^{M(1)} + 2\dot{W}_{ij} q_j^{M(1)} \varepsilon^{M(1)} + W'_i \Lambda^{M(2)} \\ &+ \dot{W}_i \varepsilon^{M(2)} + W''_i (\Lambda^{M(1)})^2 + \ddot{W}_i (\varepsilon^{M(1)})^2 + 2\ddot{W}'_i \Lambda^{M(1)} \varepsilon^{M(1)} = 0, \\ W_{ijkl} q_j^{M(1)} q_k^{M(1)} q_l^{M(1)} + 3W_{ijk} q_j^{M(1)} q_k^{M(2)} + W_{ij} q_j^{M(3)} \\ &+ 3W'_{ijk} q_j^{M(1)} q_k^{M(1)} \Lambda^{M(1)} + 3\dot{W}_{ijk} q_j^{M(1)} q_k^{M(1)} \varepsilon^{M(1)} + 3W'_{ij} q_j^{M(2)} \Lambda^{M(1)} \\ &+ 3\dot{W}_{ij} q_j^{M(2)} \varepsilon^{M(1)} + 3W'_{ij} q_j^{M(1)} \Lambda^{M(2)} + 3\dot{W}_{ij} q_j^{M(1)} \varepsilon^{M(2)} + W'_i \Lambda^{M(3)} \\ &+ \dot{W}_i \varepsilon^{M(3)} + 3W''_{ij} q_j^{M(1)} (\Lambda^{M(1)})^2 + 3\ddot{W}_{ij} q_j^{M(1)} (\varepsilon^{M(1)})^2 + 6\ddot{W}'_{ij} q_j^{M(1)} \Lambda^{M(1)} \varepsilon^{M(1)} \\ &+ 3W''_i \Lambda^{M(1)} \Lambda^{M(2)} + 3\ddot{W}_i \varepsilon^{M(1)} \varepsilon^{M(2)} + 3\dot{W}'_i \Lambda^{M(2)} \varepsilon^{M(1)} + 3\ddot{W}'_i \Lambda^{M(1)} \varepsilon^{M(2)} \\ &+ 3\ddot{W}''_i (\Lambda^{M(1)})^2 \varepsilon^{M(1)} + 3\ddot{W}'_i \Lambda^{M(1)} (\varepsilon^{M(1)})^2 + W'''_i (\Lambda^{M(1)})^3 + \ddot{W}_i (\varepsilon^{M(1)})^3 = 0, \end{aligned}$$

etc. Here as before a dot denotes partial differentiation with respect to ε . Once again a bracketed superscript is used to denote differentiation of the functions of (8.4) and (8.5) with respect to q_1^M and remembering that q_1^M is written as $q_1^M(q_1^M)$ we have

$$q_1^{M(r)} \equiv \frac{d^r q_1^M}{dq_1^{Mr}} = \delta_{1r},$$

where δ_{ij} denotes the Kronecker delta.

We shall now write down a general form of the r th-order equilibrium equation which may be written formally as

$$\frac{d^r}{dq_1^{Mr}} W_{il} [q_j^M(q_1^M), \Lambda^M(q_1^M), \varepsilon^M(q_1^M)] = 0.$$

Once again we note that all the following work on the general r th-order perturbation equations may not be of immediate value in the straightforward application of the scheme and therefore might be passed over on first reading by the nonspecialist reader who might possibly prefer to follow the rudimentary scheme presented in the original paper of Thompson.¹⁰¹ The proposed general form is

$$\begin{aligned} W_i|^{(r)} &= W_{ij} q_j^{M(r)} + G_i^r (q_j^{M(r-1)}, q_j^{M(r-2)}, \dots, q_j^{M(1)}; \\ &\quad \Lambda^{M(r-1)}, \Lambda^{M(r-2)}, \dots, \Lambda^{M(1)}; \\ &\quad \varepsilon^{M(r-1)}, \varepsilon^{M(r-2)}, \dots, \varepsilon^{M(1)}) \\ &+ W'_i \Lambda^{M(r)} + \dot{W}_i \varepsilon^{M(r)} = 0, \end{aligned}$$

and we have here introduced a new notation in which a bracketed superscript after a vertical stroke indicates the number of differentiations with respect to q_1^M of the full expression preceding the stroke. We can show this general form

to be valid by the following inductive reasoning. Let us therefore differentiate this general form to obtain $W_i|^{(r+1)}$, where

$$\begin{aligned} W_{ij} q_j^{M(r)} &\text{ becomes } \begin{cases} (W_{ijk} q_k^{M(1)} + W'_{ij} \Lambda^{M(1)} + \dot{W}_i \varepsilon^{M(1)}) q_j^{M(r)} & (\text{included in } G_i^{r+1}) \\ W_{ij} q_j^{M(r+1)}, & \end{cases} \\ G_i^r &\text{ is all included in } G_i^{r+1}, \\ W'_i \Lambda^{M(r)} &\text{ becomes } \begin{cases} (W'_{ij} q_j^{M(1)} + W''_i \Lambda^{M(1)} + \ddot{W}_i \varepsilon^{M(1)}) \Lambda^{M(r)} & (\text{included in } G_i^{r+1}) \\ W_i \Lambda^{M(r+1)}, & \end{cases} \\ \dot{W}_i \varepsilon^{M(r)} &\text{ becomes } \begin{cases} (\dot{W}_{ij} q_j^{M(1)} + \dot{W}'_i \Lambda^{M(1)} + \ddot{W}_i \varepsilon^{M(1)}) \varepsilon^{M(r)} & (\text{included in } G_i^{r+1}) \\ \dot{W}_i \varepsilon^{M(r+1)}. & \end{cases} \end{aligned}$$

Thus if the assumed form is correct for the r th-order equation it is likewise correct for the $r+1$ th-order equation; but we see from our low-order equations that the form is valid for $r=1$ and $r=2$ and so by the well known induction mechanism it follows that this form is correct in general.

We now move on to the critical state identity. Differentiating this repeatedly with respect to q_1^M we obtain

$$\begin{aligned} &[W_{ijk} q_k^{M(1)} + W'_{ij} \Lambda^{M(1)} + \dot{W}_i \varepsilon^{M(1)}] x_j + W_{ij} x_j^{(1)} = 0, \\ &[W_{ijkl} q_k^{M(1)} q_l^{M(1)} + W_{ijk} q_k^{M(2)} + 2W'_{ijk} q_k^{M(1)} \Lambda^{M(1)} + 2\dot{W}_{ijk} q_k^{M(1)} \varepsilon^{M(1)} \\ &\quad + W'_i \Lambda^{M(2)} + \dot{W}_{ij} \varepsilon^{M(2)} + W''_i (\Lambda^{M(1)})^2 + \ddot{W}_{ij} (\varepsilon^{M(1)})^2 + 2\ddot{W}'_{ij} \Lambda^{M(1)} \varepsilon^{M(1)}] x_j \\ &\quad + 2[W_{ijk} q_k^{M(1)} + W'_{ij} \Lambda^{M(1)} + \dot{W}_i \varepsilon^{M(1)}] x_j^{(1)} + W_{ij} x_j^{(2)} = 0, \\ &[W_{ijklm} q_k^{M(1)} q_l^{M(1)} q_m^{M(1)} + 3W_{ijkl} q_k^{M(1)} q_l^{M(2)} + W_{ijk} q_k^{M(3)} \\ &\quad + 3W'_{ijkl} q_k^{M(1)} q_l^{M(1)} \Lambda^{M(1)} + 3\dot{W}_{ijkl} q_k^{M(1)} q_l^{M(1)} \varepsilon^{M(1)} + 3W'_{ijk} q_k^{M(2)} \Lambda^{M(1)} \\ &\quad + 3\dot{W}_{ijk} q_k^{M(2)} \varepsilon^{M(1)} + 3\dot{W}_{ijk} q_k^{M(1)} \varepsilon^{M(2)} + W'_i \Lambda^{M(3)} + 3W'_{ij} q_k^{M(1)} \Lambda^{M(2)} \\ &\quad + \dot{W}_{ij} \varepsilon^{M(3)} + 3W''_{ijk} q_k^{M(1)} (\Lambda^{M(1)})^2 + 3\ddot{W}_{ijk} q_k^{M(1)} (\varepsilon^{M(1)})^2 \\ &\quad + 6\ddot{W}'_{ijk} q_k^{M(1)} \Lambda^{M(1)} \varepsilon^{M(1)} + 3W''_i \Lambda^{M(1)} \Lambda^{M(2)} + 3\ddot{W}_{ij} \varepsilon^{M(1)} \varepsilon^{M(2)} \\ &\quad + 3\dot{W}'_{ij} \Lambda^{M(2)} \varepsilon^{M(1)} + 3\ddot{W}'_i \Lambda^{M(1)} \varepsilon^{M(2)} + 3\ddot{W}'_{ij} (\Lambda^{M(1)})^2 \varepsilon^{M(1)} \\ &\quad + 3\ddot{W}'_{ij} \Lambda^{M(1)} (\varepsilon^{M(1)})^2 + W'''_i (\Lambda^{M(1)})^3 + \ddot{W}_i (\varepsilon^{M(1)})^3] x_j + 3[W_{ijkl} q_k^{M(1)} q_l^{M(1)} \\ &\quad + W_{ijk} q_k^{M(2)} + 2W'_{ijk} q_k^{M(1)} \Lambda^{M(1)} + 2\dot{W}_{ijk} q_k^{M(1)} \varepsilon^{M(1)} + W'_i \Lambda^{M(2)} + \dot{W}_i \varepsilon^{M(2)} \\ &\quad + W''_i (\Lambda^{M(1)})^2 + \ddot{W}_{ij} (\varepsilon^{M(1)})^2 + 2\ddot{W}'_{ij} \Lambda^{M(1)} \varepsilon^{M(1)}] x_j^{(1)} + 3[W_{ijk} q_k^{M(1)} \\ &\quad + W'_i \Lambda^{M(1)} + \dot{W}_i \varepsilon^{M(1)}] x_j^{(2)} + W_{ij} x_j^{(3)} = 0, \end{aligned}$$

etc. The normalizing condition on x_j gives us

$$\begin{aligned} x_1 &= 1, \\ x_1^{(r)} &= 0 \quad \text{for } r = 1, 2, 3, \dots, \end{aligned}$$

and since in the limit as ε^M tends to zero the spiralling eigenvector x_j must be coincident with the eigenvector of the perfect system, we can write

$$x_j^C \equiv x_j(0) = q_j^{(1)C}.$$

We shall now present a general form of the r th-order critical state equation which is written formally as

$$\frac{d^r}{dq_1^M r} \{ W_{ij} [q_1^M, q_1^{M(r-1)}, \dots, q_1^{M(1)}; A^M(q_1^M), \varepsilon^M(q_1^M)] x_j(q_1^M) \} = 0.$$

The proposed general form is

$$W_{ij} x_j|^{(r)} = H_i^r (q_j^{M(r)}, q_j^{M(r-1)}, \dots, q_j^{M(1)}; A^{M(r-1)}, A^{M(r-2)}, \dots, A^{M(1)}; \varepsilon^{M(r)}, \varepsilon^{M(r-1)}, \dots, \varepsilon^{M(1)}; x_j^{(r-1)}, x_j^{(r-2)}, \dots, x_j^{(1)}, x_j) + W'_{ij} x_j A^{M(r)} + W_{ij} x_j^{(r)} = 0,$$

which again can be shown to be valid by the following inductive reasoning. We therefore differentiate this general form with respect to q_1^M to obtain $W_{ij} x_j|^{(r+1)}$, where

H_i^r is all included in H_i^{r+1} ,

$$W'_{ij} x_j A^{M(r)} \text{ becomes } \begin{cases} (W'_{ijk} q_k^{M(1)} + W''_{ij} A^{M(1)} + \dot{W}'_{ij} \varepsilon^{M(1)}) x_j A^{M(r)} & (\text{included in } H_i^{r+1}) \\ W'_{ij} x_j^{(1)} A^{M(r)} & (\text{included in } H_i^{r+1}) \\ W'_{ij} x_j A^{M(r+1)}, \end{cases}$$

$$W_{ij} x_j^{(r)} \text{ becomes } \begin{cases} (W_{ijk} q_k^{M(1)} + W'_{ij} A^{M(1)} + \dot{W}_{ij} \varepsilon^{M(1)}) x_j^{(r)} & (\text{included in } H_i^{r+1}) \\ W_{ij} x_j^{(r+1)}. \end{cases}$$

Thus it can be seen that if the form is correct for the r th-order equation it is likewise correct for the $r+1$ th-order equation; but from the low-order equations it can easily be seen that the assumed form is correct for $r=1$ and so the form is proved to be generally valid by induction.

8.6 Perturbation patterns

General forms of the governing perturbation equations in the W -analysis for imperfect systems have been presented, and we shall now make use of these forms in developing the pattern of solution of the scheme; this will be laid beside the known perturbation pattern for the analysis of a perfect system. First we shall present the *general* patterns of solution and secondly look at the *initial* forms of the two schemes which exhibit certain interrelationships and thus allow some prediction of imperfection-sensitivity from the analysis of a

perfect system. We do this for both critical points of interest—the asymmetric point of bifurcation and the unstable-symmetric point of bifurcation.

The general forms of the two schemes are presented in Figure 83 and we note that they appear quite distinct and dissimilar at this general stage. The 'perfect'

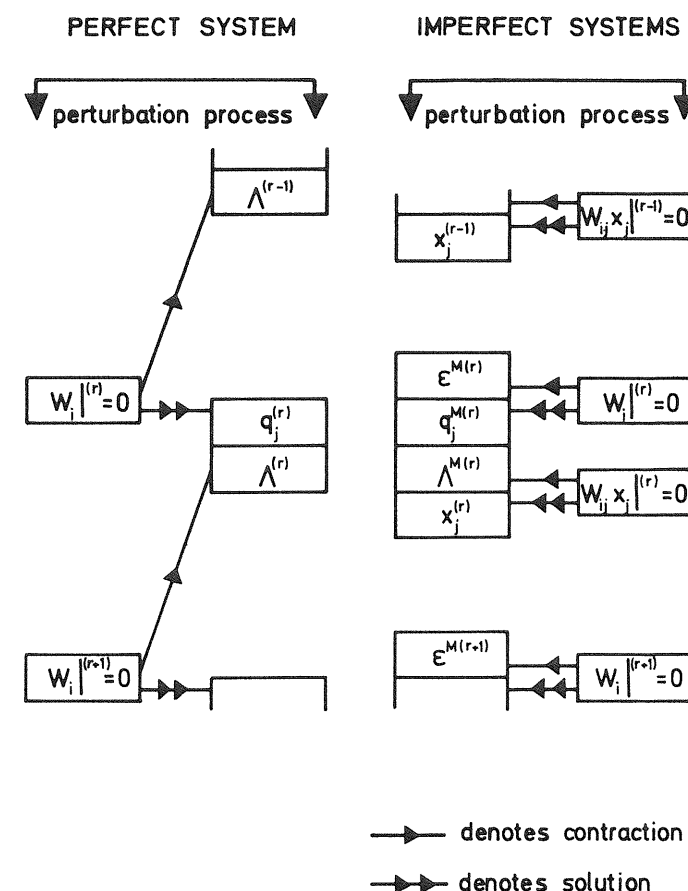


Figure 83 General patterns of the perturbation schemes

scheme was investigated in Chapter 6 so here we have merely duplicated the pattern for discrete systems shown in Figure 66. We shall again adopt the technique of induction to demonstrate that the 'imperfect' scheme follows the pattern shown here; this allows us to assume that we know the derivatives resulting from the $r-1$ th equations and show that the appropriate r th derivatives may be obtained from the r th equations. The later investigation

of the initial form of the scheme, which shows it to be valid for the starting equations, will complete the inductive reasoning.

Let us therefore consider the general form of the r th-order equilibrium equation. We assume that we know the $r - 1$ th derivatives and so G'_i is known. If we evaluate this equation at the critical point of the perfect system, the penultimate term will vanish by virtue of the properties of the W -function given in Chapter 6. Now contracting the n equations by multiplying by the post-buckling rates of the *perfect* system $q_i^{(1)c}$ and adding we find that the first term is zero by virtue of the first-order equilibrium equation of the perfect system $W_{ij}q_j^{(1)}|^c = 0$. This yields the result for the r th imperfection parameter derivative,

$$\varepsilon^{M(r)c} = - \frac{G'_i q_i^{(1)}}{W_i q_i^{(1)}} \Bigg| ^c,$$

and subsequent solution of the uncontracted set of equations,

$$W_{ij}q_j^{M(r)} + G'_i + \dot{W}_i \varepsilon^{M(r)}|^c = 0,$$

will reveal the r th derivatives $q_j^{M(r)c}$.

We next consider the general form of the r th-order critical state equation. The derivatives included in H'_i are known from the assumed $r - 1$ th derivatives and the solution of the r th equilibrium equation and so H'_i is known. If we evaluate at the critical point of the perfect system we can replace x_j^c in the penultimate term by $q_j^{(1)c}$. Furthermore, contraction of the set makes the last term zero by virtue of the first-order equilibrium equation of the perfect system $W_{ij}q_j^{(1)}|^c = 0$. This leads to an expression for the r th load derivative,

$$\Lambda^{M(r)c} = - \frac{H'_i q_i^{(1)}}{W'_{ij} q_i^{(1)} q_j^{(1)}} \Bigg| ^c,$$

and subsequent solution of the uncontracted equations,

$$H'_i + W'_{ij} q_j^{(1)} \Lambda^{M(r)} + W_{ij} x_j^{(r)}|^c = 0,$$

will reveal the r th-order derivatives of the spiralling eigenvector, $x_j^{(r)c}$. These results are therefore seen to be in agreement with the perturbation patterns of Figure 83.

We now focus attention on the initial results of the two perturbation schemes and the interaction which arises between them; this work will be of immediate significance to the numerical analyst with an interest in the phenomenon of imperfection-sensitivity. We have seen from the general results that the *same contraction mechanism* will play a continuing role throughout the ‘imperfect’ W -analysis as it did for the corresponding ‘perfect’ analysis of Chapter 6. However, the patterns of solution of the two schemes have been seen to be somewhat different as is apparent from the diagram of Figure 83.

We begin with a general treatment which corresponds to an asymmetric point of bifurcation and consider first the results of the perturbation scheme for the perfect system presented in Chapter 6: here we have a simple critical point in the sense that $W'_{ij} q_i^{(1)} q_j^{(1)}|^c \neq 0$ and in general $W_{ijk} q_i^{(1)} q_j^{(1)} q_k^{(1)}|^c \neq 0$. Starting with evaluation of the first equilibrium equation at the critical point, we employ the contraction mechanism in each subsequent set of equations and obtain from the continuing perturbation scheme

$$\begin{aligned} W_{ij} q_j^{(1)}|^c &= 0, \\ \Lambda^{(1)c} &= - \frac{W_{ijk} q_i^{(1)} q_j^{(1)} q_k^{(1)}}{2 W'_{ij} q_i^{(1)} q_j^{(1)}} \Bigg| ^c, \\ W_{ij} q_j^{(2)}|^c &= - (W_{ijk} q_j^{(1)} q_k^{(1)} + 2 W'_{ij} q_j^{(1)} \Lambda^{(1)})|^c, \end{aligned}$$

etc.

Passing on now to the corresponding perturbation scheme for imperfect systems we begin with contraction of the first-order equilibrium equations; thus multiplying by the post-buckling rates of the perfect system $q_i^{(1)c}$, adding the n equations, and evaluating at the critical point of the perfect system, we have

$$\dot{W}_i q_i^{(1)} \varepsilon^{M(1)}|^c = 0.$$

Assuming, as with the diagonalized A -analysis, that the imperfection parameter has a direct action on the buckling mode in the sense here that $\dot{W}_i q_i^{(1)}|^c \neq 0$, we have the first result of interest

$$\varepsilon^{M(1)c} = 0.$$

Evaluation of the uncontracted set of equations now yields

$$W_{ij} q_j^{M(1)}|^c = 0,$$

and a comparison with the first result of the ‘perfect’ scheme shows us that

$$q_j^{M(1)c} = q_j^{(1)c} \quad (= x_j^c).$$

Continuing, with contraction of the first-order critical state equations, we obtain after evaluation at the critical point of the perfect system and using the above result,

$$\Lambda^{M(1)c} = - \frac{W_{ijk} q_i^{(1)} q_j^{(1)} q_k^{(1)}}{W'_{ij} q_i^{(1)} q_j^{(1)}} \Bigg| ^c.$$

A comparison with the result for the slope of the post-buckling path of the perfect system gives the important interrelationship

$$\Lambda^{M(1)c} = 2 \Lambda^{(1)c}.$$

A comparison with the expression for the curvature of the post-buckling path of the perfect system gives the important interrelationship

$$\Lambda^{M(2)C} = 3\Lambda^{(2)C}.$$

The uncontracted set of second-order critical state equations can now be written after evaluation as

$$W_{ij} x_j^{(2)}|^C = - (W_{ijkl} q_j^{(1)} q_k^{(1)} q_l^{(1)} + 3W_{ijk} q_j^{(1)} q_k^{(2)} + 3W'_{ij} q_j^{(1)} \Lambda^{(2)})|^C,$$

and a comparison with the results of the ‘perfect’ scheme shows that

$$x_j^{(2)C} = q_j^{(3)C}.$$

Finally, contraction of the third-order equilibrium equation leads to the result

$$\varepsilon^{M(3)C} = \frac{2\tilde{W}_4}{\dot{W}_i q_i^{(1)}} \Big|^C.$$

The numerator of the above expression is non-zero for a symmetric point of bifurcation and again we find that having obtained a non-zero ε^M derivative there are no further interrelationships between ‘perfect’ and ‘imperfect’ perturbation schemes, so we stop the analysis. The interactions which arise only at symmetric points of bifurcation are not given specifically on Figure 84 to avoid confusion, but they are sometimes derived from identical sets of equations and these are represented in the diagram by the symbols A^s and B^s on the flow lines.

The interrelationships which have been obtained here allow a *first-order estimate of imperfection-sensitivity* to be made entirely in terms of the post-buckling derivatives of the perfect system for both an asymmetric and an unstable-symmetric point of bifurcation, as we shall see in the following section.

8.7 Asymptotic equations of imperfection-sensitivity

The ‘imperfect’ perturbation scheme generates the derivatives of Λ^M and ε^M with respect to q_1^M evaluated at the critical point of the perfect system and thereby allows these parameters to be expanded as Taylor series in terms of q_1^M . However, we can see from Figures 81 and 82 that the most convenient way of illustrating the imperfection-sensitivity of a system would be to express Λ^M as a function of ε^M . With this in mind we shall reverse the series for ε^M and substitute $q_1^M(\varepsilon^M)$ into $\Lambda^M(q_1^M)$ to find $\Lambda^M(\varepsilon^M)$; this, however, involves the reversal of an incomplete Taylor series for each of the two critical points of interest.

First we consider the asymmetric point of bifurcation. We have seen that $\varepsilon^{M(1)C}$ is equal to zero so we are left with

$$\begin{aligned}\Lambda^M &= \Lambda^C + \Lambda^{M(1)C} q_1^M + \frac{1}{2}\Lambda^{M(2)C}(q_1^M)^2 + \frac{1}{6}\Lambda^{M(3)C}(q_1^M)^3 + \dots, \\ \varepsilon^M &= \frac{1}{2}\varepsilon^{M(2)C}(q_1^M)^2 + \frac{1}{6}\varepsilon^{M(3)C}(q_1^M)^3 + \frac{1}{24}\varepsilon^{M(4)C}(q_1^M)^4 + \dots.\end{aligned}$$

Standard formulae are readily available for the reversal of a complete Taylor series but these become invalid once the linear term of the series is missing. However, a method of reversing this incomplete $\varepsilon^M(q^M)$ series has been developed,¹²⁶ so using this technique and substituting the result into the $\Lambda^M(q_1^M)$ series we obtain the complete asymptotic equation of imperfection-sensitivity for the asymmetric point of bifurcation,

$$\Lambda^M = \Lambda^C + \alpha(\varepsilon^M)^{\frac{1}{2}+} + \beta(\varepsilon^M) + \gamma(\varepsilon^M)^{1+\frac{1}{2}+} + \dots,$$

where

$$\begin{aligned}\alpha &= \pm \left(\frac{2}{\varepsilon^{M(2)C}} \right)^{\frac{1}{2}+} \Lambda^{M(1)C}, \quad \beta = \frac{\Lambda^{M(2)C}}{\varepsilon^{M(2)C}} - \frac{\Lambda^{M(1)C} \varepsilon^{M(3)C}}{3(\varepsilon^{M(2)C})^2}, \\ \gamma &= \pm \left(\frac{2}{\varepsilon^{M(2)C}} \right)^{\frac{1}{2}+} \left\{ \frac{\Lambda^{M(3)C}}{3\varepsilon^{M(2)C}} - \frac{\Lambda^{M(2)C} \varepsilon^{M(3)C}}{3(\varepsilon^{M(2)C})^2} + \frac{\Lambda^{M(1)C}}{36(\varepsilon^{M(2)C})^3} \right. \\ &\quad \left. \times [5(\varepsilon^{M(3)C})^2 - 3\varepsilon^{M(2)C} \varepsilon^{M(4)C}] \right\},\end{aligned}$$

etc. Here $\frac{1}{2}+$ denotes the positive square root only and the sign of γ is dependent upon the sign of α . If we consider only the first term of this series we obtain the first-order estimate of imperfection-sensitivity, the expected parabolic relationship. We see that the coefficient α can be written entirely in terms of the post-buckling derivatives of the perfect system from the interrelationships of the previous section.

We now repeat the process for the unstable-symmetric point of bifurcation. Here $\varepsilon^{M(1)C}$, $\Lambda^{M(1)C}$, and $\varepsilon^{M(2)C}$ are all equal to zero so our Taylor series expansions become

$$\begin{aligned}\Lambda^M &= \Lambda^C + \frac{1}{2}\Lambda^{M(2)C}(q_1^M)^2 + \frac{1}{6}\Lambda^{M(3)C}(q_1^M)^3 + \frac{1}{24}\Lambda^{M(4)C}(q_1^M)^4 + \dots, \\ \varepsilon^M &= \frac{1}{6}\varepsilon^{M(3)C}(q_1^M)^3 + \frac{1}{24}\varepsilon^{M(4)C}(q_1^M)^4 + \frac{1}{120}\varepsilon^{M(5)C}(q_1^M)^5 + \dots.\end{aligned}$$

Once again we cannot use standard formulae to reverse the incomplete $\varepsilon^M(q_1^M)$ series. However, we can again appeal to earlier work¹²⁶ for the appropriate reverse form and substitute into the $\Lambda^M(q_1^M)$ series to obtain the complete asymptotic equation of imperfection-sensitivity for the unstable-symmetric point of bifurcation

$$\Lambda^M = \Lambda^C + \alpha(\varepsilon^M)^{\frac{1}{3}} + \beta(\varepsilon^M) + \gamma(\varepsilon^M)^{\frac{4}{3}} + \dots,$$

where

$$\alpha = \frac{\Lambda^{M(2)C}}{2} \left(\frac{6}{\varepsilon^{M(3)C}} \right)^{\frac{1}{3}}, \quad \beta = \frac{1}{2} \left[\frac{2\Lambda^{M(3)C}}{\varepsilon^{M(3)C}} - \frac{\Lambda^{M(2)C} \varepsilon^{M(4)C}}{(\varepsilon^{M(3)C})^2} \right],$$

$$\gamma = \left(\frac{6}{\varepsilon^{M(3)C}} \right)^{\frac{1}{3}} \left[\frac{\Lambda^{M(4)C}}{4\varepsilon^{M(3)C}} - \frac{\Lambda^{M(3)C} \varepsilon^{M(4)C}}{4(\varepsilon^{M(3)C})^2} - \frac{\Lambda^{M(2)C} \varepsilon^{M(5)C}}{10(\varepsilon^{M(3)C})^2} + \frac{7\Lambda^{M(2)C} (\varepsilon^{M(4)C})^2}{48(\varepsilon^{M(3)C})^3} \right],$$

etc. Considering only the first term of the series we obtain the first-order estimate of imperfection-sensitivity, the expected two-thirds power law relationship. We see that the coefficient α can be written entirely in terms of the post-buckling derivatives of the perfect system from the interrelationships of the previous section.

9

STRUTS AND FRAMES

9.1 Strut on an elastic foundation

After such a considerable dose of general theory as is dealt out in the previous chapter it is usually rewarding to see the application of the theory to appropriate structural problems. With this in mind we devote this chapter to the analysis of two imperfection-sensitive structures, the first illustrating the analytical procedure for a diagonalized potential energy function and the second the procedure for a non-diagonalized potential energy function.

We start then with a harmonic analysis of the strut on an elastic foundation. A similar analysis of a strut on a continuous *nonlinear* elastic foundation is given by Bolotin:¹⁹⁸ here the foundation nonlinearity is assumed to be so strong that the eigenvalue equation for the strut can be used, leaving the foundation as the only nonlinear factor in the problem. The paper contains a *description* in fairly general terms of the four distinct critical points of this monograph, together with an interesting geometrical construction for determining the response of perfect and imperfect systems. We note also that the problem has been dealt with in continuum terms by Lekkerkerker.¹⁵⁴

Energy formulation

We consider the pin-ended strut of length l shown in Figure 85 which is loaded by the axial force P and rests on an elastic foundation of stiffness per unit length K . The strut is assumed to be axially inextensible, and the relevant bending stiffness is denoted by B . To represent an imperfection from this ideal situation we suppose that the strut carries a small lateral load ε at its mid-point. The two loads are assumed to retain their magnitude and direction as the strut deflects.

Point A of the strut originally distance x from the left-hand support is displaced to A' and this displacement is resolved into an unspecified horizontal component and a vertical component w as shown: The centre-line being inextensible, the arc length SA' is equal to x , and the deflected form of the strut is totally specified by the mathematical function $w(x)$, where x ranges from 0 to l .

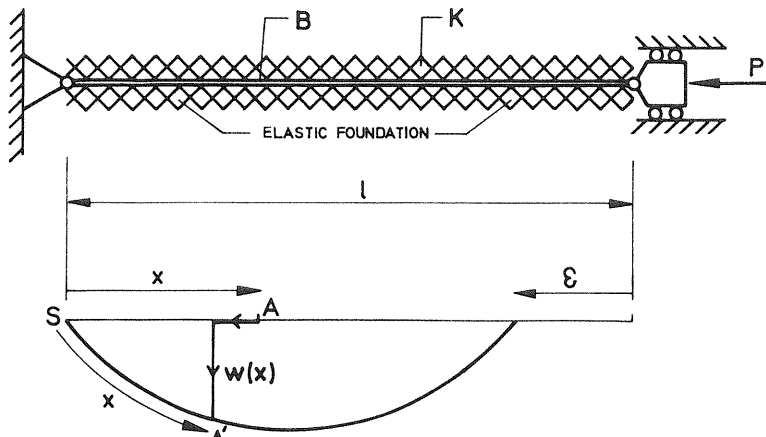


Figure 85 The strut on an elastic foundation

The foundation is assumed to consist of a large number of elastic springs tied to the strut and anchored at infinity so that they remain normal to the original centre-line as the strut deflects. The strain energy stored in these springs is then given exactly by the expression

$$U_k = \frac{1}{2}K \int_0^l w^2 dx.$$

The strain energy stored in the bending strut is of course the same as for the pin-ended strut of Chapter 1 and is given by equation (1.1) as

$$U_B = \frac{1}{2}B \int_0^l (\dot{w}^2 + \dot{w}^2 \dot{w}^2 + \dot{w}^2 \dot{w}^4 + \dots) dx.$$

Likewise, the corresponding deflection of the axial load P remains unchanged and is given by equation (1.2) as

$$\mathcal{E} = \int_0^l (\frac{1}{2}\dot{w}^2 + \frac{1}{8}\dot{w}^4 + \frac{1}{16}\dot{w}^6 + \dots) dx.$$

The corresponding deflection of the lateral load ε is of course

$$\phi = w \left(\frac{l}{2} \right).$$

The total potential energy can thus be written as

$$V = \frac{1}{2}K \int_0^l w^2 dx + \frac{1}{2}B \int_0^l (\dot{w}^2 + \dot{w}^2 \dot{w}^2 + \dot{w}^2 \dot{w}^4 + \dots) dx - P \int_0^l (\frac{1}{2}\dot{w}^2 + \frac{1}{8}\dot{w}^4 + \frac{1}{16}\dot{w}^6 + \dots) dx - \varepsilon w \left(\frac{l}{2} \right)$$

We note at this stage that the choice of imperfection as a lateral load with its point of application at the mid-point of the strut means that it can have no action on buckling modes which are harmonics of even degree; we can therefore only discuss the imperfection-sensitivity of modes of odd degree.

We begin the harmonic analysis by expanding the lateral deflection as a Fourier series

$$w(x) = \sum_{i=1}^{\infty} u_i \sin \frac{i\pi x}{l}.$$

The necessary derivatives of w can then be written down

$$\begin{aligned} \dot{w} &= \sum_{i=1}^{\infty} u_i \frac{i\pi}{l} \cos \frac{i\pi x}{l}, \\ \ddot{w} &= \sum_{i=1}^{\infty} -u_i \left(\frac{i\pi}{l} \right)^2 \sin \frac{i\pi x}{l}, \\ w^2 &= \sum_{i=1}^{\infty} \sum_{j=1}^{\infty} u_i u_j \sin \frac{i\pi x}{l} \sin \frac{j\pi x}{l}, \end{aligned}$$

etc. Substituting these into the energy functional gives us V as an algebraic function of the u_i , P and ε which we can write formally as

$$\begin{aligned} V(u_i, P, \varepsilon) &= \frac{1}{2}U_{ij}(0)u_i u_j + \frac{1}{24}U_{ijkm}(0)u_i u_j u_k u_m + \dots \\ &\quad - P[\frac{1}{2}\mathcal{E}_{ij}(0)u_i u_j + \frac{1}{24}\mathcal{E}_{ijkm}(0)u_i u_j u_k u_m + \dots] - \varepsilon \phi_i(0)u_i, \end{aligned}$$

where the dummy-suffix summation convention is employed. Comparing this with the functional we see that the coefficients will be given by

$$\begin{aligned} U_{ij}(0) &= 0 \quad \text{for } i \neq j, \\ U_{ii}(0) &= \frac{Bl}{2} \left(\frac{i\pi}{l} \right)^4 + \frac{1}{2}Kl, \\ \mathcal{E}_{ij}(0) &= 0 \quad \text{for } i \neq j, \\ \mathcal{E}_{ii}(0) &= \frac{l}{2} \left(\frac{i\pi}{l} \right)^2, \\ U_{ijkm}(0)u_i u_j u_k u_m &= 12B \left(\frac{\pi}{l} \right)^6 \sum_i \sum_j \sum_k \sum_m i^2 j^2 k m u_i u_j u_k u_m \int_0^l \sin \frac{i\pi x}{l} \\ &\quad \times \sin \frac{j\pi x}{l} \cos \frac{k\pi x}{l} \cos \frac{m\pi x}{l} dx, \\ \mathcal{E}_{ijkm}(0) &= 3ijkm \left(\frac{\pi}{l} \right)^4 \int_0^l \cos \frac{i\pi x}{l} \cos \frac{j\pi x}{l} \cos \frac{k\pi x}{l} \cos \frac{m\pi x}{l} dx, \\ \phi_i(0) &= +1 \quad \text{for } i = 1, 5, 9, \dots, \\ \phi_i(0) &= -1 \quad \text{for } i = 3, 7, 11, \dots, \\ \phi_i(0) &= 0 \quad \text{for } i = 2, 4, 6, \dots \end{aligned}$$

Here, as with the elastica analysis of Chapter 1, we have included a summation in the equality associated with U_{lkm} since this coefficient is necessarily symmetric while the integral is not.

Perfect system

If we set $\varepsilon = 0$ in the potential energy function we can directly employ the results of Chapter 6 for an analysis of the buckling behaviour of the perfect system. We see that U_{ij} and \mathcal{E}_{ij} are both diagonal forms so the results of the A -analysis can be used, and the critical loads can immediately be written as

$$P^i = \frac{U_{ii}(0)}{\mathcal{E}_{ii}(0)}$$

giving

$$\frac{P^i}{B(\pi/l)^2} = i^2 + \frac{1}{i^2}\gamma,$$

where γ is a stiffness ratio given by

$$\gamma = \frac{K}{B(\pi/l)^4}.$$

We note that these results agree with the eigenvalue analysis of Timoshenko and Gere.¹⁹⁹

Plotting P^i with γ for typical i values of 1, 2 and 3 we obtain the straight lines shown in Figure 86. We see from this diagram that the lowest critical load of the

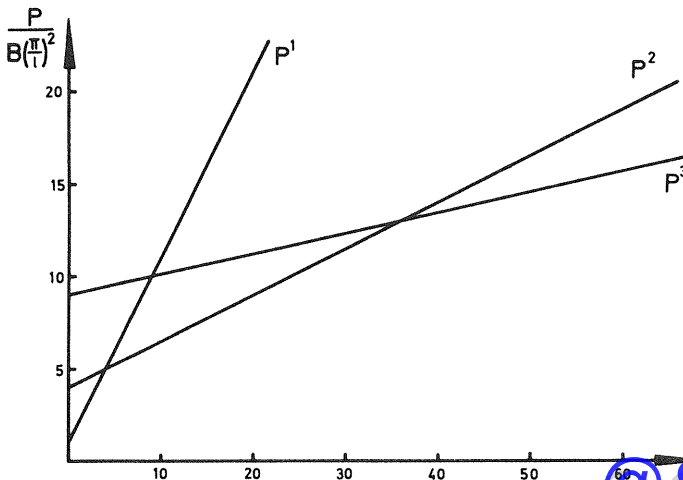


Figure 86 The variation of three critical loads with stiffness ratio

system is not necessarily given by $i = 1$ as was the case with the elastica analysis of Chapter 1. Thus assuming that the strut first buckles in t half-sin waves the critical load P^c is given by P^t and the critical principal coordinate is u_t .

Moving on now to a study of the post-buckling response of the perfect system, we see that the cubic coefficients are all zero so we can expect buckling to take place at a symmetric point of bifurcation. The necessary coefficients for the curvature of the post-buckling path can next be determined,

$$A'_{tt} = -\mathcal{E}_{tt}(0) = -\frac{l}{2} \left(\frac{t\pi}{l} \right)^2,$$

$$A_{ttt}^c = U_{ttt}(0) - P^t \mathcal{E}_{ttt}(0) = \frac{3}{8} Bl \left(\frac{\pi}{l} \right)^6 t^2 (t^4 - 3\gamma),$$

and finally, using equations (6.3) and (6.4) of the general theory, the curvature of the post-buckling path can be expressed in the form

$$\frac{P^{(2)c}}{B(\pi/l)^4} = \frac{1}{4}(t^4 - 3\gamma).$$

We note that this expression agrees with the results of Lekkerkerker.¹⁵⁴ The variation of the curvature expression with the stiffness ratio γ is shown in Figure 87. Here the singularities of $P^{(2)c}$ at $\gamma = 4$ and $\gamma = 36$ represent changes in mode form arising at conditions of coincidence of two critical loads.

Imperfect systems

Having found that over a large proportion of the stiffness ratios considered in Figure 87 the post-buckling path curvature is negative and the perfect system therefore exhibits an unstable-symmetric point of bifurcation, it now becomes necessary to examine the imperfection-sensitivity response; we must, however, remember that with our particular definition of imperfection we are only able to do this for buckling harmonics of odd degree.

Thus after replacing ε in the potential energy expression and referring to the diagonalized A -analysis of Chapter 8, we find that the only further energy coefficient we require for a first-order imperfection-sensitivity estimate is A_t^c . This we may immediately write as

$$A_t^c = -\phi_t(0) \quad \text{for } t = 1, 3, 5, \dots$$

The asymptotic variation of the peak or failure load P^M with imperfection parameter ε can now be determined from equation (8.3) to a first-order as

$$P^M = P^c - \alpha \varepsilon^{2/3},$$

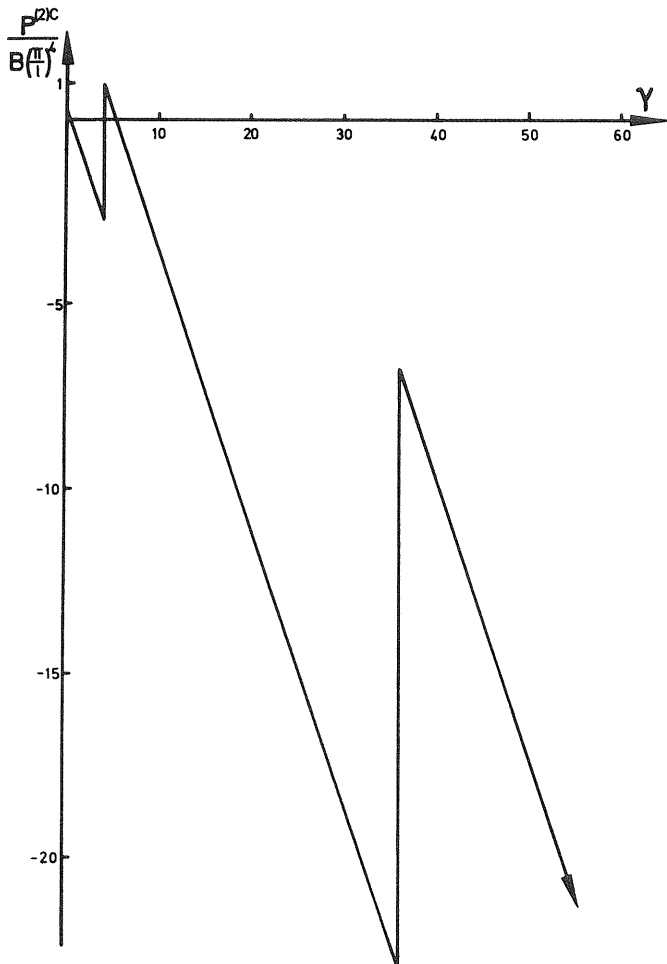


Figure 87 The variation of the curvature of the post-buckling path with stiffness ratio

where

$$\alpha = -\frac{3}{2} \left(\frac{B}{l^2 t^4} \right)^{\frac{1}{3}} (t^4 - 3\gamma)^{\frac{1}{3}},$$

and we see that we obtain the initial two-thirds power law imperfection-sensitivity relationship expected about an unstable-symmetric point of bifurcation.

9.2 Finite-element method for frames

As an illustration of the ‘perfect’ and ‘imperfect’ perturbation procedures using a non-diagonalized potential energy function, we now present an analysis of a simple two-bar frame using a finite-element formulation. This choice is considered apt because it demonstrates the salient features of more complex frame problems without obscuring them in a mass of complicated detail; it is felt that the extension to such problems should become obvious when this analysis is fully understood. Furthermore the experiments of Roorda,⁶⁰ which we mention in the general introduction of Chapter 2, provide an excellent basis for comparison and a continuum analysis of this frame by Koiter¹⁷ means that we can compare the results produced by the finite-element model with their corresponding exact values.

One of the major problems associated with post-buckling analyses of frames is generated by the necessity of considering nonlinear compatibility relationships at the joints where two or more members meet. We find here that the problem is neatly overcome by the finite-element formulation; in fact it is these nonlinear relationships which allow us to generate cubic terms of potential energy simply by using the general quadratic coefficients of strain energy and end-shortening of elements. The whole nonlinear treatment, leading to a first-order estimate of the post-buckling and imperfection-sensitivity of the system, is thus found to require little more in the way of computational effort than a standard eigenvalue analysis.

Generalized coordinates

Consider the frame of Figure 88 comprising two identical members of length l , pinned to rigid supports and rigidly joined together at right angles as shown. The frame is loaded by the dead vertical load P which retains its magnitude and direction as the system deflects. The members of the frame are assumed to be axially inextensible and the bending stiffness of each bar is denoted by B .

To study the effect of small imperfections on the response of the system we allow the load to be applied with a small eccentricity ϵl ; the behaviour of the perfect system can of course be fully investigated by setting $\epsilon = 0$. The load P is therefore assumed to act on an initially-horizontal bar which is rigidly joined to the frame at the joint and which itself is rigid in bending; the distance along the bar ϵl remains constant as the system deflects. An exaggerated representation of this loading detail is shown in Figure 88(b).

Point A of the frame, originally distance x from the pin end of the upright member is displaced to A' and we resolve this into an unspecified vertical component and a horizontal component w as shown. Furthermore point C of the frame, originally distance y from the rigid joint, is displaced to C' and we

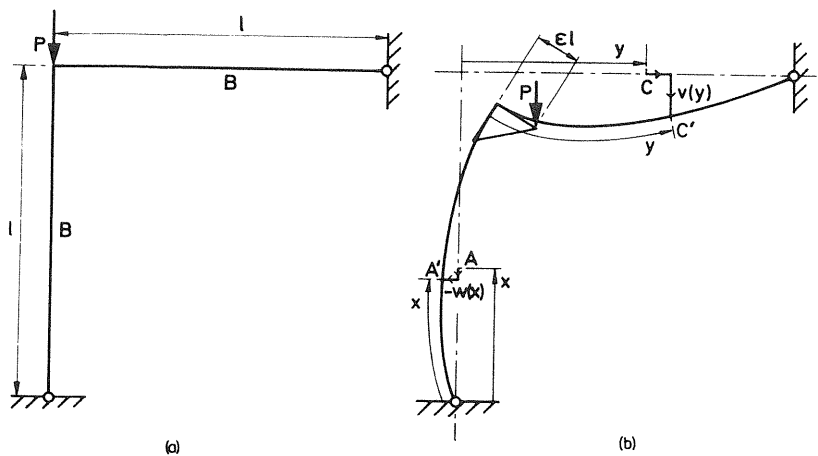


Figure 88 A two-member frame showing (a) undeflected perfect system and (b) deflected imperfect system

resolve this into an unspecified horizontal component and a vertical component v as shown. An appropriate finite-element formulation will now allow us to fabricate kinematically-admissible forms for $w(x)$ and $v(y)$ and so arrive at a nonlinear potential energy function for a finite-element model for the system.

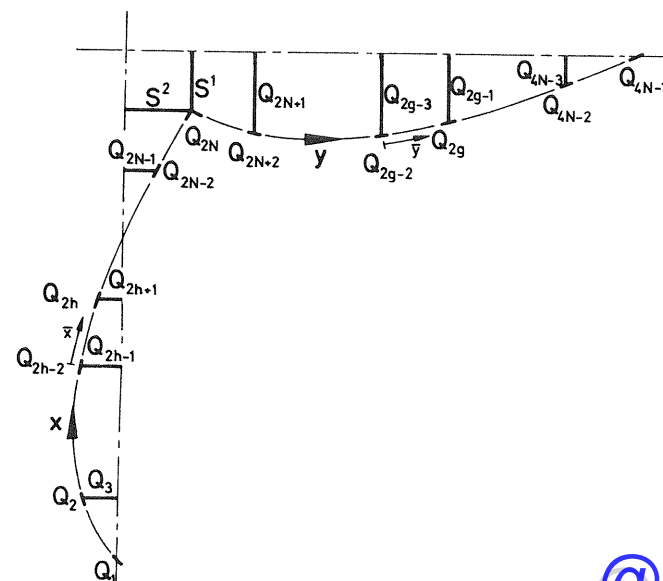


Figure 89 Finite-element fabrication of the deflection functions

We might note at this stage the functions $w(x)$ and $v(y)$ do not represent the physical shape of the deflected system if plotted in rectangular coordinates.

Thus for a finite-element representation we divide both the x -domain and the y -domain into $N + 1$ equally spaced stations. Each internal station is given an arbitrary displacement w or v and an arbitrary first derivative dw/dx or dv/dy , whilst in accordance with the boundary conditions of the problem the stations at the pin-joints are given arbitrary first derivatives but no displacement; the displacements at the rigid joint are not made arbitrary but are denoted by the end-shortening functions S^1 and S^2 as shown in Figure 89. The totality of the arbitrary displacements and first derivatives become the generalized coordinates of a discrete problem and are denoted by Q_i , the ordering of these $4N - 1$ coordinates being shown in Figure 89.

A third-order polynomial is now fitted in each region giving an overall deflected form which is continuous in displacement and first derivative but which admits discontinuities in its second derivative at the stations. Considering the general h th interval on the vertical member with its local independent variable \bar{x} (Figure 89) this third-order polynomial is

$$\begin{aligned} w^h &= Q_{2h-2} \left[\bar{x} - 2\left(\frac{n}{l}\right) \bar{x}^2 + \left(\frac{n}{l}\right)^2 \bar{x}^3 \right] + Q_{2h-1} \left[1 - 3\left(\frac{n}{l}\right)^2 \bar{x}^2 + 2\left(\frac{n}{l}\right)^3 \bar{x}^3 \right] \\ &\quad + Q_{2h} \left[-\left(\frac{n}{l}\right) \bar{x}^2 + \left(\frac{n}{l}\right)^2 \bar{x}^3 \right] + Q_{2h+1} \left[3\left(\frac{n}{l}\right)^2 \bar{x}^2 - 2\left(\frac{n}{l}\right)^3 \bar{x}^3 \right]. \end{aligned}$$

There is of course a similar expression for a typical region of the horizontal member.

The curvature of an element $d\bar{x}$ of the h th region is given by

$$\chi = \frac{d}{d\bar{x}} \sin^{-1} \dot{w}^h = \dot{w}^h [1 - (\dot{w}^h)^2]^{-\frac{1}{2}},$$

where a dot denotes differentiation with respect to \bar{x} . We thus have the strain energy functional for the region

$$\begin{aligned} U^h &= \frac{1}{2} B \int_0^{l/n} \chi^2 d\bar{x} \\ &= \frac{1}{2} B \int_0^{l/n} (\dot{w}^h)^2 [1 - (\dot{w}^h)^2]^{-1} d\bar{x} \\ &= \frac{1}{2} B \int_0^{l/n} [(\dot{w}^h)^2 + (\dot{w}^h)^2 (\ddot{w}^h)^2 + (\dot{w}^h)^2 (\dot{w}^h)^4 + \dots] d\bar{x}. \end{aligned}$$

The end-shortening of the general h th region is given by

$$\begin{aligned} S^h &= \frac{l}{n} - \int_0^{l/n} [1 - (\dot{w}^h)^2]^{\frac{1}{2}} d\bar{x} \\ &= \int_0^{l/n} [\frac{1}{2} (\dot{w}^h)^2 + \frac{1}{8} (\dot{w}^h)^4 + \frac{1}{16} (\dot{w}^h)^6 + \dots] d\bar{x}, \end{aligned}$$

and we note that the leading term is quadratic in both the strain energy and end-shortening functionals. There are of course entirely similar expressions for a typical g th region of the horizontal member.

Substitution of our third-order polynomial for w^h into these expressions gives the strain energy and end-shortening of the element in terms of the generalized coordinates bounding the region, except for the important elements adjacent to the rigid joint where one generalized coordinate is replaced by S^1 or S^2 . Summation over the complete frame now gives the total strain energy U and summation over each member of the frame gives expressions for S^1 and S^2 as follows

$$U = \sum_{h=1}^{h=N} U^h + \sum_{g=N+1}^{g=2N} U^g,$$

$$S^1 = \sum_{h=1}^{h=N} S^h, \quad S^2 = \sum_{g=N+1}^{g=2N} S^g.$$

The corresponding deflection of the dead load P is given by

$$\begin{aligned} \mathcal{E} &= S^1 + \varepsilon l \sin \theta \\ &= S^1 + \varepsilon l Q_{2N}, \end{aligned}$$

where θ is the angle of rotation of the rigid joint. The total potential energy function can thus be written

$$\begin{aligned} V &= U - P\mathcal{E} \\ &= \sum_{h=1}^{h=N} U^h + \sum_{g=N+1}^{g=2N} U^g - P \sum_{h=1}^{h=N} S^h - P\varepsilon l Q_{2N} \end{aligned}$$

and we see that V has been obtained in the form

$$V = U[Q_i, S^\alpha(Q_i, S^\beta)] - PS^1[Q_i, S^2(Q_i, S^1)] - P\varepsilon l Q_{2N},$$

where in general i takes the values 1 to $n = 4N - 1$ and $\alpha = 1$ or 2.

Perfect system

Before we can appeal to the general theory of Chapter 6 we must first ensure that the potential energy is in a suitable form for analysis. Setting $\varepsilon = 0$ to study the perfect system, the fundamental path and sliding transformation can be easily shown to be trivial so that $q_i = Q_i$ and we can write the non-diagonalized potential energy function as

$$W = W[q_i, S^\alpha(q_i, S^\beta), A].$$

The subsequent eigenvalue problem and perturbation scheme for the slope of the post-buckling path require derivatives of $W(q_i, A)$ so writing

$$W(q_i, A) \equiv W[q_i, S^\alpha(q_i, S^\beta), A],$$

we obtain by differentiation

$$\begin{aligned} W_t &= W_t + W_\alpha[S_t^\alpha + S_\beta^\alpha S_t^\beta + S_\beta^\alpha S_\gamma^\beta S_t^\gamma + \dots], \\ W'_t &= W'_t + W'_\alpha[S_t^\alpha + S_\beta^\alpha S_t^\beta + S_\beta^\alpha S_\gamma^\beta S_t^\gamma + \dots], \\ W_{ij} &= W_{ij} + W_{ia}[S_j^\alpha + S_\beta^\alpha S_j^\beta + \dots] + W_{ja}[S_i^\alpha + S_\beta^\alpha S_i^\beta + \dots] \\ &\quad + W_{\alpha\beta}[S_j^\beta + S_\gamma^\beta S_j^\gamma + \dots][S_i^\alpha + S_\gamma^\alpha S_i^\gamma + \dots] \\ &\quad + W_\alpha[S_{ij}^\alpha + S_{i\beta}^\alpha S_j^\beta + S_{j\beta}^\alpha S_i^\beta + S_\beta^\alpha S_{ij}^\beta + \dots], \end{aligned}$$

etc., where

$$W_\alpha \equiv \frac{\partial W}{\partial S^\alpha}, \quad S_\beta^\alpha \equiv \frac{\partial S^\alpha}{\partial S^\beta}, \quad W_{\alpha\beta} \equiv \frac{\partial^2 W}{\partial S^\alpha \partial S^\beta},$$

etc., the other subscripts and primes carrying the same significance as before. Here as elsewhere in this analysis a summation convention is employed over repeated subscripts and superscripts with summation over Latin subscripts being from 1 to n and over Greek indices from 1 to 2.

From the general theory we know that the critical load of this perfect system depends on the quadratic form $W_{ij}(0, A)$ so evaluating W_{ij} on the fundamental path we obtain

$$W_{ij}^F = W_{ij}^F = U_{ij}(0) - PS_{ij}^1(0).$$

This conveniently trivial relationship is obtained because the linear terms of the expansion $S^\alpha(q_i, S^\beta)$ is zero and also $W_\alpha^F = 0$. The critical load P^C can now be found from the stability requirement

$$|W_{ij}^C| = |U_{ij}(0) - P^C S_{ij}^1(0)| = 0.$$

Thus using a computer and varying the loading parameter systematically until the determinant approaches zero, the value of P^C can readily be found.

Returning to the W -analysis of the general theory, we now make use of the perturbation scheme of Chapter 6 for the post-buckling path derivatives. Here we select the slope of the rigid joint q_t ($t = 2N$) as the independent variable; the identity $q_t^{(1)} = 1$ then allows the first mode equation $W_{ij} q_t^{(1)}|^C = 0$ to be rewritten as

$$W_{is}^C q_s^{(1)C} = -W_{it}^C \quad (s \neq t).$$

We thus have n equations in $n - 1$ unknowns; simply disregarding the t th equation the remaining non-singular set may be solved on the computer for the mode derivatives $q_s^{(1)C}$.

The W derivatives which are required for the slope of the post-buckling path can be written after evaluation at C as

$$\begin{aligned} W'_{ij}^C &= W'_{ij} = -S_{ij}^1(0), \\ W'_{ijk}^C &= W_{i\alpha} S_{jk}^\alpha + W_{j\alpha} S_{ik}^\alpha + W_{k\alpha} S_{ij}^\alpha \\ &= [U_{i\alpha}(0) - P^C S_{i\alpha}^1(0)] S_{jk}^\alpha(0) + [U_{j\alpha}(0) - P^C S_{j\alpha}^1(0)] S_{ik}^\alpha(0) \\ &\quad + [U_{k\alpha}(0) - P^C S_{k\alpha}^1(0)] S_{ij}^\alpha(0), \end{aligned}$$

and again we note that these results rely heavily on the fact that the linear term of the expansion $S^\alpha(q_i, S^\beta)$ is zero. The non-vanishing cubic coefficient clearly demonstrates the development of third-order terms from a finite-element formulation comprising no terms of odd orders. Knowing the mode derivatives $q_j^{(1)C}$ and the required W derivatives the slope of the post-buckling path can now be evaluated by simple summation on the computer.

The necessary computations for the critical load and post-buckling slope of our finite-element model were performed for values of N —the number of elements in each member—from 1 to 16. The answers were found to converge rapidly to the exact values given by Koiter¹⁷ and this convergence from $N = 2$ to $N = 16$ is shown in Figure 90; the values for $N = 1$ were found to lie well outside the scale of the present plots, and to include these would have rendered the graphs less meaningful.

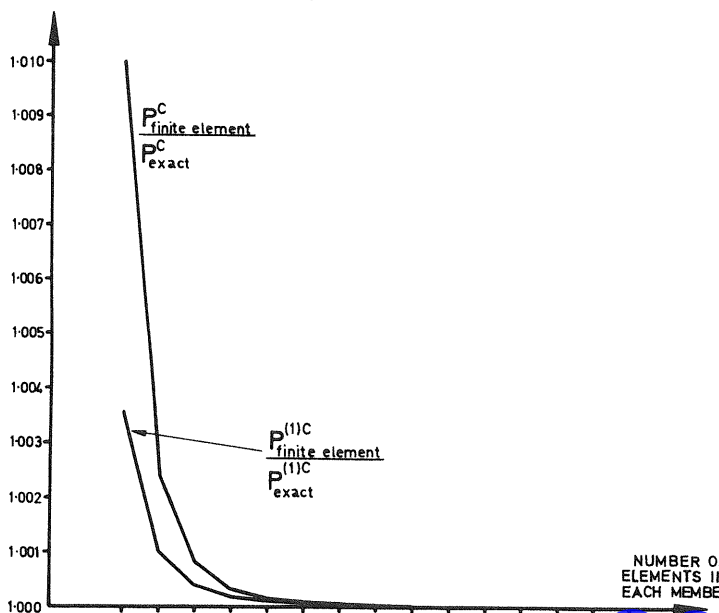


Figure 90 Convergence of the finite-element critical load and post-buckling slope

Imperfect systems

Having seen that the perfect system experiences an asymmetric point of bifurcation, we know that the imperfection-sensitivity relationship can be expected to be initially parabolic in form from the general theory of Chapter 8. To obtain the first coefficient of the appropriate asymptotic equation we have the following results for a non-diagonalized potential energy function

$$\begin{aligned} A^{M(1)C} &= 2A^{(1)C}, \\ \varepsilon^{M(2)C} &= \left. \frac{W_{ijk} q_i^{(1)} q_j^{(1)} q_k^{(1)}}{W_i q_i^{(1)}} \right|^C. \end{aligned}$$

Thus applying these to our frame problem, we find that the only further W derivative required is \dot{W}_i so writing

$$W(q_i, A, \varepsilon) = W[q_i, S^\alpha(q_i, S^\beta), A, \varepsilon],$$

we obtain by differentiation as before

$$\dot{W}_i = \dot{W}_i + \dot{W}_\alpha [S_i^\alpha + S_\beta^\alpha S_i^\beta + S_\beta^\alpha S_\gamma^\beta S_i^\gamma + \dots].$$

Evaluating at the critical point C of the perfect system, this expression is conveniently simplified by vanishing linear terms in the $S^\alpha(q_i, S^\beta)$ expansions as before and we obtain the following results

$$\begin{aligned} \dot{W}_i^C &= \dot{W}_i = -P^C I, \\ \dot{W}_s^C &= \dot{W}_s^C = 0 \quad \text{for } s \neq i. \end{aligned}$$

The necessary summation required for $\varepsilon^{M(2)C}$ is thus reduced to merely a single term and we can obtain a first-order estimate of imperfection-sensitivity without any further appeal to the computer. The leading term of the $A^M(\varepsilon^M)$ relationship for the asymmetric point of bifurcation can now be determined from the complete asymptotic equation of imperfection-sensitivity given in Chapter 8

$$A^M = A^C + \alpha(\varepsilon^M)^{\frac{1}{2}+} + \beta(\varepsilon^M) + \dots,$$

where

$$\alpha = \pm \left(\frac{2}{\varepsilon^{M(2)C}} \right)^{\frac{1}{2}+} A^{M(1)C}.$$

Here we remember that a superscript $\frac{1}{2}+$ denotes the positive square root only.

The necessary calculations for the coefficients $\varepsilon^{M(2)C}$ and α of the finite-element model were performed for the values of N from 1 to 16 as with the perfect analysis. We again find that the convergence of these approximate

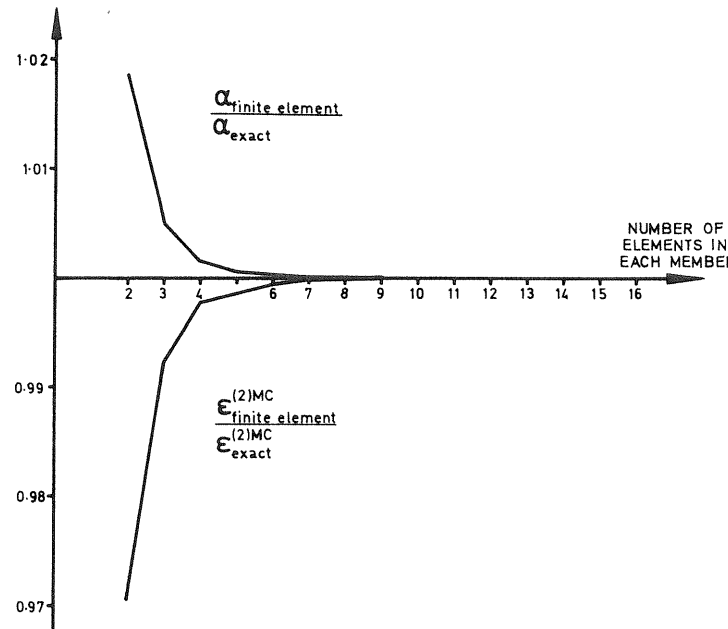


Figure 91 Convergence of the finite-element coefficients for a first-order imperfection-sensitivity analysis

results to the exact answers of Koiter¹⁷ is encouragingly good and this convergence from $N = 2$ to $N = 16$ is shown in Figure 91: the values for $N = 1$ again lie well outside the scale of these plots and so are not included since they would merely serve to obscure the subsequent convergence.

Correlation with experiments

Before a comparison between our theoretical results and the experimental data of Roorda⁶⁰ is feasible, it is necessary to recast the result for the slope of the post-buckling path in terms of the natural deformation parameter of experiment—the angle of rotation of the rigid joint θ . Thus writing

$$P(\theta) = P[Q_{2N}(\theta)],$$

we obtain by differentiation

$$\frac{dP}{d\theta} = \frac{dP}{dQ_{2N}} \cdot \frac{dQ_{2N}}{d\theta}.$$

Now we know that $Q_{2N} = \sin \theta$ so evaluating at the critical point C we obtain

$$\left. \frac{dP}{d\theta} \right|_C = \left. \frac{dP}{dQ_{2N}} \right|_C,$$

and the slope of the post-buckling path obtained by analysis can be used in a direct comparison with experiment.

The results of Roorda's experiments together with our theoretical predictions of the first-order post-buckling and imperfection-sensitivity analyses are shown in Figure 92. The left-hand diagram compares the predicted post-buckling path of the perfect system with two sets of experimental data

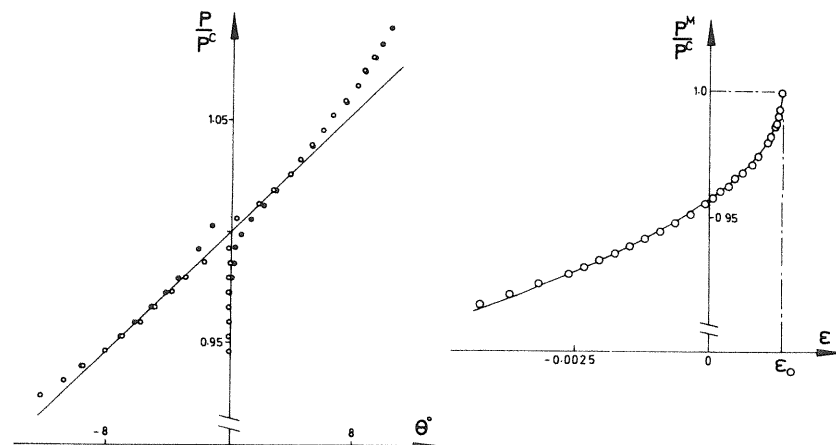


Figure 92 Comparison between the present theory and the experiments of Roorda

corresponding to the smallest effective values of positive and negative eccentricity of applied load which the apparatus would allow; here the closed circles represent equilibrium states for the smallest possible positive value of effective ϵ and the open circles represent equilibrium states for the smallest possible negative value of effective ϵ . The straight line is the theoretical prediction for the post-buckling path and we can see from the diagram that agreement between theory and experiment is most satisfactory.

The right-hand diagram of Figure 92 compares the experimental and theoretical evidence of imperfection-sensitivity; the open circles represent experimental points and the continuous line denotes the curve predicted by the first-order imperfection analysis. Small geometric irregularities are of course unavoidable in any real structural system and we find that the particular frame used in Roorda's experiments required a small positive eccentricity $\epsilon_0 l$ to

nullify the effect of these imperfections. Adjusting our theoretical curve accordingly, we find that experiment and theory are again in remarkable agreement.

As we have seen, the finite-element model represents a good approximation to this continuum at least where a first-order post-buckling and imperfection-sensitivity analysis is concerned; in fact the results lie within three percent of the exact values for as few as two elements per member. It is interesting to note that we have obtained the necessary cubic terms without having to evaluate coefficients of order higher than quadratic (the order of terms required by a linear eigenvalue analysis). It is felt that a similar finite-element treatment would be useful in nonlinear studies of more complex systems.

The link between the post-buckling of a perfect system and the imperfection-sensitivity of associated imperfect systems is clearly demonstrated in this illustration of the W -analysis; the interrelationships between perfect and imperfect studies are extensive enough so as to render the latter trivial to a first order.

Finally we note that an interesting study of the buckling response of frames, including the derivation of a nonlinear virtual-work equation, has been made recently by Brown.²⁰⁰

10

COINCIDENT BRANCHING POINTS

10.1 Introduction

After looking at the distinct critical points in some depth, our attention now falls on the somewhat more complex situation which arises when two or more such points coincide. Here we shall apply our perturbation procedures to m coincident branching points, giving rise to a single m -fold compound branching point, but this treatment differs from earlier work in the early elimination of passive coordinates; it is felt that this elimination offers significant theoretical and analytical advantages. The general theory of this chapter is fully illustrated in the next by an analysis of the simultaneous rotationally-symmetric branching behaviour of a complete spherical shell under external pressure.

The process of elimination of passive coordinates is performed by a perturbation analysis on $n - m$ of the governing equilibrium equations, thereby reducing the number of degrees of freedom of the problem to m . The work of Dong and Wolf²⁰¹ on the stability analysis of structures by a reduced system of generalized coordinates may be relevant here. Such a procedure can of course be applied to the analysis of a *distinct* branching point simply by setting $m = 1$, and a worthwhile alternative approach to the branching studies of Chapter 6 is thus provided; it is felt that, although the two methods overlap to the extent of generating identical equations, the difference in conceptual approach can give to this new procedure a very real value.¹²⁷

Having generated a new potential energy function with just m degrees of freedom, it is first essential to show that the normal equilibrium and stability conditions hold over the transformation. This having been done we can then operate exclusively in terms of the new function and seek to generate a perturbation scheme for the post-buckling path derivatives of the system. For a compound branching point, however, we do not obtain a sequence of linear problems; in fact the first non-trivial perturbation equations are a set of m simultaneous quadratics. These of course generate a number of possible post-buckling solutions and we find from the theorem of Bezout that the maximum possible number is $2^m - 1$. We also find that this perturbation approach differs slightly from our earlier schemes, in that the perturbation parameter must remain free, and cannot be specified at an early stage in the

analysis. This generates solution rays in a rate space but these will then become the post-buckling path tangents when mapped directly into load-coordinate space.

Following the pattern laid down in some of the earlier work, we first write the theory in terms of the diagonalized A -function in order to develop a degree of insight into the phenomena which are involved; a particular diagonalizing transformation which passes smoothly through a compound branching point is presented as an illustrative example. The general perturbation equations are examined in some detail for the case of two coincident branching points ($m = 2$) and the nonlinear coupling action between the active principal coordinates is demonstrated. The important special case in which the total potential energy function is symmetric (even) in one of the active coordinates is considered and explicit solutions are presented; these are directly employed in Chapter 11 in the analysis of the spherical shell.

Finally we present the general W -analysis for compound branching. This of course has the advantage of not resorting to a diagonalization scheme and thus is better suited to numerical analysis. It is felt that this theory could also be useful in problems involving not simultaneous, but *near-simultaneous* branching points, which often exhibit violent path contortions unsuited to direct perturbation methods. These contortions disappear with the coalescence of critical points, so it may well be worth artificially enforcing simultaneity by some 'fudge' of the analysis or by considering a slightly different problem to that originally posed.

10.2 Analysis with diagonalization

We start the analysis with the transformed energy function

$$A(u_i, \Lambda) \equiv V[Q_i^c(\Lambda) + \alpha_{ij}(\Lambda) u_j, \Lambda],$$

with the properties arising from its derivation

$$\begin{aligned} A_i(0, \Lambda) &= A'_i(0, \Lambda) = A''_i(0, \Lambda) = \dots = 0, \\ A_{ij}(0, \Lambda) &= A'_{ij}(0, \Lambda) = A''_{ij}(0, \Lambda) = \dots = 0 \quad \text{for } i \neq j. \end{aligned}$$

The energy function being diagonalized, the derivatives $A_{ii}(0, \Lambda)$ are a set of n stability coefficients, and we now deviate from the earlier work focusing attention on m *coincident* branching points which together constitute a *compound* branching point C lying on the fundamental path; here m stability coefficients are simultaneously zero. We therefore have m principal coordinates which are associated with the vanishing stability coefficients and we refer to these as the *active* coordinates, adopting Latin subscripts for their use. The $n - m$ principal coordinates which are associated with the non-vanishing stability coefficients will be referred to as the *passive* coordinates and we adopt

Greek subscripts for their use. We shall suppose that this is the *first* critical point of the system and consider the fundamental path in a region close to this point in which no other critical points are present. Thus we can write

$$\begin{aligned} A_{ii}^C &= A_{ii}(0, \Lambda^C) = 0, \\ A_{\alpha\alpha}^C &= A_{\alpha\alpha}(0, \Lambda^C) \neq 0, \end{aligned}$$

where Λ^C is the critical value of Λ . Also

$$A_{\alpha\alpha}^F = A_{\alpha\alpha}(0, \Lambda) > 0$$

in the region of interest. We note that the dummy-suffix summation convention may still be employed, where summations over Latin suffices will range over the m active values and summations over Greek suffices will range over the $n - m$ passive values.

In the earlier work the general diagonalization process has been used in the region of a distinct critical point, and as evidence for its present validity we shall now show how a particular smooth diagonalizing transformation can be generated for a compound problem containing two generalized coordinates. To do this we consider the W -function in two generalized coordinates giving the quadratic form

$$\frac{1}{2}W_{ij}(\Lambda)q_i q_j = \frac{1}{2}W_{11}(\Lambda)q_1^2 + W_{12}(\Lambda)q_1 q_2 + \frac{1}{2}W_{22}(\Lambda)q_2^2,$$

which by a process of completion of a square may be written

$$\frac{1}{2}W_{ij}(\Lambda)q_i q_j = \frac{1}{2}W_{11}\left(q_1 + \frac{W_{12}}{W_{11}}q_2\right)^2 + \left(\frac{1}{2}W_{22} - \frac{W_{12}^2}{2W_{11}}\right)q_2^2.$$

We now write

$$\begin{aligned} u_1 &= q_1 + \frac{W_{12}(\Lambda)}{W_{11}(\Lambda)}q_2, \\ u_2 &= q_2, \end{aligned}$$

to obtain

$$\frac{1}{2}W_{ij}(\Lambda)q_i q_j = \frac{1}{2}A_{ii}(\Lambda)u_i^2 = \frac{1}{2}A_{11}u_1^2 + \frac{1}{2}A_{22}u_2^2,$$

where

$$A_{11} = W_{11}, \quad A_{22} = W_{22} - \frac{W_{12}^2}{W_{11}}.$$

The relationship between the two sets of axes is shown in Figure 93; the u_1 axis remains fixed in the direction of q_1 while the u_2 axis rotates with Λ .

Consider now this particular diagonalization process in the vicinity of a compound critical equilibrium state at which $W_{ij} = 0$. We must immediately

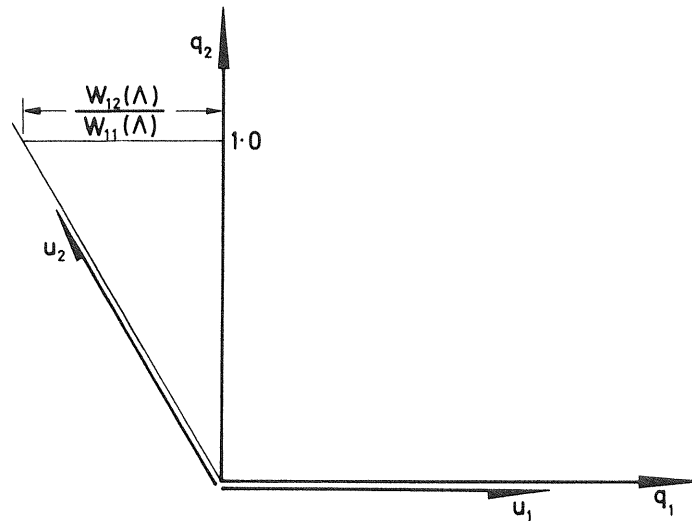


Figure 93 A particular two-degree-of-freedom example of the diagonalizing transformation $q_i = \alpha_{ij}(A) u_j$

suspect the above analysis in which we have been blindly dividing by W_{11} which is now zero when $A = A^C$. We may write the original quadratic form as

$$\frac{1}{2}W_{ij}(A)q_i q_j = \frac{1}{2}[W_{ij}^C + W_{ij}^C(A - A^C) + \frac{1}{2}W_{ij}^C(A - A^C)^2 + \dots]q_i q_j.$$

The first term is of course identically zero so we may extract $(A - A^C)$ to give

$$\frac{1}{2}W_{ij}(A)q_i q_j = \frac{1}{2}(A - A^C)[W_{ij}^C + \frac{1}{2}W_{ij}^C(A - A^C) + \dots]q_i q_j.$$

It now becomes possible to operate on the expansion within the square brackets as before. In this way we can convince ourselves that the illustrated diagonalization process works smoothly through a compound branching point.

A diagonalization scheme based on a completion of the square routine such as the above works smoothly through a single distinct branching point and, as we have seen, through a compound branching point. We would not, however, recommend that it be used for a continuous diagonalization through two distinct critical points, nearly coincident or otherwise, as there is a strong likelihood that this would generate a singularity in the transformation at some value of A .

Elimination of passive coordinates

We now seek to express the passive coordinates in a parametric form by use of $n - m$ of the governing equilibrium equations, and thence eliminate them

from the analysis. This has the effect of reducing the number of degrees of freedom to m .

The $n - m$ equilibrium equations

$$A_\alpha(u_i, u_\beta, A) = 0$$

contain $n + 1$ unknowns and so the problem may be reduced to contain $m + 1$ independent variables. This enables us to write the passive coordinates in the parametric form

$$u_\beta = u_\beta(u_i, A)$$

and we seek to find partial derivatives with respect to the independent variables which will enable us to employ systematic Taylor series expansions of these coordinates. Anticipating this representation we may substitute the parametric forms into the equilibrium equations $A_\alpha = 0$ to give the identity

$$A_\alpha[u_i, u_\beta(u_i, A), A] \equiv 0.$$

The left-hand side is now a function of the $m + 1$ independent variables u_i and A , so we may differentiate with respect to these variables as many times as we please. Thus, differentiating repeatedly, we can generate the ordered equilibrium equations

$$\frac{\partial}{\partial u_i} A_\alpha = A_{\alpha i} + A_{\alpha\beta} u_{\beta i} = 0,$$

$$\frac{\partial}{\partial A} A_\alpha = A_{\alpha\beta} u'_\beta + A'_\alpha = 0,$$

$$\frac{\partial^2}{\partial u_i \partial u_j} A_\alpha = A_{\alpha ij} + A_{\alpha\beta i} u_{\beta j} + A_{\alpha\beta j} u_{\beta i} + A_{\alpha\gamma i} u_{\beta j} u_{\gamma j} + A_{\alpha\beta i} u_{\beta j} = 0,$$

$$\frac{\partial^2}{\partial u_i \partial A} A_\alpha = A_{\alpha\beta i} u'_\beta + A'_{\alpha i} + A_{\alpha\gamma i} u_{\beta i} u'_\gamma + A'_{\alpha\beta i} u_{\beta i} + A_{\alpha\beta i} u'_{\beta i} = 0,$$

$$\frac{\partial^2}{\partial A^2} A_\alpha = A_{\alpha\beta i} u'_\beta u'_i + 2A'_{\alpha\beta i} u'_\beta + A_{\alpha\beta i} u''_\beta + A''_\alpha = 0,$$

etc. Here a subscript again denotes partial differentiation with respect to the corresponding generalized coordinate and a prime denotes partial differentiation with respect to A so

$$u_{\beta i} \equiv \frac{\partial u_\beta}{\partial u_i}, \quad u'_\beta \equiv \frac{\partial u_\beta}{\partial A},$$

$$u_{\beta ij} \equiv \frac{\partial^2 u_\beta}{\partial u_i \partial u_j}, \quad u'_{\beta i} \equiv \frac{\partial^2 u_\beta}{\partial u_i \partial A},$$

etc. We may evaluate these equations on the fundamental path F in the region of the critical point, where we know

$$\begin{aligned} A_i^F &= A'_i^F = A''_i^F = \cdots = 0, \\ A_\alpha^F &= A'_\alpha^F = A''_\alpha^F = \cdots = 0, \\ A_{ij}^F &= A'_{ij}^F = A''_{ij}^F = \cdots = 0 \quad \text{for } i \neq j, \\ A_{\alpha\beta}^F &= A'_{\alpha\beta}^F = A''_{\alpha\beta}^F = \cdots = 0 \quad \text{for } \alpha \neq \beta, \\ A_{\alpha i}^F &= A'_{\alpha i}^F = A''_{\alpha i}^F = \cdots = 0. \end{aligned}$$

This leads to a systematic evaluation of the required derivatives,

$$\begin{aligned} u_{\alpha i}^F &= u'_\alpha^F = 0, \\ u_{\alpha i j}^F &= -\left. \frac{A_{\alpha i j}}{A_{\alpha \alpha}} \right|_F, \\ u''_{\alpha i}^F &= u''_\alpha^F = 0, \end{aligned}$$

etc. We note that the denominator in all cases is $A_{\alpha \alpha}^F$ which is non-zero in the region of interest; we therefore generate no infinite derivatives and the scheme is justified.

We now state some general results concerning the evaluated derivatives. These emerge from the inductive reasoning which is fully presented in Appendix II and they may be written

$$\begin{aligned} u_\alpha^F &= u''_\alpha^F = u'''_\alpha^F = \cdots = 0 \\ u_{\alpha i}^F &= u'_{\alpha i}^F = u''_{\alpha i}^F = \cdots = 0. \end{aligned}$$

The process which has been presented above constitutes a valid perturbation scheme and with the series expansions of $u_\alpha(u_i, \Lambda)$ in terms of the known u_α derivatives, leads to a new energy function with m degrees of freedom defined by

$$\mathcal{A}(u_i, \Lambda) \equiv A[u_i, u_\alpha(u_i, \Lambda), \Lambda].$$

The derivatives of this new energy function may be obtained in terms of the known derivatives by direct differentiation,

$$\begin{aligned} \mathcal{A}_i &= A_i + A_\alpha u_{\alpha i}, \\ \mathcal{A}' &= A_\alpha u'_\alpha + A', \\ \mathcal{A}_{ij} &= A_{ij} + A_{\alpha i} u_{\alpha j} + A_{\alpha j} u_{\alpha i} + A_{\alpha\beta} u_{\alpha i} u_{\beta j} + A_\alpha u_{\alpha i j}, \\ \mathcal{A}'_i &= A_{\alpha i} u'_\alpha + A'_i + A_{\alpha\beta} u_{\alpha i} u'_\beta + A'_\alpha u_{\alpha i} + A_\alpha u'_{\alpha i}, \\ \mathcal{A}'_{ij} &= A_{\alpha i j} u'_\alpha + A'_{ij} + A_{\alpha\beta i} u_{\alpha j} u'_\beta + A'_{\alpha i} u_{\alpha j} + A_{\alpha i} u'_{\alpha j} + A_{\alpha\beta j} u_{\alpha i} u'_\beta + A'_{\alpha j} u_{\alpha i} \\ &\quad + A_{\alpha j} u'_{\alpha i} + A_{\alpha\beta j} u_{\alpha i} u_{\beta j} + A'_{\alpha\beta} u_{\alpha i} u_{\beta j} + A_{\alpha\beta} u'_{\alpha i} u_{\beta j} + A_{\alpha\beta} u_{\alpha i} u'_{\beta j} + A_{\alpha\beta} u_{\alpha i j} u'_\beta, \\ \mathcal{A}_{ijk} &= A_{ijk} + A_{\alpha i j} u_{\alpha k} + A_{\alpha i k} u_{\alpha j} + A_{\alpha\beta i} u_{\alpha j} u_{\beta k} + A_{\alpha i} u_{\alpha j k} + A_{\alpha i} u_{\alpha k j} \\ &\quad + A_{\alpha\beta j} u_{\alpha i} u_{\beta k} + A_{\alpha j} u_{\alpha i k} + A_{\alpha\beta k} u_{\alpha i} u_{\beta j} + A_{\alpha\beta} u_{\alpha i} u_{\beta j} u_{\beta k} + A_{\alpha\beta} u_{\alpha i} u_{\alpha k} u_{\beta j}, \\ &\quad + A_{\alpha\beta} u_{\alpha i} u_{\beta j k} + A_{\alpha k} u_{\alpha i j} + A_{\alpha\beta} u_{\alpha i j} u_{\beta k} + A_\alpha u_{\alpha i j k}. \end{aligned}$$

etc. The evaluation of these \mathcal{A} -derivatives on the fundamental path in the region of the critical point leads to

$$\begin{aligned} \mathcal{A}_i^F &= 0, \\ \mathcal{A}'^F &= A'^F, \\ \mathcal{A}_{ij}^F &= A_{ij}^F = 0 \quad \text{for } i \neq j, \\ \mathcal{A}_{ii}^F &= A_{ii}^F, \\ \mathcal{A}'_i^F &= 0, \\ \mathcal{A}'_{ij}^F &= A'_{ij}^F = 0 \quad \text{for } i \neq j, \\ \mathcal{A}_{ii}^F &= A_{ii}^F, \\ \mathcal{A}_{ijk}^F &= A_{ijk}^F, \end{aligned} \tag{10.1}$$

etc.

We now refer to further general results obtained from the induction procedures of Appendix II. One of these, given by equation (A.1), can be seen to represent the preservation of a familiar condition associated with the use of a set of incremental coordinates. In a more recognizable form it may be stated

$$\mathcal{A}_i^F = \mathcal{A}'_i^F = \mathcal{A}''_i^F = \cdots = 0.$$

This same result may alternatively be obtained as follows. We see from the above analysis that $\mathcal{A}_i^F = 0$ everywhere on the fundamental path in the region of interest. Considering this region in $\Lambda-u_i$ space, the fundamental path is synonymous with the Λ -axis, and therefore \mathcal{A}_i is zero everywhere along the Λ -axis. We may therefore conclude that all the derivatives of \mathcal{A}_i with respect to Λ are zero on this axis, since a Taylor expansion along the Λ -axis must result in \mathcal{A}_i being zero everywhere.

For the final general result we draw on equation (A.2) of Appendix II. This result may be interpreted in a more normal way

$$\begin{aligned} \mathcal{A}_{ij}^F &= \mathcal{A}'_{ij}^F = \mathcal{A}''_{ij}^F = \cdots = 0 \quad \text{for } i \neq j, \\ \mathcal{A}_{ii}^F &= A_{ii}^F, \\ \mathcal{A}'_{ii}^F &= A'_{ii}^F, \\ \mathcal{A}''_{ii}^F &= A''_{ii}^F, \end{aligned}$$

etc., and we see that it includes the important conclusion that the diagonalization condition is fully preserved over the transformation. Again this result may be alternatively obtained as follows. We have seen in the above analysis that $\mathcal{A}_{ij} = A_{ij}$ everywhere on the fundamental path in the region of interest. Considering this region in $\Lambda-u_i$ space, the fundamental path is synonymous with the Λ -axis, and therefore $\mathcal{A}_{ij} = A_{ij}$ everywhere along the Λ -axis. We may therefore conclude that all the derivatives of \mathcal{A}_{ij} with respect to Λ must

equal their corresponding derivatives of A_{ij} with respect to Λ since a Taylor series expansion along the Λ -axis must result in \mathcal{A}_{ij} being equal to A_{ij} everywhere.

Preservation of equilibrium and stability conditions

Before we can proceed with our general treatment it is necessary to show that the normal equilibrium and stability conditions are fully preserved over the transformation from $A(u_i, u_\alpha, \Lambda)$ to $\mathcal{A}(u_i, \Lambda)$.

The question of the equilibrium condition can be simply resolved analytically as follows. The necessary and sufficient condition for equilibrium is that both $A_i = 0$ and $A_\alpha = 0$. The transformation process makes use of the $n - m$ equilibrium equations $A_\alpha = 0$, so we are left after transformation with the necessary and sufficient condition for equilibrium as $A_i = 0$. Now we know from the elimination of passive coordinates that

$$\mathcal{A}_i = A_i + A_\alpha u_{\alpha i},$$

and we note that the second term of the right-hand side vanishes—before evaluation on the fundamental path—by virtue of the equations $A_\alpha = 0$. This then leaves $\mathcal{A}_i = A_i$ and we may conclude that the necessary and sufficient condition for equilibrium is $\mathcal{A}_i = 0$. This constitutes a full preservation of the normal equilibrium condition.

It is the nature of the stability condition that no complete analytical proof readily suggests itself. However, it is possible to show analytically that the condition is preserved for non-critical positions of equilibrium on the fundamental path and so this is the natural first step towards a more general proof. We remember from Chapter 6 that if the A_{ii}^F and $A_{\alpha\alpha}^F$ are all greater than zero then the fundamental path is thoroughly stable. Now we know that in the region of the critical point $A_{\alpha\alpha}^F > 0$ and so the necessary and sufficient condition for stability at non-critical positions on the fundamental path is now $A_{ii}^F > 0$. However, from the elimination of passive coordinates we have seen that $\mathcal{A}_{ii}^F = A_{ii}^F$ with all non-diagonal terms vanishing and so we may conclude that the necessary and sufficient condition for thorough stability of the fundamental path is $\mathcal{A}_{ii}^F > 0$.

We believe the stability condition to be *fully* preserved in general on the basis of the following heuristic reasoning, although we feel that a rigorous analytical proof would be extremely difficult to obtain.

Let us consider the behaviour of a system in the neighbourhood of a compound critical point, the point itself being stable with respect to the non-critical (passive) principal coordinates u_α so that A is a minimum with respect to these coordinates. The expansions $u_\alpha(u_i, \Lambda)$ which generate the \mathcal{A} -function lead to the concept of a ‘hypersurface of activity’ in the $n + 1$ -dimensional

$u_i - u_\alpha - \Lambda$ space, each point on the surface being uniquely defined by specifying the values of the active coordinates u_i and the loading parameter Λ ; the \mathcal{A} -function itself supplies the energy level on this surface. All equilibrium paths will lie on the hypersurface since a necessary although not sufficient condition for equilibrium is that the potential energy should be stationary with respect to the passive coordinates. An example of a hypersurface of activity is the ‘curved surface’ of Hunt,¹²⁷ which is generated for a distinct critical point and hence can be pictured in a three-dimensional space with u_1 (active), u_s (passive) and Λ as the axes.

It should be noted that although the concept of a hypersurface of activity is a powerful one, the surface itself is not independent of the choice of diagonalizing transformation. Had we chosen a different diagonalizing transformation with a different set of principal coordinates we would not obtain the same hypersurface of activity.

To illustrate the ensuing argument it is of course desirable to draw some pictures, but having only three visual dimensions available any such figures will be of necessity highly schematic. Fortunately, however, the loading parameter Λ is held fixed throughout the discussion and so need not be considered, while it is quite easy to visualize the total potential energy as a scalar variable with appropriate contour surfaces. We are left with the n coordinates u_i and u_α and can thus either designate two axes to the active coordinates u_i or two axes to the passive coordinates u_α . To obtain the maximum visual aid we shall choose to follow both of these alternatives and the present arguments are thus illustrated schematically in Figures 94 and 95. In Figure 94 only one axis is assigned to the active coordinates u_i , while in Figure 95 only one axis is assigned to the passive coordinates u_α .

Let us now consider the system at a fixed Λ level (not necessarily at the critical load Λ^C) and as a preliminary manoeuvre fix the values of the active coordinates u_i . The total potential energy A is now a function of the passive coordinates only, and it is clear from continuity that in the immediate neighbourhood of the compound critical point this function $A(u_\alpha)$ must yield a *minimum* on the activity hypersurface. This condition holds for any set of assigned values of the active coordinates u_i , as shown schematically in Figure 94.

We consider now an equilibrium state E , on the hypersurface but not necessarily on the fundamental path, and to examine its stability we must study the change of potential energy along all coordinate paths (not equilibrium paths) leading out of this state. Some of these paths will lie in the hypersurface $A_\alpha = 0$ and some will not, and it is our intention to show that for an examination of stability it is only necessary to consider those paths that lie in the activity surface. That is to say it is only necessary to examine the form of the new energy function $\mathcal{A}(u_\alpha)$.

We observe first that if a path in the surface yields a falling total potential energy then the equilibrium state is certainly unstable; thus if \mathcal{A} is not a mini-

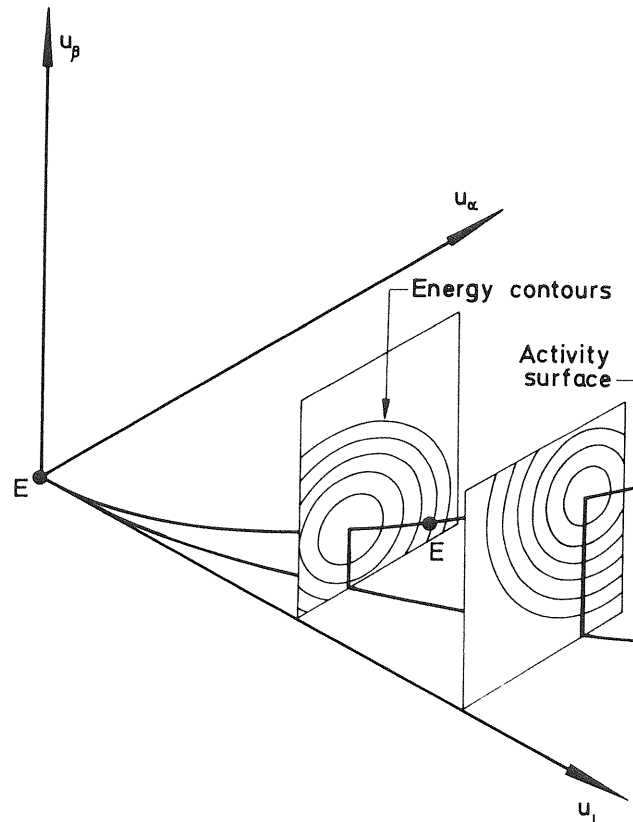


Figure 94 A schematic view of coordinate space showing one active and two passive coordinates

mum we certainly have instability. Let us suppose secondly that all paths in the surface yield a rising total potential energy. In this case any path deviating from the surface will certainly rise since points on the surface represent minima with respect to the passive coordinates. This point can be followed carefully in Figure 95 in which a trial path from E must penetrate the drawn cylinder, the most crucial height for such a penetration being that of the activity surface; here we have assumed that the active coordinates participate in any significant trial and so trial paths which are orthogonal to the active coordinates need not be considered. It follows that the equilibrium state is now stable so that a minimum of \mathcal{A} is seen to imply stability.

We see that we have now achieved our objective of showing that a minimum of \mathcal{A} with respect to the active coordinates is both necessary and sufficient for

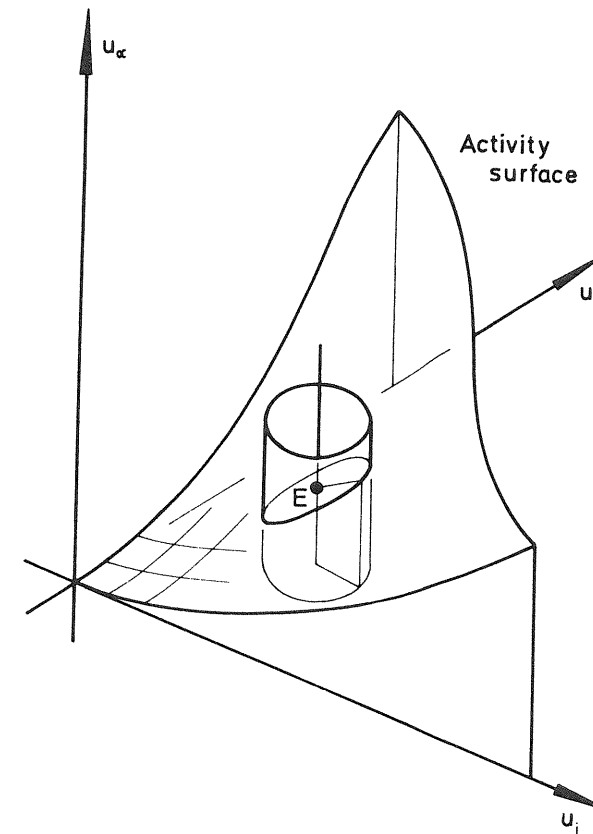


Figure 95 A schematic view of coordinate space showing two active and one passive coordinate

the stability of an equilibrium state in the vicinity of our compound critical point. In other words, the normal stability condition is preserved over the elimination of passive coordinates.

Perturbation equations and the theorem of Bezout

It is now possible to continue with our general theory. We seek to express any post-buckling equilibrium paths which emerge from the compound critical equilibrium state in the parametric form

$$u_j = u_j(s), \quad \Lambda = \Lambda(s),$$

in which s is an unspecified but suitable expansion parameter.

These parametric equations can now be substituted into the equilibrium equations $\mathcal{A}_i = 0$ to give the identity

$$\mathcal{A}_i[u_j(s), \Lambda(s)] \equiv 0.$$

Here the left-hand side is simply a function of the independent parameter s so we can differentiate these equations with respect to s as many times as we please. Thus, differentiating repeatedly, we generate the ordered equilibrium equations

$$\mathcal{A}_{ij} \dot{u}_j + \mathcal{A}'_i \dot{\Lambda} = 0,$$

$$\mathcal{A}_{ijk} \ddot{u}_j \dot{u}_k + 2\mathcal{A}'_{ij} \dot{u}_j \dot{\Lambda} + \mathcal{A}_{ij} \ddot{u}_j + \mathcal{A}''_i \dot{\Lambda}^2 + \mathcal{A}'_i \ddot{\Lambda} = 0,$$

etc., in which a dot denotes differentiation with respect to s . Evaluating these ordered equilibrium equations at the critical point $u_i = 0$, $\Lambda = \Lambda^c$ and remembering the earlier derived properties of the \mathcal{A} -function, we see that the first equation gives no information while the second equation takes the form

$$\mathcal{A}_{ijk} \ddot{u}_j \dot{u}_k + 2\mathcal{A}'_{ii} \dot{u}_i \dot{\Lambda}|^c = 0, \quad \text{no summation over } i.$$

These equations constitute m simultaneous quadratics in $m+1$ unknowns and therefore contain a number of possible solution rays. They may be regarded as homogeneous equations but are obviously non-general. Thus the coefficient of $\dot{u}_i \dot{u}_j$ in the k th equation equals the coefficient of $\dot{u}_j \dot{u}_k$ in the i th equation, which in turn equals the coefficient of $\dot{u}_k \dot{u}_i$ in the j th equation, and we note in particular the absence of all $\dot{\Lambda}^2$ terms. However, applying Bezout's theorem¹⁸⁷ to this non-general set of homogeneous equations, we see we may generate a maximum number of 2^m solution rays in the $\dot{\Lambda}-\dot{u}_i$ rate space; the significance of this particular coordinate space will be discussed at a later stage. Now one of these rays will correspond to the fundamental path ($\dot{u}_i = 0$) and so the maximum number of possible post-buckling solutions is $2^m - 1$.

These equations require delicate handling. For instance we might be tempted to eliminate $\dot{\Lambda}$ between pairs of equations thereby producing a non-general homogeneous set of $m-1$ cubic equations in m unknowns. The straightforward application of Bezout's theorem to this new set of equations gives the maximum number of possible solution rays as 3^{m-1} ; which we note is greater than 2^m for $m > 2$. Further examination of this process, however, reveals the possibility of the inclusion of a number of spurious solutions and so this approach, which at first glance seems reasonable, is invalidated.

We have discussed the number of solutions produced by the set of simultaneous quadratics, but have not yet said anything about the significance of these solutions. The perturbation parameter s has remained undefined throughout the analysis, and as a result we have generated possible solution rays in the 'rate space' $\dot{\Lambda}-\dot{u}_i$. These solution rays will be of the form

$$\dot{u}_i = k_i \dot{u}_1,$$

$$\dot{\Lambda} = k \dot{u}_1,$$

and these lead to the relevant relationships in $\Lambda-u_i$ space,

$$\frac{\partial u_i}{\partial u_1} = k_i,$$

$$\frac{\partial \Lambda}{\partial u_1} = k.$$

We may conclude that the solution rays in rate space, which are produced by solution of the perturbation equations *keeping the perturbation parameter free*, become the path tangents when mapped directly into coordinate space. This process is conceptually different from our earlier perturbation solutions for distinct critical points, where the perturbation parameter was for convenience fixed at an early stage in the analysis and we solved directly for the path tangents; we remember that there was a unique path tangent in this earlier case so the perturbation parameter did not need to be kept free providing it contained a component in the direction of the post-buckling path.

Some particular solutions

The first relevant perturbation equations for two coincident critical points ($m = 2$), which we shall assume for ease of formulation to be associated with the u_1 and u_2 principal coordinates, may be written in full as

$$\begin{aligned} \mathcal{A}_{111} \dot{u}_1^2 + 2\mathcal{A}_{112} \dot{u}_1 \dot{u}_2 + \mathcal{A}_{122} \dot{u}_2^2 + 2\mathcal{A}'_{11} \dot{u}_1 \dot{\Lambda}|^c &= 0, \\ \mathcal{A}_{112} \dot{u}_1^2 + 2\mathcal{A}_{122} \dot{u}_1 \dot{u}_2 + \mathcal{A}_{222} \dot{u}_2^2 + 2\mathcal{A}'_{22} \dot{u}_2 \dot{\Lambda}|^c &= 0, \end{aligned}$$

and we are looking for particular solutions to these equations in interesting special cases (for instance when one or more of the coefficients vanish). We shall not, however, consider the complex and rare case in which either or both of the coefficients \mathcal{A}'_{11}^c and \mathcal{A}'_{22}^c vanish.

First let us consider the case when $\mathcal{A}_{222}^c = 0$. We see it is possible to extract \dot{u}_1/\dot{u}_2 as a factor from one of the equations to obtain

$$\frac{\dot{u}_1}{\dot{u}_2} \left[\mathcal{A}_{111} \frac{\dot{u}_1}{\dot{u}_2} + 2\mathcal{A}_{112} + 2\mathcal{A}'_{11} \frac{\dot{\Lambda}}{\dot{u}_2} \right]^c = 0,$$

$$\mathcal{A}_{112} \left(\frac{\dot{u}_1}{\dot{u}_2} \right)^2 + \mathcal{A}_{222} + 2\mathcal{A}'_{22} \frac{\dot{\Lambda}}{\dot{u}_2} \Big|^c = 0,$$

and one of the three possible solution rays is given by

$$\frac{\dot{u}_1}{\dot{u}_2} \Big|^c = 0, \quad \frac{\dot{\Lambda}}{\dot{u}_2} \Big|^c = -\frac{\mathcal{A}_{222}}{2\mathcal{A}'_{22}} \Big|^c.$$

This is the solution we should obtain from an analysis in the u_2 mode assuming the critical point to be distinct; it is obtained if, and only if, the coefficient \mathcal{A}_{122}^C is zero. The other two solutions may or may not exist, but if they do they give rise to complicated expressions which are not presented explicitly here. It is, however, possible to obtain a second solution coincident with the first under the further condition

$$2\mathcal{A}_{112}^C \mathcal{A}_{22}^C = \mathcal{A}_{222}^C \mathcal{A}_{11}^C,$$

in which case we may write the third solution ray explicitly as

$$\left| \frac{\dot{u}_1}{\dot{u}_2} \right|^C = \left| \frac{\mathcal{A}_{111} \mathcal{A}'_{22}}{\mathcal{A}_{112} \mathcal{A}'_{11}} \right|^C, \quad \left| \frac{\dot{A}}{\dot{u}_2} \right|^C = - \left| \frac{(\mathcal{A}_{111})^2 \mathcal{A}'_{22} + 2(\mathcal{A}_{112})^2 \mathcal{A}'_{11}}{2(\mathcal{A}'_{11})^2 \mathcal{A}_{112}} \right|^C.$$

We now have considered all interesting special cases in which only one coefficient vanishes. If the coefficient \mathcal{A}_{112}^C is zero we of course draw the same conclusions with the roles of the modes reversed and if either \mathcal{A}_{111}^C or \mathcal{A}_{222}^C is zero it is not possible to extract any simple solutions from the equations.

We now consider some special cases in which two of the coefficients vanish. First let us look at the situation when both \mathcal{A}_{112}^C and \mathcal{A}_{222}^C are equal to zero. As can be seen above, we may extract \dot{u}_1/\dot{u}_2 as a factor from one equation, and \dot{u}_2/\dot{u}_1 as a factor from the other equation leaving the three solution rays

$$\begin{aligned} 1 \quad & \left| \frac{\dot{u}_1}{\dot{u}_2} \right|^C = 0, \quad \left| \frac{\dot{A}}{\dot{u}_2} \right|^C = - \left| \frac{\mathcal{A}_{222}}{2\mathcal{A}'_{22}} \right|^C, \\ 2 \quad & \left| \frac{\dot{u}_2}{\dot{u}_1} \right|^C = 0, \quad \left| \frac{\dot{A}}{\dot{u}_1} \right|^C = - \left| \frac{\mathcal{A}_{111}}{2\mathcal{A}'_{11}} \right|^C, \\ 3 \quad & \left| \frac{\dot{u}_1}{\dot{u}_2} \right|^C = \left| \frac{\mathcal{A}_{222} \mathcal{A}'_{11}}{\mathcal{A}_{111} \mathcal{A}'_{22}} \right|^C, \quad \left| \frac{\dot{A}}{\dot{u}_1} \right|^C = - \left| \frac{\mathcal{A}_{111}}{2\mathcal{A}'_{11}} \right|^C, \quad \left| \frac{\dot{A}}{\dot{u}_2} \right|^C = - \left| \frac{\mathcal{A}_{222}}{2\mathcal{A}'_{22}} \right|^C. \end{aligned}$$

These three solutions are pictured in rate space in Figure 96. As might be expected we have the two solutions which are in one mode alone—the solutions which would naively be produced by two separate analyses assuming distinct critical points—but these are combined in a third solution which we can see results from the simultaneous occurrence of the other two.

The second special case in which two coefficients vanish is to be found under conditions of symmetry in one mode. Consider a system which is symmetric in the u_1 mode; by this we mean that the potential energy function carries the same value for $-u_1$ as for $+u_1$ and hence the coefficients \mathcal{A}_{111}^C and \mathcal{A}_{122}^C are zero since these are coefficients of odd powers of u_1 in the potential energy expression. We note that physical systems commonly display this type of symmetry and indeed the simultaneous rotationally-symmetric buckling of a complete

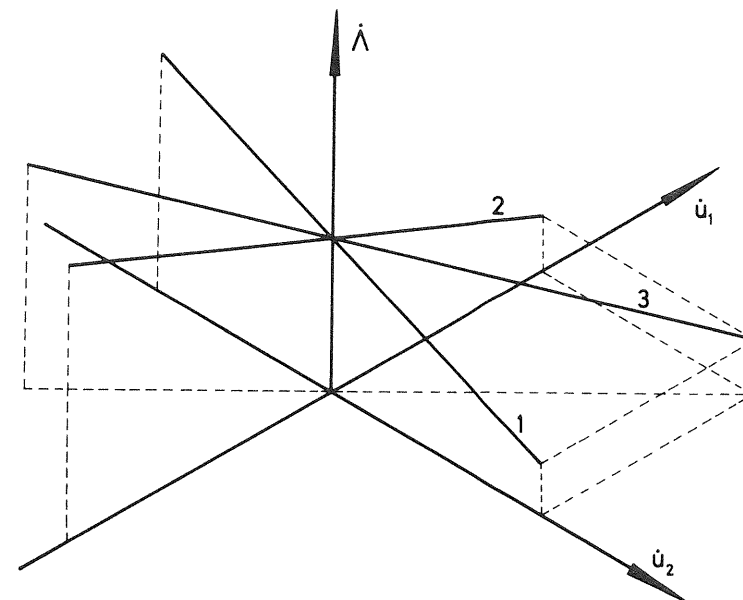


Figure 96 Possible post-buckling paths for a 2-fold compound critical point with the coefficients \mathcal{A}_{112}^C and \mathcal{A}_{222}^C equal to zero

spherical shell falls into this category as we shall see in Chapter 11. We first obtain our expected solution in the u_2 direction

$$1 \quad \left| \frac{\dot{u}_1}{\dot{u}_2} \right|^C = 0, \quad \left| \frac{\dot{A}}{\dot{u}_2} \right|^C = - \left| \frac{\mathcal{A}_{222}}{2\mathcal{A}'_{22}} \right|^C,$$

and we also obtain two other possible solutions which can now be written explicitly as

$$2, 3 \quad \left| \frac{\dot{u}_1}{\dot{u}_2} \right|^C = \pm \sqrt{\left(\frac{2\mathcal{A}'_{22}}{\mathcal{A}'_{11}} - \frac{\mathcal{A}_{222}}{\mathcal{A}_{112}} \right)}, \quad \left| \frac{\dot{A}}{\dot{u}_2} \right|^C = - \left| \frac{\mathcal{A}_{112}}{\mathcal{A}'_{11}} \right|^C.$$

This post-buckling behaviour is shown in rate space in Figure 97. The first solution lies in the u_2 direction and the other two, if they exist, lie symmetrically opposed about the u_2 -axis. Under the further condition $2\mathcal{A}_{112}^C \mathcal{A}_{22}^C = \mathcal{A}_{222}^C \mathcal{A}_{11}^C$ introduced earlier the second and third solutions have approached the first solution until they all lie coincidentally in the u_2 mode.

These then are some particular cases which may be of interest. It is possible to give further specific cases, but it was felt that the above examples illustrate all the interesting phenomena. The only other situation of obvious importance

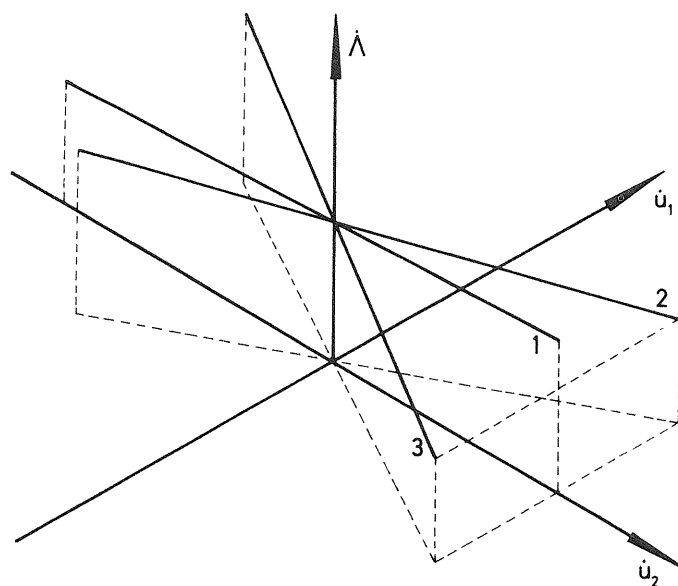


Figure 97 Possible post-buckling paths for a 2-fold compound critical point with a potential energy function which is symmetric in u_1 ($\mathcal{A}_{111}^C = \mathcal{A}_{122}^C = 0$)

is the system which is symmetrical in two modes at once. Unfortunately the analysis of this problem is out of the scope of the present work since it generates a case in which all the cubic coefficients vanish and we are obliged to consider higher-order equations.

Critical state stability analysis

Koiter⁵⁻²² has stressed the significance of the stability of the critical state itself and with this in mind we shall now investigate the stability of our compound branching point. We adopt our \mathcal{A} -function for the analysis since we have seen the normal stability condition to be preserved over the transformation to \mathcal{A} in the region of, and indeed at, the critical point.

As in the earlier work we keep A fixed at the value A^C and examine the variation of \mathcal{A} along all coordinate paths leading from the equilibrium state. To do this we write a general path from the equilibrium state in the parametric form

$$u_i = u_i(s),$$

where as before s is some suitable parameter, vanishing at C , which we need not specify.

The variation of \mathcal{A} along this path is then given by the identity

$$\mathcal{A}(s) \equiv \mathcal{A}[u_i(s), A^C],$$

and we expand this variation as a function of s as follows

$$\mathcal{A}(s) = \dot{\mathcal{A}}^C s + \frac{1}{2} \ddot{\mathcal{A}}^C s^2 + \frac{1}{6} \dddot{\mathcal{A}}^C s^3 + \dots,$$

where a dot, as before, denotes differentiation with respect to s . We may now differentiate the identity with respect to s as many times as we please, to obtain

$$\begin{aligned}\dot{\mathcal{A}} &= \mathcal{A}_i \dot{u}_i, \\ \ddot{\mathcal{A}} &= \mathcal{A}_{ij} \dot{u}_i \dot{u}_j + \mathcal{A}_i \ddot{u}_i, \\ \dddot{\mathcal{A}} &= \mathcal{A}_{ijk} \dot{u}_i \dot{u}_j \dot{u}_k + 3\mathcal{A}_{ij} \dot{u}_i \dot{u}_j + \mathcal{A}_i \dddot{u}_i,\end{aligned}$$

etc., and evaluate at the critical point C , which leads to

$$\begin{aligned}\dot{\mathcal{A}}^C &= \ddot{\mathcal{A}}^C = 0, \\ \ddot{\mathcal{A}}^C &= \mathcal{A}_{ijk}^C \dot{u}_i^C \dot{u}_j^C \dot{u}_k^C,\end{aligned}$$

etc.

This shows that $\ddot{\mathcal{A}}^C$ is a cubic in the rates \dot{u}_i^C and we can now consider all possible values of $\ddot{\mathcal{A}}^C$ by a representation in the rate space $\mathcal{A}^C - \dot{u}_i^C$. Let us first consider the behaviour of a general cubic form

$$F = F_{ijk} x_i x_j x_k,$$

with the associated coordinate space $F - x_i$. We write a particular ray as

$$x_i = l_i x$$

and hence

$$F = F_{ijk} l_i l_j l_k x^3.$$

Returning to $\ddot{\mathcal{A}}^C$, this means we may write it as a cubic in one variable for any particular set of rates, and so if it is anywhere non-zero we can find a set of rates that will make $\ddot{\mathcal{A}}^C$, and hence our expanded form of \mathcal{A} , negative. Clearly for $\ddot{\mathcal{A}}^C$ to be everywhere zero all the coefficients \mathcal{A}_{ijk}^C must vanish and so we may conclude that a *necessary but not sufficient* condition for stability is that all the coefficients \mathcal{A}_{ijk}^C are zero.

Should this condition be satisfied, the stability of the critical equilibrium state must be examined in the light of higher-order terms. With vanishing cubic coefficients, an extension of the differentiation process leads to

$$\dddot{\mathcal{A}}^C = \mathcal{A}_{ijkl}^C \dot{u}_i^C \dot{u}_j^C \dot{u}_k^C \dot{u}_l^C$$

and, now having a quartic in rate space, we may continue the examination in a similar way to the cubic.

Koiter⁵⁻²² has stressed that the response of a family of imperfect structural systems in the vicinity of a critical equilibrium state of some perfect system is

dependent on the stability or instability of the critical equilibrium state itself. With this in mind we refer back to the General Introduction of Chapter 2 in which a far-field stability test is proposed for problems involving coincident critical points; these may well be too complex to analyse in full detail and can thus be usefully classified as either ‘stable in the large’ or ‘unstable in the large’.

10.3 General branching analysis

We start this non-diagonalized theory for the numerical analysis of compound branching with the transformed energy function

$$W(q_i, \Lambda) \equiv V[Q_i^F(\Lambda) + q_i, \Lambda],$$

which has the properties arising from its derivation

$$W_i(0, \Lambda) = W'_i(0, \Lambda) = W''_i(0, \Lambda) = \dots = 0.$$

We now assume that a point C lies on the fundamental path at $\Lambda = \Lambda^C$ such that the matrix W_{ij} at C is singular and of rank $n - m$. This condition defines C as an *m-fold compound branching point* and we may write

$$|W_{ij}^C| \equiv |W_{ij}(0, \Lambda^C)| = 0.$$

Following the example of the A -analysis, the next step is to eliminate $n - m$ of the generalized coordinates from the analysis by expressing them in terms of the remaining m generalized coordinates and the loading parameter; this is again achieved via the corresponding $n - m$ equilibrium equations. The q_i are therefore separated into two groups, m of them becoming the active coordinates and henceforth given Latin subscripts, while $n - m$ of them become the passive coordinates and are henceforth given Greek subscripts. This segregation must be performed under the condition that $W_{\alpha\beta}^C$ is a non-singular matrix and hence

$$|W_{\alpha\beta}^C| \equiv |W_{\alpha\beta}(0, \Lambda^C)| \neq 0.$$

It is a property of the singular W_{ij} matrix of rank $n - m$, which defines the *m-fold critical point*, that a valid segregation can always be found for a given set of generalized coordinates. Alternatively the condition may be stated: *the subspace spanned by the passive coordinates q_α must have no non-trivial intersection with the subspace spanned by the buckling modes*.

Elimination of passive coordinates

As with the A -analysis, the $n - m$ equilibrium equations

$$W_\alpha(q_i, q_\beta, \Lambda) = 0$$

contain $n + 1$ unknowns and so the problem may be reduced to contain $m + 1$ independent variables. This enables us to write the passive coordinates in the parametric form

$$q_\beta = q_\beta(q_i, \Lambda)$$

and we seek to find partial derivatives with respect to the independent variables which will enable us to employ systematic Taylor series expansions of these coordinates. Anticipating this representation we may substitute the parametric forms into the equilibrium equations $W_\alpha = 0$ to give the identity

$$W_\alpha[q_i, q_\beta(q_i, \Lambda), \Lambda] \equiv 0.$$

The left-hand side is now a function of the $m + 1$ independent variables q_i and Λ , so we may differentiate with respect to these variables as many times as we please. Thus differentiating repeatedly, we can generate the ordered equilibrium equations

$$\begin{aligned} \frac{\partial}{\partial q_i} W_\alpha &= W_{\alpha i} + W_{\alpha\beta} q_{\beta i} = 0, \\ \frac{\partial}{\partial \Lambda} W_\alpha &= W_{\alpha\beta} q'_\beta + W'_\alpha = 0, \\ \frac{\partial^2}{\partial q_i \partial q_j} W_\alpha &= W_{\alpha ij} + W_{\alpha\beta i} q_{\beta j} + W_{\alpha\beta j} q_{\beta i} + W_{\alpha\gamma i} q_{\beta i} q_{\gamma j} + W_{\alpha\beta} q_{\beta i j} = 0, \\ \frac{\partial^2}{\partial q_i \partial \Lambda} W_\alpha &= W_{\alpha\beta i} q'_\beta + W'_{\alpha i} + W_{\alpha\gamma i} q_{\beta i} q'_\gamma + W'_{\alpha\beta} q_{\beta i} + W_{\alpha\beta} q'_{\beta i} = 0, \\ \frac{\partial^2}{\partial \Lambda^2} W_\alpha &= W_{\alpha\beta i} q'_\beta q'_\gamma + 2W'_{\alpha\beta} q'_\beta + W_{\alpha\beta} q''_\beta + W''_\alpha = 0, \end{aligned} \quad (10.2)$$

etc. Here, following the convention of the A -analysis, we have

$$\begin{aligned} q_{\beta i} &\equiv \frac{\partial q_\beta}{\partial q_i}, & q'_\beta &\equiv \frac{\partial q_\beta}{\partial \Lambda}, \\ q_{\beta i j} &\equiv \frac{\partial^2 q_\beta}{\partial q_i \partial q_j}, & q'_{\beta i} &\equiv \frac{\partial^2 q_\beta}{\partial q_i \partial \Lambda}, \end{aligned}$$

etc.

As before we evaluate these equations on the fundamental path to obtain an ordered series of sequentially linear equations which may be readily solved for the required q_β derivatives. The first such equation is

$$W_{\alpha\beta} q_{\beta i}|^F = -W_{\alpha i}^F$$

and we find that this is a standard form with the result that each $q_{\beta i}^F$ can be written explicitly as the ratio of two determinants, the denominator being the complete determinant of $W_{\alpha\beta}^F$ and the numerator being the determinant of this same matrix with the particular $W_{\alpha\beta}^F$ elements replaced by $-W_{\alpha i}^F$. The remaining evaluated equations yield

$$\begin{aligned} q'_\beta|^F &= 0, \\ W_{\alpha\beta} q_{\beta i j}|^F &= -(W_{\alpha i j} + W_{\alpha\beta i} q_{\beta j} + W_{\alpha\beta j} q_{\beta i} + W_{\alpha\gamma i} q_{\beta i} q_{\gamma j})|^F, \\ W_{\alpha\beta} q_{\beta i}|^F &= -(W_{\alpha i} + W'_{\alpha\beta} q_{\beta i})|^F, \\ q''_\beta|^F &= 0, \end{aligned}$$

etc. It is clear that this is a valid scheme of non-singular linear equations. By employing inductive reasoning similar to that given in Appendix II in terms of the diagonalized A -function, we can write the general result

$$q_{\beta}^F = q_{\beta}''^F = q_{\beta}'''^F = \dots = 0.$$

The sequential solution of these perturbation equations leads to the coefficients of the Taylor series expansions $q_{\alpha}(q_i, \Lambda)$ which can then be used to define a new energy function with only m degrees of freedom as follows

$$\mathcal{W}(q_i, \Lambda) \equiv W[q_i, q_{\alpha}(q_i, \Lambda), \Lambda].$$

The derivatives of this new energy function may be obtained in terms of the known derivatives by direct differentiation,

$$\begin{aligned} \mathcal{W}_i &= W_i + W_{\alpha} q_{\alpha i}, \\ \mathcal{W}' &= W_{\alpha} q'_{\alpha} + W', \\ \mathcal{W}_{ij} &= W_{ij} + W_{\alpha i} q_{\alpha j} + W_{\alpha j} q_{\alpha i} + W_{\alpha \beta} q_{\alpha i} q_{\beta j} + W_{\alpha} q_{\alpha i j}, \\ \mathcal{W}'_i &= W_{\alpha i} q'_{\alpha} + W'_i + W_{\alpha \beta} q_{\alpha i} q'_{\beta} + W'_{\alpha} q_{\alpha i} + W_{\alpha} q'_{\alpha i}, \\ \mathcal{W}_{ijk} &= W_{ijk} + W_{\alpha i j} q_{\alpha k} + W_{\alpha i k} q_{\alpha j} + W_{\alpha \beta i} q_{\alpha j} q_{\beta k} + W_{\alpha i} q_{\alpha j k} + W_{\alpha j k} q_{\alpha i} \\ &\quad + W_{\alpha \beta j} q_{\alpha i} q_{\beta k} + W_{\alpha j} q_{\alpha i k} + W_{\alpha \beta k} q_{\alpha i} q_{\beta j} + W_{\alpha \beta y} q_{\alpha i} q_{\beta j} q_{\gamma k} + W_{\alpha \beta} q_{\alpha i k} q_{\beta j} \\ &\quad + W_{\alpha \beta} q_{\alpha i} q_{\beta j k} + W_{\alpha k} q_{\alpha i j} + W_{\alpha b} q_{\alpha i j} q_{\beta k} + W_{\alpha} q_{\alpha i j k}, \\ \mathcal{W}'_{ij} &= W_{\alpha i j} q'_{\alpha} + W'_{ij} + W_{\alpha \beta} q_{\alpha j} q'_{\beta} + W'_{\alpha i} q_{\alpha j} + W_{\alpha i} q'_{\alpha j} + W_{\alpha \beta j} q_{\alpha i} q'_{\beta} \\ &\quad + W'_{\alpha j} q_{\alpha i} + W_{\alpha j} q'_{\alpha i} + W_{\alpha \beta y} q_{\alpha i} q_{\beta j} q'_{\gamma} + W'_{\alpha \beta} q_{\alpha i} q_{\beta j} + W_{\alpha \beta} q'_{\alpha i} q_{\beta j} \\ &\quad + W_{\alpha \beta} q_{\alpha i} q'_{\beta j} + W_{\alpha \beta} q_{\alpha i j} q'_{\beta} + W'_{\alpha} q_{\alpha i j} + W_{\alpha} q'_{\alpha i j}, \end{aligned}$$

etc. Before we come to evaluate these equations on the fundamental path, we can show that the equilibrium condition is preserved over the transformation to the \mathcal{W} -function following the reasoning of the analysis with diagonalization. The necessary and sufficient condition for equilibrium is that both $W_i = 0$ and $W_{\alpha} = 0$. The transformation process makes use of the $n - m$ equilibrium equations $W_{\alpha} = 0$, so we are left after transformation with the necessary and sufficient condition for equilibrium as $W_i = 0$. Now the second term of the right-hand side in the first of the above equations vanishes by virtue of the equations $W_{\alpha} = 0$; this then leaves $\mathcal{W}_i = W_i$ and we may conclude that the necessary and sufficient condition for equilibrium is $\mathcal{W}_i = 0$. This constitutes a full preservation of the normal equilibrium condition and leads to the following properties, which are associated with the use of a set of incremental coordinates, also being maintained,

$$\mathcal{W}_i(0, \Lambda) = \mathcal{W}'_i(0, \Lambda) = \mathcal{W}''_i(0, \Lambda) = \dots = 0.$$

Evaluating the above derivatives on the fundamental path in the region of the critical point and using the earlier result for $q_{\beta i}^F$ from the elimination of passive coordinates, we obtain

$$\begin{aligned} \mathcal{W}_i^F &= 0, \\ \mathcal{W}'^F &= W'^F, \\ \mathcal{W}_{ij}^F &= W_{ij} + W_{\alpha i} q_{\alpha j}|^F, \\ \mathcal{W}'_i^F &= 0, \\ \mathcal{W}_{ijk}^F &= W_{ijk} + W_{\alpha j k} q_{\alpha i} + W_{\alpha i k} q_{\alpha j} + W_{\alpha i j} q_{\alpha k} + W_{\alpha \beta i} q_{\alpha j} q_{\beta k} + W_{\alpha \beta j} q_{\alpha i} q_{\beta k} \\ &\quad + W_{\alpha \beta k} q_{\alpha i} q_{\beta j} + W_{\alpha \beta y} q_{\alpha i} q_{\beta j} q_{\gamma k}|^F, \\ \mathcal{W}'_{ij}^F &= W'_{ij} + W'_{\alpha i} q_{\alpha j} + W'_{\alpha j} q_{\alpha i} + W'_{\alpha \beta} q_{\alpha i} q_{\beta j}|^F, \end{aligned} \tag{10.3}$$

etc. We note that up to the stage presented explicitly here, we require only the derivatives $q_{\alpha i}^F$ from the earlier perturbation scheme. Considering now the derivative \mathcal{W}_{ij}^F together with the known result for $q_{\alpha i}^F$, a little careful thought leads to the conclusion that \mathcal{W}_{ij}^F may be written as the ratio of two determinants, the denominator being the non-zero determinant of $W_{\alpha \beta}^F$ and the numerator being the determinant of a minor of order $n - m + 1$ of the full W -matrix. At the compound critical point the full W -matrix is singular and of rank $n - m$ so any minor of order greater than $n - m$ is singular. This therefore yields the important result

$$\mathcal{W}_{ij}^C = 0,$$

and \mathcal{W}_{ij}^C is thus a null matrix.

Post-buckling solutions

We are now at liberty to operate exclusively in terms of the transformed \mathcal{W} -function. We thus seek to express any *post-buckling* equilibrium paths which emerge from the compound critical equilibrium state in the parametric form

$$q_j = q_j(s), \quad \Lambda = \Lambda(s),$$

where, as in the \mathcal{A} -analysis, s is an unspecified but suitable expansion parameter.

These parametric equations can now be substituted into the equilibrium equations $\mathcal{W}_i = 0$ to give the identity

$$\mathcal{W}_i[q_j(s), \Lambda(s)] \equiv 0.$$

Here the left-hand side is simply a function of the independent parameter s so we can differentiate these equations with respect to s as many times as we please. Thus, differentiating repeatedly, we generate the ordered equilibrium equations

$$\mathcal{W}_{ij} \dot{q}_j + \mathcal{W}'_i \dot{\Lambda} = 0,$$

$$\mathcal{W}_{ijk} q_j \dot{q}_k + 2\mathcal{W}'_{ij} \dot{q}_j \dot{\Lambda} + \mathcal{W}_{ij} \ddot{q}_j + \mathcal{W}''_i \dot{\Lambda}^2 + \mathcal{W}'_i \ddot{\Lambda} = 0,$$

etc., where as before a dot denotes differentiation with respect to s . Evaluating these ordered equilibrium equations at the critical point $q_i = 0$, $\Lambda = \Lambda^C$ and remembering the earlier derived properties of the \mathcal{W} -function, we see that the first equation gives no information while the second equation takes the form

$$\mathcal{W}_{ijk}\dot{q}_j\dot{q}_k + 2\mathcal{W}'_{ij}\dot{q}_j\Lambda|_C = 0.$$

As with the diagonalized analysis, these equations for the post-buckling path tangents constitute m homogeneous quadratics in $m + 1$ unknowns, so by the theorem of Bezout¹⁸⁷ we have a maximum number of 2^m solutions. Again one of these corresponds to the fundamental path so we underline the earlier result that under asymmetric conditions the maximum number of possible *post-buckling* solutions emerging from an m -fold compound branching point is $2^m - 1$.

In the diagonalized analysis we pictured the post-buckling solutions in rate space, but for the purposes of numerical analysis it is felt that the quadratics are more readily handled with the inclusion of a further equation which specifies the independent path parameter s . Of course once s has been specified it is possible that one or more post-buckling path tangents are not included amongst the solutions since the s -axis may be orthogonal to these tangents. For safety it is therefore suggested that one should take s to be each of the q_i -axes in turn. Thus if $s = q_i$ we can substitute the expressions

$$\dot{q}_i = 1, \quad \ddot{q}_i = \ddot{q}_j = \dots = 0$$

into the above equations and solve for the remaining path derivatives. This of course may result in some duplication of solutions but it does ensure that the slope of every post-buckling path is determined.

10.4 Erosion of an optimum design

In the final chapter of this Monograph we explore the role of optimization as a generator of structural instability in general, and of compound branching in particular. The latter is indeed demanded by F. R. Shanley's so-called principle of *simultaneous mode design* which is formulated by Spunt as follows: 'A given form will be optimum if all failure modes which can possibly intersect occur simultaneously under the action of the load environment'.

Unfortunately simultaneous buckling can give rise to unexpected nonlinear coupling, which can bring with it quite severe imperfection-sensitivity and experimental scatter as observed in the buckling of shells. We shall see examples of this in Chapter 12 which is devoted to interaction phenomena in the compound failure of columns, and the role of the associated imperfection-sensitivity in eroding the benefits of a nominally optimum design is analysed in Section 13.8.

To close this chapter on compound branching we thought it appropriate to present a simple two-degree-of-freedom buckling model due to Augusti¹⁹⁷ which shows most elegantly how the coalescence of two quite stable post-buckling modes can generate highly unstable compound buckling and associated imperfection-sensitivity. We shall observe the approach and coalescence of the two primary critical points and for the secondary bifurcation which runs in we can illustrate our general theory of Sections 6.3 and 8.3 for a distinct critical point lying on a nonlinear fundamental path.

For this model it is then shown, following Thompson and Supple,¹³⁶ that a simple optimization problem can be posed which calls for the simultaneity of the two primary critical loads, and the erosion of this optimum is examined. It is seen that the compound imperfection-sensitivity can indeed quite seriously modify and perhaps destroy the apparent optimum, and the key role of secondary bifurcation is delineated.

The Augusti model

We consider then the model of Figure 98 which consists of a light rigid link of length L carrying a dead vertical load P . It is supported at its pinned end by rotational springs of stiffness c_1 and c_2 tied to the orthogonal coordinate axes as shown. Deflection of the link is specified by the two angles spanned by the springs, Q_1 and Q_2 , and we introduce the generalized coordinates

$$u_1 = \frac{\pi}{2} - Q_1$$

$$u_2 = \frac{\pi}{2} - Q_2.$$

We shall suppose that the 'perfect' system rests vertically under zero load, and then introduce a family of imperfect systems by supposing that the springs are initially too short so that in the unloaded configuration $u_1 = u_1^0$ and $u_2 = u_2^0$. We shall see that equal initial imperfections are the most serious for the structure, and so we shall straight away write

$$u_1^0 = u_2^0 = \epsilon,$$

where ϵ is now our single imperfection parameter.

For a perfect or an imperfect system the strain energy is

$$U = \frac{1}{2}c_1(u_1 - u_1^0)^2 + \frac{1}{2}c_2(u_2 - u_2^0)^2$$

and the corresponding deflection of the load P can be written as

$$\mathcal{E} = -L\{1 - \sin^2 u_1 - \sin^2 u_2\}^{\frac{1}{2}}.$$

The total potential energy is thus

$$V(u_1, u_2, P) = \frac{1}{2}c_1(u_1 - u_1^0)^2 + \frac{1}{2}c_2(u_2 - u_2^0)^2 + PL\{1 - \sin^2 u_1 - \sin^2 u_2\}^{\frac{1}{2}}$$

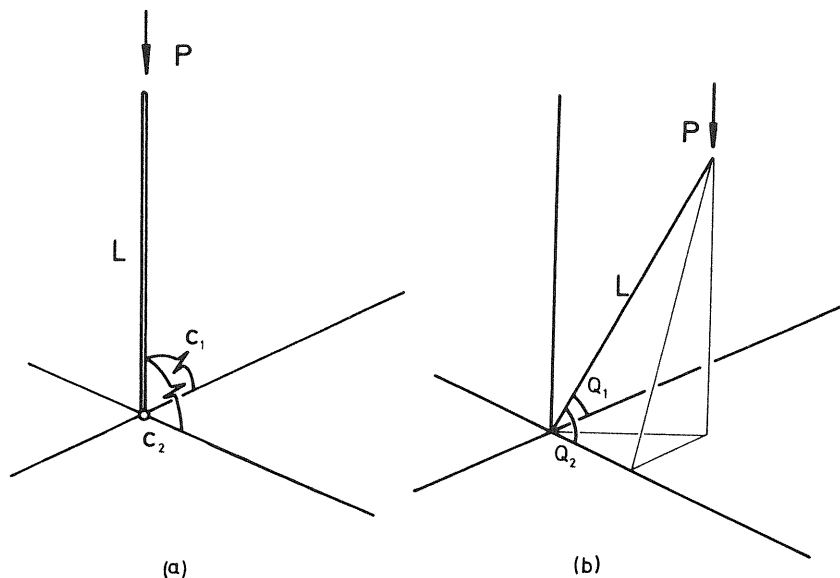


Figure 98 The Augusti model showing (a) the undeflected perfect system and (b) the deflected imperfect system

and expanding the trigonometric functions we shall truncate this to give

$$V = \frac{1}{2}c_1 u_1^2 + \frac{1}{2}c_2 u_2^2 + PL\{-\frac{1}{2}u_1^2 - \frac{1}{2}u_2^2 + \frac{1}{24}u_1^4 + \frac{1}{24}u_2^4 - \frac{1}{4}u_1^2 u_2^2\} - \epsilon(c_1 u_1 + c_2 u_2).$$

Exact analyses will now be based on this approximate total potential energy function which effectively defines the *analytical model* under consideration.

By inspection we see that buckling of the perfect system will occur at the smaller of the two critical loads

$$P_1 = \frac{c_1}{L}, \quad P_2 = \frac{c_2}{L},$$

and we now introduce the concept of optimization by imagining that a given amount of spring stiffness, k , is available for apportioning between the angular springs, so that

$$c_1 + c_2 = k.$$

Taking a simple linear distribution such that

$$\begin{aligned} c_1 &= \beta k, \\ c_2 &= (1 - \beta)k, \end{aligned}$$

we shall first look for the value of the *design parameter* β which maximizes the load-carrying capacity subject to there being no instability. Figure 99 includes

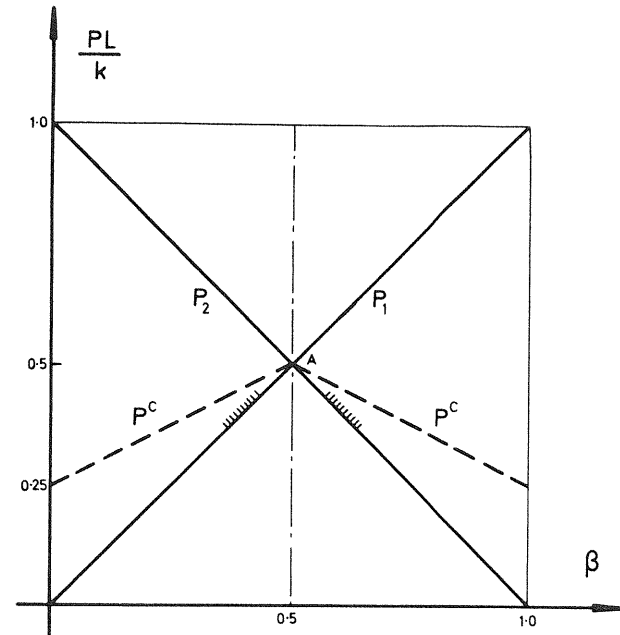


Figure 99 Variation of the bifurcation loads with the design parameter

a plot of the primary critical loads P_1 and P_2 against β and shows the intuitively obvious result that $\beta = \frac{1}{2}$ optimizes P , and we note that optimization defined in this simple manner calls for simultaneity of the buckling loads.

Let us first study the response of the system for the non-coincident case in which $c_1 \neq c_2$. The equilibrium equations of the perfect system,

$$\begin{aligned} V_1 &= c_1 u_1 + PL\{-u_1 + \frac{1}{6}u_1^3 - \frac{1}{2}u_1 u_2^2\} = 0, \\ V_2 &= c_2 u_2 + PL\{-u_2 + \frac{1}{6}u_2^3 - \frac{1}{2}u_2 u_1^2\} = 0, \end{aligned}$$

reveal the existence of four equilibrium paths as shown in Figure 100(a). Here, supposing that $c_1 < c_2$, we have the trivial fundamental path (a) given by

$$u_1 = u_2 = 0 \quad \text{for all } P,$$

the two uncoupled primary post-buckling paths (b) and (c) given by

$$\begin{aligned} u_2 &= 0, \quad u_1^2 = 6\left(1 - \frac{c_1}{PL}\right), \\ u_1 &= 0, \quad u_2^2 = 6\left(1 - \frac{c_2}{PL}\right), \end{aligned}$$

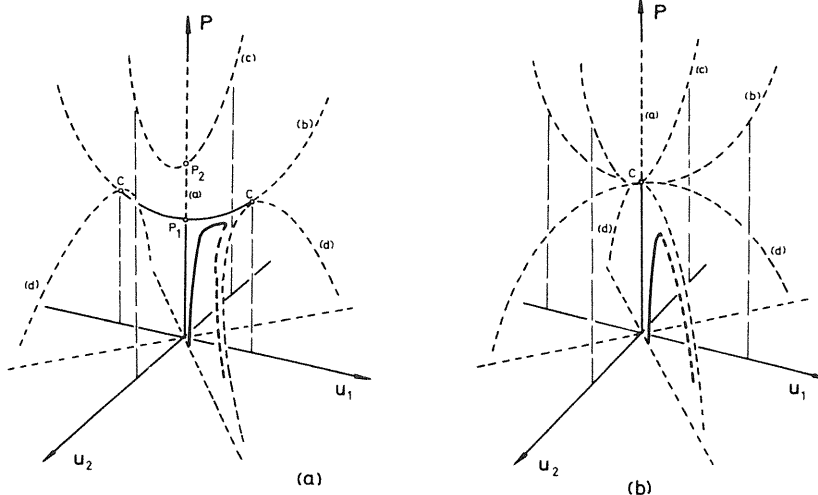


Figure 100 Equilibrium paths of perfect and imperfect systems for (a) separated primary critical points and (b) coincident critical points

and a coupled solution (d) for which $u_1 \neq 0, u_2 \neq 0$, given by

$$\begin{aligned} c_1 + PL\{-1 + \frac{1}{6}u_1^2 - \frac{1}{2}u_2^2\} &= 0, \\ c_2 + PL\{-1 + \frac{1}{6}u_2^2 - \frac{1}{2}u_1^2\} &= 0. \end{aligned}$$

The latter falling path is seen to bifurcate from the lower of the two primary paths at the critical equilibrium state C , and we can identify this coupling action as one of the hyperbolic forms delineated by Supple.^{75,83}

Secondary branching

For a finite separation such that $c_1 \ll c_2$ imperfect systems will fail at limit points close to the critical equilibrium state C , as indicated in the figure, and to study the imperfection-sensitivity about this point we shall now make an asymptotic branching study treating path (b) as fundamental. The fundamental path is thus given by

$$u_1^F(P) = \left\{ 6 \left(1 - \frac{c_1}{PL} \right) \right\}^{\frac{1}{2}},$$

$$u_2^F(P) = 0,$$

and we introduce the incremental coordinates v_1 and v_2 measured from the fundamental solution by setting

$$\begin{aligned} u_1 &= u_1^F(P) + v_1, \\ u_2 &= v_2. \end{aligned}$$

We define next our transformed energy function

$$W(v_1, v_2, P, \varepsilon) \equiv V[u_1^F(P) + v_1, v_2, P, \varepsilon]$$

with the derivatives

$$\begin{aligned} W_{11} &= V_{11} = c_1 + PL\{-1 + \frac{1}{2}u_1^2 - \frac{1}{2}u_2^2\}, \\ W_{22} &= V_{22} = c_2 + PL\{-1 + \frac{1}{2}u_2^2 - \frac{1}{2}u_1^2\}, \\ W_{12} &= V_{12} = PL\{-u_1 u_2\}, \end{aligned}$$

and evaluating on the fundamental path (b) we have

$$W_{12}^F = 0.$$

We see that we already have a diagonal system, so W can be equated to our diagonalized A -function of Chapters 6 and 8. The two stability coefficients are

$$\begin{aligned} W_{11}^F &= c_1 + PL\{-1 + \frac{1}{2}u_1^2\}|^F, \\ W_{22}^F &= c_2 + PL\{-1 - \frac{1}{2}u_1^2\}|^F, \end{aligned}$$

and substituting for $u_1^F(P)$ we have

$$\begin{aligned} W_{11}^F &= 2PL - 2c_1, \\ W_{22}^F &= c_2 + 3c_1 - 4PL. \end{aligned}$$

The critical equilibrium state C is clearly associated with the vanishing of W_{22}^F so the critical load is given by

$$P^c = \frac{3c_1 + c_2}{4L}.$$

In terms of our design parameter we have

$$P^c = \frac{k}{L}(\frac{1}{4} + \frac{1}{2}\beta)$$

giving us the variation shown in Figure 99, and we see that as β tends to $\frac{1}{2}$ this secondary point of bifurcation will coalesce with the two primary critical points. This load P^c is of course the real failure load of the perfect system, and noting that it takes its maximum value at $\beta = \frac{1}{2}$ we see that our provisional optimization scheme based on initial instability has produced a truly optimum design based on collapse.

Now we have seen that the asymptotic equations for a symmetric point of bifurcation can be written in the form

$$P^{(2)c} = -\frac{\tilde{A}_{1111}}{3A'_{11}} \Bigg|_c^c,$$

where

$$\begin{aligned}\tilde{A}_{1111}^c &= A_{1111} - 3 \sum_2^n \frac{(A_{s11})^2}{A_{ss}} \Bigg|_c^c, \\ P^M &= P^c - \frac{1}{2}(\tilde{A}_{1111}^c)^{\frac{1}{3}} \frac{(3\tilde{A}_1^c \varepsilon)^{\frac{1}{3}}}{A_{11}^c}.\end{aligned}$$

Here $P^{(2)c}$ is the initial post-buckling curvature of the perfect system, and P^M is the peak load of an imperfect system. They are given in terms of A , the diagonalized incremental energy function, which we can here simply equate to W if we transpose the subscripts 1 and 2. This is necessary because in the general theory a subscript 1 relates to the critical principal coordinate, while here it is v_2 that is critical. The necessary derivatives of W are

$$\begin{aligned}W_{11}^c &= \frac{1}{2}(c_2 - c_1), \quad W_{111}^c = PLu_1|_c^c, \\ W_{222}^c &= 0, \quad W_{221}^c = -PLu_1|_c^c, \\ W_{2222}^c &= PL|_c^c, \quad W_{22}^c = -4L, \quad \dot{W}_2^c = -c_2,\end{aligned}$$

and substituting these we obtain

$$\begin{aligned}\tilde{A}_{1111}^c &= -8PL|_c^c = -2(3c_1 + c_2), \\ P^{(2)c} &= -\frac{3c_1 + c_2}{6L}, \\ P^M &= \frac{1}{4L} [(3c_1 + c_2) - (\frac{3}{2})^{\frac{1}{3}}(3c_1 + c_2)^{\frac{1}{3}}\varepsilon^{\frac{1}{3}}c_2^{\frac{1}{3}}].\end{aligned}$$

These then are the results of our bifurcation study of C , and we see that we have an unstable-symmetric point of bifurcation with the well known two-thirds power law for the imperfection-sensitivity.

Imperfection-sensitivity at coalescence

Let us now examine the behaviour of the system under the optimum condition $\beta = \frac{1}{2}$, so that $c_1 = c_2 = c$, say. For the perfect system we have a compound point of bifurcation with

$$P_1 = P_2 = P^c = \frac{c}{L}$$

and we see that the paths (a), (b) and (c) can be written down as before. The coupled paths (d) undergo some modification, and can be written as

$$u_1^2 = u_2^2 = 3 \left(\frac{c}{PL} - 1 \right).$$

We see that as β tends to $\frac{1}{2}$ the coupled paths have collapsed onto the compound critical point, in the manner delineated by Chilver⁷⁰ and Supple,⁷⁵ leaving us with the two downwards-curving coupled paths shown in Figure 100(b).

It remains to study the imperfection-sensitivity corresponding to this coincident case, and with equal imperfections as specified we can restrict attention to the 45° plane by writing $u_1 = u_2 = u$. In this plane we now have the total potential energy function

$$V = cu^2 + PL\{-u^2 - \frac{1}{6}u^4\} - 2ceu,$$

and we can again make use of the above general asymptotic equations for a distinct critical point. Energy derivatives are

$$\begin{aligned}V_{111}^c &= 0, \quad V_{1111}^c = -4PL|_c^c, \\ V_{11}'^c &= -2L, \quad \dot{V}_1^c = -2c,\end{aligned}$$

and we obtain

$$\begin{aligned}P^{(2)c} &= -\frac{2c}{3L}, \\ P^M &= \frac{1}{4L} [4c - (\frac{3}{2})^{\frac{1}{3}}(4c)^{\frac{1}{3}}\varepsilon^{\frac{1}{3}}c^{\frac{1}{3}}2^{\frac{1}{3}}].\end{aligned}$$

This then is the imperfection-sensitivity at the optimum, and we note that it is *more severe* by a factor of $4^{\frac{1}{3}}$ than that of the finite separation study which does of course break down in the limit as β tends to $\frac{1}{2}$.

Using the two asymptotic formulae, and guided by the results of a companion numerical study that was included in Reference 136, we can now suggest the curves of Figure 101 for the imperfection-sensitivity of our analytical model. Here the two solid curves are sketched for initial imperfections of $u_1^0 = u_2^0 = 2$ degrees and $u_1^0 = u_2^0 = 5$ degrees respectively. We see that there is a marked flattening of the optimum as the imperfection is increased, and it is clear that, possibly for this system, but certainly for a *quite similar* system, the optimum could be completely destroyed by the appearance of a central dimple as suggested by the broken line. The mechanics of the erosion are clearly seen, and depend crucially on the approach of the secondary bifurcation.

The present study emphasizes the need to evaluate *all* the post-buckling equilibrium paths which may be present in a given problem. Optimization based solely on classical critical loads tends to produce designs with compound

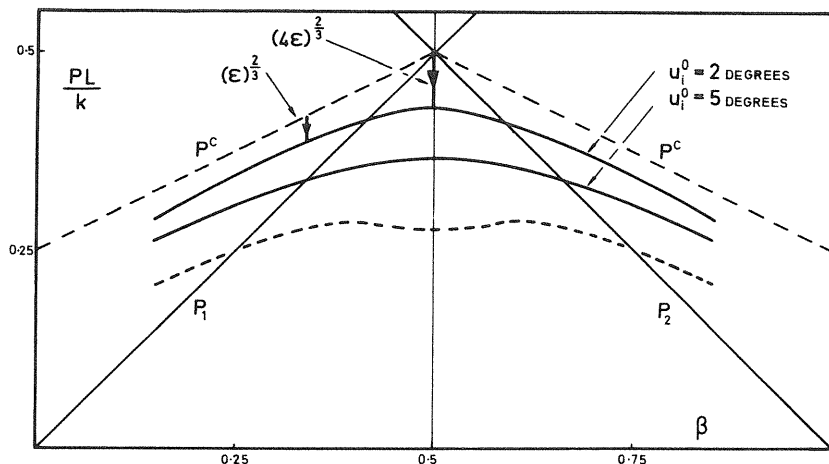


Figure 101 Erosion of the optimum design by compound imperfection-sensitivity

branching points, and these in turn tend to generate nonlinear coupled paths. If there is severe imperfection-sensitivity associated with the coupling then the optimization process cast in this form may be invalid. We conclude, therefore, that any optimization scheme which is to be applied to a structural system displaying multi-mode buckling must be *so defined* as to take into account the complete post-buckling characteristics including the effects of unavoidable manufacturing imperfections.

11

THE SPHERICAL SHELL

11.1 Introduction

Following the classic work of Kármán and Tsien²⁰² who showed for the first time the relevance of the large-deflection post-buckling behaviour of thin elastic shells, the complete spherical shell has been the subject of innumerable investigations attempting to close the gap between the theoretical and experimental failure loads. The early experimental results are reviewed in the works of Thompson,^{57, 203, 204} and more recent studies at Stanford University have already been mentioned in the General Introduction of Chapter 2.

On the theoretical side the recent imperfection-sensitivity studies of Koiter²¹ and Hutchinson³⁰ are particularly significant and it is now well established that the notorious discrepancy in the buckling of elastic spheres and cylinders is attributable to inevitable manufacturing imperfections in the test specimens. An excellent review of these two problems can be found in the article by Hutchinson and Koiter.⁴⁴

We shall not here attempt a complete study of the complex branching behaviour of the spherical shell as delineated by Koiter,²¹ but will content ourselves by retrieving his results for the *initial rotationally-symmetric* post-buckling. In this, the nonlinear coupling action between *two simultaneous buckling modes* that arises at certain thickness-radius ratios will be considered as an excellent and non-trivial example of the preceding general theory.

It is now well known that under rotationally-symmetric conditions a linear eigenvalue analysis reveals eigenfunctions for the normal deflection which are the Legendre functions $P_n(\cos \theta)$, where θ is the independent variable angle of Figure 102 and n can take the values 2, 3, 4, ... For a thin shell the *critical* eigenfunction will correspond to a large n , the particular value depending on the thickness-radius ratio of the shell. Moreover at certain thickness-radius ratios we find that two adjacent values of n give the same critical load so that we have a *two-fold compound critical point*.

An examination of the Legendre functions shows that when n is odd the corresponding deformation of the shell is 'skew-symmetric' about the equator, so that an inwards deflection of the north pole will be accompanied by an outwards deflection of the south pole. On the other hand when n is even the

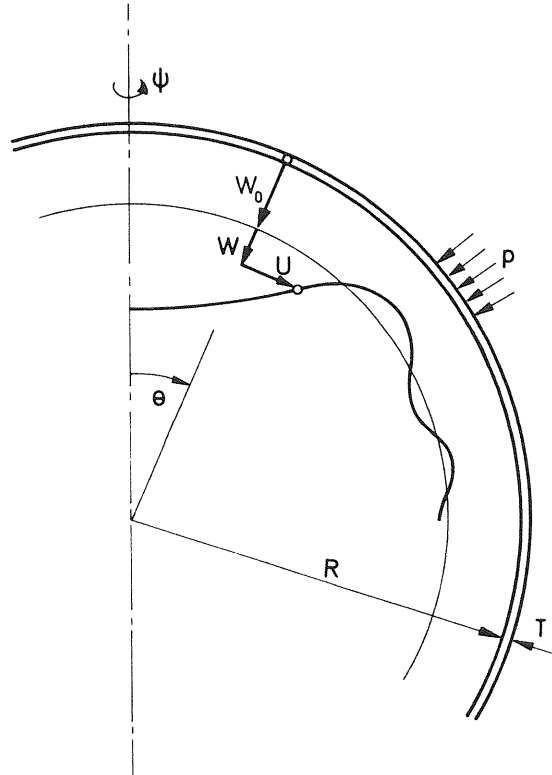


Figure 102 The geometry and notation of the spherical shell

deformation is symmetric about the equator, an inwards deflection of the north pole being accompanied by an inwards deflection of the south pole. It is thus clear that at a *distinct* branching point for which n is odd, the non-trivial equilibrium path will have zero initial slope due to the skew-symmetry of the deformation, while if n is even the initial slope may be, and in fact is, non-zero.⁵⁷ Furthermore, at the *compound* branching point of interest the potential energy is symmetric in one of the critical principal coordinates enabling us ultimately to appeal to the particular solutions of Chapter 10 for the slopes of the post-buckling paths.

Differential equations relevant to the spherical shell have been analysed in an asymptotic manner by Reissner^{205, 206} and these studies throw light on the relationship between the continuum and discrete-coordinate approaches: in particular the role of the suppression of secular terms is pinpointed as in our study of the elastica in Chapter 1. The relationship between the discrete

coordinate studies and the general continuum theory of Koiter is studied briefly in the paper by Haftka, Mallett and Nachbar.²⁰⁷

Although the following analysis for the spherical shell is somewhat complex in comparison with the elastica analysis of Chapter 1, there remain important parallels in the two examples. In each case the displacement of the system is represented by an infinite modal expansion using appropriate orthogonal functions, the amplitudes of the modes becoming the generalized coordinates of our discrete theory. However, in the spherical shell example we find it necessary, under rotationally-symmetric conditions, to provide a series expansion in Legendre functions for each of two displacements shown in Figure 102, the normal component W and the tangential component U . This of course gives two distinct sets of generalized coordinates and we find that the diagonalized nature of the quadratic form of potential energy is thereby destroyed, the off-diagonal terms being generated by corresponding pairs in the two series expansions.

The potential energy nevertheless remains in a near-diagonal form and we find we are thus presented with two alternative methods of analysis. First using a simple completion of the square routine we can quite easily diagonalize the quadratic form of potential energy and so utilize the A -analysis of the general theory; alternatively we can leave the potential energy in its non-diagonalized form and make use of the results of the W -analysis. For a complete illustration of the general theory both courses are followed here, but after the elimination of passive coordinates it is found that the two analyses are identical, the same two-degree-of-freedom diagonalized potential energy function being generated by each perturbation scheme.

11.2 Energy formulation

Energy functional

Following the general theory we shall first write down an expression for the change in total potential energy experienced by the system as the shell is displaced from the fundamental uniformly-contracted state to an ‘adjacent’ or ‘buckled’ state. Assuming rotational symmetry, we introduce the displacements of the middle-surface, W_t normal to the middle-surface and U tangential to the middle-surface, as shown in Figure 102. The normal displacement W_t is written as the sum of the uniform contraction W_0 and the ‘buckling’ component W . The displacements are finally divided by R , the radius of the shell, to give the corresponding lower-case symbols u and $w = w_t - w_0$. The required energy increase will thus be a *functional* of the displacements $u(\theta)$ and $w(\theta)$, where θ is the variable angle of Figure 102.

We first consider the strain energy of the shell. For 'moderately large' deflections of a thin spherical shell suffering rotationally-symmetric deformations, the middle-surface strains, ε_θ and ε_ψ , can be written

$$\begin{aligned}\varepsilon_\theta &= u' - w_t + \frac{1}{2}w_t' = (u' - w + \frac{1}{2}w'^2) - w_0, \\ \varepsilon_\psi &= u \cot \theta - w_t = (u \cot \theta - w) - w_0,\end{aligned}$$

where a prime now denotes differentiation with respect to θ . Since the wavelength of the buckling deformation is small, the changes in curvature of the middle-surface can be written as

$$\begin{aligned}\chi_\theta &= \frac{1}{R}(w''), \\ \chi_\psi &= \frac{1}{R}(w' \cot \theta).\end{aligned}$$

The strain energy per unit area of the undeformed middle-surface is now given⁷ by

$$\begin{aligned}K &= \frac{1}{2} \cdot \frac{ET}{1-v^2} [\varepsilon_\theta^2 + \varepsilon_\psi^2 + 2v\varepsilon_\theta\varepsilon_\psi] \\ &\quad + \frac{1}{2} \cdot \frac{ET^3}{12(1-v^2)} [\chi_\theta^2 + \chi_\psi^2 + 2v\chi_\theta\chi_\psi],\end{aligned}$$

where E is Young's modulus, v is Poisson's ratio, and T is the shell thickness. The strain energy of the deformed shell is thus given by

$$\begin{aligned}J_E &= \int_0^\pi 2\pi R^2 K \sin \theta d\theta \\ &= \frac{\pi ETR^2}{1-v^2} \int_0^\pi \{2w_0^2(1+v) \sin \theta + 2w_0(1+v) \sin \theta [2w - u' - u \cot \theta] \\ &\quad + \sin \theta [(u' - w)^2 + (u \cot \theta - w)^2 + 2v(u' - w)(u \cot \theta - w)] \\ &\quad - w_0(1+v) \sin \theta [w'^2] + \sin \theta [(w'^2)(u' - vu \cot \theta - w(1+v))] \\ &\quad + \sin \theta [\frac{1}{4}w'^4]\} d\theta + \frac{\pi ETR^2}{1-v^2} \cdot \frac{T^2}{12R^2} \int_0^\pi \\ &\quad \times \sin \theta [w''^2 + (w' \cot \theta)^2 + 2vw''w' \cot \theta] d\theta.\end{aligned}$$

We must now consider the potential energy of the load, J_L , which can be written as the product of the uniform external pressure p and the internal volume of the deformed shell. An exact expression for this is given by Thompson,⁵⁷ but an adequate form is nevertheless given by the simply-derived approximate expression

$$J_L = -p2\pi R^3 \int_0^\pi w \sin \theta d\theta,$$

which can be obtained from the exact equation by dropping the irrelevant 'constant', linearizing, neglecting w_0 in comparison with unity and using integration by parts.

We are now able to write down a first expansion of the energy functional $W(u, w) = J_E + J_L$ in terms of the pressure p and the (as yet unknown) uniform contraction w_0 . It is felt that no confusion will arise from the use of the symbol W for the energy functional which is consistent with the general theory, since the component W of W_t makes no further appearance in the analysis having been replaced by its dimensionless form w . Thus expanding $W(u, w)$ in the form

$$W(u, w) = W_0 + W_1(u, w) + W_2(u, w) + W_3(u, w) + \dots,$$

where $W_m(u, w)$ is the sum of all terms which are of m th degree in the 'buckling' displacements and their derivatives, we have

$$\begin{aligned}W_1(u, w) &= \frac{\pi ETR^2}{1-v^2} \int_0^\pi \{2w_0(1+v)[2w - u' - u \cot \theta] - 4\Lambda[w]\} \sin \theta d\theta, \\ W_2(u, w) &= \frac{\pi ETR^2}{1-v^2} \int_0^\pi \{[(u' - w)^2 + (u \cot \theta - w)^2 + 2v(u' - w)(u \cot \theta - w)] \\ &\quad - w_0(1+v)[w'^2] + \alpha[w''^2 + w'^2 \cot^2 \theta + 2vw''w' \cot \theta]\} \sin \theta d\theta, \\ W_3(u, w) &= \frac{\pi ETR^2}{1-v^2} \int_0^\pi \{[w'^2][u' - vu \cot \theta - w(1+v)]\} \sin \theta d\theta, \\ W_4(u, w) &= \frac{\pi ETR^2}{1-v^2} \int_0^\pi \frac{1}{4}[w'^4] \sin \theta d\theta.\end{aligned}$$

Here we have disregarded the immaterial constant W_0 , $\alpha \equiv (T/R)^2/12$ and Λ is a dimensionless load parameter defined by the equation

$$\Lambda \equiv \frac{pR(1-v^2)}{2ET}.$$

We note that the series terminates with the term of fourth degree.

Using integration by parts, u and u' drop out of the expression for W_1 and we are left with

$$W_1(u, w) = \frac{\pi ETR^2}{1-v^2} 4[w_0(1+v) - \Lambda] \int_0^\pi w \sin \theta d\theta.$$

Now since the fundamental state, involving the normal deflection W_0 and zero tangential deflection, is a state of equilibrium this functional must be identically zero and we see that this is so when

$$w_0 = \frac{\Lambda}{1+v}.$$

This corresponds to the well known membrane solution.

Substituting for w_0 we can now write a second expansion of the energy functional as

$$W(u, w, A) = W_2^0 + W_3 + W_4 + AW'_2,$$

where

$$\begin{aligned} W_2^0 &= \frac{\pi ETR^2}{1-v^2} \int_0^\pi \{[(u' - w)^2 + (u \cot \theta - w)^2 + 2v(u' - w)(u \cot \theta - w)] \\ &\quad + \alpha[w''^2 + w'^2 \cot^2 \theta + 2vw''w' \cot \theta]\} \sin \theta d\theta, \end{aligned}$$

$$W_3 = \frac{\pi ETR^2}{1-v^2} \int_0^\pi \{[w'^2] [u' + vu \cot \theta - w(1+v)]\} \sin \theta d\theta,$$

$$W_4 = \frac{\pi ETR^2}{1-v^2} \int_0^\pi \frac{1}{4}[w'^4] \sin \theta d\theta,$$

$$W'_2 = -\frac{\pi ETR^2}{1-v^2} \int_0^\pi w'^2 \sin \theta d\theta.$$

Expansion in Legendre functions

Following the example of the earlier work we may complete the eigenvalue and post-buckling analyses by the introduction of Legendre functions. We can thus write $w(\theta)$ and $u(\theta)$ in the form

$$w(\theta) = \sum_{n=0}^{+\infty} a_n P_n(\cos \theta),$$

$$u(\theta) = \sum_{n=0}^{+\infty} b_n P'_n(\cos \theta),$$

these being completely general expressions satisfying the boundary conditions of the problem.²⁰⁸ We shall assume that these expressions can be repeatedly differentiated term by term. The Legendre function $P_n(\cos \theta)$ of degree n satisfies the Legendre differential equation

$$P''_n + P'_n \cot \theta + n(n+1)P_n = 0$$

and by writing $z = \cos \theta$ this equation may also be written

$$(1-z^2)\ddot{P}_n - 2z\dot{P}_n + n(n+1)P_n = 0,$$

where a dot now denotes differentiation with respect to z . We find we require a certain adaptability in handling these functions and shall need to interchange between $P'_n(\cos \theta)$ and $\dot{P}_n(z)$, etc. We therefore write the required relationship

$$P'_n = -\dot{P}_n \sin \theta.$$

It is now possible to substitute the expanded forms for $w(\theta)$ and $u(\theta)$ into the second expansion of the potential energy function. For the sake of brevity let us only consider here a typical term—the first term of W_2^0 —which is written

$$\begin{aligned} T_1 &= \frac{\pi ETR^2}{1-v^2} \int_0^\pi u'^2 \sin \theta d\theta \\ &= \frac{\pi ETR^2}{1-v^2} b_n b_m \int_0^\pi P'_n P'_m \sin \theta d\theta. \end{aligned}$$

Here the dummy-suffix summation convention is employed with all summations ranging from 0 to ∞ . We may now eliminate the second derivatives by use of the Legendre differential equation and so this becomes

$$\begin{aligned} T_1 &= \frac{\pi ETR^2}{1-v^2} b_n b_m \left\{ \int_0^\pi P'_n P'_m \cot^2 \theta \sin \theta d\theta + m(m+1) \int_0^\pi P'_n P_m \cot \theta \sin \theta d\theta \right. \\ &\quad \left. + n(n+1) \int_0^\pi P_n P'_m \cot \theta \sin \theta d\theta + nm(n+1)(m+1) \int_0^\pi P_n P_m \sin \theta d\theta \right\}. \end{aligned}$$

Now, making use of the earlier relationship for first derivatives, whilst noting that

$$\int_0^\pi \sin \theta d\theta \text{ becomes } \int_{-1}^{+1} dz,$$

this becomes

$$\begin{aligned} T_1 &= \frac{\pi ETR^2}{1-v^2} b_n b_m \left\{ \int_{-1}^{+1} \dot{P}_n \dot{P}_m z^2 dz - m(m+1) \int_{-1}^{+1} \dot{P}_n \dot{P}_m z dz \right. \\ &\quad \left. - n(n+1) \int_{-1}^{+1} P_n \dot{P}_m z dz + nm(n+1)(m+1) \int_{-1}^{+1} P_n \dot{P}_m dz \right\}. \end{aligned}$$

Quadratic coefficients

If we treat the remaining twelve terms of W_2^0 and the single term of W'_2 in a similar way to that of T_1 we may obtain the quadratic terms of the total potential energy function in the form

$$\begin{aligned} W_2 &= W_2^0 + AW'_2 \\ &= \frac{\pi ETR^2}{1-v^2} a_n a_m \left\{ 2(1+v) \int_{-1}^{+1} P_n P_m dz + \alpha \left[nm(n+1)(m+1) \int_{-1}^{+1} P_n P_m dz \right. \right. \\ &\quad \left. - m(m+1) \int_{-1}^{+1} \dot{P}_n \dot{P}_m z dz - n(n+1) \int_{-1}^{+1} P_n \dot{P}_m z dz + 2vn(n+1) \right. \\ &\quad \left. \times \left[\int_{-1}^{+1} P_n P_m dz + 2(1-v) \int_{-1}^{+1} \dot{P}_n \dot{P}_m z^2 dz \right] - A \int_{-1}^{+1} \dot{P}_n \dot{P}_m (1-z^2) dz \right\} \end{aligned}$$

$$\begin{aligned}
& + \frac{\pi ETR^2}{1-v^2} b_n b_m \left\{ nm(n+1)(m+1) \int_{-1}^{+1} P_n P_m dz - m(m+1) \right. \\
& \times \int_{-1}^{+1} \dot{P}_n P_m z dz - n(n+1) \int_{-1}^{+1} P_n \dot{P}_m z dz + 2vn(n+1) \int_{-1}^{+1} P_n \dot{P}_m z dz \\
& + 2(1-v) \int_{-1}^{+1} \dot{P}_n \dot{P}_m z^2 dz \Big\} + \frac{\pi ETR^2}{1-v^2} a_m b_n \\
& \times \left\{ 2n(n+1)(1+v) \int_{-1}^{+1} P_n P_m dz \right\}.
\end{aligned}$$

We note that we have a common combination of integrals in the $a_n a_m$ and $b_n b_m$ expressions, so extracting this form we write

$$\begin{aligned}
F_{nm}^1 &= 2 \int_{-1}^{+1} \dot{P}_n \dot{P}_m z^2 dz - m(m+1) \int_{-1}^{+1} \dot{P}_n P_m z dz - n(n+1) \int_{-1}^{+1} P_n \dot{P}_m z dz, \\
F_{nm}^2 &= -2v \left\{ \int_{-1}^{+1} \dot{P}_n \dot{P}_m z^2 dz - n(n+1) \int_{-1}^{+1} P_n \dot{P}_m z dz \right\}.
\end{aligned}$$

Now if we consider $m < n$, two substitutions into standard recurrence formulae given by Whittaker and Watson,²⁰⁸ integration by parts, the use of series expansions of $\dot{P}_m z$, \dot{P}_m and \ddot{P}_m ,²⁰⁹ and finally consideration of the orthogonal properties of Legendre functions lead to the result

$$F_{nm}^1 = 2[P_n \dot{P}_m]_{-1}^{+1} - m(m+1) \int_{-1}^{+1} \dot{P}_n P_m z dz.$$

Further series expansions of \dot{P}_m and $\dot{P}_n z$ and a close consideration of the terms generated gives rise to the conclusion that if both m and n are either odd or even the first term sums as an arithmetic progression to $2m(m+1)$ and the second term becomes $-2m(m+1)$: furthermore if m is odd and n is even or vice versa both terms are zero. By symmetry we draw the same conclusions for $n < m$ and hence

$$F_{nm}^1 = 0 \quad \text{for } n \neq m.$$

We now pass on to F_{nm}^2 . This expression is non-symmetric in the sense that it will be altered by interchanging m and n , i.e. $F_{nm}^2 \neq F_{mn}^2$; but the general theory demands symmetry so we must account for this by calculating $\frac{1}{2}(F_{nm}^2 + F_{mn}^2)$ as the coefficients of the general theory. The required integrals for F_{nm}^2 have already been examined so we may conclude immediately that if m is odd and n is even or vice versa then F_{nm}^2 is zero. If both m and n are either even or odd we have

$$F_{nm}^2 = 2vn(n+1) \quad \text{for } n < m,$$

$$F_{nm}^2 = -2vm(m+1) \quad \text{for } m < n,$$

and hence from the second relationship by interchanging m and n we obtain the inverse

$$F_{mn}^2 = -2vn(n+1) \quad \text{for } n < m.$$

The symmetry condition therefore gives the coefficient of the general theory as zero for $n < m$ and by similar reasoning for $m < n$.

Finally we consider the W'_2 term. From the recurrence formulae, series expansions of \dot{P}_m and $\dot{P}_m z$, and the orthogonal properties of Legendre functions it can be shown that

$$\int_{-1}^{+1} \dot{P}_n \dot{P}_m z^2 dz = \int_{-1}^{+1} \dot{P}_n \dot{P}_m dz$$

for $m < n$ and by symmetry for $n < m$. Thus

$$-\int_{-1}^{+1} \dot{P}_n \dot{P}_m (1-z^2) dz = 0 \quad \text{for } m \neq n.$$

We now write down some non-zero results which may be calculated using the now familiar operations on integrals of Legendre function products,

$$\int_{-1}^{+1} (\dot{P}_n)^2 z^2 dz = \frac{n}{2}(n+1)(2n-1) \int_{-1}^{+1} (\dot{P}_n)^2 dz,$$

$$\int_{-1}^{+1} P_n \dot{P}_n z dz = n \int_{-1}^{+1} (\dot{P}_n)^2 dz,$$

$$\int_{-1}^{+1} (\dot{P}_n)^2 (1-z^2) dz = n(n+1) \int_{-1}^{+1} (\dot{P}_n)^2 dz,$$

and the standard result

$$\int_{-1}^{+1} (\dot{P}_n)^2 dz = \frac{2}{2n+1}.$$

The results obtained above allow us to express W_2 in the form

$$W_2 = \frac{1}{2}(K_i a_i^2 + 2H_i a_i b_i + M_i b_i^2 + \Lambda N_i a_i^2)$$

with all other possible coefficients zero, where the K_i etc. are now the coefficients of a Taylor expansion of the energy function and are given by

$$K_i = \frac{2\pi ETR^2}{1-v^2} \{2(1+v) + \alpha[i^2(i+1)^2 - i(i+1)(1-v)]\} \int_{-1}^{+1} (P_i)^2 dz,$$

$$H_i = \frac{2\pi ETR^2}{1-v^2} \{i(i+1)(1+v)\} \int_{-1}^{+1} (P_i)^2 dz,$$

$$M_i = \frac{2\pi ETR^2}{1-v^2} \{i^2(i+1)^2 - i(i+1)(1-v)\} \int_{-1}^{+1} (P_i)^2 dz,$$

$$N_i = \frac{2\pi ETR^2}{1-v^2} i(i+1) \int_{-1}^{+1} (P_i)^2 dz.$$

11.3 Analysis in principal coordinates

Diagonalization and eigenvalue problem

Having obtained the quadratic terms of potential energy in a near-diagonal form, the eigenvalue problem is most easily solved by the introduction of a linear coordinate transformation to complete the diagonalization. We therefore start with our derived form for W_2 and complete the square to obtain

$$W_2 = \frac{1}{2} [K_i a_i^2 - D_i a_i^2 + (D_i^\frac{1}{2} a_i + M_i^\frac{1}{2} b_i)^2 + \Lambda N_i a_i^2],$$

where

$$D_i^\frac{1}{2} M_i^\frac{1}{2} = H_i,$$

so that

$$D_i = \frac{H_i^2}{M_i} = \frac{2\pi ETR^2}{1-v^2} \left\{ \frac{i(i+1)(1+v)^2}{i(i+1)-(1-v)} \right\} \int_{-1}^{+1} (P_i)^2 dz.$$

We now change coordinates from the set of a_i and b_i to the new set of a_i and x_i , where

$$x_i = D_i^\frac{1}{2} a_i + M_i^\frac{1}{2} b_i$$

so that

$$b_i = \frac{1}{M_i^\frac{1}{2}} (x_i - D_i^\frac{1}{2} a_i).$$

This gives W_2 in a diagonalized form which in line with the notation of the general theory we write as

$$A_2 = \frac{1}{2} [(K_i - D_i) a_i^2 + x_i^2 + \Lambda N_i a_i^2]$$

and we see that a_i and x_i are now the principal coordinates.

Let us now write down the modes which are associated with these principal coordinates. First if only a typical $a_r \neq 0$ we have the mode associated with this coordinate as

$$w(\theta) = a_r P_r,$$

$$u(\theta) = -\sqrt{\frac{D_r}{M_r}} a_r P'_r,$$

and we see that whereas previously there was no $u(\theta)$ component in the a_r mode, after diagonalization this is no longer the case. If only a typical $x_s \neq 0$ we have the mode associated with this coordinate as

$$w(\theta) = 0,$$

$$u(\theta) = \frac{1}{\sqrt{M_s}} x_s P'_s,$$

and we see that there is no $w(\theta)$ component in the x_s mode. Thus we may expect the x_i coordinates to play an extremely passive role in a buckling analysis. This is underlined by an examination of the diagonalized form of A_2 in which we see that we always have stability with respect to the principal coordinates x_i .

The critical load Λ^n associated with a_n is given by

$$(K_n - D_n) + \Lambda^n N_n = 0$$

and hence

$$\Lambda^n = \frac{D_n - K_n}{N_n}.$$

Now we know n to be large for a thin shell and so it is advisable at this stage to neglect 1 in comparison with n^2 following the earlier work.^{21, 57} This approximation may be used advantageously at various stages in the analysis and we adopt it wherever useful, but always with care and with an explicit reference. Within this approximation Λ^n may be reduced to

$$\Lambda^n = \frac{1-v^2}{n(n+1)} + \alpha n(n+1).$$

If we now treat Λ^n as a continuous function of n we have the situation illustrated schematically in Figure 103, in which the integer values of n are shown as solid lines. We find by simple differentiation that

$$s(s+1) = \sqrt{\frac{1-v^2}{\alpha}}$$

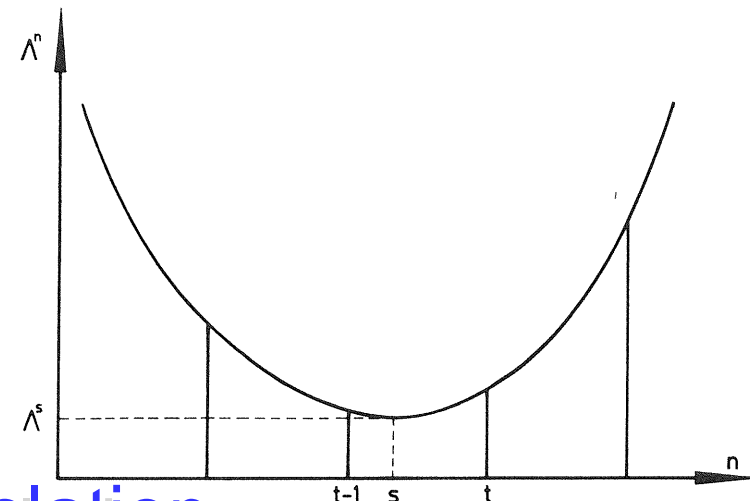


Figure 103 Λ^n treated as a continuous function of n with integers shown as solid lines

and

$$A^s = 2\sqrt{[\alpha(1 - v^2)]}.$$

Neglecting 1 in comparison with n^2 the nearest possible integer value of n gives $A^n = A^s$ which can easily be shown to be true by considering the maximum possible separation between the loads. Thus

$$A^c = A^s = 2\sqrt{[\alpha(1 - v^2)]}.$$

The buckling mode in the case of a distinct critical point has the integral n giving the lowest A ; for the schematic illustration of Figure 103 this critical mode will be P_{t-1} . However, it may happen—and this is the situation of major concern here—that we have two coincident critical loads, $A^t = A^{t-1}$, in which case we obtain simultaneous rotationally-symmetric buckling. For this to occur we must have

$$\frac{1 - v^2}{t(t + 1)} + \alpha t(t + 1) = \frac{1 - v^2}{(t - 1)t} + \alpha(t - 1)t$$

giving

$$\frac{1 - v^2}{\alpha} = t^2(t^2 - 1).$$

For this simultaneous buckling A^c is still given by A^s , and the buckling modes are now associated with P_t and P_{t-1} .

Cubic coefficients

A post-buckling analysis requires us to evaluate certain of the cubic coefficients in the expanded form of W_3 . Substituting the series expansions for $w(\theta)$ and $u(\theta)$ and eliminating the second derivatives of Legendre functions by the use of the Legendre differential equation gives W_3 in the form

$$W_3 = \frac{\pi ETR^2}{1 - v^2} \left\{ -(1 - v) a_l a_m b_n \int_0^\pi P'_l P'_m P'_n \cos \theta d\theta - n(n + 1) a_l a_m b_n \right. \\ \left. \times \int_0^\pi P'_l P'_m P_n \sin \theta d\theta - (1 + v) a_l a_m a_n \int_0^\pi P'_l P'_m P_n \sin \theta d\theta \right\}.$$

We next transform coordinates to the diagonalized set a_i and x_i . This generates the cubic form of the diagonalized A -function which may be written

$$A_3 = \frac{\pi ETR^2}{1 - v^2} \left\{ (1 - v) \sqrt{\frac{D_n}{M_n}} a_l a_m a_n \int_0^\pi P'_l P'_m P'_n \cos \theta d\theta \right. \\ \left. + \left[n(n + 1) \sqrt{\frac{D_n}{M_n}} - (1 + v) \right] a_l a_m a_n \int_0^\pi P'_l P'_m P_n \sin \theta d\theta \right\}.$$

$$- \frac{(1 - v)}{\sqrt{M_n}} a_l a_m x_n \int_0^\pi P'_l P'_m P'_n \cos \theta d\theta - \frac{n(n + 1)}{\sqrt{M_n}} a_l a_m x_n \\ \times \int_0^\pi P'_l P'_m P_n \sin \theta d\theta \Big\}.$$

Now we find from the definitions of M_n and D_n that

$$\sqrt{\frac{D_n}{M_n}} = \frac{1 + v}{n(n + 1) - (1 - v)}$$

and so A_3 becomes

$$A_3 = \frac{\pi ETR^2}{n(n + 1) - (1 - v)} a_l a_m a_n \left\{ \int_0^\pi P'_l P'_m P'_n \cos \theta d\theta + \int_0^\pi P'_l P'_m P_n \sin \theta d\theta \right\} \\ + \frac{\pi ETR^2}{(1 - v^2)\sqrt{M_n}} a_l a_m x_n \left\{ -(1 - v) \int_0^\pi P'_l P'_m P'_n \cos \theta d\theta - n(n + 1) \right. \\ \left. \times \int_0^\pi P'_l P'_m P_n \sin \theta d\theta \right\}.$$

This may also be written

$$A_3 = \frac{1}{6} A_{lmn} a_l a_m a_n + \frac{1}{2} \tilde{A}_{lmn} a_l a_m x_n$$

in which A_{lmn} and \tilde{A}_{lmn} are now the cubic coefficients in a Taylor expansion of the potential energy function.

We shall now stipulate a further condition of this analysis, namely that we assume t to be an even integer. This suggests a critical load associated with the coincidence of a Legendre function of even order and another of odd order and degree one lower. However, the associated problem in which t is odd will follow a similar pattern of analysis and we investigate it no further here, merely pointing out that Koiter²¹ states that the two problems generate the same results; his analysis includes at times a less rigorous assumption than ours in which he neglects 1 in comparison with t but we may at least conclude from his evidence that the two associated problems give rise to very similar post-buckling responses.

Anticipating the elimination of passive coordinates in the following analysis we find we need only evaluate the coefficients A_{ttt} and $A_{t-1,t-1,t}$ which may now be written

$$A_{ttt} = \frac{6\pi ETR^2}{t(t + 1) - (1 - v)} \left\{ \int_0^\pi (P'_t)^3 \cos \theta d\theta + \int_0^\pi (P'_t)^2 P_t \sin \theta d\theta \right\},$$

$$A_{t-1,t-1,t} = \frac{2\pi ETR^2}{t(t + 1) - (1 - v)} \left\{ \int_0^\pi (P'_{t-1})^2 P'_t \cos \theta d\theta + \int_0^\pi (P'_{t-1})^2 P_t \sin \theta d\theta \right\}$$

$$+ \frac{4\pi ETR^2}{(t - 1)t - (1 - v)} \left\{ \int_0^\pi (P'_{t-1})^2 P'_t \cos \theta d\theta + \int_0^\pi P'_{t-1} P'_t P_{t-1} \sin \theta d\theta \right\}.$$

A summation is included in $A_{t-1,t-1,t}$ since the general theory demands symmetric coefficients; by this we mean that a coefficient is unchanged by interchanging subscripts. The required integrals are not symmetric and so we enforce symmetry by this summation.

We now list some properties of these integrals which may be obtained by constructive use of integration by parts and the Legendre differential equation,

$$\int_0^\pi (P'_t)^3 \cos \theta d\theta = -\frac{3t(t+1)}{2} \int_0^\pi (P'_t)^2 P_t \sin \theta d\theta,$$

$$\int_0^\pi (P'_t)^2 P_t \sin \theta d\theta = \frac{t(t+1)}{2} \int_0^\pi (P'_t)^3 \sin \theta d\theta,$$

$$\begin{aligned} \int_0^\pi (P'_{t-1})^2 P'_t \cos \theta d\theta &= -t(t-1) \int_0^\pi P'_{t-1} P'_t P_{t-1} \sin \theta d\theta - \frac{t(t+1)}{2} \\ &\quad \times \int_0^\pi (P'_{t-1})^2 P_t \sin \theta d\theta, \end{aligned}$$

$$\int_0^\pi P'_{t-1} P'_t P_{t-1} \sin \theta d\theta = \frac{t(t+1)}{2} \int_0^\pi (P_{t-1})^2 P_t \sin \theta d\theta,$$

$$\int_0^\pi (P'_{t-1})^2 P_t \sin \theta d\theta = \frac{t(t-3)}{2} \int_0^\pi (P_{t-1})^2 P_t \sin \theta d\theta.$$

If we now neglect 1 in comparison with t^2 these properties reduce the required derivatives to the form

$$A_{ttt} = -\frac{9}{2} \pi ETR^2 t(t+1) \int_0^\pi (P_t)^3 \sin \theta d\theta,$$

$$A_{t-1,t-1,t} = -\frac{\pi ETR^2}{2(t-1)} t(3t+1)(3t-5) \int_0^\pi (P_{t-1})^2 P_t \sin \theta d\theta.$$

Thompson⁵⁷ evaluates the integral of the first expression by adopting the result of Adams.²¹⁰ This states that

$$\int_{-1}^{+1} P_\alpha(z) P_\beta(z) P_\gamma(z) dz = \frac{2}{2\epsilon+1} \frac{A[\epsilon-\alpha] A[\epsilon-\beta] A[\epsilon-\gamma]}{A[\epsilon]},$$

where

$$\epsilon = \frac{\alpha + \beta + \gamma}{2},$$

$$A[y] \equiv \frac{1 \cdot 3 \cdot 5 \cdot \dots \cdot (2y-1)}{1 \cdot 2 \cdot 3 \cdot \dots \cdot y} \equiv \frac{(2y-1)! 2^{-(y-1)}}{y!(y-1)!}.$$

Here no one of the quantities α , β , and γ must be greater than the sum of the other two, and $\alpha + \beta + \gamma$ must be an even integer. Thus we set $\alpha = \beta = \gamma = t$ and since t is an even integer we have

$$\int_0^\pi [P_t(\cos \theta)]^3 \sin \theta d\theta = \int_{-1}^{+1} [P_t(z)]^3 dz = \frac{2}{3t+1} \cdot \frac{A[t/2]^3}{A[3t/2]}.$$

Also if $\alpha = \beta = t-1$ and $\gamma = t$ we have

$$\begin{aligned} \int_0^\pi [P_{t-1}(\cos \theta)]^2 P_t(\cos \theta) \sin \theta d\theta &= \int_{-1}^{+1} [P_{t-1}(z)]^2 P_t(z) dz \\ &= \frac{2}{3t-1} \cdot \frac{A[t/2]^2 A[t/2-1]}{A[3t/2-1]}. \end{aligned}$$

We can now write a general result which emerges from the definition of $A[y]$,

$$A[y-1] \equiv \frac{y}{2y-1} A[y],$$

and so the above result becomes

$$\int_0^\pi (P_{t-1})^2 P_t \sin \theta d\theta = \frac{3t+1}{3(t-1)} \int_{-1}^{+1} (P_t)^3 dz.$$

Finally we find the only remaining integral by employing asymptotic expansions of the factorials and neglecting 1 in comparison with t^2 . We see that

$$\int_{-1}^{+1} (P_t)^3 dz = \frac{4\sqrt{3}}{3\pi} \frac{1}{t(t+1)},$$

giving finally after some manipulation with the condition which neglects 1 in comparison with t^2 ,

$$A_{ttt} = A_{t-1,t-1,t} = -6\sqrt{3} ETR^2.$$

Post-buckling solutions

The first step in a post-buckling analysis must be to follow a scheme for the elimination of the passive coordinates. The scheme has of course already been developed in general terms in Chapter 10 and so here we need merely to translate the general results of this process expressed by equations (10.1) to the notation of the spherical shell. This having been done we can then appeal directly to the known post-buckling solutions for a two-fold compound branching point and a potential energy function which is symmetric in one of the modes; these particular results are presented explicitly in Section 10.2. We note that the potential energy function for the sphere must be symmetric in the mode associated with a Legendre function of degree $t-1$ since $t-1$ is odd; it has previously been pointed out that a Legendre function of odd order

is 'skew-symmetric' about the equator of the sphere and therefore must induce the same change in potential energy with an amplitude of $+a$ as with an amplitude of $-a$.

Thus, after elimination of the passive coordinates, we are left with a new potential energy function $\mathcal{A}(a_{t-1}, a_t, \Lambda)$ with only two degrees of freedom and the following derivatives obtained from equations (10.1),

$$\begin{aligned}\mathcal{A}'^F_{tt} &= A'^F_{tt} = K_t - D_t + \Lambda N_t, \\ \mathcal{A}'^F_{t-1t-1} &= A'^F_{t-1t-1} = K_{t-1} - D_{t-1} + \Lambda N_{t-1}, \\ \mathcal{A}'^F_{tt} &= A'^F_{tt} = N_t, \\ \mathcal{A}'^F_{t-1t-1} &= A'^F_{t-1t-1} = N_{t-1}, \\ \mathcal{A}'^F_{ttt} &= A'^F_{ttt}, \\ \mathcal{A}'^F_{t-1t-1t} &= A'^F_{t-1t-1t},\end{aligned}$$

which after some algebra lead to the results of interest,

$$\begin{aligned}\mathcal{A}'^F_{tt} &= \frac{2\pi ETR^2}{1-v^2} \left\{ 2(1-v^2) \frac{t}{t-1} - t(t+1)\Lambda \right\} \frac{2}{2t+1}, \\ \mathcal{A}'^F_{t-1t-1} &= \frac{2\pi ETR^2}{1-v^2} \left\{ 2(1-v^2) \frac{t}{t+1} - (t-1)t\Lambda \right\} \frac{2}{2t-1}, \\ \mathcal{A}'^C_{tt} &= -\frac{4\pi ETR^2}{1-v^2} \frac{t(t+1)}{2t+1}, \\ \mathcal{A}'^C_{t-1t-1} &= -\frac{4\pi ETR^2}{1-v^2} \frac{(t-1)t}{2t-1}, \\ \mathcal{A}'^C_{ttt} &= \mathcal{A}'^C_{t-1t-1t} = -6\sqrt{3}ETR^2.\end{aligned}$$

The first two of these results constitute the quadratic coefficients of potential energy on the fundamental path and have been included to enable a comparison with Koiter's work,²¹ we find after using his approximation of neglecting 1 in comparison with t that the two analyses are in direct agreement. The same may also be said of the cubic terms.

The post-buckling path tangents can now be determined from the particular solutions of Section 10.2. In terms of the critical modes $t-1$ and t we obtain the results

$$\begin{aligned}1 \quad \frac{\dot{a}_{t-1}}{\dot{a}_t} \Big|_c &= 0, \quad \frac{\dot{\Lambda}}{\dot{a}_t} \Big|_c = -\frac{\mathcal{A}_{ttt}}{2\mathcal{A}'_{tt}}, \\ 2 \quad \frac{\dot{a}_{t-1}}{\dot{a}_t} \Big|_c &= +\sqrt{\left(\frac{2\mathcal{A}'_{tt}}{\mathcal{A}'_{t-1t-1}} - \frac{\mathcal{A}_{ttt}}{\mathcal{A}_{t-1t-1t}} \right)} \Big|_c, \quad \frac{\dot{\Lambda}}{\dot{a}_t} \Big|_c = -\frac{\mathcal{A}_{t-1t-1t}}{\mathcal{A}'_{t-1t-1}}, \\ 3 \quad \frac{\dot{a}_{t-1}}{\dot{a}_t} \Big|_c &= -\sqrt{\left(\frac{2\mathcal{A}'_{tt}}{\mathcal{A}'_{t-1t-1}} - \frac{\mathcal{A}_{ttt}}{\mathcal{A}_{t-1t-1t}} \right)} \Big|_c, \quad \frac{\dot{\Lambda}}{\dot{a}_t} \Big|_c = -\frac{\mathcal{A}_{t-1t-1t}}{\mathcal{A}'_{t-1t-1}}.\end{aligned}$$

These are of course expressed in terms of the post-buckling rates but we again note that the solution rays in rate space may be mapped directly into coordinate space to give the post-buckling tangents. Substituting our known \mathcal{A} -derivatives and neglecting 1 in comparison with t^2 these may be reduced to

$$\begin{aligned}1 \quad \frac{\dot{a}_{t-1}}{\dot{a}_t} \Big|_c &= 0, \quad \frac{\dot{\Lambda}}{\dot{a}_t} \Big|_c = -\frac{3\sqrt{3}(1-v^2)}{2\pi(t+\frac{1}{2})}, \\ 2 \quad \frac{\dot{a}_{t-1}}{\dot{a}_t} \Big|_c &= +\sqrt{\left(\frac{t+\frac{3}{2}}{t-\frac{1}{2}} \right)}, \quad \frac{\dot{\Lambda}}{\dot{a}_t} \Big|_c = -\frac{3\sqrt{3}(1-v^2)}{\pi(t-\frac{1}{2})}, \\ 3 \quad \frac{\dot{a}_{t-1}}{\dot{a}_t} \Big|_c &= -\sqrt{\left(\frac{t+\frac{3}{2}}{t-\frac{1}{2}} \right)}, \quad \frac{\dot{\Lambda}}{\dot{a}_t} \Big|_c = -\frac{3\sqrt{3}(1-v^2)}{\pi(t-\frac{1}{2})}.\end{aligned}$$

These solution rays in rate space (or tangents in coordinate space) are shown in Figure 104. The first solution is of course the post-buckling path of non-zero slope given by Thompson's analysis of the distinct critical point,⁵⁷ while the other two solutions are symmetrically opposed about the a_t (or a_{t-1}) axis as we would expect. We note that if we neglect 1 in comparison with t these solutions agree with those of Koiter.²¹

Each of the two coupled modes obtained from our compound branching analysis combines a Legendre function of even degree t which is symmetrically disposed about the equator of the sphere with one of odd degree $t-1$ which is skew-symmetric about the equator. It is thus clear that for a given reduction in load the deflection of the north pole is largely preserved, while the deflection of the south pole is much reduced and the deformation pattern approaches the 'single dimple' post-buckling shape observed experimentally.¹⁵⁰

Finally let us consider the situation when the two critical points are not coincident but are separated by a small-but-finite load increment on the fundamental path. In this case we would expect the post-buckling behaviour at each critical point to be given by an analysis which treats it as distinct, whereas the large-deflection behaviour would resemble the post-buckling paths of the above analysis. This situation was envisaged by Chilver⁷⁰ who has presented the plan view of these paths in coordinate space in Figure 4 of this reference. We have here interpreted Chilver's result for the special case of the spherical shell in Figure 105, which shows the plan view of the post-buckling equilibrium paths when the critical loads are (a) well separated, (b) a small-but-finite distance apart, and finally (c) completely coincident. We see that Thompson's 'asymmetric' path in the a_t direction, which appears unchanged in our simultaneous buckling solution, will clearly exist for any, large or small, separation of the critical loads. However, in case (b) of Figure 105 the path of zero slope in the a_{t-1} direction, while retaining symmetry about the a_t axis is

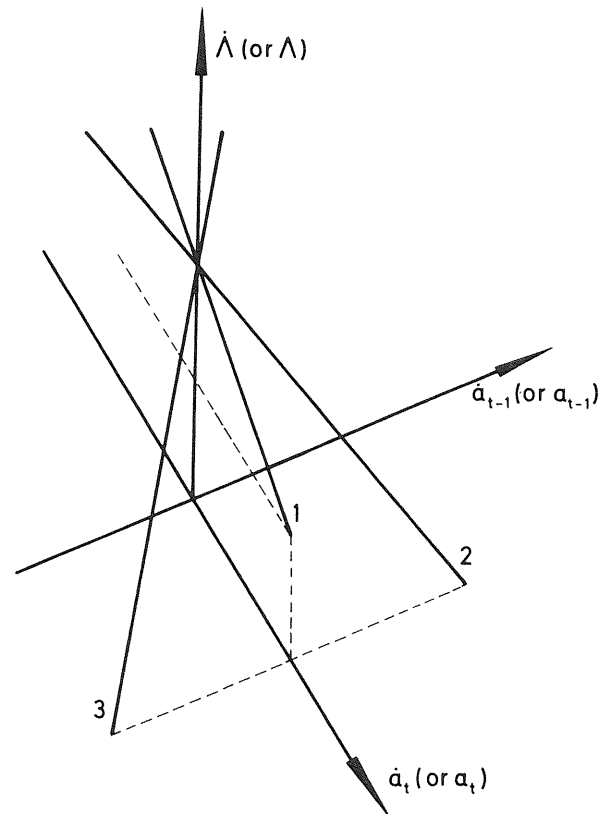


Figure 104 The post-buckling solutions for the rotationally-symmetric branching of a complete spherical shell

altered by increasing deflections until it resembles the paths of non-zero slope which are given by the second and third solutions above. This implies the existence of the further complementary path, again symmetric about the a_t axis and close to these paths, which does not pass through the fundamental path.

11.4 Analysis in original coordinates

We next illustrate the W -analysis for compound branching by presenting a post-buckling study of the same spherical shell problem without resorting to a diagonalizing transformation. We note that although this process is conceptually different from the earlier diagonalized treatment, the only significant

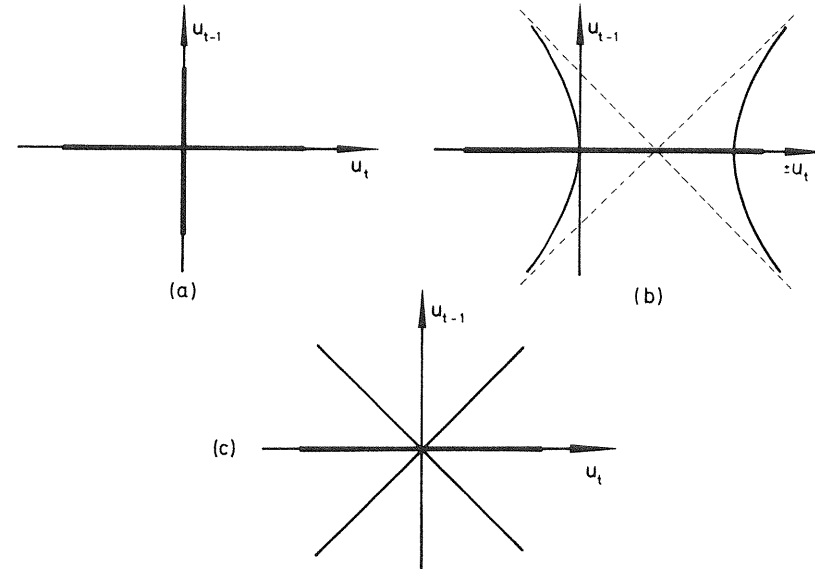


Figure 105 Path contortions during the coalescence of the critical points of the spherical shell

analytical difference is in the elimination of passive coordinates; this transforming process is not dependent on the critical value of Λ and so we are able to follow the scheme of the general theory without first having to perform a non-diagonalized eigenvalue analysis to find the appropriate critical load.

We remember from Section 11.2 that the quadratic terms of potential energy are finally obtained in the form

$$W_2 = \frac{1}{2}(K_i a_i^2 + 2H_i a_i b_i + M_i b_i^2 + \Lambda N_i a_i^2),$$

where the K_i , etc. are the coefficients of a Taylor expansion of the potential energy and are given explicitly in the above section. The cubic terms are written

$$W_3 = \frac{\pi ETR^2}{1 - v^2} \left\{ -(1 - v) a_i a_m b_n \int_0^\pi P'_l P'_m P'_n \cos \theta d\theta - n(n+1) a_i a_m b_n \right. \\ \left. \times \int_0^\pi P'_l P'_m P_n \sin \theta d\theta - (1 + v) a_i a_m a_n \int_0^\pi P'_l P'_m P_n \sin \theta d\theta \right\}.$$

Elimination of passive coordinates

The first step in this process must be to find a valid segregation between active and passive coordinates. We know that we have a two-fold compound

branching point on the fundamental path and from our knowledge of the problem it becomes clear that the coordinates a_{t-1} and a_t must play the active role in the analysis. We therefore have to eliminate two types of passive coordinates, first the complete set of b_i coordinates and secondly the remaining a_i coordinates which we henceforth write as a_s , where $s \neq t-1$ or t . Now in the diagonalized analysis we were able to appeal directly to the results of the elimination of passive coordinates perturbation scheme since all of the required derivatives of passive coordinates were known to be zero from the general theory, but without diagonalization this is no longer the case; it therefore becomes necessary to look at the non-diagonalized perturbation scheme in more detail.

Equations (10.2) tell us that

$$\frac{\partial}{\partial q_i} W_\alpha = W_{\alpha i} + W_{\alpha\beta} q_\beta = 0$$

in the notation of the general theory. We shall first write these equations explicitly for the active coordinate $q_i = a_{t-1}$. Setting $q_\alpha = b_j$ we obtain

$$\begin{aligned} M_s \frac{\partial b_s}{\partial a_{t-1}} + H_s \frac{\partial a_s}{\partial a_{t-1}} &\Big|^\text{F} = 0, \\ H_{t-1} + M_{t-1} \frac{\partial b_{t-1}}{\partial a_{t-1}} &\Big|^\text{F} = 0, \\ M_t \frac{\partial b_t}{\partial a_{t-1}} &\Big|^\text{F} = 0, \end{aligned}$$

and then setting $q_\alpha = a_s$ yields

$$H_s \frac{\partial b_s}{\partial a_{t-1}} + (K_s + \Lambda N_s) \frac{\partial a_s}{\partial a_{t-1}} \Big|^\text{F} = 0.$$

The solutions to these equations are

$$\begin{aligned} \frac{\partial b_s}{\partial a_{t-1}} \Big|^\text{F} &= \frac{\partial a_s}{\partial a_{t-1}} \Big|^\text{F} = \frac{\partial b_t}{\partial a_{t-1}} \Big|^\text{F} = 0, \\ \frac{\partial b_{t-1}}{\partial a_{t-1}} \Big|^\text{F} &= -\frac{H_{t-1}}{M_{t-1}}. \end{aligned}$$

Secondly by setting $q_i = a_t$ we obtain from a similar set of equations

$$\begin{aligned} \frac{\partial b_s}{\partial a_t} \Big|^\text{F} &= \frac{\partial a_s}{\partial a_t} \Big|^\text{F} = \frac{\partial b_{t-1}}{\partial a_t} \Big|^\text{F} = 0, \\ \frac{\partial b_t}{\partial a_t} \Big|^\text{F} &= -\frac{H_t}{M_t}. \end{aligned}$$

The substitution of these results into equations (10.3) of the general theory now leads to the necessary derivatives of a new energy function $\mathcal{W}(a_{t-1}, a_t, \Lambda)$ as follows

$$\begin{aligned} \mathcal{W}_{tt}^F &= K_t - \frac{H_t^2}{M_t} + \Lambda N_t, \\ \mathcal{W}_{t-1,t-1}^F &= K_{t-1} - \frac{H_{t-1}^2}{M_{t-1}} + \Lambda N_{t-1}, \\ \mathcal{W}_{t-1,t}^F &= \mathcal{W}'_{t-1,t}^F = 0, \\ \mathcal{W}'_{tt}^F &= N_t, \\ \mathcal{W}'_{t-1,t-1}^F &= N_{t-1}, \\ \mathcal{W}_{ttt}^F &= \frac{6\pi ETR^2}{t(t+1)-(1-v)} \left\{ \int_0^\pi (P'_t)^3 \cos \theta d\theta + \int_0^\pi (P'_t)^2 P_t \sin \theta d\theta \right\}, \\ \mathcal{W}_{t-1,t-1,t}^F &= \frac{2\pi ETR^2}{t(t+1)-(1-v)} \left\{ \int_0^\pi (P'_{t-1})^2 P'_t \cos \theta d\theta + \int_0^\pi (P'_{t-1})^2 P_t \sin \theta d\theta \right\} \\ &\quad + \frac{4\pi ETR^2}{t(t-1)-(1-v)} \left\{ \int_0^\pi (P'_{t-1})^2 P'_t \cos \theta d\theta \right. \\ &\quad \left. + \int_0^\pi P'_{t-1} P'_t P_{t-1} \sin \theta d\theta \right\}, \\ \mathcal{W}_{t-1,tt}^F &= \mathcal{W}_{t-1,t-1,t-1}^F = 0. \end{aligned}$$

Here as before we have assumed that t is an even integer. We find that the \mathcal{W} -function is in fact diagonalized and on closer inspection it is revealed that each of the above derivatives is equal to the corresponding derivative of the earlier \mathcal{A} -function. We therefore need take this analysis no further here, merely pointing out that both eigenvalue and post-buckling analyses will naturally generate the same results as the diagonalized analysis of the previous section.

Finally it is worth noting that the buckling of shells other than spherical has been briefly summarized in the General Introduction of Chapter 2. Excellent review articles have been presented by Fung and Sechler²¹¹ in 1960 and by Hutchinson and Koiter⁴⁴ in 1970.

12

COMPOUND FAILURE OF COLUMNS

12.1 Introduction

In Chapter 13, which closes this monograph, we shall delineate the role of branching studies in the important field of structural optimization, and as a preliminary to this we first examine some coupling phenomena in the compound failure of columns or struts. Here we shall not make rigorous application of our general branching theory, but rather present some simple *ad hoc* engineering analyses: but in the spirit of the general studies we shall focus attention on the asymptotic equations of imperfection-sensitivity and we shall see that they have exactly the same form as those derived earlier in the monograph. In this way some useful unity of outlook is achieved.

12.2 The thin-walled strut

Analysis of Van der Neut

We examine first the behaviour of an idealized thin-walled compression member following the analysis of Van der Neut.¹⁴⁵ The cross-section of the strut is shown in Figure 106 and comprises two flanges of thickness h and breadth b . The depth of the cross-section is $2c$ and we restrict attention to bending about the axis XX . The flange plates are assumed to be simply supported along their long edges by an unspecified web which merely serves to maintain the structural integrity of the system and does not contribute to the transmission of axial stresses.

The member is assumed to be linearly elastic throughout with Young's Modulus E , Poisson's Ratio ν and second moment of area I , and it carries an axial compressive load K . The length of the strut is L , where $h \ll b \ll L$, and both of the ends are assumed to be pin-jointed.

Clearly we have two important loads for the system. If the flange plates do not buckle, the column will become unstable at the *overall* Euler buckling load

$$K_e = \frac{\pi^2 EI}{L^2}.$$

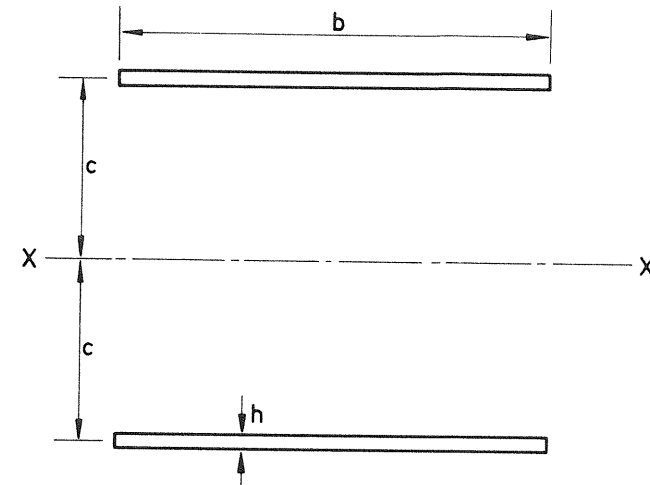


Figure 106 Van der Neut's idealized cross-section

Conversely, if the column axis does not bend, the simply-supported flange plates would become unstable at the *local* buckling load

$$K_l = \frac{2\pi^2 E}{3(1-\nu^2)} \cdot \frac{h^3}{b}.$$

Now, following Van der Neut, we will deem the strut to have failed once its centroidal axis first bends at the *bending* buckling load K_b , this being a reasonable assumption because although an Euler column exhibits a stable-symmetric point of bifurcation its post-buckling strength is very limited. Thus if $K_e < K_b$ the strut will clearly 'fail' by simple Euler buckling at $K_b = K_e$. Alternatively, if $K_l \ll K_e$ the simply-supported flange plates will buckle at $K = K_l$. This stable-symmetric buckling does not, however, exhaust the load-carrying capacity of the plates which can carry an appreciable load in the initial post-buckling range with, however, an effective Young's Modulus of ηE , where η is of the order of 1/2·45. It is clear then that the column will eventually fail by overall Euler action at a load given by

$$K_b = \eta K_e.$$

This tangent modulus approach of course assumes that the new reduced stiffness is 'smeared' along the whole length of the strut. Finally we have a domain of compound failure at $K_b = K_l$ in which overall buckling and local buckling occur simultaneously, giving us the three domains of Figures 107 and 108. In the latter figure the ratio K_e/K_l is to be thought of as a geometric

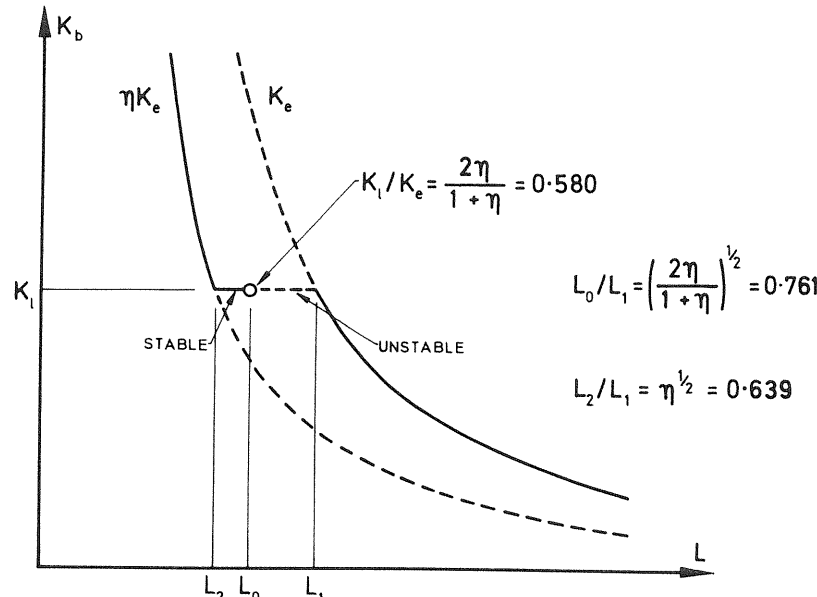


Figure 107 Summary of the response of the perfect system (after Van der Neut 1968)

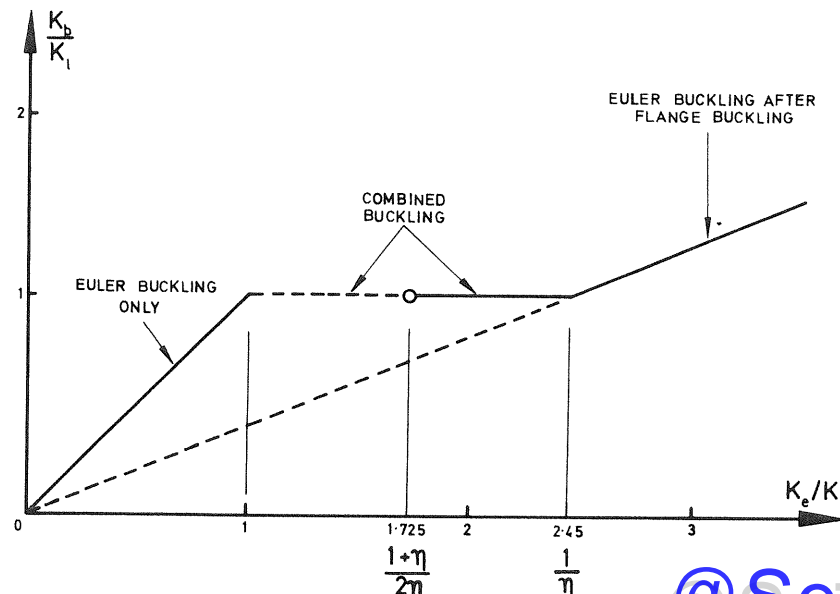


Figure 108 Convenient representation of the response of the perfect system (after Van der Neut 1968)

parameter for our family of struts, and by a Shanley-type analysis Van der Neut showed that the initial post-buckling in the combine mode changes from being unstable to stable at a value of

$$\frac{K_e}{K_l} = \frac{1+\eta}{2\eta}.$$

So far we have only considered perfect systems but we shall now imagine each flange plate to have an initial imperfection in the form of its sinusoidal buckling mode of amplitude αh . The effective value of the Young's Modulus of the plates will then change gradually on loading from E to ηE as the local buckling develops, so knowing the response of the plates it would be an easy matter to compute the bending load which would be given approximately by

$$K_b = \eta(K) K_e.$$

This calculation was in fact made by Van der Neut¹⁴⁵ and his results are shown in Figure 109 for values of α between 0 and 0.4.

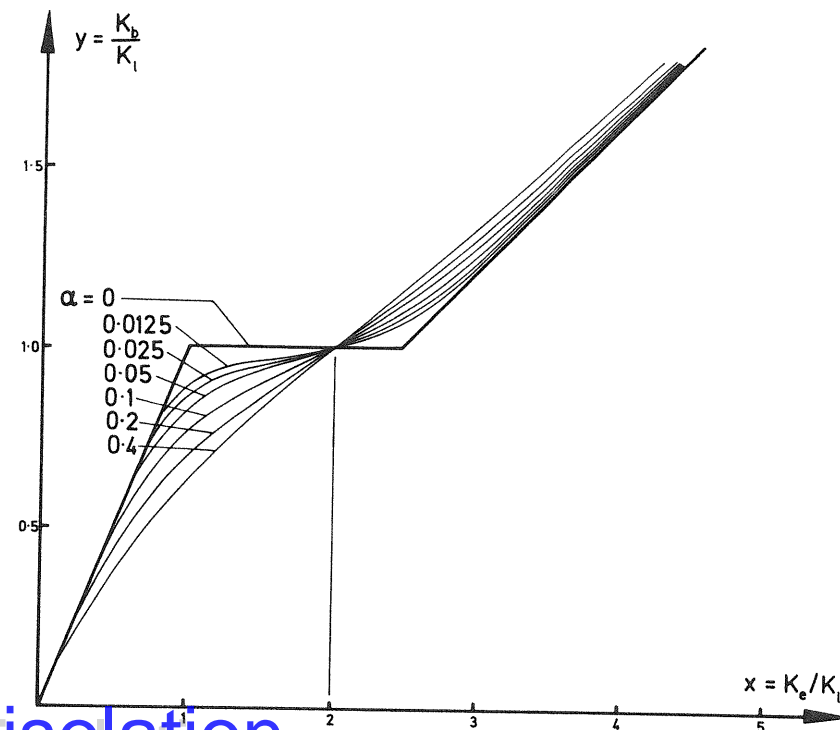


Figure 109 The response of imperfect systems obtained by Van der Neut (after Van der Neut 1968)

We see that there is a quite severe imperfection-sensitivity when the geometric parameter $x = K_e/K_i$ takes the value one due to an interaction between the two buckling modes which decays away as the ratio changes from unity. The imperfection curves pass through a single point at $x = 2$ which rather curiously is not exactly the value at which the Shanley analysis predicts a change in the post-buckling stability. For $x > 2$ imperfections are seen to be beneficial.

In Section 13.8 we shall use these results to examine quantitatively how the compounded imperfection-sensitivity at $x = 1$ tends to erode the benefits of a simultaneous mode design.

Analysis of Koiter

These results of Van der Neut have been confirmed quite recently by Koiter and Kuiken, who made a careful application of Koiter's general branching theory to the same structural model. As well as offering some welcome support for the 'smearing' approximation, this new study highlights the mechanics of the nonlinear interaction between the buckling modes and gives in addition useful asymptotic power laws of the type derived in this monograph.

The indices of these laws are shown in the diagram of Figure 110 and we see that for $x = 1$ we have a severe imperfection-sensitivity governed by a one-half power law as for an asymmetric point of bifurcation. For $x > 1$ we have a

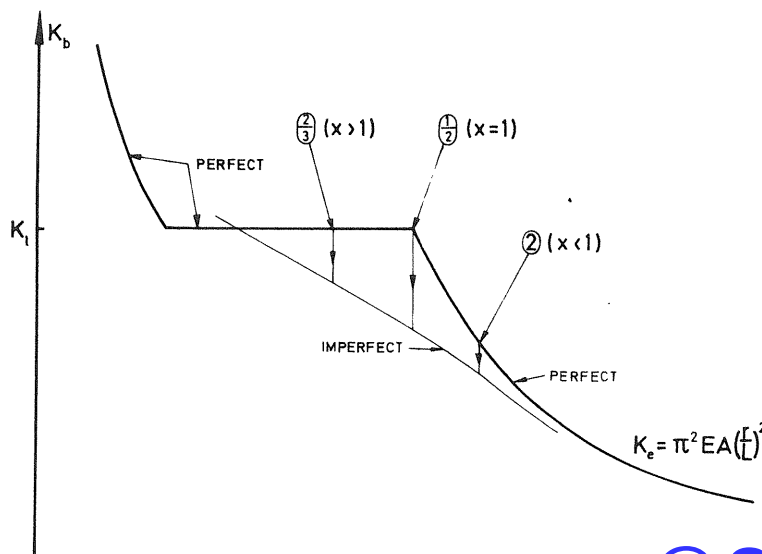


Figure 110 Asymptotic results for thin-walled columns²¹⁷

less severe two-thirds power law as for an unstable-symmetric point of bifurcation, while for $x < 1$ we have a very mild imperfection-sensitivity governed by a power of two. We shall show in the following section that an identical set of indices arises in the response of reticulated columns.

We shall not here reproduce the Koiter and Kuiken analysis, but simply note that it can be analogued by the three-degree-of-freedom energy function

$$A(u_1, A, \varepsilon) = (1 - A)(u_1^2 + u_2^2) + (A_E - A)u_3^2 + 2Cu_3(u_2^2 - u_1^2) + u_1^4 + u_2^4 - 2A\varepsilon(u_1 + u_2),$$

where C is a constant and A_E represents the geometric parameter x .

12.3 The reticulated strut

In view of the above imperfection-sensitivity for thin-walled columns, it seems reasonable to suppose that a similar phenomenon will occur in the buckling of a reticulated or triangulated column such as that shown in Figure 111: and after the confirmed success of the 'smearing' analysis with its effective value of E , it is tempting to try a similar engineering analysis for a reticulated column. This we shall now do, and we obtain, interestingly enough, the *same set of indices* that we have just observed in Koiter's analysis of the thin-walled column.

This result is all the more remarkable because we have based our 'smeared' analysis on a linear eigenvalue approximation for the component short columns. So we see that a linearized 'smeared' analysis supplies us with large-deflection information that could only be obtained rigorously by a nonlinear branching study along the lines of the Koiter and Kuiken analysis.

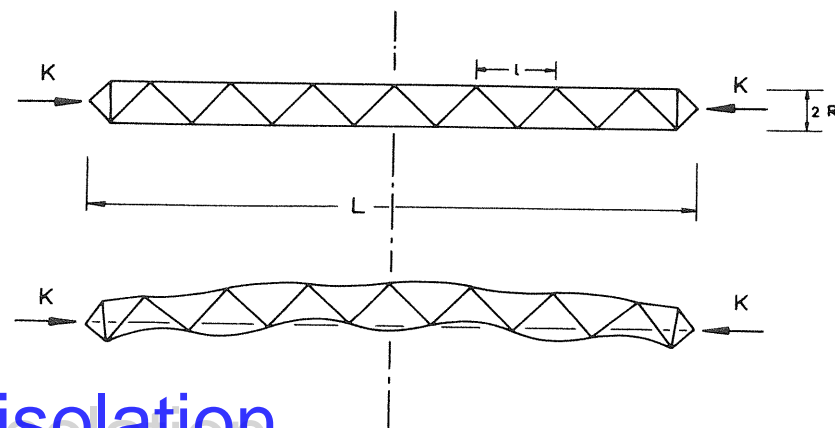


Figure 111 A reticulated or triangulated column

This having been said, we must hasten to add that for reticulated structures of more complex shape an engineering analysis will usually not be available, so that recourse must be made to a general branching theory. We have added our simple analysis here merely to draw attention to the dangers of imperfection-sensitivity in large reticulated structures which will be particularly severe if use is made of the principle of simultaneous mode design.

Theory

We consider a built-up column of overall length L , pinned at its ends and carrying an axial compressive load K . Each flange of this column is assumed to comprise a chain of short pin-ended struts of length l , where $1 \ll L$. The structural integrity of the overall column is maintained by an unspecified web, which could perhaps be a triangulation as in Figure 111. The web is assumed to play no part in the transmission of axial forces, but serves to locate the small pins at a distance R from the centre line and to carry shear forces as the main column deflects.

For the small struts we write the modulus as E , area a , length l , load P , second moment of area i and radius of gyration r . For the large column we have similarly E , $A = 2a$, L , $K = 2P$, $I = AR^2$ and R .

We can now write down two uncoupled failure loads as follows. In the absence of any 'local' buckling of the short struts, the main column will buckle at the *Euler buckling load*

$$K_E = \frac{\pi^2 E A R^2}{L^2}.$$

In the absence of this overall buckling, the elemental struts would fail at the *local buckling load*

$$K_L = 2 \frac{\pi^2 E a r^2}{l^2}.$$

The ratio of these two buckling loads we write as a geometric parameter

$$x = \frac{K_E}{K_L} = \frac{R^2 l^2}{L^2 r^2}.$$

We shall now assume that the elemental struts are all (equally) imperfect with an initial sinusoidal amplitude b_0 , so that local deformations develop from the first application of load. In this circumstance, the main column will buckle at a load close to the *tangent modulus load* corresponding to the current effective axial stiffness of the short struts, and it is this load that we shall proceed to evaluate.

To assess the deteriorating axial stiffness of the short columns we now perform a linear eigenvalue analysis, assuming for the time being that they are axially incompressible and drawing on the exact formulation of Chapter 1. The change in lateral deflection is written as

$$w = w_T - w_0$$

so the change of curvature is

$$\chi = \ddot{w}$$

and the total potential energy functional becomes

$$V = \frac{1}{2} E i \int_0^l \ddot{w}^2 dx - \frac{1}{2} P \int_0^l (\dot{w}^2 + 2 \dot{w} \dot{w}_0) dx.$$

Writing

$$w_0(x) = b_0 \sin \frac{\pi x}{l},$$

$$w(x) = b \sin \frac{\pi x}{l},$$

we obtain

$$V = \frac{1}{2} I \left(\frac{\pi}{l} \right)^2 \left\{ \frac{1}{2} E i \left(\frac{\pi}{l} \right)^2 b^2 - \frac{1}{2} P b^2 - P b b_0 \right\}$$

and setting $\partial V / \partial b = 0$ gives us

$$b = \frac{P b_0}{P_L - P},$$

where

$$P_L = \frac{\pi^2 E i}{l^2}.$$

We might note in passing that it is this relationship between b and P that gives us the well known Southwell plot. The change in end shortening is then

$$\epsilon = \frac{1}{2} b_0^2 l \left(\frac{\pi}{l} \right)^2 \frac{P(P_L - \frac{1}{2} P)}{(P_L - P)^2}$$

and differentiating to find the incremental stiffness we have

$$\frac{d\epsilon}{dP} = \frac{1}{2} b_0^2 l \left(\frac{\pi}{l} \right)^2 \frac{P_L^2}{(P_L - P)^3}.$$

So far we have assumed the elemental struts to be axially incompressible, but it is now adequate for our present purposes simply to add in an EA term to give us the effective current Young's Modulus

$$\tilde{E} = 1 \left/ \left(\frac{1}{E} + \frac{a d\epsilon}{l dP} \right) \right.$$

which becomes

$$\tilde{E} = E \left(1 + \frac{ab_0^2}{2i} \frac{P_L^3}{(P_L - P)^3} \right)^{-1}.$$

Finally, using this as an effective value of Young's Modulus in the well known Euler formula we obtain the buckling load

$$K_B = \frac{\pi^2 \tilde{E} I}{L^2}$$

and the relation

$$y = x \frac{(1-y)^3}{\alpha^2 + (1-y)^3},$$

where $y = K_B/K_L$ and

$$\alpha^2 = \frac{b_0^2}{2r^2}.$$

With $\alpha = 0$ for zero imperfection we see that y is equal to x or 1, and we have the situation shown schematically in Figure 112 which is completely analogous to Figure 109 for the thin-walled strut.

For the completely coincident case of $x = 1$ we can readily derive the asymptotic formula of imperfection-sensitivity

$$1 - y = \alpha^{\frac{1}{3}}.$$

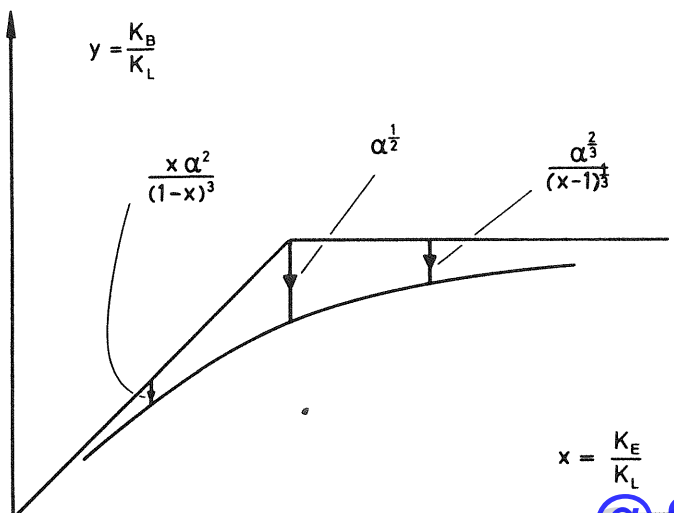


Figure 112 Convenient representation of the response of the reticulated column

For $x > 1$ we have similarly

$$1 - y = \frac{\alpha^{\frac{1}{3}}}{(x-1)^{\frac{1}{3}}},$$

while for $x < 1$ we have

$$x - y = \frac{x\alpha^2}{(1-x)^3}.$$

We see that the power indices of $\frac{1}{3}$, $\frac{1}{2}$, 2 which are shown in Figure 113 are identical to those of Koiter and Kuiken shown in Figure 110. It is interesting to note, therefore, that the Koiter and Kuiken indices are simply a function of the plate buckling, rather than the plate post-buckling, since we have retrieved them without mention of element post-buckling.

We finally draw attention to the magnified imperfection-sensitivity of $\alpha^{\frac{1}{3}}$ which is induced by interactive effects between the overall and local buckling, a theme to which we shall be returning in Chapter 13.

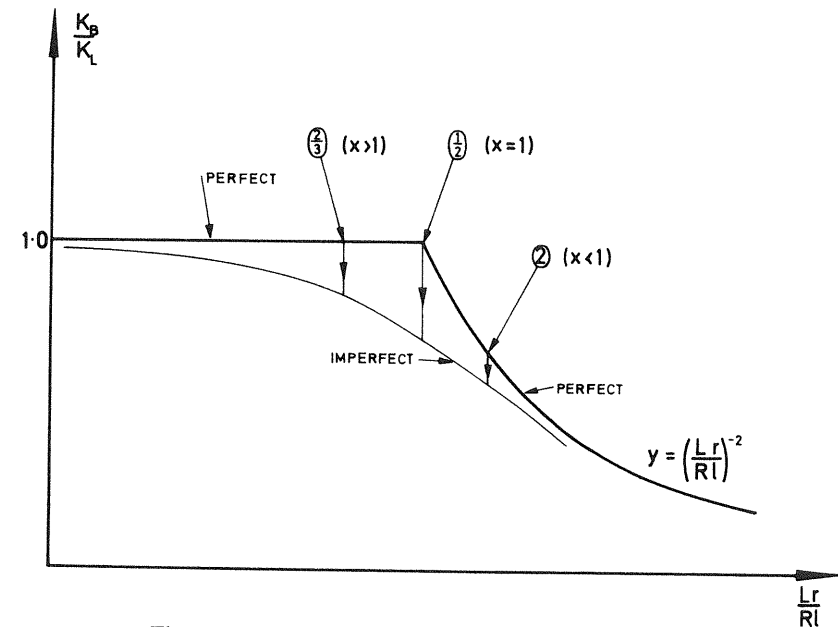


Figure 113 Asymptotic results for reticulated columns

Experiments

It is felt that some simple and illuminating experiments could usefully be performed on such a reticulated column, and we here make a few observations on the experimental problem.

which becomes

$$\tilde{E} = E \left(1 + \frac{ab_0^2}{2i} \frac{P_L^3}{(P_L - P)^3} \right)^{-1}.$$

Finally, using this as an effective value of Young's Modulus in the well known Euler formula we obtain the buckling load

$$K_B = \frac{\pi^2 \tilde{E} I}{L^2}$$

and the relation

$$y = x \frac{(1-y)^3}{\alpha^2 + (1-y)^3},$$

where $y = K_B/K_L$ and

$$\alpha^2 = \frac{b_0^2}{2r^2}.$$

With $\alpha = 0$ for zero imperfection we see that y is equal to x or 1, and we have the situation shown schematically in Figure 112 which is completely analogous to Figure 109 for the thin-walled strut.

For the completely coincident case of $x = 1$ we can readily derive the asymptotic formula of imperfection-sensitivity

$$1 - y = \alpha^{\frac{1}{3}}.$$

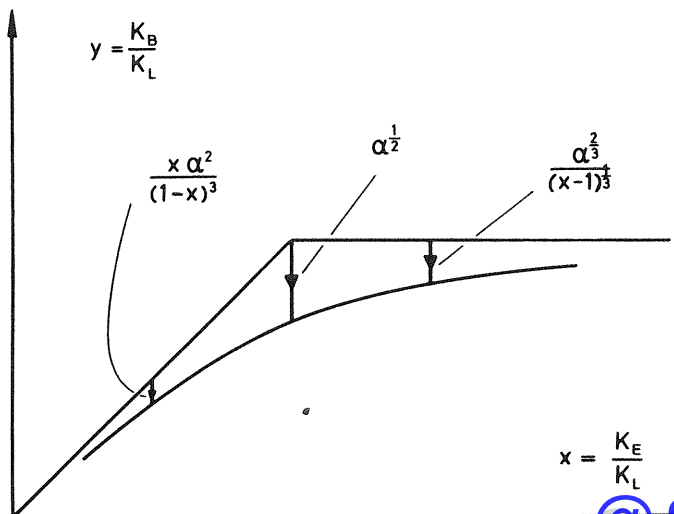


Figure 112 Convenient representation of the response of the reticulated column

For $x > 1$ we have similarly

$$1 - y = \frac{\alpha^{\frac{1}{3}}}{(x-1)^{\frac{1}{3}}},$$

while for $x < 1$ we have

$$x - y = \frac{x\alpha^2}{(1-x)^3}.$$

We see that the power indices of $\frac{1}{3}$, $\frac{1}{2}$, 2 which are shown in Figure 113 are identical to those of Koiter and Kuiken shown in Figure 110. It is interesting to note, therefore, that the Koiter and Kuiken indices are simply a function of the plate buckling, rather than the plate post-buckling, since we have retrieved them without mention of element post-buckling.

We finally draw attention to the magnified imperfection-sensitivity of $\alpha^{\frac{1}{3}}$ which is induced by interactive effects between the overall and local buckling, a theme to which we shall be returning in Chapter 13.

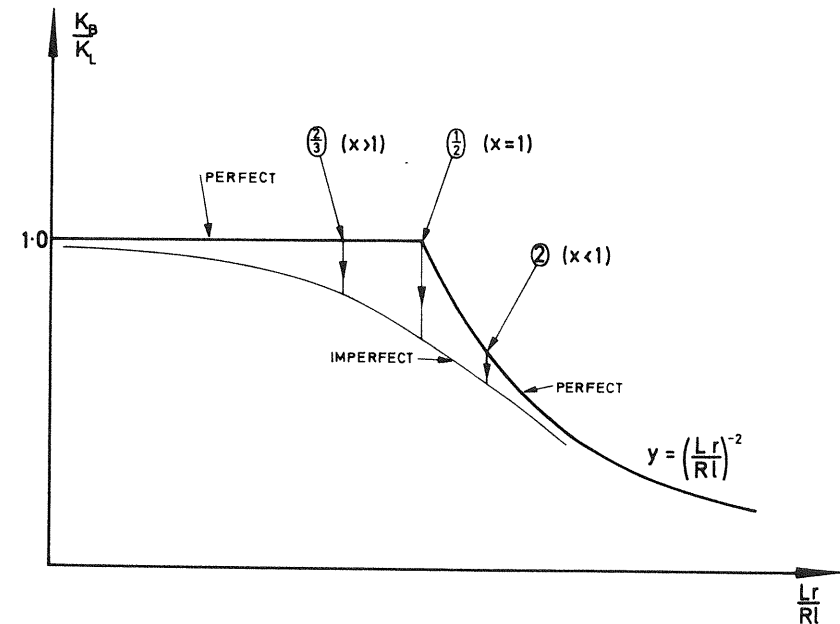


Figure 113 Asymptotic results for reticulated columns

Experiments

It is felt that some simple and illuminating experiments could usefully be performed on such a reticulated column, and we here make a few observations on the experimental problem.

Assuming that we were to make a triangulated column similar to that of Figure 111 we can observe that the minor slenderness-ratio l/r is held to a fairly large value by the yield strain of the material. This means that to approach the simultaneous buckling at $x = 1$ the major slenderness-ratio L/R must also be large, which will pose some experimental problems that can be alleviated by the use of a rubber or plastic material.

This difficulty is not influenced by the number of bays, which should therefore be as small as is consistent with the 'smearing' approximation since joints are expensive to manufacture. It follows that the rigid diagonal members should be very inclined, rather than at 45° as shown in Figure 111.

12.4 The mild-steel strut

To compare and contrast with the work of the two preceding sections, we shall now look at the compound failure characteristics of a compact mild-steel column.

We consider, then, the situation of Figure 114 in which a pair of coaxial compressive forces is resisted by a curved member made from mild steel and of length L , cross-sectional area A and height a_0 as shown. We shall assume that all deformations take place in the plane of the paper with the corresponding bending stiffness EAr^2 , where E is the Young's Modulus and r is the appropriate radius of gyration: the cross-section is of course assumed to be symmetric about the relevant centroidal axis.

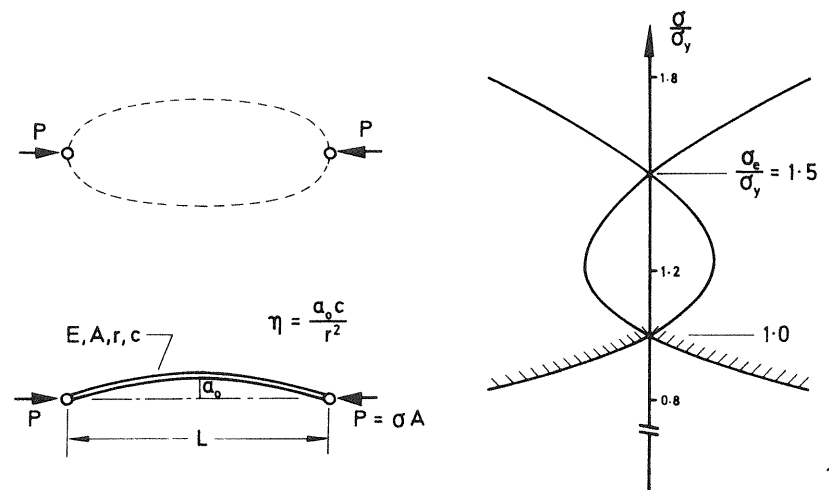


Figure 114 The compact mild-steel column with the imperfection-sensitivity for $\sigma_e > \sigma_y$

For this column we shall focus attention on two primary modes of failure, the squash mode which arises when the stress $\sigma = P/A$ in a short, thick, perfect column reaches the yield stress of the steel σ_y , and the elastic buckling mode which arises when the stress in a long, slender, perfect column reaches the Euler buckling stress given by

$$\sigma_e = \pi^2 E \left(\frac{r}{L} \right)^2.$$

The failure criterion for the initially curved members is now taken as the occurrence of first yield which will be located in an extreme fibre at the centre of the strut, so we can use the well known Perry equation

$$\sigma = \frac{1}{2} [\sigma_y + (1 + \eta) \sigma_e] \pm \sqrt{\{ \frac{1}{4} [\sigma_y + (1 + \eta) \sigma_e]^2 - \sigma_y \sigma_e \}}.$$

Here η can be regarded as a dimensionless imperfection parameter defined by

$$\eta = \frac{a_0 c}{r^2},$$

where c is the distance from the centroidal axis to the extreme fibre in the plane of interest.

Three examples of imperfection-sensitivity curves obtained from this equation for columns of differing σ_y/σ_e ratios are here presented in Figures 114 and 115. In each of these cases the Perry equation in its present form yields

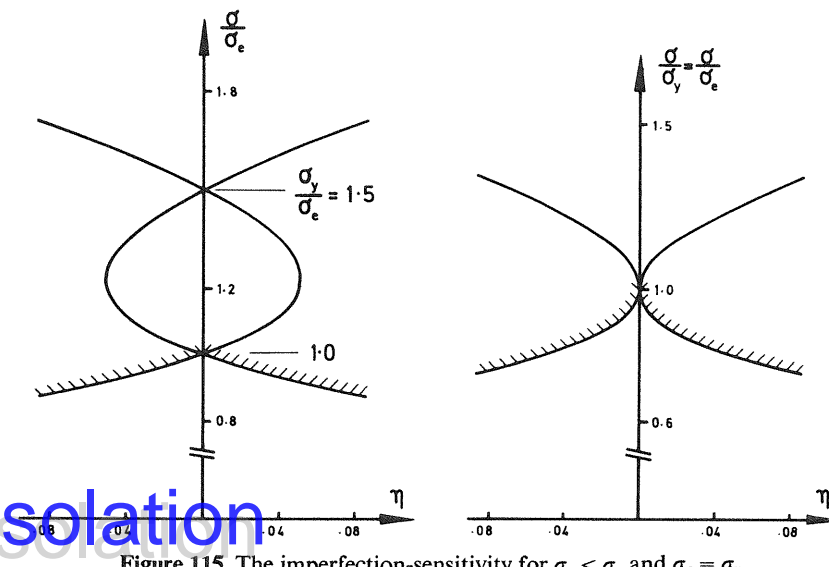


Figure 115 The imperfection-sensitivity for $\sigma_e < \sigma_y$ and $\sigma_e = \sigma_y$

one branch of the complete curve, the second (mirror-image) branch coming from an appeal to the symmetry properties of our system. Moreover, the complete Perry equation, including both positive and negative square roots as above, generates two mathematical solutions to the failure stress for a particular column, the meaningful solution of course being that with the lowest

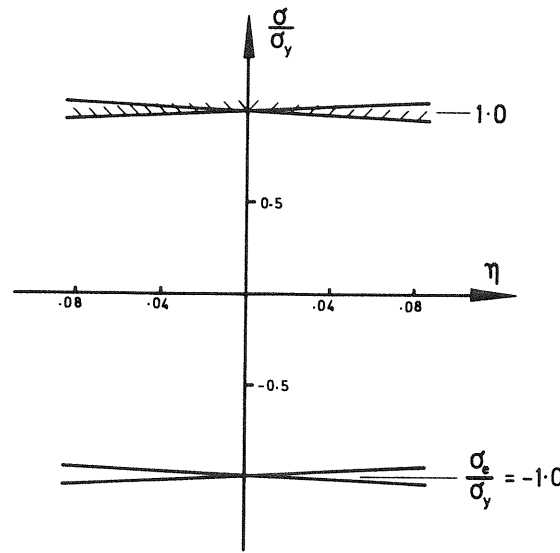


Figure 116 The imperfection-sensitivity with the column in tension

numerical value. The hatched portions of each figure thus give the appropriate imperfection-sensitivity plot for a family of perfect and imperfect columns derived by varying the dimensionless imperfection η . We see that this imperfection-sensitivity is markedly more severe when $\sigma_y = \sigma_e$, supporting our thesis that coincidence of failure modes can result in increased imperfection-sensitivity.

The Perry equation presented above is valid only for columns loaded in compression since σ_y represents a compressive yield stress. However, by reversing the sign of σ_y , we are able to generate for purposes of comparison a second Perry equation which is valid merely for columns loaded in tension and a typical set of curves obtained from this second analysis is presented in Figure 116. Again the hatched portion of the diagram represents the valid imperfection-sensitivity relationship, the other mathematical solutions having been included as before but being meaningless in any practical sense. Clearly the full imperfection-sensitivity relationship for a particular family of columns

loaded either in tension or compression can be obtained by superimposing the hatched portions of the two appropriate curves generated by the two Perry analyses.

From the form of the plots that we have been considering we might expect that in the general case when $\sigma_y \neq \sigma_e$ the failure stress would vary initially linearly with imperfection. That this is indeed the case can be seen from an asymptotic expansion of the Perry equation in which the σ - η relationship becomes either

$$\sigma/\sigma_e = 1 - \frac{1}{\gamma - 1} \eta + \text{order } \eta^2,$$

or alternatively

$$\sigma/\sigma_y = 1 + \frac{1}{\gamma - 1} \eta + \text{order } \eta^2,$$

where $\gamma = \sigma_y/\sigma_e$. Plotting the variation of the slopes of these expressions, $\beta = -1/(\gamma - 1)$ or $+1/(\gamma - 1)$, we obtain the full rectangular hyperbola shown in Figure 117: here an unbroken line represents the valid β at a particular γ , the corresponding broken line being related to the asymptotic expansion which gives non-meaningful mathematical solutions. It can be shown quite simply from the form of this hyperbola that a given column has a greater sensitivity to imperfections when loaded in compression than when loaded in tension.

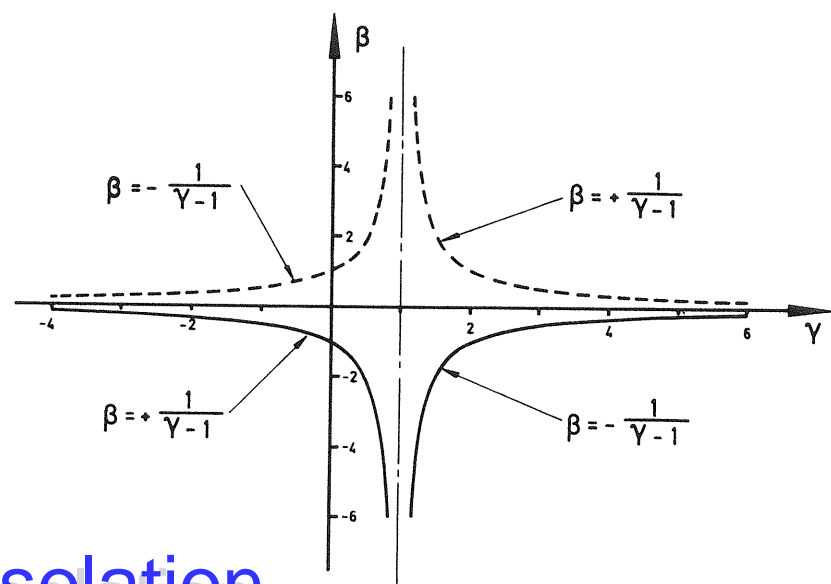


Figure 117 Variation of the linear coefficient β in the asymptotic expansion

Furthermore, we have an infinite slope of the imperfection-sensitivity relationship at $\gamma = 1$ as we have seen in the earlier plot of the closed-form Perry equation, and in this case an asymptotic analysis reveals a more severe one-half power law as follows

$$\sigma/\sigma_e = \sigma/\sigma_y = 1 \pm \eta^{\frac{1}{2}} + \text{order } \eta.$$

Finally, to provide some degree of comparison with the thin-walled and reticulated columns, we can draw the load to slenderness-ratio plot of Figure 118, and we see that this schematic diagram is closely analogous to that of

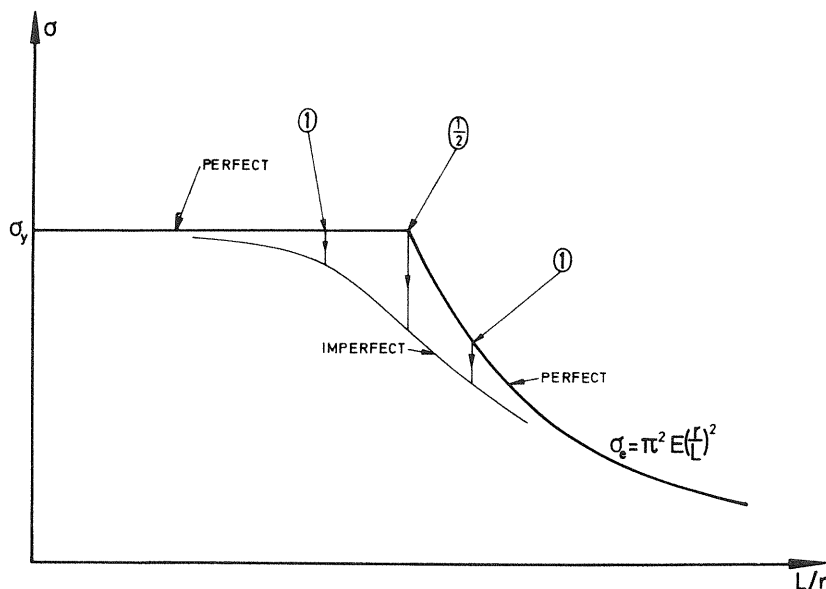


Figure 118 Asymptotic results for the mild-steel column (compare Figure 110)

Figure 110, the yield stress playing the same role for the compact column as did the local buckling stress in the earlier examples. We find that in the case of the compact yielding column the imperfection-sensitivity indices are $(1, \frac{1}{2}, 1)$ as compared with $(\frac{2}{3}, \frac{1}{2}, 2)$ for the thin-walled and reticulated columns.

Once again we note that the principle of simultaneous mode design is leading us to a potentially dangerous compound instability.

13

STRUCTURAL OPTIMIZATION

13.1 Introduction

One field in which the branching studies of the general theory of elastic stability will acquire increasing importance is that of structural optimization, where ever more severe instabilities are being generated by the continuing search for greater structural efficiency. This tendency was noted in Reference 105 and in a little more detail in a recent letter,²¹² and it seems appropriate to conclude this monograph with a further development of this theme as a pointer to the problems and potential dangers of structural optimization.

We proceed then to examine the thesis that a process of optimization leads almost inevitably to designs which exhibit the notorious failure characteristics often associated with the buckling of thin elastic shells. Here the idealized perfect structure exhibits an unstable and often compound branching point and would fail by an explosive instability, while nominally perfect real structures containing inevitable initial imperfections fail at scattered loads which can be quite considerably lower than that of the idealization. Our line of reasoning is sketched in Figure 119, and we shall observe that an increasing degree of optimization implies an increasingly severe instability by demanding in turn an unstable bifurcation, a very unstable bifurcation and finally a very unstable *compound* bifurcation. The last of these is especially dangerous as it may involve an unexpected nonlinear coupling action.

To see that a process of optimization will often lead to a bifurcation we appeal to the old adage that for efficient structural design, forces should be carried as far as possible by direct membrane stresses rather than by bending action. Some such membrane stresses can be expected to be compressive, particularly in civil engineering structures which stand rather than hang, and it is of course precisely direct compressive action that gives rise to bifurcational buckling. The symmetry of many optimum designs is a further generator of branching behaviour. We can next observe that an optimum design is by its very nature imperfection-sensitive, since any deviation from the idealized optimum design must yield a lower failure load. Combining these two observations we can infer that an optimum design is likely to exhibit an *unstable point of bifurcation*.

Furthermore, we have an infinite slope of the imperfection-sensitivity relationship at $\gamma = 1$ as we have seen in the earlier plot of the closed-form Perry equation, and in this case an asymptotic analysis reveals a more severe one-half power law as follows

$$\sigma/\sigma_e = \sigma/\sigma_y = 1 \pm \eta^{\frac{1}{2}} + \text{order } \eta.$$

Finally, to provide some degree of comparison with the thin-walled and reticulated columns, we can draw the load to slenderness-ratio plot of Figure 118, and we see that this schematic diagram is closely analogous to that of

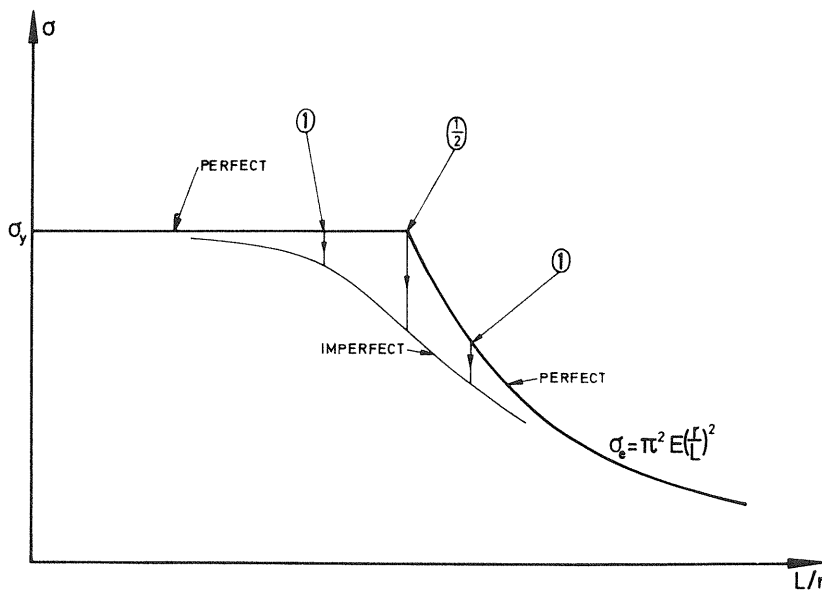


Figure 118 Asymptotic results for the mild-steel column (compare Figure 110)

Figure 110, the yield stress playing the same role for the compact column as did the local buckling stress in the earlier examples. We find that in the case of the compact yielding column the imperfection-sensitivity indices are $(1, \frac{1}{2}, 1)$ as compared with $(\frac{3}{2}, \frac{1}{2}, 2)$ for the thin-walled and reticulated columns.

Once again we note that the principle of simultaneous mode design is leading us to a potentially dangerous compound instability.

13

STRUCTURAL OPTIMIZATION

13.1 Introduction

One field in which the branching studies of the general theory of elastic stability will acquire increasing importance is that of structural optimization, where ever more severe instabilities are being generated by the continuing search for greater structural efficiency. This tendency was noted in Reference 105 and in a little more detail in a recent letter,²¹² and it seems appropriate to conclude this monograph with a further development of this theme as a pointer to the problems and potential dangers of structural optimization.

We proceed then to examine the thesis that a process of optimization leads almost inevitably to designs which exhibit the notorious failure characteristics often associated with the buckling of thin elastic shells. Here the idealized perfect structure exhibits an unstable and often compound branching point and would fail by an explosive instability, while nominally perfect real structures containing inevitable initial imperfections fail at scattered loads which can be quite considerably lower than that of the idealization. Our line of reasoning is sketched in Figure 119, and we shall observe that an increasing degree of optimization implies an increasingly severe instability by demanding in turn an unstable bifurcation, a very unstable bifurcation and finally a very unstable *compound* bifurcation. The last of these is especially dangerous as it may involve an unexpected nonlinear coupling action.

To see that a process of optimization will often lead to a bifurcation we appeal to the old adage that for efficient structural design, forces should be carried as far as possible by direct membrane stresses rather than by bending action. Some such membrane stresses can be expected to be compressive, particularly in civil engineering structures which stand rather than hang, and it is of course precisely direct compressive action that gives rise to bifurcational buckling. The symmetry of many optimum designs is a further generator of branching behaviour. We can next observe that an optimum design is by its very nature imperfection-sensitive, since any deviation from the idealized optimum design must yield a lower failure load. Combining these two observations, we can infer that an optimum design is likely to exhibit an *unstable point of bifurcation*.

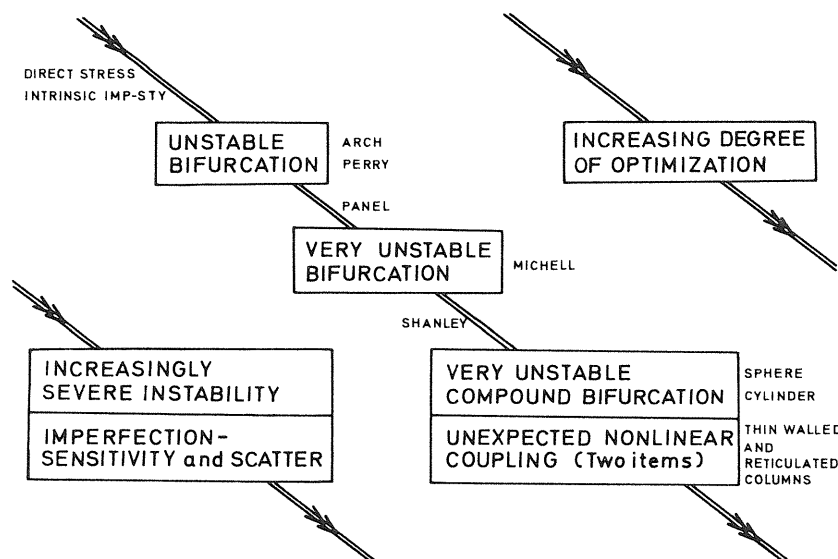


Figure 119 Optimization as a generator of structural instability

As specific examples of this we shall discuss the design of an optimal elastic arch in Section 13.2 and the design of a mild-steel beam-column in Section 13.3.

The next feature to emerge from a careful consideration of structural optimization is that the severity of failure will tend to increase with the degree of optimization achieved, and this is nicely displayed by the cylindrical panel of Section 13.4. Here the critical load of the structure can be progressively raised by increasing the curvature of the panel, but this gain is at the expense of the post-buckling behaviour and associated imperfection-sensitivity which are becoming more and more severe. A further example illustrating the same tendency is the minimum weight Michell truss of Section 13.5 which is a superb design for carrying the applied vertical load, but is actually a mechanism for horizontal movement of the centre pin. The design is thus violently unstable, and has effectively an infinitely severe imperfection-sensitivity since it offers no resistance at all to a horizontal disturbance.

The suggestion so far is that a process of optimization leads to increasingly severe bifurcational instabilities, but worse is yet to come. In a complete structure of any complexity, optimization appears to demand simultaneity of failure loads²¹³ and this concept advanced by Shanley is already a significant feature in the design of large composite structures. Unfortunately for this design philosophy, the nonlinear coupling of even apparently unrelated and mild failures can give rise to extremely severe post-buckling behaviour, as was

predicted by Koiter and Skaloud²¹⁴ in 1962. One might say that a loss of stiffness in one mode precipitates an explosive failure in another.

Two classical examples of this nonlinear coupling are the spherical and cylindrical shells discussed in Sections 13.6 and 13.7. As we would intuitively expect, these are both highly efficient designs for carrying their uniform compressive loads, but due to the simultaneity of many buckling modes the shells exhibit a most violent failure characteristic. This is associated with a severe imperfection-sensitivity which can lower the load-carrying capacity of even a carefully manufactured laboratory specimen by a factor of three.

This coupling phenomenon, long understood in the field of shell buckling, has recently been observed in the local and overall buckling of plate assemblages by Van der Neut.²¹⁵ Such assemblages have conventionally been regarded as quite safe in the post-buckling range, so we have here a dangerous situation in which current procedures may lead to unsafe design, which could be a contributory factor in the recent failures of box-girder bridges. In this connection we can stress that the phenomenon will only be revealed analytically if both ingredients, namely *nonlinearity* and *coupling*, are included in the study of either perfect or imperfect systems. Linear buckling studies and uncoupled nonlinear studies will simply fail to locate the danger.

This significant contribution of Van der Neut has been outlined in the preceding chapter, where we have shown that a precisely similar situation arises in the compound failure of reticulated columns. A somewhat similar phenomenon is in fact concealed in the well known Perry analysis of mild-steel columns, as we have demonstrated.

Optimization, then, is a generator of severe imperfection-sensitivity and this might clearly erode the benefits of a nominally optimum design. We have already seen this in the case of the simple link model of Chapter 10, and in Section 13.8 we present a quantitative study of this erosion for the thin-walled column using the graphical results of Van der Neut. Here we see that the nominal optimum can be highly modified, and indeed almost completely destroyed, by modest flange imperfections.

We conclude the chapter, and indeed the monograph, by drawing some tentative conclusions from this examination of the dangers of structural optimization.²¹⁵

13.2 The elastic arch

As an illustration of the manner in which an unstable (symmetric) point of bifurcation can arise in the solution of an optimization problem, let us consider the shallow arch of Figure 120. Taking the imperfection-sensitivity data from the experiment of Roorda, which we have presented in Figure 44 of Chapter 2, we can regard his additional offset simply as some measure ε of the asymmetry

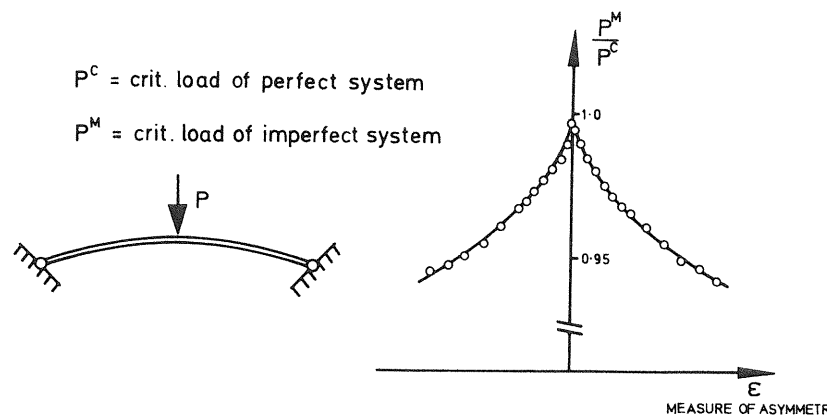


Figure 120 The symmetric arch as an optimum design (after Roorda 1965)

of the arch, to give the graph shown. Supposing now that ϵ were a design parameter under our control, we see that the greatest load-carrying capacity is achieved by the symmetric configuration for which $\epsilon = 0$, which thus represents the optimum design. This is clearly a sharp optimum, associated as it is with a two-thirds power law, so the ideal optimum load-carrying capacity would be essentially unattainable in practice.

Arches of this type demonstrate an interesting phenomenon directly associated with the sharpness of this optimum. If an arch is endowed with some degree of asymmetry it may in fact be possible, by removing material from one half of the arch, to move towards the optimum design, thereby *increasing* the load-carrying capacity of the system.

A similar sharp optimum design can be expected in the behaviour of shallow spherical domes which exhibit an unstable-symmetric point of bifurcation associated with the development of non-symmetric deformations.

13.3 The yielding strut

As a second illustration of the generation of an unstable bifurcating situation, let us consider the design problem posed in Figure 114. Here a pair of coaxial equal and opposite compressive forces are to be carried by a uniform curved member of given cross-section made from mild steel.

Thinking of a_0 as a design parameter, we can first observe that the straight column will have the *minimum* weight of the family. But, taking first yield as a good criterion of collapse, we have seen from the analysis of Chapter 12 that the straight member gives us the *greatest* load-carrying capacity. Therefore, since weight is a minimum and load is a maximum, it follows *a fortiori* that the

optimum load to weight ratio is obtained from the straight member for which $a_0 = 0$.

The optimum is fairly mild when $\sigma_y \neq \sigma_e$, but when the two failure modes occur simultaneously the optimum becomes more severe, as we have observed.

13.4 The cylindrical panel

To illustrate the tendency for an increasing degree of optimization to generate an increasingly severe failure characteristic, we turn now to the buckling behaviour of the family of axially compressed cylindrical panels illustrated in Figure 121. Here the family is generated by varying the curvature of the panel, and we adopt this as our design parameter. The designs under consideration thus embrace in the limit a flat plate, for which the curvature is zero.

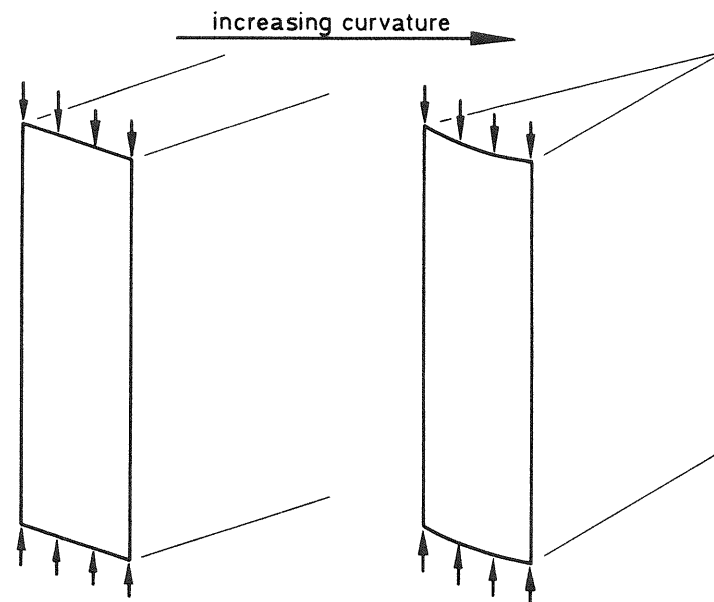


Figure 121 A family of curved panels

The buckling and post-buckling behaviours of long narrow panels of this type have been discussed by Koiter,⁶ and they are summarized schematically here in Figure 122. The boundary conditions considered suppress radial deflection waves along the longitudinal edges, these boundary conditions being chosen as the nearest simple approximation to the state of a panel included in a longitudinally-stiffened cylindrical shell, an important practical problem. The work shows that if we keep the structural weight constant, the

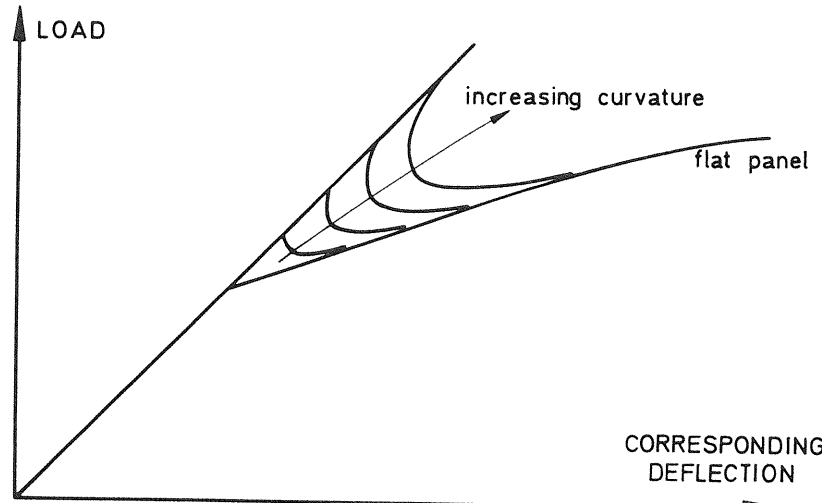


Figure 122 The response of the curved panels

critical bifurcation load can be pushed up by increasing the panel curvature. Unfortunately, at the same time, the initial post-buckling response is becoming increasingly unstable since the structure under consideration is changing from a flat plate to a highly curved shell. The advanced post-buckling response is however largely independent of the curvature, and approaches the behaviour of the flat plate of the same width. The increasingly severe initial post-buckling does of course imply an increasingly severe imperfection-sensitivity, so once again a scheme of optimization is leading us to an unpredictable situation.

13.5 The Michell truss

As a somewhat different item, which nevertheless serves to illustrate our general theme, let us now consider the Michell truss of Figure 123 which is the minimum weight pin-jointed frame to support a load half-way between two fixed supports at the same level.²¹⁶ Here we have a highly optimized situation in which the layout of the structure has been carefully chosen to carry a prescribed load. Unfortunately, however, the frame can carry no horizontal load at all, as it is in fact a mechanism having thus no stiffness or stability against horizontal perturbations: it has effectively an infinitely severe imperfection-sensitivity.

This then is a good example of the concept that in designing a structure one should not put all the eggs in the same basket.

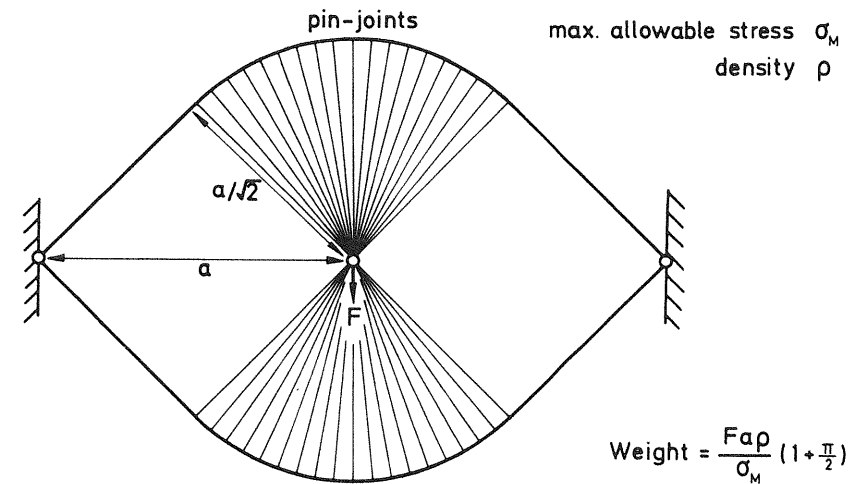


Figure 123 The Michell truss as an unstable optimum

13.6 The complete spherical shell

As our first example embracing a compound failure, let us consider the problem of designing a pressure vessel of a given elastic material to carry a uniform external pressure. We shall suppose that the volume to be enclosed is a prescribed quantity, and that a shell of given uniform thickness is to be employed.

Now the *minimum* weight shell to satisfy these geometric conditions is clearly a sphere, and we know from Koiter's elastic buckling studies that the (perfect) sphere will also give us the *maximum* load-carrying capacity. Thus since weight is minimum and pressure is maximum, the sphere will *a fortiori* give us the best load to weight ratio, and we clearly have the optimum solution to our problem.

However the complete spherical shell is well known to exhibit highly unstable compound branching with the extreme imperfection-sensitivity shown in Figure 124, which is here reproduced from the work of Koiter;²¹ in this diagram the imperfection parameter is taken as the root mean square of the imperfection magnitude to thickness ratio, thereby combining the imperfection-sensitivities for shells of differing radius to thickness ratios on the same curve. The sharply optimum character of the perfect sphere is well demonstrated, and we find for a typical shell with a radius to thickness ratio of 82 and an imperfection amplitude of about two-thirds of the shell thickness that the load-carrying capacity has dropped by a factor of two.

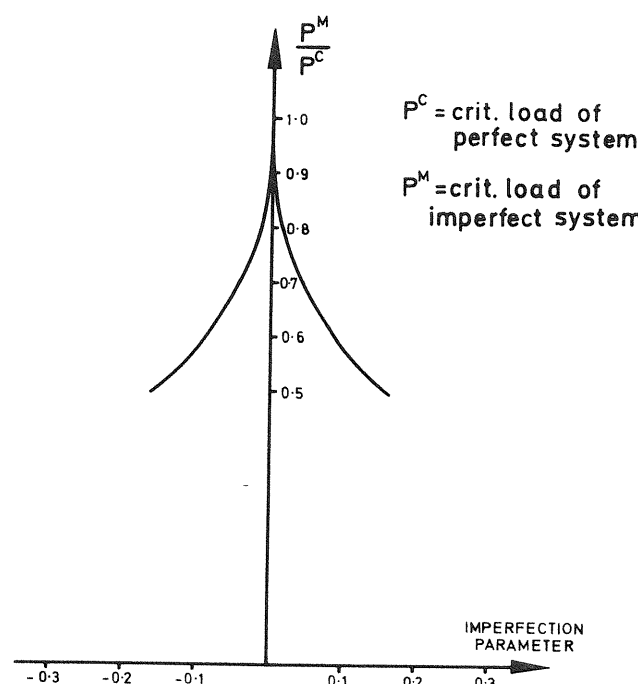


Figure 124 The imperfection-sensitivity of a spherical shell
 (after Koiter 1969)

This then is an important example in which an extreme optimum design involving compound failure modes yields a highly unstable structure prone to dramatic failure and severe imperfection-sensitivity.

13.7 The complete cylindrical shell

An entirely similar situation arises in the elastic buckling of a complete cylindrical shell under uniform axial compression. Here the idealized perfect structure is again an obviously optimum form for resisting the applied loading, while failure is once more associated with a multiplicity of buckling modes.

The imperfection-sensitivity arising from the nonlinear interaction of these modes is reproduced from the work of Koiter in Figure 125. We see that it is extremely severe, with an imperfection amplitude of just one-fifth of the shell thickness reducing the load-carrying capacity by a factor of two. The optimum design represented by the idealized perfect cylinder is thus totally unattainable in practice.

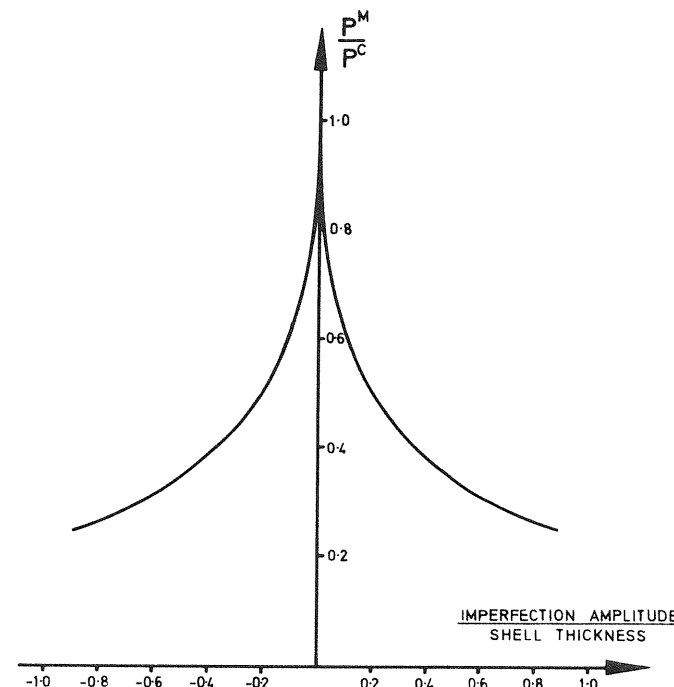


Figure 125 The imperfection-sensitivity of a cylindrical shell (after Koiter 1969)

13.8 The thin-walled column

We shall be concerned in this final section with the erosion of nominally optimum designs by the imperfection-sensitivity of coupled failure modes. The mechanics of such an erosion have already been carefully examined in Section 10.4 for a simple model cantilever, and we shall here make a more pragmatic study for a thin-walled compression member following Thompson and Lewis.²¹³ In this we shall not look too carefully at the mechanics of the problem but shall aim to get practically-relevant results by drawing on the numerical calculations of Van der Neut which we presented in Figure 109. We might observe that these calculations have been confirmed by a careful branching study due to Koiter and Kuiken,²¹⁷ while similar results for related structural forms have been obtained in References 218–220.

In contemplating the design of a thin-walled column it is clear that by increasing the overall dimensions of the cross-section, b and c , we can push up the overall Euler buckling load of the column. However, at constant weight

this can only be done by reducing the thickness of the walls, and so is at the expense of the local buckling load which will be coming down. We thus might expect an optimum solution at an intersection point as shown schematically in Figure 126. The question then arises as to how this apparent optimum might be eroded away by the enhanced imperfection-sensitivity which is expected at this coincident point.

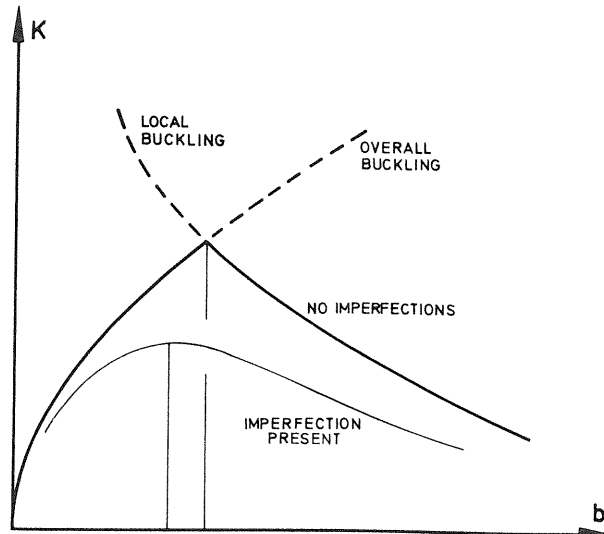


Figure 126 An apparent optimum for a thin-walled column

To study this, let us suppose that we wish to design a pin-ended strut with the idealized cross-section of Van der Neut which is shown in Figure 106. We shall suppose that the length of the strut L is a prescribed quantity and that the material of construction is specified so that the Young's Modulus E and density ρ are also fixed. The yield stress of the material is supposed to be sufficiently high to ensure elastic behaviour at all times. We suppose that the cross-section is to be maintained square so that $b = 2c$, and we shall assume that $h \ll b \ll L$.

We now set ourselves the task of maximizing the load-carrying capacity of the column, as estimated by Van der Neut's bending buckling load K_b , subject to the constraint that the weight shall be held constant. With prescribed density this means that the cross-sectional area is a constant so we can write

$$bh = k,$$

and we are left with one independent design variable which we take as b .

Now the curves of Figure 109 give us $y(x)$ for various values of the imperfection parameter α , which we recall is the ratio of the plate imperfection amplitude to the wall thickness. Here $x = K_e/K_l$ and $y = K_b/K_l$ and using the expressions for K_e and K_l we have

$$x = \frac{3(1 - \nu^2)}{4k^2 L^2} \cdot b^6,$$

so that

$$b = \left\{ x \cdot \frac{4k^2 L^2}{3(1 - \nu^2)} \right\}^{1/6}.$$

We see that x varies monotonically with b , and so we can retain x as a measure of b .

The bending buckling load K_b can be written in terms of y as

$$K_b = \frac{2\pi E k^3}{3(1 - \nu^2)} y b^{-4},$$

and substituting for b we obtain

$$K_b = R y x^{-4},$$

where R is a constant. Thus to find the optimum load-carrying capacity of the strut we merely have to maximize

$$P(x) \equiv K_b/R = y(x) x^{-4},$$

where $y(x)$ can be obtained from the curves of Figure 109.

For the perfect system where $\alpha = 0$ we already have the required information to proceed analytically. In the first domain of Figure 108 where $y = x$ we obtain

$$P(x) = x^4,$$

while in the third domain of this diagram where $y = \eta x$ the relationship becomes

$$P(x) = \eta x^4.$$

Finally in the central domain where combined buckling takes place we have $y = 1$ and so obtain

$$P(x) = x^{-4}.$$

We now find that, by plotting the variation of $P(x)$ with x for the three domains of Figure 108 this diagram is transformed to that of Figure 127 which clearly illustrates a local optimum of the load-carrying capacity at A , where $K_e = K_l$.

In the presence of imperfections we must make use of the information presented graphically in Figure 109 to construct the corresponding $P(x)$ curves. These are shown in Figure 128 for values of the imperfection amplitude up to 0.4 times the flange thickness.

Before commenting on these two figures we must observe that they show only a locally optimum value of load at A , and it would seem that we might obtain

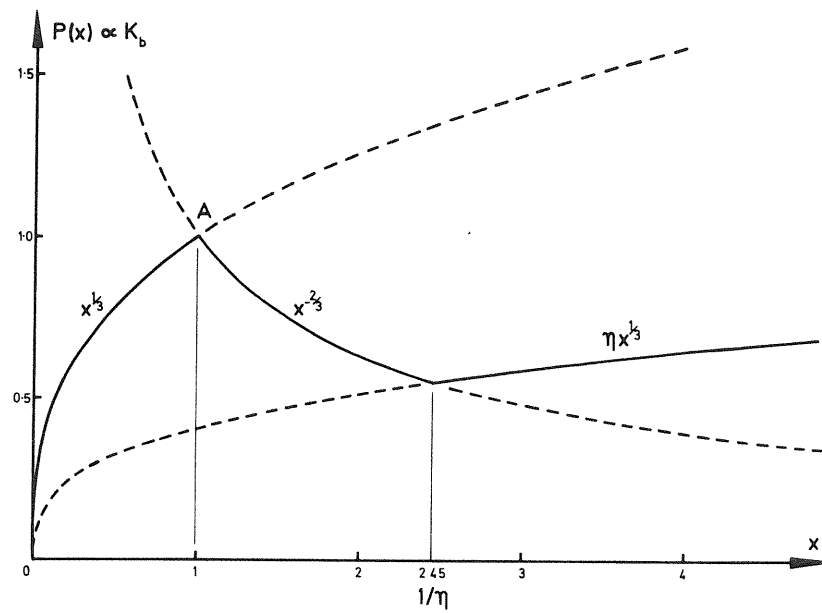


Figure 127 The optimum design for the Van der Neut model

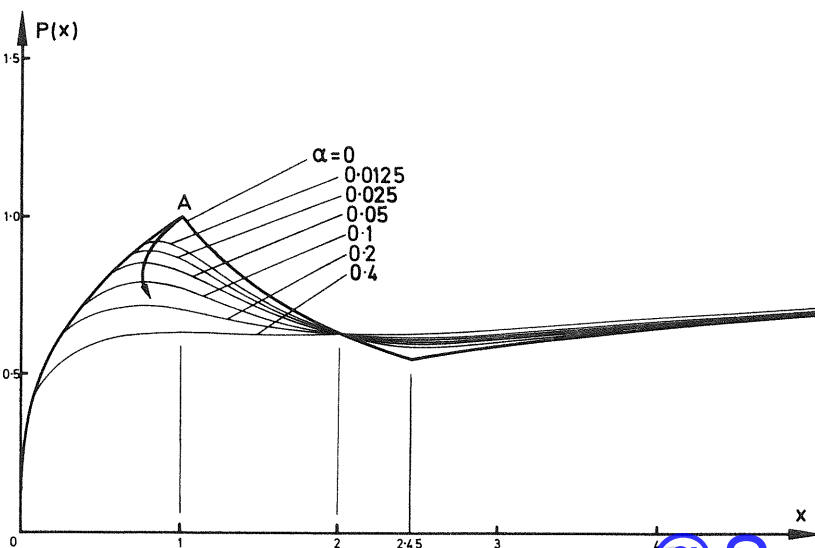


Figure 128 The erosion of the optimum by flange imperfections

higher values for P by making x large. However, this implies that the flange buckling would be increasingly severe before column bending takes place, and two new effects would set in. First, in any practical circumstance, yielding of the material could be expected thereby destroying the validity of the curves for large x . Secondly, even if the material remained linearly elastic, the post-buckling stiffness which we have assumed to be constant is likely to fall off with load, and once again the curves are suspect where x is large as demonstrated in the original article.²¹³ It is therefore reasonable to suppose that $K_e = K_l$ in fact gives a *complete* as opposed to a *local* optimum.

Referring back to Figures 127 and 128 we can now see the extent to which the optimum has been eroded away by the imperfections assumed to be present in the flanges. First we note that the optimum is essentially lost by the time the imperfection amplitude becomes about one-third of the plate thickness, so that the cautionary remarks of Hutchinson and Koiter⁴⁴ are completely borne out. Secondly, we see that as the imperfection increases the maximum shifts initially to the left so that it pays to make $K_e < K_l$, which contradicts the simple argument that it is advisable to set $K_e > K_l$ on the grounds that flange buckling does not exhaust the load-carrying capacity of the system. This initial shift is in fact to be expected from the asymptotic results of Koiter and Kuiken²¹⁷ which we have summarized schematically in the load to slenderness ratio plot of Figure 110: here the indices of the asymptotic expansions $\gamma(\alpha)$ show that the imperfection-sensitivity is fundamentally more severe for $x > 1$ than for $x < 1$.

13.9 Concluding remarks

The diversity of structural forms examined in this concluding chapter establish quite clearly that an increasing degree of optimization will bring in its wake an increasingly unstable failure characteristic. We note in particular the dangers inherent in the so-called principle of simultaneous mode design, and the growing need for the sophisticated branching studies of this monograph.

The impact of these conclusions on design is not immediately apparent, but it will clearly vary from field to field since the philosophies of aerospace structures differ quite radically from those of civil engineering structures. Thus a weight-conscious aircraft designer may be tempted to accept the unpleasant failure characteristics and continue to seek the highest possible optimization allowing as best he can for the random manufacturing tolerances. A civil engineer on the other hand may prefer to abandon a high degree of optimization and aim to build structures with mild failure characteristics, in the same way as he might prefer the ductility and energy absorption of a mild steel as against the brittle fracture of a high-strength steel.

Perhaps we can close with the question expressed by Pugsley.²²¹ Shall our structures be designed to be just stable, or in some way more than stable?

APPENDIX I BASIC THEOREMS

We give here the original forms of the two basic theorems which are discussed and sharpened in Section 2.4, together with the corresponding analytical proofs from Reference 118.

Theorem 1. *An initially-stable (fundamental) equilibrium path rising monotonically with the loading parameter cannot become (thoroughly) unstable without intersecting a second distinct (post-buckling) equilibrium path.*

Theorem 2. *An initially-stable (fundamental) equilibrium path rising monotonically with the loading parameter cannot approach an unstable critical equilibrium state (from which the system would snap dynamically) without the approach of a second distinct (post-buckling) equilibrium path at subcritical values of the loading parameter.*

We consider a general system with one degree of freedom described by the total potential energy function $V(Q_1, \Lambda)$ and assume the existence of a single-valued fundamental equilibrium path given by $Q_1 = Q_1^F(\Lambda)$. A sliding (incremental) coordinate q_1 is defined by the equation $Q_1 = Q_1^F(\Lambda) + q_1$, so that the equilibrium paths of the system can be mapped into a new load-coordinate space generated by the points (q_1, Λ) in which the fundamental path will be coincident with the load axis and given by $q_1 = 0$.

The new potential energy function

$$W(q_1, \Lambda) \equiv V[Q_1^F(\Lambda) + q_1, \Lambda]$$

is now introduced, and we note that the equilibrium and stability conditions carry over unchanged to this function. For small Λ the fundamental path is assumed to be thoroughly stable with $C(\Lambda) = W_{11}^F$ greater than zero and we suppose that moving along the path with increasing Λ this stability coefficient drops to zero at the critical equilibrium state $q_1 = 0$, $\Lambda = \Lambda^C$. Expanding $W(q_1, \Lambda)$ as a power or Taylor series about this critical equilibrium state we have

$$W = \sum_{i=0}^{i=\infty} \sum_{j=0}^{j=\infty} W_j^i(q_1)^j (\lambda)^i,$$

where $\lambda = \Lambda - \Lambda^C$, and differentiating with respect to q_1 we can write

$$W_1 = \sum_{i=0}^{i=\infty} \sum_{j=1}^{j=\infty} j W_j^i(q_1)^{j-1} (\lambda)^i.$$

The fundamental equilibrium path being given by $q_1 = 0$, this derivative must vanish with q_1 for all λ , so the first column must vanish leaving

$$W_1 = \sum_{i=0}^{i=\infty} \sum_{j=2}^{j=\infty} j W_j^i(q_1)^{j-1} (\lambda)^i.$$

To prove Theorem 1 we note that the new leading column can be identified as $q_1 C(\lambda)$, where $C(\lambda)$ represents the variation of the stability coefficient along the fundamental path. Thus $C(0) = 0$, and if the fundamental path is to thoroughly lose its initial stability $C(\lambda)$ must become negative so for the first non-vanishing coefficient of the column, i must be odd. Thus the first term of the new leading column must vanish and the first non-zero term can be written as $2 W_2^u q_1(\lambda)^u$, where u is odd.

The terms with i greater than u in the equilibrium equation $W_1 = 0$ will be small in comparison with this non-zero term when q_1 and λ are small, and so can be dropped in a local first-order analysis. Thus for such an analysis we can write the equilibrium equation

$$W_1 = \sum_{i=0}^{i=u} \sum_{j=2}^{j=\infty} j W_j^i(q_1)^{j-1} (\lambda)^i = 0$$

which has the form

$$(\lambda)^u [q_1 + O(q_1^2)] + (\lambda)^{u-1} O(q_1^2) + (\lambda)^{u-2} O(q_1^2) + \cdots + \lambda O(q_1^2) + O(q_1^2) = 0.$$

Cancelling q_1 for the fundamental solution leaves an equation, satisfied by $q_1 = \lambda = 0$, which will always have at least one real solution for λ corresponding to a prescribed value of q_1 . Thus there will be at least one real (post-buckling) equilibrium path intersecting the fundamental equilibrium path at the critical equilibrium state and the first theorem is proved.

We proceed now to Theorem 2 and we note that the stability of the critical equilibrium state itself depends on the first row of the W expansion. In this, the leading term is simply an arbitrary constant, the second term vanishes because the state is one of equilibrium and the third term vanishes because the equilibrium state is critical. Examining the remaining terms we see that for instability of the critical equilibrium state either the first non-zero term must be odd or the coefficient must be negative. Supposing that the first non-zero term is $W_1^0(q_1)^r$ we see that for a local first-order analysis we can drop higher values of j in the original equilibrium equation which becomes

$$W_1 = \sum_{i=0}^{i=\infty} \sum_{j=2}^{j=r} j W_j^i(q_1)^{j-1} (\lambda)^i = 0.$$

Supposing now that the first non-zero term in the $j = 2$ column is $2W_2^u q_1(\lambda)^u$ and dropping small terms in comparison with non-zero terms, the equilibrium equation becomes, after cancelling q_1 for the fundamental solution,

$$\begin{aligned} R(q_1) &= (q_1)^{r-2} r W_r^0 + (q_1)^{r-3} O(\lambda) + (q_1)^{r-4} O(\lambda) + \cdots + q_1 O(\lambda) + 2W_2^u(\lambda)^u \\ &= 0. \end{aligned}$$

This is satisfied by $q_1 = \lambda = 0$.

Now if r is odd this equation must have at least one real solution for both positive and negative λ , and thus a (post-buckling) equilibrium path must approach from below. If r is even W_r^0 must be negative for instability so for 'large' positive or negative q_1 the function $R(q_1)$ will be negative. But for zero q_1 the function has the sign of $W_2^u(\lambda)^u$ which for the circumstances under consideration is positive for negative λ whether u is odd or even. Thus there must be two solutions satisfying $R(q_1) = 0$ for negative λ and again there is a real (post-buckling) equilibrium path approaching from below. Thus the second theorem is proved.

APPENDIX II INDUCTION TECHNIQUES

We are interested first of all in the ordered series of equilibrium equations, generated by a perturbation scheme, which are used in the process of elimination of passive coordinates expressed in terms of the diagonalized A -function. These equations are derived in the coincident branching analysis of Chapter 10, but some of them are worthy of study in greater detail than was presented here. We shall also be looking at general forms for some of the associated \mathcal{A} -derivatives.

First let us look at the equation for $(\partial^r/\partial A^r) A_\alpha$ which may conveniently be written in the general form

$$\frac{\partial^r}{\partial A^r} A_\alpha = F_\alpha^r(u_\beta^{(r-1)}, u_\beta^{(r-2)}, \dots, u_\beta^{(1)}; \text{no constant}) + A_{\alpha\beta} u_\beta^{(r)} + A_\alpha^{(r)} = 0.$$

We remember from the earlier work that a bracketed superscript on an A or u_β derivative would denote partial differentiation with respect to the independent variable of the perturbation scheme; here we have $m + 1$ independent variables u_i and A , but in this particular case we choose a bracketed superscript to represent the number of partial differentiations with respect to A . The form of this equation may be shown to be valid by employing inductive reasoning. Let us therefore differentiate it with respect to A , thereby generating $(\partial^{r+1}/\partial A^{r+1}) A_\alpha$. Here

F_α^r is all included in F_α^{r+1} ,

$$A_{\alpha\beta} u_\beta^{(r)} \text{ becomes } \begin{cases} A_{\alpha\beta\gamma} u_\beta^{(r)} u_\gamma^{(1)} + A_{\alpha\beta}^{(1)} u_\beta^{(r)} & (\text{included in } F_\alpha^{r+1}) \\ A_{\alpha\beta} u_\beta^{(r+1)}, \end{cases}$$

$$A_\alpha^{(r)} \text{ becomes } \begin{cases} A_{\alpha\beta}^{(r)} u_\beta^{(1)} & (\text{included in } F_\alpha^{r+1}) \\ A_\alpha^{(r+1)}. \end{cases}$$

So it can be seen that if the form is correct for the r th equation it is likewise true for the $(r+1)$ th equation; but from our original equations we know the form to be valid for $r = 1$ and so by the well known induction mechanism it follows that the form is correct in general.

Let us now assume that the derivatives $u_{\beta}^{(r-1)F}, u_{\beta}^{(r-2)F}, \dots, u_{\beta}^{(1)F}$ are all equal to zero when we evaluate on the fundamental path in the region of the critical point. It will then follow that F_{α}^r is zero and keeping in mind the properties of the A -function we obtain

$$u_{\alpha}^{(r)F} = - \frac{A_{\alpha i}^{(r)}}{A_{\alpha \alpha}} \Big|_F = 0.$$

However, we know that $u_{\beta}^{(1)F} = u_{\beta}^{(2)F} = 0$ from the original evaluations and hence it follows from inductive reasoning that all F_{α}^r and $u_{\alpha}^{(r)F}$ are equal to zero.

The second convenient general form which we shall consider is in the equation for $(\partial/\partial u_i \partial A^{r-1}) A_{\alpha}$. Thus writing

$$\begin{aligned} \frac{\partial r}{\partial u_i \partial A^{r-1}} A_{\alpha} &= G_{\alpha}^r(u_{\beta}^{(r)}, u_{\beta}^{(r-1)}, \dots, u_{\beta}^{(1)}; u_{\beta i}^{(r-1)}, u_{\beta i}^{(r-2)}, \dots, u_{\beta i}; \text{no constant}) \\ &\quad + A_{\alpha i}^{(r)} + A_{\alpha \beta} u_{\beta i}^{(r)} = 0, \end{aligned}$$

we obtain $(\partial^{r+1}/\partial u_i \partial A^r) A_{\alpha}$ by partial differentiation with respect to A , where

G_{α}^r is all included in G_{α}^{r+1} ,

$$A_{\alpha i}^{(r)} \quad \text{becomes} \quad \begin{cases} A_{\alpha \beta i}^{(1)} u_{\beta}^{(r)} & (\text{included in } G_{\alpha}^{r+1}) \\ A_{\alpha i}^{(r+1)}, & \end{cases}$$

$$A_{\alpha \beta} u_{\beta i}^{(r)} \quad \text{becomes} \quad \begin{cases} A_{\alpha \beta \gamma} u_{\beta i}^{(r)} u_{\gamma}^{(1)} + A_{\alpha \beta}^{(1)} u_{\beta i}^{(r)} & (\text{included in } G_{\alpha}^{r+1}) \\ A_{\alpha \beta} u_{\beta i}^{(r+1)}. & \end{cases}$$

Again we find that the general form holds over differentiation with respect to A ; but from the original equations of Chapter 10 we know the form to be valid for $r = 1$ and so by induction it follows that it is correct in general.

Let us now assume that the derivatives $u_{\beta i}^{(r-1)F}, u_{\beta i}^{(r-2)F}, \dots, u_{\beta i}^{(1)F}$ are all equal to zero when we evaluate on the fundamental path in the region of the critical point. Making use of the previous result in which all the $u_{\beta}^{(r)F}$ are equal to zero and remembering the diagonalized properties of the A -function, we can then write

$$u_{\alpha i}^{(r)F} = - \frac{A_{\alpha i}^{(r)}}{A_{\alpha \alpha}} \Big|_F = 0.$$

Again we know our assumption to be correct for $r = 1$, and so by induction it may be concluded that all G_{α}^r and $u_{\alpha i}^{(r)F}$ are equal to zero.

We shall now apply our induction techniques to the \mathcal{A} -derivatives which emerge from the elimination of passive coordinates. First we write a general form for $\mathcal{A}_i^{(r)}$ as

$$\mathcal{A}_i^{(r)} = H_i^r(u_{\alpha}^{(r)}, u_{\alpha}^{(r-1)}, \dots, u_{\alpha}^{(1)}; u_{\alpha i}^{(r)}, u_{\alpha i}^{(r-1)}, \dots, u_{\alpha i}; \text{no constant}) + A_i^{(r)}.$$

Partial differentiation with respect to A will generate $\mathcal{A}_i^{(r+1)}$, where

H_i^r is all included in H_i^{r+1} ,

$$A_i^{(r)} \quad \text{becomes} \quad \begin{cases} A_{\alpha i}^{(r)} u_{\alpha}^{(1)} & (\text{included in } H_i^{r+1}) \\ A_i^{(r+1)}. & \end{cases}$$

The familiar arguments are now called into play. The general form holds over differentiation with respect to A ; it is also correct for $r = 1$ and so is justified. If we now evaluate on the appropriate region of the fundamental path, we can see from the earlier results that H_i^r is zero and so it follows that

$$\mathcal{A}_i^{(r)F} = A_i^{(r)F} = 0. \quad (\text{A.1})$$

This constitutes a full preservation over the transformation of a condition associated with the use of a set of incremental coordinates and is presented in a more recognizable form in Chapter 10.

The second general form of \mathcal{A} -derivative which we shall consider here is $\mathcal{A}_{ij}^{(r)}$, written

$$\begin{aligned} \mathcal{A}_{ij}^{(r)} &= I_{ij}^r(u_{\alpha i}^{(r)}, u_{\alpha i}^{(r-1)}, \dots, u_{\alpha i}; u_{\alpha j}^{(r)}, u_{\alpha j}^{(r-1)}, \dots, u_{\alpha j}; u_{\alpha}^{(r)}, \\ &\quad u_{\alpha}^{(r-1)}, \dots, u_{\alpha}^{(1)}; \text{no constant}) \\ &\quad + J_{\alpha}^r(u_{\beta}^{(r)}, u_{\beta}^{(r-1)}, \dots, u_{\beta}^{(1)}; \text{no constant}) u_{\alpha i j} \\ &\quad + K_{\alpha}^r(u_{\beta}^{(r-1)}, u_{\beta}^{(r-2)}, \dots, u_{\beta}^{(1)}; \text{no constant}) u_{\alpha i j}^{(1)} \\ &\quad + L_{\alpha}^r(u_{\beta}^{(r-2)}, u_{\beta}^{(r-3)}, \dots, u_{\beta}^{(1)}; \text{no constant}) u_{\alpha i j}^{(2)} + \dots + r A_{\alpha \beta} u_{\beta}^{(1)} u_{\alpha i j}^{(r-1)} \\ &\quad + A_{\alpha} u_{\alpha i j}^{(r)} + r A_{\alpha}^{(1)} u_{\alpha i j}^{(r-1)} + \dots + r A_{\alpha}^{(r-1)} u_{\alpha i j}^{(1)} + A_{\alpha}^{(r)} u_{\alpha i j} + A_{ij}^{(r)}. \end{aligned}$$

Partial differentiation of this form with respect to A leads to $\mathcal{A}_{ij}^{(r+1)}$, where

I_{ij}^r is all included in I_{ij}^{r+1} ,

$$J_{\alpha}^r u_{\alpha i j} \quad \text{becomes} \quad \begin{cases} J_{\alpha}^{r+1} u_{\alpha i j} \\ J_{\alpha}^{r+1} u_{\alpha i j}^{(1)} & (\text{included in } K_{\alpha}^{r+1}), \end{cases}$$

$$\begin{aligned} K_{\alpha}^r u_{\alpha i j}^{(1)} &\quad \text{becomes} \quad \begin{cases} K_{\alpha}^{r+1} u_{\alpha i j}^{(1)} \\ K_{\alpha}^{r+1} u_{\alpha i j}^{(2)} & (\text{included in } L_{\alpha}^{r+1}), \end{cases} \\ &\quad \dots \text{etc.} \dots \end{aligned}$$

$$\begin{aligned}
rA_{\alpha\beta} u_{\beta}^{(1)} u_{\alpha ij}^{(r-1)} &\text{ becomes } \left\{ \begin{array}{l} rA_{\alpha\beta} u_{\beta}^{(1)} |^{(1)} u_{\alpha ij}^{(r-1)} \text{ (included in new previous term)} \\ rA_{\alpha\beta} u_{\beta}^{(1)} u_{\alpha ij}^{(r)}, \end{array} \right\} (r+1) A_{\alpha\beta} u_{\beta}^{(1)} u_{\alpha ij}^{(r)} \\
A_{\alpha} u_{\alpha ij}^{(r)} &\text{ becomes } \left\{ \begin{array}{l} A_{\alpha\beta} u_{\beta}^{(1)} u_{\alpha ij}^{(r)} \\ A_{\alpha} u_{\alpha ij}^{(r+1)} \\ A_{\alpha}^{(1)} u_{\alpha ij}^{(r)}, \end{array} \right\} (r+1) A_{\alpha}^{(1)} u_{\alpha ij}^{(r)} \\
rA_{\alpha}^{(1)} u_{\alpha ij}^{(r-1)} &\text{ becomes } \left\{ \begin{array}{l} rA_{\alpha\beta}^{(1)} u_{\beta}^{(1)} u_{\alpha ij}^{(r-1)} \text{ (included in new } J_{\alpha}^{r+1}, K_{\alpha}^{r+1}, \text{ etc. terms)} \\ rA_{\alpha}^{(2)} u_{\alpha ij}^{(r-1)} \text{ (included in new following term)} \end{array} \right. \\
&\dots \text{etc.} \dots \\
rA_{\alpha}^{(r-1)} u_{\alpha ij}^{(1)} &\text{ becomes } \left\{ \begin{array}{l} rA_{\alpha}^{(r-1)} u_{\alpha ij}^{(2)} \text{ (included in new previous term)} \\ rA_{\alpha\beta}^{(r-1)} u_{\beta}^{(1)} u_{\alpha ij}^{(1)} \text{ (included in } K_{\alpha}^{r+1}) \\ rA_{\alpha}^{(r)} u_{\alpha ij}^{(1)}, \end{array} \right\} (r+1) A_{\alpha}^{(r)} u_{\alpha ij}^{(1)} \\
A_{\alpha}^{(r)} u_{\alpha ij} &\text{ becomes } \left\{ \begin{array}{l} A_{\alpha\beta}^{(r)} u_{\beta}^{(1)} u_{\alpha ij} \text{ (included in } J_{\alpha}^{r+1}) \\ A_{\alpha}^{(r+1)} u_{\alpha ij}, \end{array} \right. \\
A_{ij}^{(r)} &\text{ becomes } \left\{ \begin{array}{l} A_{\alpha}^{(r)} u_{\alpha}^{(1)} \text{ (included in } I_{ij}^{r+1}) \\ A_{ij}^{(r+1)}, \end{array} \right.
\end{aligned}$$

a bracketed superscript after a vertical stroke here denoting partial differentiation of the full expression preceding the stroke. We see the general form to be preserved over the differentiations and know it to hold for $r=1$ so by induction it is generally valid. Evaluation on the fundamental path in the region of interest now leads to

$$I_{ij}^F = J_{\alpha}^F = K_{\alpha}^F = \dots = rA_{\alpha\beta} u_{\beta}^{(1)} u_{\alpha ij}^{(r-1)}|^F = 0.$$

Furthermore we know that $A_{\alpha}^{(r)F}$ is equal to zero for all r and so we can draw the general conclusion

$$\mathcal{A}_{ij}^{(r)F} = A_{ij}^{(r)F}. \quad (\text{A.2})$$

This represents a full preservation of the diagonalization of the total potential energy over the transformation and is presented in a more recognizable form in Chapter 10.

REFERENCES

1. L. Euler, *Methodus Inveniendi Lineas Curvas Maximi Minimive Proprietate Gaudentes* (Appendix, De curvis elasticis), Marcum Michaelem Bousquet, Lausanne and Geneva, 1744.
2. J. L. Lagrange, *Mécanique Analytique*, Courcier, Paris, 1788.
3. H. Poincaré, Sur l'Équilibre d'Une Masse Fluide Animée d'Un Mouvement de Rotation, *Acta. math.*, **7**, 259 (1885).
4. A. Liapunov, *Problème Général de la Stabilité du Mouvement*, Kharkov, 1892. French translation in *Ann. fac. sci. univ. Toulouse*, **9**, 1907; reproduced in *Ann. Math. Studies*, **17**, Princeton Univ. Press, Princeton, N.J., 1949.
5. W. T. Koiter, On the Stability of Elastic Equilibrium, Dissertation, Delft, Holland, 1945. (An english translation is now available as *NASA, Tech. Trans.*, **F 10**, 833, 1967.)
6. W. T. Koiter, Buckling and post-buckling behaviour of a cylindrical panel under axial compression, *Rpts Trans. Nat. Aero. Res. Inst. Amsterdam*, **20**, 71 (1956).
7. W. T. Koiter, 'A consistent first approximation in the general theory of thin elastic shells', in *The Theory of Thin Elastic Shells* (Ed. W. T. Koiter), North Holland Publishing Co., Amsterdam, 1960.
8. W. T. Koiter, A systematic simplification of the general equations in the linear theory of thin shells, *Proc. K. ned. Akad. Wet.*, Series B, **64**, 612 (1961).
9. W. T. Koiter, *Theory of Elastic Stability and Post-buckling Behaviour*: Chapter 1, Basic concepts, Delft Report, September 1962; Chapter 2, Simple examples, Delft Report, November 1962; Chapter 3, Stability of equilibrium of continuous bodies, Brown Report No. 79, April 1962; Appendix, Notes on tensor analysis in three dimensional Euclidean space, Brown Report No. 80, October 1962.
10. W. T. Koiter, On the concept of stability of equilibrium for continuous bodies, *Proc. K. ned. Akad. Wet.*, Series B, **66**, 173 (1963).
11. W. T. Koiter, The effect of axisymmetric imperfections on the buckling of cylindrical shells under axial compression, *Proc. K. ned. Akad. Wet.*, Series B, **66**, 265 (1963).
12. W. T. Koiter, 'Elastic stability and post-buckling behaviour' in *Nonlinear Problems* (Ed. R. E. Langer), Univ. of Wisconsin Press, Madison, 1963.
13. W. T. Koiter, On the dynamic boundary conditions in the theory of thin shells, *Proc. K. ned. Akad. Wet.*, Series B, **67**, 117 (1964).
14. W. T. Koiter, On the instability of equilibrium in the absence of a minimum of the potential energy, *Proc. K. ned. Akad. Wet.*, Series B, **68**, 107 (1965).
15. W. T. Koiter, The energy criterion of stability for continuous elastic bodies, *Proc. K. ned. Akad. Wet.*, Series B, **68**, 178 (1965).

16. W. T. Koiter, General equations of elastic stability for thin shells, *Proc. Symp. Theory of Shells, Donnell Anniversary Volume*, Houston, 1966.
17. W. T. Koiter, 'Post-buckling analysis of a simple two-bar frame', in *Recent Progress in Applied Mechanics* (Ed. B. Broberg, J. Hult and F. Niordson), Almquist and Wiksell, Stockholm, 1967.
18. W. T. Koiter, Purpose and achievements of research in elastic stability, *Proc. fourth Tech. Conf., Soc. for Engng Sci.*, Raleigh, 1966.
19. W. T. Koiter, On the nonlinear theory of thin elastic shells, *Proc. K. ned. Akad. Wet.*, Series B; I Introductory sections, **69**, 1 (1966), II Basic shell equations, **69**, 18 (1966), III Simplified shell equations, **69**, 33 (1966).
20. W. T. Koiter, A sufficient condition for the stability of shallow shells, *Proc. K. ned. Akad. Wet.*, Series B, **70**, 367 (1967).
21. W. T. Koiter, The nonlinear buckling problem of a complete spherical shell under uniform external pressure, *Proc. K. ned. Akad. Wet.*, Series B, **72**, 40 (1969).
22. W. T. Koiter, On the foundations of the linear theory of thin elastic shells, *Proc. K. ned. Akad. Wet.*, Series B; Part I, **73**, 169 (1970), Part II, **73**, 183 (1970).
23. B. Budiansky and J. W. Hutchinson, Dynamic buckling of imperfection-sensitive structures, *Proc. XI Internat. Cong. Appl. Mech.*, Munich, 1964 (Springer-Verlag).
24. J. W. Hutchinson, Axial buckling of pressurized imperfect cylindrical shells, *A.I.A.A. Journal*, **3**, 1461 (1965).
25. J. W. Hutchinson, Buckling of imperfect cylindrical shells under axial compression and external pressure, *A.I.A.A. Journal*, **3**, 1968 (1965).
26. B. Budiansky, 'Dynamic buckling of elastic structures: criteria and estimates', in *Dynamic Stability of Structures* (Ed. G. Herrmann), Pergamon Press, Oxford, 1966.
27. B. Budiansky and J. W. Hutchinson, A survey of some buckling problems, *A.I.A.A. Journal*, **4**, 1505 (1966).
28. J. W. Hutchinson and B. Budiansky, Dynamic buckling estimates, *A.I.A.A. Journal*, **4**, 525 (1966).
29. B. Budiansky, Post-buckling behaviour of cylinders in torsion, *Proc. Second IUTAM Symp., Theory of Thin Shells*, Copenhagen, 1967 (Springer-Verlag).
30. J. W. Hutchinson, Imperfection sensitivity of externally pressurized spherical shells, *J. appl. Mech.*, **34**, 49 (1967).
31. J. W. Hutchinson, Initial post-buckling behaviour of toroidal shell segments, *Int. J. Solids Structures*, **3**, 97 (1967).
32. J. W. Hutchinson and J. C. Amazigo, Imperfection-sensitivity of eccentrically stiffened cylindrical shells, *A.I.A.A. Journal*, **5**, 392 (1967).
33. B. Budiansky, Notes on nonlinear shell theory, *J. appl. Mech.*, **35**, 393 (1968).
34. B. Budiansky and J. C. Amazigo, Initial post-buckling behaviour of cylindrical shells under external pressure, *J. Math. Phys.*, **47**, 223 (1968).
35. J. R. Fitch, The buckling and post-buckling behaviour of spherical caps under concentrated load, *Int. J. Solids Structures*, **4**, 421 (1968).
36. J. W. Hutchinson, Buckling and initial post-buckling behaviour of oval cylindrical shells under axial compression, *J. appl. Mech.*, **35**, 66 (1968).
37. J. C. Amazigo, Buckling under axial compression of long cylindrical shells with random axisymmetric imperfections, *Q. appl. Math.*, **26**, 537 (1969).
38. D. A. Danielson, Buckling and initial post-buckling behaviour of spheroidal shells under pressure, *A.I.A.A. Journal*, **7**, 936 (1969).
39. D. A. Danielson, Dynamic buckling loads of imperfection-sensitive structures from perturbation procedures, *A.I.A.A. Journal*, **7**, 1506 (1969).

40. W. B. Fraser and B. Budiansky, The buckling of a column with random initial deflections, *J. appl. Mech.*, **36**, 233 (1969).
41. J. W. Hutchinson and J. C. Frauenthal, Elastic postbuckling behaviour of stiffened and barreled cylindrical shells, *J. appl. Mech.*, **36**, 784 (1969).
42. J. C. Amazigo, B. Budiansky and G. F. Carrier, Asymptotic analyses of the buckling of imperfect columns on nonlinear elastic foundations, *Int. J. Solids Structures*, **6**, 1341 (1970).
43. J. R. Fitch and B. Budiansky, Buckling and post-buckling behaviour of spherical caps under axi-symmetric load, *A.I.A.A. Journal*, **8**, 686 (1970).
44. J. W. Hutchinson and W. T. Koiter, Postbuckling theory, *Appl. Mech. Rev.*, **23**, 1353 (1970).
45. J. C. Amazigo, Buckling of stochastically imperfect columns on nonlinear elastic foundations, *Q. appl. Math.*, **29**, 403 (1971).
46. J. C. Amazigo and W. B. Fraser, Buckling under external pressure of cylindrical shells with dimple shaped initial imperfections, *Int. J. Solids Structures*, **7**, 883 (1971).
47. J. W. Hutchinson, R. C. Tennyson and D. B. Muggeridge, Effect of a local axisymmetric imperfection on the buckling behaviour of a circular cylindrical shell under axial compression, *A.I.A.A. Journal*, **9**, 48 (1971).
48. W. B. Stephens, Imperfection sensitivity of axially compressed stringer reinforced cylindrical panels under internal pressure. *A.I.A.A. Journal*, **9**, 1713 (1971).
49. H. Ziegler, On the concept of elastic stability, *Advances in Applied Mechanics*, **4**, 351 (1956). (Academic Press, New York.)
50. H. Ziegler, *Principles of Structural Stability*, Blaisdell Publishing Co. (A division of Ginn and Co.), Waltham, Mass., 1968.
51. G. Herrmann, Stability of equilibrium of elastic systems subjected to non-conservative forces, *Appl. Mech. Rev.*, **20**, 103 (1967).
52. J. M. T. Thompson, Basic principles in the general theory of elastic stability, *J. Mech. Phys. Solids*, **11**, 13 (1963).
53. S. J. Britvec and A. H. Chilver, Elastic buckling of rigidly-jointed braced frames, *J. Engng Mech. Div. Am. Soc. civ. Engrs*, **89**, 217 (1963).
54. J. M. T. Thompson, Basic concepts of elastic stability, *Dept. of Aeronautics and Astronautics, Stanford University*, Rpt. No. 146, February 1963.
55. J. W. Appeltauer and T. A. Barta, Critical loads of plane frames, *Concr. constr. Engng.*, **59**, 293 (1964).
56. J. M. T. Thompson, 'The post-buckling of a spherical shell by computer analysis', in *World Conference on Shell Structures* (Ed. S. J. Medwadowski, et al.), National Academy of Sciences, Washington, 1964.
57. J. M. T. Thompson, The rotationally-symmetric branching behaviour of a complete spherical shell, *Proc. K. ned. Akad. Wet.*, Series B, **67**, 295 (1964).
58. J. M. T. Thompson, Eigenvalue branching configurations and the Rayleigh-Ritz procedure, *Q. appl. Math.*, **22**, 244 (1964).
59. J. Roorda, The Instability of Imperfect Elastic Structures, Ph.D. Thesis, University College, London, 1965.
60. J. Roorda, Stability of structures with small imperfections, *J. Engng. Mech. Div. Am. Soc. civ. Engrs*, **91**, 87 (1965).
61. J. Roorda, The buckling behaviour of imperfect structural systems, *J. Mech. Phys. Solids*, **13**, 267 (1965).
62. J. M. T. Thompson, Discrete branching points in the general theory of elastic stability, *J. Mech. Phys. Solids*, **13**, 295 (1965).

63. S. C. Tillman, The Elastic Instability of Shallow Spherical Shells, Ph.D. Thesis, University College London, 1965.
64. M. H. R. Godley, Elastic Buckling of Plane Frames, Ph.D. Thesis, University College London, 1966.
65. S. H. Perry, Statistical Variation of Buckling Strength, Ph.D. Thesis, University College London, 1966.
66. W. J. Supple, Coupled Buckling Modes of Structures, Ph.D. Thesis, University College London, 1966.
67. J. M. T. Thompson, 'Dynamic buckling under step loading', in *Dynamic Stability of Structures* (Ed. G. Herrmann), Pergamon Press, Oxford, 1966.
68. A. C. Walker, Local instability in plates and channel struts, *J. struct. Div. Am. Soc. civ. Engrs*, **92**, 39 (1966).
69. T. A. Barta, 'On the torsional-flexural buckling of thin-walled elastic bars with monosymmetric open cross-section', in *Thin-walled Structures* (Ed. A. H. Chilver), Chatto and Windus, London, 1967.
70. A. H. Chilver, Coupled modes of elastic buckling, *J. Mech. Phys. Solids*, **15**, 15 (1967).
71. A. H. Chilver, *Thin-walled Structures*, Chatto and Windus, London, 1967.
72. M. H. R. Godley and A. H. Chilver, The elastic post-buckling behaviour of unbraced plane frames, *Int. J. mech. Sci.*, **9**, 323 (1967).
73. K. Huseyin, Elastic Stability of Structures under Combined Loading, Ph.D. Thesis, University College London, 1967.
74. J. Roorda, Some thoughts on the Southwell plot, *J. Engng Mech. Div. Am. Soc. civ. Engrs*, **93**, 37 (1967).
75. W. J. Supple, Coupled branching configurations in the elastic buckling of symmetric structural systems, *Int. J. mech. Sci.*, **9**, 97 (1967).
76. W. J. Supple and A. H. Chilver, 'Elastic post-buckling of compressed rectangular plates', in *Thin-walled Structures* (Ed. A. H. Chilver), Chatto and Windus, London, 1967.
77. J. M. T. Thompson, Localized Rayleigh functions for structural and stress analysis, *Int. J. Solids Structures*, **3**, 285 (1967).
78. J. M. T. Thompson, The estimation of elastic critical loads, *J. Mech. Phys. Solids*, **15**, 311 (1967).
79. J. M. T. Thompson, Towards a general statistical theory of imperfection-sensitivity in elastic post-buckling, *J. Mech. Phys. Solids*, **15**, 413 (1967).
80. A. C. Walker, 'Flat rectangular plates subjected to a linearly-varying edge compressive loading', in *Thin-walled Structures* (Ed. A. H. Chilver), Chatto and Windus, London, 1967.
81. A. C. Walker, Rayleigh-Ritz method for plate flexure, *J. Engng Mech. Div. Am. Soc. civ. Engrs*, **93**, 139 (1967).
82. J. Roorda, On the buckling of symmetric structural systems with first and second order imperfections, *Int. J. Solids Structures*, **4**, 1137 (1968).
83. W. J. Supple, On the change in buckle pattern in elastic structures, *Int. J. mech. Sci.*, **10**, 737 (1968).
84. J. M. T. Thompson and A. C. Walker, The nonlinear perturbation analysis of discrete structural systems, *Int. J. Solids Structures*, **4**, 757 (1968).
85. A. C. Walker, Maximum loads for eccentrically loaded thin-walled channel struts, *Publs int. Ass. Bridge struct. Engng*, **28-II**, 169 (1968).
86. A. C. Walker, An analytical study of the rotationally-symmetric nonlinear buckling of a complete spherical shell under external pressure, *Int. J. mech. Sci.*, **10**, 695 (1968).

87. A. C. Walker and D. G. Hall, An analysis of the large deflections of beams using the Rayleigh-Ritz Finite Element method, *Aeronaut. Q.*, **19**, 357 (1968).
88. T. A. Barta, A comparative survey of the theories for elastic circular cylindrical shells, *Proc. Int. Colloquium, Progress of Shell Structures in the Last Ten Years and its Future Development*, Madrid, 1969 (IASS).
89. T. A. Barta, A contribution to a nonlinear engineering shell theory, *Proc. IUTAM Symp. Instability of Continuous Systems*, Herrenalb, 1969 (Springer-Verlag).
90. I. W. Burgess, Some One-way Buckling Phenomena, Ph.D. Thesis, University College London, 1969.
91. A. H. Chilver and K. C. Johns, Coupled modes of buckling in some continuous systems, *Proc. IUTAM Symp. Instability of Continuous Systems*, Herrenalb, 1969 (Springer-Verlag).
92. J. G. A. Croll, The buckling of hyperboloidal cooling towers under lateral loading, *Proc. Int. Colloquium, Progress of Shell Structures in the Last Ten Years and its Future Development*, Madrid, 1969 (IASS).
93. J. G. A. Croll and A. C. Walker, On the unification of the finite-difference and finite-element methods, *Proc. Fifth International Congress on the Application of Mathematics in Engineering*, Weimar, 1969.
94. J. G. A. Croll, The influence of shape on the stresses in cooling towers, *Proc. Instn civ. Engrs*, **42**, 383 (1969).
95. D. G. Hall, Numerical Analysis of Nonlinear Behaviour of Structural Elements, Ph.D. Thesis, University College London, 1969.
96. K. Huseyin, The convexity of the stability boundary of symmetric structural systems, *Acta mech.*, **8**, 205 (1969).
97. K. C. Johns, Elastic Buckling Behaviour at Coincident Branching Points, Ph.D. Thesis, University College London, 1969.
98. M. S. Rolls, The Elastic Stability of Discontinuous Structural Systems, Ph.D. Thesis, University College London, 1969.
99. J. Roorda, Some statistical aspects of the buckling of imperfection-sensitive structures, *J. Mech. Phys. Solids*, **17**, 111 (1969).
100. W. J. Supple, Initial post-buckling behaviour of a class of elastic structural systems, *Int. J. Nonlinear Mechanics*, **4**, 23 (1969).
101. J. M. T. Thompson, The branching analysis of perfect and imperfect discrete structural systems, *J. Mech. Phys. Solids*, **17**, 1 (1969).
102. J. M. T. Thompson and A. C. Walker, A general theory for the branching analysis of discrete structural systems, *Int. J. Solids Structures*, **5**, 281 (1969).
103. J. M. T. Thompson and G. W. Hunt, Perturbation patterns in nonlinear branching theory, *Proc. IUTAM Symp. Instability of Continuous Systems*, Herrenalb, 1969 (Springer-Verlag).
104. J. M. T. Thompson and G. W. Hunt, Comparative perturbation studies of the elastica, *Int. J. mech. Sci.*, **11**, 999 (1969).
105. J. M. T. Thompson, A general theory for the equilibrium and stability of discrete conservative systems, *Z. angew. Math. Phys.*, **20**, 797 (1969).
106. A. C. Walker, A nonlinear finite element analysis of shallow circular arches, *Int. J. Solids Structures*, **5**, 97 (1969).
107. A. C. Walker, The post-buckling behaviour of simply-supported square plates, *Aeronaut. Q.*, **20**, 203 (1969).
108. A. C. Walker, A method of solution for nonlinear simultaneous algebraic equations, *Int. J. Numerical Methods in Engng*, **1**, 177 (1969).

109. J. G. A. Croll, Hermitian methods for the approximate solution of partial differential equations, *J. Inst. Maths Applics.*, **6**, 365 (1970).
110. M. H. R. Godley and A. H. Chilver, Elastic buckling of overbraced frames, *J. mech. Engng Sci.*, **12**, 238 (1970).
111. B. Hayman, The Stability of Degenerate Structures, Ph.D. Thesis, University College London, 1970.
112. K. Huseyin, The stability boundary of systems with one degree of freedom, *Meccanica*, **5**, 306 and **5**, 312 (1970).
113. K. Huseyin, Fundamental principles in the buckling of structures under combined loading, *Int. J. Solids Structures*, **6**, 479 (1970).
114. K. Huseyin, The elastic stability of structural systems with independent loading parameters, *Int. J. Solids Structures*, **6**, 677 (1970).
115. J. Roorda and A. H. Chilver, Frame buckling: an illustration of the perturbation technique, *Int. J. Nonlinear Mechanics*, **5**, 235 (1970).
116. W. J. Supple, Changes of wave-form of plates in the post-buckling range, *Int. J. Solids Structures*, **6**, 1243 (1970).
117. J. M. T. Thompson, A new approach to elastic branching analysis, *J. Mech. Phys. Solids*, **18**, 29 (1970).
118. J. M. T. Thompson, Basic theorems of elastic stability, *Int. J. Engng Sci.*, **8**, 307 (1970).
119. S. C. Tillman, On the buckling behaviour of shallow spherical caps under a uniform pressure load, *Int. J. Solids Structures*, **6**, 37 (1970).
120. I. W. Burgess, On the equilibrium and stability of discrete one-way structural systems, *Int. J. Solids Structures*, **7**, 667 (1971).
121. I. W. Burgess, The buckling of a radially constrained imperfect circular ring, *Int. J. mech. Sci.*, **13**, 741 (1971).
122. A. H. Chilver, 'The role of structural materials and forms', in *A Discussion on Architectural Aerodynamics* (Ed. M. J. Lighthill and A. Silverleaf), *Phil. Trans. R. Soc.*, **269**, 321 (1971).
123. J. G. A. Croll, Continuum perturbation method in the branching analysis of conservative systems, *Int. J. mech. Sci.*, **13**, 605 (1971).
124. J. G. A. Croll and A. C. Walker, The finite-difference and localized Ritz methods, *Int. J. Numerical Methods in Engng*, **3**, 155 (1971).
125. D. Ho, Higher order approximations in the calculation of elastic buckling loads of imperfect systems, *Int. J. Non-linear Mechanics*, **6**, 649 (1971).
126. G. W. Hunt, Perturbation Techniques in Elastic Stability, Ph.D. Thesis, University College London, 1971.
127. G. W. Hunt, The discrete branching point as a one degree of freedom phenomenon, *Int. J. Solids Structures*, **7**, 495 (1971).
128. K. Huseyin, The post-buckling behaviour of structures under combined loading, *Z. angew. Math. Mech.*, **51**, 177 (1971).
129. K. Huseyin, Instability of symmetric structural systems with independent loading parameters, *Q. appl. Math.*, **28**, 571 (1971).
130. K. Huseyin and J. Roorda, The loading frequency relationship in multiple eigenvalue problems, *J. appl. Mech.*, **38**, 1007 (1971).
131. K. C. Johns and A. H. Chilver, Multiple path generation at coincident branching points, *Int. J. mech. Sci.*, **13**, 899 (1971).
132. J. M. T. Thompson, On the simulation of a gravitational field by a centrifugal field, *Int. J. mech. Sci.*, **13**, 979 (1971).
133. J. M. T. Thompson and G. W. Hunt, A theory for the numerical analysis of compound branching, *Z. angew. Math. Phys.*, **22**, 1001 (1971).

134. A. C. Walker, J. G. A. Croll and E. Wilson, Experimental models to illustrate the nonlinear behaviour of elastic structures, *Bull. mech. Engng Educ.*, **10**, 247 (1971).
135. J. M. T. Thompson and G. M. Lewis, Continuum and finite element branching studies of the circular plate, *Computers and Structures*, **2**, 511 (1972).
136. J. M. T. Thompson and W. J. Supple, Erosion of optimum designs by compound branching phenomena, *J. Mech. Phys. Solids*, **21**, 135 (1973).
137. M. J. Sewell, The static perturbation technique in buckling problems, *J. Mech. Phys. Solids*, **13**, 247 (1965).
138. M. J. Sewell, On the connexion between stability and the shape of the equilibrium surface, *J. Mech. Phys. Solids*, **14**, 203 (1966).
139. M. J. Sewell, A general theory of equilibrium paths through critical points, *Proc. R. Soc., Series A*, **306**, 201 (1968).
140. M. J. Sewell, A method of post-buckling analysis, *J. Mech. Phys. Solids*, **17**, 219 (1969).
141. M. J. Sewell, On the branching of equilibrium paths, *Proc. R. Soc., Series A*, **315**, 499 (1970).
142. R. A. Lyttleton, *The Stability of Rotating Liquid Masses*, Cambridge University Press, Cambridge, 1953.
143. P. Ledoux, 'Stellar Stability', in *Handbuch der Physik*, Vol. LI (Ed. S. Flugge), Springer-Verlag, Berlin, 1958.
144. S. T. Mau and R. H. Gallagher, A finite element procedure for nonlinear pre-buckling and initial post-buckling analysis, *NASA, CR*, August 1971.
145. A. van der Neut, The interaction of local buckling and column failure of thin-walled compression members, *Proc. XII Internat. Cong. Appl. Mech.*, Stanford, 1968 (Springer-Verlag).
146. J. L. Synge and B. A. Griffith, *Principles of Mechanics*, McGraw-Hill, New York, 1959.
147. B. Fraeij de Veubeke, 'Displacement and equilibrium models in the finite element method', in *Stress Analysis* (Ed. O. C. Zienkiewicz and G. S. Holister), Wiley, London, 1965.
148. J. M. T. Thompson, Stability of elastic structures and their loading devices, *J. mech. Engng Sci.*, **3**, 153 (1961).
149. D. G. Ashwell, 'Nonlinear problems', in *Handbook of Engineering Mechanics* (Ed. W. Flugge), McGraw-Hill, New York, 1962.
150. J. M. T. Thompson, The elastic instability of a complete spherical shell, *Aeronaut. Q.*, **13**, 189 (1962).
151. S. J. Britvec, The theory of elastica in the nonlinear behaviour of plane frameworks, *Int. J. mech. Sci.*, **7**, 661 (1965).
152. R. Haftka and W. Nachbar, Post-buckling analysis of an elastically-restrained column, *Int. J. Solids Structures*, **6**, 1433 (1970).
153. G. F. Carrier, On the buckling of elastic rings, *J. Math. Phys.*, **26**, 94 (1947).
154. J. G. Lekkerkerker, On the stability of an elastically supported beam subjected to its smallest buckling load, *Proc. K. ned. Akad. Wet., Series B*, **65**, 190 (1962).
155. Y. C. Fung and A. Kaplan, Buckling of low arches or curved beams of small curvature, *NACA Tech. Nt.* 2840, 1952.
156. S. J. Britvec, Elastic buckling of pin-jointed frames, *Int. J. mech. Sci.*, **5**, 447 (1963).
157. S. J. Britvec, Overall stability of pin-jointed frameworks after the onset of elastic buckling, *Ing.-Arch.*, **32**, 443 (1963).

158. K. O. Friedrichs and J. J. Stoker, The nonlinear boundary value problem of the buckled plate, *Proc. natn. Acad. Sci., U.S.A.*, **25**, 535 (1939).
159. K. O. Friedrichs and J. J. Stoker, The nonlinear boundary value problem of the buckled plate, *Am. J. Math.*, **63**, 839 (1941).
160. K. O. Friedrichs and J. J. Stoker, Buckling of the circular plate beyond the critical thrust, *J. appl. Mech.*, **9**, 7 (1942).
161. S. R. Bodner, The post-buckling behaviour of a clamped circular plate, *Q. appl. Math.*, **12**, 397 (1955).
162. G. G. Pope, The buckling behaviour in axial compression of slightly-curved panels, including the effect of shear deformability, *Int. J. Solids Structures*, **4**, 323 (1968).
163. N. Akkas and N. R. Bauld, Static and dynamic buckling behaviour of clamped shallow conical shells, *Int. J. mech. Sci.*, **13**, 689 (1971).
164. N. Akkas and N. R. Bauld, Buckling and post-buckling of spherical caps, *J. Engng. Mech. Div. Am. Soc. civ. Engrs.*, **97**, 727 (1971).
165. N. Akkas and N. R. Bauld, Buckling and post-buckling behaviour of clamped shallow spherical shells under axisymmetric ring loads, *J. appl. Mech.*, **38**, 996 (1971).
166. N. Akkas and N. R. Bauld, Buckling and initial post-buckling behaviour of clamped shallow spherical sandwich shells, *Int. J. Solids Structures*, **7**, 1229 (1971).
167. B. O. Almroth, A. M. C. Holmes and D. O. Brush, An experimental study of the buckling of cylinders under axial compression, *Experimental Mechanics*, **4**, 263 (1964).
168. R. L. Carlson, R. L. Sendelbeck and N. J. Hoff, Experimental studies of the buckling of complete spherical shells, *Experimental Mechanics*, **7**, 281 (1967).
169. L. Berke and R. L. Carlson, Experimental studies of the post-buckling behaviour of complete spherical shells, *Experimental Mechanics*, **8**, 548 (1968).
170. J. M. T. Thompson, Making of thin metal shells for model stress analysis, *J. mech. Engng Sci.*, **2**, 105 (1960).
171. D. A. Evensen, High speed photographic observation of the buckling of thin cylinders, *Experimental Mechanics*, **4**, 110 (1964).
172. R. C. Tennyson, Buckling modes of circular cylindrical shells under axial compression, *A.I.A.A. Journal*, **7**, 1481 (1969).
173. N. J. Hoff, Buckling of thin shells, *Von Karman 80th Anniversary Lecture*, May 1961 (Institute of the Aerospace Sciences, New York).
174. W. Nachbar and N. J. Hoff, The buckling of a free edge of an axially compressed circular cylindrical shell, *Q. appl. Math.*, **20**, 267 (1962).
175. N. J. Hoff and L. W. Rehfield, Buckling of axially compressed circular cylindrical shells at stresses smaller than the classical critical value, *J. appl. Mech.*, **32**, 542 (1965).
176. N. J. Hoff, W. A. Madsen and J. Mayers, Post-buckling equilibrium of axially compressed circular cylindrical shells, *A.I.A.A. Journal*, **4**, 126 (1966).
177. A. E. Green and J. E. Adkins, *Large Elastic Deformations*, Clarendon Press, Oxford, 1960.
178. H. Alexander, The tensile instability of an inflated cylindrical membrane as affected by an axial load, *Int. J. mech. Sci.*, **13**, 87 (1971).
179. H. Alexander, Tensile instability of initially spherical balloons, *Int. J. Engng Sci.*, **9**, 151 (1971).
180. J. P. Miles, Bifurcation in plastic flow under uniaxial tension, *J. Mech. Phys. Solids*, **19**, 89 (1971).

181. W. H. Chen, Necking of a bar, *Int. J. Solids Structures*, **7**, 685 (1971).
182. R. N. Dubey and S. T. Ariaratnam, Necking instabilities in elastic-plastic plates, *Int. J. Engng Sci.*, **10**, 145 (1972).
183. V. I. Vozlinskii, On the relations between the bifurcation of the equilibria of conservative systems and the stability distribution on the equilibria curve, *Prikl. Mat. Mekh.*, **31**, 418 (1967).
184. R. E. Bellman, *Perturbation Techniques in Mathematics, Physics and Engineering*, elastic foundations, *Q. appl. Math.*, **29**, 403 (1971).
185. J. B. Keller, *Perturbation Theory*, Notes on a series of six lectures presented at the Dept. of Mathematics, Michigan State University, East Lansing, Michigan, March 1968.
186. J. B. Keller and S. Antman, *Bifurcation Theory and Nonlinear Eigenvalue Problems*, Benjamin, New York, 1969.
187. B. L. van der Waerden, *Modern Algebra*, F. Ungar, New York, 1950.
188. J. La Salle and S. Lefschetz, *Stability by Liapunov's Direct Method with Applications*, Academic Press, New York, 1961.
189. N. G. Chetayev, *The Stability of Motion*, translated from the Russian by M. Nadler, Pergamon Press, New York, 1961.
190. W. L. Ferrar, *Algebra: A text book of determinants, matrices and algebraic forms*, Clarendon Press, Oxford, 1957.
191. E. F. Masur and H. L. Schreyer, A second approximation to the problem of elastic stability, *Proc. Symp. Theory of Shells, Donnell Anniversary Volume*, Houston, 1966.
192. K. E. Bisschopp and D. C. Drucker, Large deflection of cantilever beams, *Q. appl. Math.*, **3**, 272 (1945).
193. R. T. Haftka, R. H. Mallett and W. Nachbar, Adaption of Koiter's method to finite element analysis of snap-through buckling behaviour, *Int. J. Solids Structures*, **7**, 1427 (1971).
194. N. Bazley and B. Zwahlen, Estimation of the bifurcation coefficient for nonlinear eigenvalue problems, *Z. angew. Math. Phys.*, **20**, 281 (1969).
195. E. H. Mansfield, Some identities on structural flexibility after buckling, *Aeronaut. Q.*, **9**, 300 (1958).
196. G. G. Pope, On the bifurcational buckling of elastic beams, plates and shallow shells, *Aeronaut. Q.*, **19**, 20 (1968).
197. G. Augusti, Stabilità' di strutture elastiche elementari in presenza di grandi spostamenti, *Atti Accad. Sci. fis. mat., Napoli*, Serie 3^a, **4**, No. 5 (1964).
198. V. V. Bolotin, Nonlinear theory of elasticity and stability in the case of large deflections, *Raschety na Prochnost*, No. 3, Mashgiz, Moscow, 1958.
199. S. P. Timoshenko and J. M. Gere, *Theory of Elastic Stability*, McGraw-Hill, New York, 1961.
200. E. H. Brown, The failure of frames, *Proc. R. Soc., Series A*, **319**, 405 (1970).
201. S. B. Dong and J. A. Wolf, Stability analysis of structures by a reduced system of generalized coordinates, *Int. J. Solids Structures*, **6**, 1377 (1970).
202. T. von Kármán and H. S. Tsien, The buckling of spherical shells by external pressure, *J. aeronaut. Sci.*, **7**, 43 (1939).
203. J. M. T. Thompson, 'Elastic buckling of thin spherical shells', in *Nuclear Reactor Containment Buildings and Pressure Vessels* (Ed. A. S. T. Thomson, et al.), Butterworths, London, 1960.
204. J. M. T. Thompson, The Elastic Instability of Spherical Shells, Ph.D. Thesis, Cambridge University, 1961.

205. E. Reissner, On post-buckling behaviour and imperfection-sensitivity of thin elastic plates on a nonlinear elastic foundation, *Stud. appl. Math.*, **49**, 45 (1970).
206. E. Reissner, A note on post-buckling behaviour of pressurized shallow spherical shells, *J. appl. Mech.*, **37**, 533 (1970).
207. R. T. Haftka, R. H. Mallett and W. Nachbar, Relation of the static perturbation technique to Koiter's method, *Israel J. Tech.*, **9**, 553 (1971).
208. E. T. Whittaker and G. N. Watson, *A Course of Modern Analysis*, Cambridge University Press, Cambridge, 1969.
209. T. M. MacRobert, *Spherical Harmonics*, Methuen, London, 1947.
210. J. C. Adams, On the expression of the product of any two Legendre's coefficients by means of a series of Legendre's coefficients, *Proc. R. Soc.*, **27**, 63 (1878).
211. Y. C. Fung and E. E. Sechler, 'Instability of thin elastic shells', in *Structural Mechanics* (Ed. J. N. Goodier and N. J. Hoff), Pergamon Press, Oxford, 1960.
212. J. M. T. Thompson, Optimization as a generator of structural instability, Letter to the Editor, *Int. J. mech. Sci.*, **14**, 627 (1972).
213. J. M. T. Thompson and G. M. Lewis, On the optimum design of thin-walled compression members, *J. Mech. Phys. Solids*, **20**, 101 (1972).
214. W. T. Koiter and M. Skaloud, Interventions, pages 64–68, 103 and 104 in *Comportement Postcritiques des Plaques Utilisées en Construction métallique*, Colloque International tenu à l'Université de Liège, 1962. *Mémoires de la Société Royale des Sciences de Liège*, 5^{me} série, tome VIII, fascicule 5.
215. J. M. T. Thompson and G. W. Hunt, 'Dangers of structural optimization', *International Symposium on Optimization in Civil Engineering*, Liverpool, 1973. To be published in *Engineering Optimization*, a new Journal by Gordon and Breach, edited by A. B. Templeman.
216. A. G. M. Michell, The limits of economy of material in frame structures, *Phil. Mag.*, **8**, 589 (1904).
217. W. T. Koiter and G. D. C. Kuiken, The interaction between local buckling and overall buckling on the behaviour of built-up columns, *Rpt. No. 447, Laboratory of Engineering Mechanics, Delft*, May 1971.
218. T. R. Graves-Smith, 'The ultimate strength of locally buckled columns of arbitrary length', in *Thin-Walled Steel Structures* (Ed. K. C. Rockey and H. V. Hill), Crosby and Lockwood, London, 1969.
219. T. R. Graves-Smith, The effect of initial imperfections on the strength of thin-walled box columns, *Int. J. mech. Sci.*, **13**, 911 (1971).
220. V. Tvergaard, Imperfection-sensitivity of a wide integrally stiffened panel under compression, *Rpt. No. 19, The Danish Centre for Applied Mathematics and Mechanics, The Technical University of Denmark*, December, 1971.
221. A. G. Pugsley, *The Safety of Structures*, Edward Arnold, London, 1966.

BIBLIOGRAPHY

A valuable text book introducing the nonlinear features of elastic stability, just completed by our colleagues at University College London

J. G. A. Croll and A. C. Walker, *Elements of Structural Stability*, Macmillan, London, 1972.

Books on elastic stability with a mechanics flavour

H. Leipholz, *Stability Theory*, Academic Press, New York, 1970

A. Pfluger, *Stabilitätsprobleme der Elastostatik*, Springer, Berlin, 1964.

H. Ziegler, *Principles of Structural Stability*, Blaisdell, Waltham, Mass, 1968.

Standard engineering texts on structural stability

F. Bleich, *Buckling Strength of Metal Structures*, McGraw-Hill, New York, 1952.

G. Burgermeister, H. Steup and H. Kretzschmar, *Stabilitätstheorie*, Vols I and II, Deutscher Verlag der Wissenschaften, Berlin, 1957, 1963.

C. F. Kollbrunner and M. Meister, *Knicken (also Ausbeulen)* Springer, Berlin, 1961 (1958).

S. P. Timoshenko and J. M. Gere, *Theory of Elastic Stability*, McGraw-Hill, New York, 1961.

A. S. Volmir, *Stability of Deformable Systems*, NASA, AD628 508 (1965).

A recent book on structural optimization

L. Spunt, *Optimum Structural Design*, Prentice-Hall, Englewood Cliffs, N.J., 1971.

INDEX

- A*-analysis, compound branching, 222–236
imperfect systems, 181–187
perfect system, 98, 150–154
Active coordinates, *see* Generalized coordinates
Adkins, J. E., 61
Akkas, N., 60
Alexander, H., 61
Almroth, B. O., 60
Amazigo, J. C., 60, 69
Antman, S., 83
Arches, 1–5, 48, 51, 57, 59, 75–76, 132, 189, 289
Ariaratnam, S. T., 61
Ashwell, D. G., 57
Asymmetric point of bifurcation, *see* Bifurcation points
Asymptotic equations of imperfection-sensitivity, 202–204
Augusti, G., 8, 11, 191, 243
Axioms, 50, 87
Bauld, N. R., 60
Beams, 112, 117–126
Bellman, R. E., 78
Bessel functions, 167, 169
Bezout's theorem, 84, 221, 231–233, 242
Bifurcation points, vii, 65, 99, 134–140, 141–159, 221, 287
asymmetric point of bifurcation, 21, 52, 68, 135, 147, 149, 153, 154, 183, 199, 203
imperfect systems, 181–204
secondary branching, 47, 246
stable-symmetric point of bifurcation, 9, 54, 68, 138, 147, 149, 153, 154, 187
unstable-symmetric point of bifurcation, 14, 55, 68, 139, 147, 149, 153, 154, 189, 200, 203
Bleich, F., 317
Bolotin, V. V., 205
Boundary conditions, 112
Tale, 31, 111–116
Box-girder bridges, 289
Branching points, *see* Bifurcation points
Britvec, S. J., 46, 59, 60
Brown, E. H., 220
Brush, D. O., 60
Buckling, vii
one-way, 47
simultaneous, vii, 47, 49, 242, 262
Buckling modes, 24, 38, 102, 262
Budiansky, B., 46, 60, 61, 69
Burgermeister, G., 317
Burgess, I. W., 47
Calculus of variations, 29, 111, 119, 164
Cantilevers, hinged, 5–9
proped, 9–14
Carlson, R. L., 60
Carrier, G. F., 59, 69
Chetayev, N. G., 87
Chilver, A. H., v, 46, 47, 249, 267
Circular plates, *see* Plates, circular
Conical shells, 60
Continuous systems, vii, 26, 110, 117, 155, 160, 205, 251
Contraction mechanism, continuous systems, 168, 177
discrete systems, 145, 146, 177, 198
Corresponding deflection of the load, 17, 107, 130, 137, 140, 148
Cosmology, 61
Critical points, bifurcations, *see* Bifurcation points
coincident, vii, 221–250, 262
compound, vii, 47, 221–250, 251, 265, 287, 293
distinct, vii, 66, 71, 79, 91
limit point, *see* Limit point
nearly-coincident, 46, 222, 267
Critical state equations, 195
general forms, 196
Critical state stability, 93–98, 236–238
Croll, J. G. A., vi, 47, 161, 168, 177, 191, 317
Crystallography, 61
Cylindrical shells, 60, 291, 294
D-analysis, 90, 95, 105, 127, 180
Danielson, D. A., 59

- Degenerating structures, 47
Degree of instability, 90, 99, 131
Degrees of freedom, infinite, 26, 253
one, 2, 5, 9, 15, 63, 132, 146, 189, 300
two, 21, 57, 108, 142, 188, 243
Diagonalization, 22, 47, 89, 98, 101, 141, 150, 151, 158, 223–224, 260
Discrete systems, vii, 49
Domes, 51, 59, 60, 290
Donnell equations, 156, 159
Dubey, R. N., 61
- Eigenvalue analysis, *see* Linear eigenvalue analysis
Elastica, 26–45, 99, 114, 253
Elimination of passive coordinates, 65, 221, 224–228, 238–241, 263, 265, 269
Equilibrium, critical, vii, 91
neutral, vii
normal, vii, 103–126, 132
stable, 91
unstable, 91
Equilibrium condition, 87, 228, 240
Equilibrium equations, 84, 104, 128, 143, 152, 194, 225, 232, 233, 239, 241
general forms, 144, 194, 303, 304
Equilibrium path, 98
complementary, 9, 73, 268
fundamental, vii, 6, 141
natural, 9
post-buckling, vii, 6, 143, 146, 152, 231, 241
primary, vii, 64
secondary, vii, 64
Euler, L., 46
Euler equation, beam, 119
circular plate, 164
hanging bar, 111
strut, 29
Evensen, D. A., 60
Exchange of stabilities, 53, 137, 154
Experiments, 60, 71–76, 219, 281
Far-field stability test, 70, 238
Finite-difference method, 47
Finite-element method, 40–44, 47, 49, 78, 81, 99, 110–116, 124–126, 170–178, 211–220
Fitch, J. R., 60
Follower force, 88
Fourier harmonics, 37
Fraeijs de Veubeke, B., 49

- Frames, 47, 59, 60, 71–75, 211–220, 292
Friedrichs, K. O., 60, 168, 178
Fung, Y. C., 59, 271
Gallagher, R. H., 48
Generalized coordinates, 49, 86, 93
active, 222, 238
incremental, 89, 132
passive, 222, 238
principal, 22, 49, 90, 187, 260
sliding, 98, 141, 142, 160, 192
sliding and rotating, 98, 130, 141, 150, 152, 153, 159, 181
Gere, J. M., 26, 44, 208, 317
Godley, M. H. R., 47
Graves-Smith, T. R., 295
Green, A. E., 61
Griffith, B. A., 49, 86
Haftka, R. T., 59, 131, 253
Hamilton's equations, 86
Hanging bar, 110–116
Harmonic analysis, beam, 122–124
spherical shell, 256–271
strut, 37–40, 99, 209
Hayman, B., 47
Herrmann, G., 46
Hoff, N. J., 60, 61
Holmes, A. M. C., 60
Holonomic systems, 86
Huseyin, K., 47
Hutchinson, J. W., 46, 60, 61, 251, 271, 299
Hypersurface of activity, 229
Imperfections, 7, 61, 65–69, 71–76, 181, 205, 211, 243, 287, 297
stochastic, 69
two, 15, 243
Imperfection-sensitivity, 71–76, 202, 219, 242, 248, 276, 280, 283, 287–299
asymmetric point of bifurcation, 20, 66, 183, 203
limit point, 181
power laws, 69, 203, 204, 276, 281, 286
unstable-symmetric point of bifurcation, 13, 67, 187, 203
Induction, 145, 195–197, 303–306
Johns, K. C., 47
Kaplan, A., 59
Kármán, T. von. v. 160, 251

- Kármán plate equations, 160
Keller, J. B., 78, 83
Kelly, A., 61
Kemp, K. O., v
Kinematically-admissible displacement field, 110
Kinetic energy function, 86, 87
Kirchhoff uniqueness theorem, 104
Koiter, W. T., v, vi, 14, 46, 60, 61, 69, 74, 87, 154, 191, 211, 216, 218, 236, 237, 251, 253, 261, 263, 266, 267, 271, 276, 277, 281, 289, 291, 293, 294, 295, 299
Kollbrunner, C. F., 317
Kretzschmar, H., 317
Kuiken, G. D. C., 276, 277, 281, 295, 299
Lagrange, J. L., 46, 86
La Salle, J., 87
Ledoux, P., 48, 61
Lefschetz, S., 87
Legendre functions, 251, 253, 256
Leipholz, H., 83, 317
Lekkerkerker, J. G., 59, 205, 209
Lewis, G. M., 48, 81, 160, 172, 177, 288, 295, 299
Liapunov, A., 46, 50, 86
Limit point, 5, 51, 68, 129–134, 148, 180
Linear eigenvalue analysis, 26, 32, 159, 260, 279
Link models, 1–26, 99, 189, 243
Loading parameter, 50, 86–88
Localized Ritz procedure, 112–115
Lyttleton, R. A., 48, 61
Macmillan, N. H., 61
Madsen, W. A., 61
Mallett, R. H., 131, 253
Mansfield, E. H., 150
Mapping, 142, 151
Masur, E. F., 105, 150
Mau, S. T., 48
Mayers, J., 61
Meister, M., 317
Metastability, 57
Michell, A. G. M., 292
Miles, J. P., 61
Multiple loading, 47
Nayfeh, W., 52, 61, 131, 253
Necking, 61
Nonlinear compatibility, 211

- Optimization, 48, 242, 244, 272, 287–299
Oval cylindrical shells, 60
Panels, 60, 291
Passive coordinates, *see* Generalized coordinates
Pearson, C. E., 158
Perturbation methods, 78, 103–105
compound branching, 231–233, 241–242
continuous systems, 29–35, 120–122, 165–170
elimination of passive coordinates, 225–227, 239–241
imperfect systems, 19, 182–187, 193–202
perfect system, 16, 127, 133, 143–148, 152–153
Perturbation parameter, 105, 143, 193, 232, 242
Perturbation patterns, 147, 196–202
Pfluger, A., 317
Plates, 60, 114, 290
circular, 160–176
Poincaré, H., v, 46, 48, 53, 137, 151
Pope, G. G., 60, 150
Post-buckling path, *see* Equilibrium path
Post-buckling path derivatives, 145, 146, 147, 153, 184, 185, 233–235
Potential energy function, 86, 91
Principal coordinates, *see* Generalized coordinates
Pugsley, A. G., 299
Rayleigh functions, 110, 112
Rayleigh–Ritz analysis, 49, 108, 110, 112, 146
Rehfield, L. W., 61
Reissner, E., 252
Rigid loading system, 71
Rings, 59, 155–159
Roorda, J., 46, 59, 71, 151, 181, 211, 218, 219, 289
Rubber structures, 61
Saddle point, 24, 91
Schreyer, H. L., 105
Scleronomic systems, 86
Sechler, E. E., 271
Sendelbeck, R. L., 60
Sewell, M. J., vi, 48, 78, 79, 84, 85, 98, 106
Shanley, F. D., 242, 260

Degenerating structures, 47
Degree of instability, 90, 99, 131
Degrees of freedom, infinite, 26, 253
one, 2, 5, 9, 15, 63, 132, 146, 189, 300
two, 21, 57, 108, 142, 188, 243
Diagonalization, 22, 47, 89, 98, 101, 141, 150, 151, 158, 223–224, 260
Discrete systems, vii, 49
Domes, 51, 59, 60, 290
Donnell equations, 156, 159
Dubey, R. N., 61
Eigenvalue analysis, *see* Linear eigenvalue analysis
Elastica, 26–45, 99, 114, 253
Elimination of passive coordinates, 65, 221, 224–228, 238–241, 263, 265, 269
Equilibrium, critical, vii, 91
neutral, vii
normal, vii, 103–126, 132
stable, 91
unstable, 91
Equilibrium condition, 87, 228, 240
Equilibrium equations, 84, 104, 128, 143, 152, 194, 225, 232, 233, 239, 241
general forms, 144, 194, 303, 304
Equilibrium path, 98
complementary, 9, 73, 268
fundamental, vii, 6, 141
natural, 9
post-buckling, vii, 6, 143, 146, 152, 231, 241
primary, vii, 64
secondary, vii, 64
Euler, L., 46
Euler equation, beam, 119
circular plate, 164
hanging bar, 111
strut, 29
Evensen, D. A., 60
Exchange of stabilities, 53, 137, 154
Experiments, 60, 71–76, 219, 281
Far-field stability test, 70, 238
Finite-difference method, 47
Finite-element method, 40–44, 47, 49, 78, 81, 99, 110–116, 124–126, 170–178, 211–220
Fitch, J. R., 60
Follower force, 88
Fourier harmonics, 37
Fraeijs de Veubeke, B., 49

Frames, 47, 59, 60, 71–75, 211–220, 292
Friedrichs, K. O., 60, 168, 178
Fung, Y. C., 59, 271
Gallagher, R. H., 48
Generalized coordinates, 49, 86, 93
active, 222, 238
incremental, 89, 132
passive, 222, 238
principal, 22, 49, 90, 187, 260
sliding, 98, 141, 142, 160, 192
sliding and rotating, 98, 130, 141, 150, 152, 153, 159, 181
Gere, J. M., 26, 44, 208, 317
Godley, M. H. R., 47
Graves-Smith, T. R., 295
Green, A. E., 61
Griffith, B. A., 49, 86
Haftka, R. T., 59, 131, 253
Hamilton's equations, 86
Hanging bar, 110–116
Harmonic analysis, beam, 122–124
spherical shell, 256–271
strut, 37–40, 99, 209
Hayman, B., 47
Herrmann, G., 46
Hoff, N. J., 60, 61
Holmes, A. M. C., 60
Holonomic systems, 86
Huseyin, K., 47
Hutchinson, J. W., 46, 60, 61, 251, 271, 299
Hypersurface of activity, 229
Imperfections, 7, 61, 65–69, 71–76, 181, 205, 211, 243, 287, 297
stochastic, 69
two, 15, 243
Imperfection-sensitivity, 71–76, 202, 219, 242, 248, 276, 280, 283, 287–299
asymmetric point of bifurcation, 20, 66, 183, 203
limit point, 181
power laws, 69, 203, 204, 276, 281, 286
unstable-symmetric point of bifurcation, 13, 67, 187, 203
Induction, 145, 195–197, 303–306
Johns, K. C., 47
Kaplan, A., 59
Kármán, T. von. v. 160, 251

Kármán plate equations, 160
Keller, J. B., 78, 83
Kelly, A., 61
Kemp, K. O., v
Kinematically-admissible displacement field, 110
Kinetic energy function, 86, 87
Kirchhoff uniqueness theorem, 104
Koiter, W. T., v, vi, 14, 46, 60, 61, 69, 74, 87, 154, 191, 211, 216, 218, 236, 237, 251, 253, 261, 263, 266, 267, 271, 276, 277, 281, 289, 291, 293, 294, 295, 299
Kollbrunner, C. F., 317
Kretzschmar, H., 317
Kuiken, G. D. C., 276, 277, 281, 295, 299
Lagrange, J. L., 46, 86
La Salle, J., 87
Ledoux, P., 48, 61
Lefschetz, S., 87
Legendre functions, 251, 253, 256
Leipholz, H., 83, 317
Lekkerkerker, J. G., 59, 205, 209
Lewis, G. M., 48, 81, 160, 172, 177, 288, 295, 299
Liapunov, A., 46, 50, 86
Limit point, 5, 51, 68, 129–134, 148, 180
Linear eigenvalue analysis, 26, 32, 159, 260, 279
Link models, 1–26, 99, 189, 243
Loading parameter, 50, 86–88
Localized Ritz procedure, 112–115
Lyttleton, R. A., 48, 61
Macmillan, N. H., 61
Madsen, W. A., 61
Mallett, R. H., 131, 253
Mansfield, E. H., 150
Mapping, 142, 151
Masur, E. F., 105, 150
Mau, S. T., 48
Mayers, J., 61
Meister, M., 317
Metastability, 57
Michell, A. G. M., 292
Miles, J. P., 61
Multiple loading, 47
Nachbar, W., 51, 31, 251
Necking, 61
Nonlinear compatibility, 211
Optimization, 48, 242, 244, 272, 287–299
Oval cylindrical shells, 60
Panels, 60, 291
Passive coordinates, *see* Generalized coordinates
Pearson, C. E., 158
Perturbation methods, 78, 103–105
compound branching, 231–233, 241–242
continuous systems, 29–35, 120–122, 165–170
elimination of passive coordinates, 225–227, 239–241
imperfect systems, 19, 182–187, 193–202
perfect system, 16, 127, 133, 143–148, 152–153
Perturbation parameter, 105, 143, 193, 232, 242
Perturbation patterns, 147, 196–202
Pfluger, A., 317
Plates, 60, 114, 290
circular, 160–176
Poincaré, H., v, 46, 48, 53, 137, 151
Pope, G. G., 60, 150
Post-buckling path, *see* Equilibrium path
Post-buckling path derivatives, 145, 146, 147, 153, 184, 185, 233–235
Potential energy function, 86, 91
Principal coordinates, *see* Generalized coordinates
Pugsley, A. G., 299
Rayleigh functions, 110, 112
Rayleigh–Ritz analysis, 49, 108, 110, 112, 146
Rehfield, L. W., 61
Reissner, E., 252
Rigid loading system, 71
Rings, 59, 155–159
Roorda, J., 46, 59, 71, 151, 181, 211, 218, 219, 289
Rubber structures, 61
Saddle point, 24, 91
Schreyer, H. L., 105
Scleronomic systems, 86
Sechler, E. E., 271
Sendelbeck, R. L., 60
Sewell, M. J., vi, 48, 78, 79, 84, 85, 98, 106
Shanley F R 242 288

- Simultaneous buckling, *see* Buckling
 Simultaneous mode design, 242, 278
 Skaloud, M., 289
 Southwell plot, 279
 Specialized system, 50, 78, 88, 106–110,
 129, 130, 137, 140, 148
 Spherical shells, 48, 59, 60, 156, 235,
 251–271, 293
 Spheroidal shells, 59
 Spiralling eigenvector, 193, 198
 Spunt, L., 242, 317
 Stability coefficients, 7, 23, 90, 99, 101,
 127, 130, 137, 139, 151, 222
 Stability condition, 23, 87, 228–231, 237
 Stability definition, 86
 Stability determinant, 26, 91, 99, 104,
 128, 131, 143, 151, 153, 181
 Stable-symmetric point of bifurcation,
 see Bifurcation points
 Steup, H., 317
 Stoker, J. J., 60, 168, 178
 Strut on an elastic foundation, 59, 205–
 210
 Struts, 59
 buckled, 76
 mild-steel, 282–286, 290
 pin-ended, 26–45
 reticulated, 277–282
 thin-walled, 272–277, 294
 two-hinged, 21–26
- Supple, W. J., 47, 243, 246, 249
 Suppression of secular terms, 33, 252
 Symmetry, 57, 234, 251, 265, 287, 290
 Synge, J. L., 49, 86
- Tennyson, R. C., 60
 Theorems, 61–65, 108, 146, 300
 Timoshenko, S. P., 26, 44, 208, 317
 Toroidal shell segments, 60
 Tsien, H. S., v, 251
 Tvergaard, V., 295
- Unstable-symmetric point of bifurcation,
 see Bifurcation points
- van der Neut, A., 49, 273–276, 289, 295,
 296
 Volmir, A. S., 317
 Vozlinskii, V. I., 65
- Walker, A. C., vi, 47, 78, 81, 191, 317
W-analysis, compound branching, 238–
 242
 imperfect systems, 191–202
 perfect system, 35, 79, 142–150
 Watson, G. N., 256, 258
 Whittaker, E. T., 256, 258
- Ziegler, H., 46, 48, 317